Numerical Modelling of a Geosynthetically Reinforced Sand mass Undermined by a Subgrade Void

by

Debbie Munian

Submitted in fulfilment of the academic requirements of

Master of Science

In Civil Engineering

School of Engineering

College of Agriculture, Engineering and Science

University of KwaZulu-Natal

KwaZulu-Natal

South Africa

Date (July 2016)

PREFACE

The research contained in this dissertation was completed by the candidate while based in the Discipline of Civil Engineering, of the College of Agriculture, Engineering and Science, University of KwaZulu-Natal, Howard College, South Africa. Contributions towards the purchase of software and laboratory equipment used by the candidate were received by the Discipline of Civil Engineering from Kaytech (a subsidiary of Kaymac (Pty) Ltd and the Geotechnical Interest Group of South Africa).

The contents of this work have not been submitted in any form to another university and, except where the work of others is acknowledged in the text, the results reported are due to investigations by the candidate.

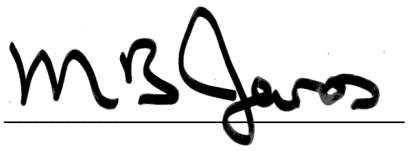

Signed: Malcom Jaros

Date: 28th July 2016

DECLARATION 1: PLAGIARISM

I, Debbie Munian, declare that:

(i) the research reported in this dissertation, except where otherwise indicated or acknowledged, is my original work;

(ii) this dissertation has not been submitted in full or in part for any degree or examination to any other university

(iii) this dissertation does not contain other persons' data, pictures, graphs or other information, unless specifically acknowledged as being sourced from other persons;

(iv) this dissertation does not contain other persons' writing, unless specifically acknowledged as being sourced from other researchers. Where other written sources have been quoted, then:

a) their words have been re-written but the general information attributed to them has been referenced;

b) where their exact words have been used, their writing has been placed inside quotation marks, and referenced;

(v) where I have used material for which publications followed, I have indicated in detail my role in the work;

(vi) this dissertation is primarily a collection of material, prepared by myself, published as journal articles or presented as a poster and oral presentations at conferences. In some cases, additional material has been included;

(vii) this dissertation does not contain text, graphics or tables copied and pasted from the Internet, unless specifically acknowledged, and the source being detailed in the dissertation and in the References sections.

Signed: Debbie Munian

Date: 28/07/2016

ABSTRACT

The South African railway network is highly developed and the vast span of existing rail lines require maintenance and upkeep to ensure smooth running of locomotives. One of the problems faced by the rail industry is instability in the formation level due to the development of sinkholes. Sinkholes and voids commonly form in karstic topography as a result of dolomite related subsidence but may also result from man-made processes such as mining. Roads and railway lines extend for hundreds of kilometres, occasionally over terrain prone to sinkhole formation, making construction over such terrain unavoidable. In order to prevent catastrophic failure in a railway line, the formation must be reinforced over sinkhole prone areas. Geosynthetic reinforcement is identified as a potential means of spanning developing subgrade voids by providing a temporary means of support in the event of a sinkhole. A laboratory model using single and multiple layers of geosynthetic reinforcement was thus developed at the UKZN geotechnical laboratory. Building physical models however is often expensive and time consuming. The research contained in this dissertation explored the use of numerical modelling in simulating the behaviour of a geosynthetically reinforced sand mass when undermined by a subgrade void. Finite element analysis software was used to provide a numerical representation of the physical laboratory model. Exploration into how best FEM can be used in predicting the behaviour of a reinforced fill layer undermined by a subgrade void is thus required. The FEM simulation should provide results within a reasonable degree of accuracy when compared to the experimental model. Through the course of the investigation the parameters governing the behaviour of the finite element model were identified and modified/varied in order to improve the accuracy of the numerical results. In addition to the numerical model, an analytical investigation in which design methods for reinforcement are used to predict the behaviour of a reinforced fill layer took place.

ACKNOWLEDGEMENTS

I would like to thank Mr Malcom Jaros, my supervisor for his input and direction in compiling the dissertation. I would also like to thank Mr Freek Shaw, and the Strand 7 FEM analysis team for their assistance and direction in the numerical modelling process.

Many thanks to the Transnet Freight Rail team, Kaytech Fabrics, Christian Psiorz from Geotextiles Africa and Hermanus de Lange who performed the experimental model within the University of Kwa Zulu Natal.

Lastly I would like to thank my family, God and my friends for their support, encouragement and help.

TABLE OF CONTENTS

Page

LIST OF TABLES

Table **Page**

LIST OF FIGURES

Figure **Page**

LIST OF ABBREVIATIONS

Symbol	Definition
FEM	Finite element method
FEA	Finite element analysis
FDM	Finite difference method
DEM	Discrete element method
RAFAEL	Renforcement des Assises Ferroviaires et Autoroutières contre les Effrondrements Localisés
LVDT's	Linear variable differential transformers
ICFEP	Imperial college finite element program
TFR	Transnet freight rail
AXI	Axisymmetric
PS	Plane strain

LIST OF SYMBOLS

Symbol	Definition
E	Young's modulus
ε	Strain
σ	Stress
K_0	Coefficient of earth pressure at rest
c	Cohesion
φ	Angle of internal friction
τ	Shear strength
V	Volume
γ	Unit weight of soil
H	Height
D	Void diameter
D_s	Diameter of settlement trough/cone
d_s	Soil surface settlement
d	Geosynthetic reinforcement deflection
θ_d	Angle of void propagation
w_s	Surcharge on soil surface
T_{max}	Maximum tension in geosynthetic
ε_{max}	Maximum strain in geosynthetic
C_e	Coefficient of expansion
μ	Poisson's ratio
g	Gravitational acceleration
T	Tensile modulus of geosynthetic reinforcement
T_{ult}	Ultimate tensile force in geosynthetic reinforcement
e	Void ratio
L_b	Geosynthetic anchorage length

1. CHAPTER 1: INTRODUCTION

1.1 Research rationale

A good transportation system is a vital and basic requirement for a functional society. The railway industry in particular, allows for transport of large quantities of goods as well as providing commuters with a means of transport. In areas underlain by karst dolomite rock landforms, sinkholes are an unpredictable and serious threat to the stability of surface structures including roads and railway lines (Bakhshipour, et al., 2013). For the railway industry specifically it poses a larger threat in that relatively minor subsidence can result in movement of the railway line sufficient to cause train derailment.

To safeguard individual buildings/structures over subsidence-prone formations deep pile foundations and ground improvement techniques such as grout infilling are employed. However when roads and railway lines that can extend for thousands of kilometres are considered such measures are too costly. A more cost effective means of reinforcing long stretches of subgrade is thus required.

Studies have identified various means of protection against sinkhole development that have been used in past designs, including deep compaction, cementitious stabilisation, steel cable and mesh reinforcement in formation layers/subgrade or use of a concrete grade-beam. The research undertaken focusses on the use of geosynthetic reinforcement in the subgrade to span over subterranean voids. Further research in this technique is required in terms of improvements in the strength, durability and cost effectiveness of modern geosynthetics and there is a need to develop new concepts and analytical techniques to optimise the utilisation of such materials in the design of subgrade reinforcement. Field trials where sinkholes are simulated are expensive and time consuming. The development of an analytical procedure for predicting the behaviour of a reinforced fill layer when undermined by a subgrade void would assist in saving time and experimental costs.

Past studies employing the use of Finite element methods (FEM) of geosynthetic reinforcement in soil have identified limitations in the type of elements used to model the geosynthetic reinforcement when the large strains associated with sinkhole development occur.

The objective of the investigation was to assess the results produced by a finite element analysis in terms of the deformations that take place in a reinforced fill layer over a developing sub grade void. The finite element analysis results produced in terms of the soil and geosynthetic deformations must match the experimental data from the laboratory model.

1.2 Justification

Numerical methods in general will help optimise the field of engineering in that expensive, time consuming experiments can be simulated using FEM instead of being physically built. The process of numerical modelling requires an in-depth understanding of the model characteristics and the engineering principles governing the design.

This investigation sought to explore the usefulness of FEM in modelling the behaviour of a reinforced fill layer to a sufficient degree of accuracy. This was done by comparing the FEM results to a laboratory experiment that was previously performed. In addition to the experimental and numerical model, an analytical assessment of the current geosynthetic design methods used in practice took place. After the validity of the numerical model had been established, a parametric investigation into the key design parameters governing the behaviour of the fill layer was undertaken.

1.3 Aims

The aim of the research was to investigate the application of finite element analysis as a means of predicting the behaviour of a reinforced soil fill layer undermined by a subgrade void.

1.4 Objectives

- The research will provide an enhanced understanding of the behaviour of a reinforced fill layer when undermined by a subgrade void.
- Provide a better understanding of numerical modelling and how this application can be used in geotechnical applications
- Identify the key parameters that influence geosynthetic reinforcement design bridging subgrade voids

1.5 Summary Table

The table below shows a summary of the type of models considered in the investigation

Table 1.1: Summary of models developed and investigated through the course of research

References	Type of Model	Model Name	Model Description
University of Kwa-Zulu Natal Geotechnical laboratory: Physical laboratory testing	Experimental	Unreinforced	600, 300mm Height
			300mm Void diameter
		Reinforced	300mm Height
			150, 200, 300mm Void diameter
			1 - 6 Layers reinforcement
Analytical calculations based on both the South African national standards and methods developed by the RAFAEL research team	Analytical	SANS 207: 2006	300 mm Height
			150, 200, 300mm Void diameter
			Basal reinforcement
			Reinforcement design for rail on embankment
		RAFAEL	300mm Height
			150, 200, 300mm Void diameter
			Basal reinforcement
Strand 7 Finite Element Analysis Program	Numerical	Reinforced experimental model	300mm Height
			150, 200, 300mm Void diameter
			1 - 6 Layers reinforcement
			3 D Model
			1- 2 Layers Reinforcement
			Plane strain model
			Axisymmetric model
		Potts (2007) Case study	80, 240mm Height
			80, 160mm Void diameter
		Parametric investigation	Standard Heavy haul line
			1- 4 Layers Reinforcement

1.6 Outline of dissertation structure

Chapter 2 is the literature review in which past experimental models performed using geosynthetically reinforced fill layers were considered. This chapter investigated the factors governing numerical modelling and past research performed in this field. The literature review also covered a theoretical assessment of the current analytical design methods used in practice. The chapter concluded with an overview of related research projects performed in the past in the form of case studies.

Chapter 3 presents the experimental model development and the model results. The experimental model was used as a basis for the development of the FEM model.

Chapter 4 is a review of the geosynthetic design techniques used in current practice in which the deflections/geometry of the soil surface and the geosynthetic reinforcement predicted from these techniques have been assessed and compared to the experimental model.

Chapter 5 focussed on the method employed in the development of the numerical model.

Chapter 6 is a presentation of the numerical FEM results for the selected experimental models.

Chapter 7 focused on a parametric FEM investigation in which a numerical model of a rail substructure and superstructure were developed. The parametric study helped to identify the key design parameters that affect the performance of a reinforced fill layer undermined by a subgrade void, in a railway specific environment.

Chapter 8 is the conclusions and recommendations section. In this chapter the results of the numerical, experimental, analytical and parametric study have been summarised and conclusions were drawn from these sections. Recommendations indicate the scope of future work yet to be covered and improvements to the current experimental/numerical procedure have been suggested.

2. CHAPTER 2: LITERATURE REVIEW

2.1 Introduction

Through the course of the literature review past experimental studies and analytical methods related to reinforcing soil against sinkholes were considered. Investigation into reinforcement methods that were historically used took place. These methods were assessed with regard to how applicable they were to a railway specific environment.

Historically engineering concepts such as movement of soil and soil arching have been applied in sinkhole reinforcement design. These engineering principles were used to formulate theoretical conclusions and observe whether the FEA model behaved in accordance to theory.

There has been past research into the use of basal (single layer) geosynthetic reinforcement to span subgrade voids (Potts, 2007). The research covered through the course of the investigation considered basal geosynthetic reinforcement as well as multi-layered reinforcement.

In FEA modelling the manner in which the geosynthetic fabric was represented has been a subject of scrutiny. Different geosynthetic modelling techniques used were investigated and these findings were taken into account when performing the actual FEM model.

The software selected for the numerical modelling process was the Strand 7 FEM program, used in Transnet Freight Rail offices for a variety of applications. Previous investigations into the use of Strand 7 in modelling geosynthetic fabric has taken place and was documented in the case study Kae (2003) and Grabe (2003). In Kae (2003), the geosynthetic modelling process was in the developmental phase and no exact method was proposed. The modelling process was further refined in Grabe (2003), where 1d truss elements were used to represent the geosynthetic layer. The findings of the literature review will allow refinement of the FEM design and provide guidance to the future research that must take place.

2.2 The formation of sub grade voids:

Sinkholes may result from natural conditions or manmade processes, e.g. tunnelling or mining. Substrata of predominantly calcium carbonate, magnesium carbonate or other soluble minerals are prone to sinkhole formation. Voids may form in the mineral structure due to downward percolation of rainwater which tends to be acidic in nature, this can result in dissolution of the calcium/magnesium carbonate minerals.

Water seepage results in development and expansion of a cavity, until a point is reached where collapse of the overlying soil occurs (Augarde, et al., 2003). Such conditions are typified as Karstic conditions which are complex land forms that resulted from the dissolution of soluble rocks (Oosthuizen & Richardson, 2011). On a section of the Gautrain line, running from Pretoria to Johannesburg, the formation of sinkholes was attributed to “the collapse of solution cavities in the underlying dolomite rock” Jaros et al. (2009). Collapse of old mine works can also result in sinkhole formation.

Sinkholes are generally bowl-like in shape but fissure-like cracks are not uncommon (e.g. slope cracks). Through the course of research sinkholes with a crater-like geometry were considered.

2.3 Numerical methods

Physically modelling the occurrence of a large scale sinkhole is a time consuming and expensive process. In especially complex applications, it may be difficult, inaccurate and sometimes impossible to physically perform the procedure. In such cases, it may be more suitable to use alternate methods to get the required results, e.g. analytical methods, numerical models. Engineering research and investigations require the use of laboratory tests and analytical models in order to validate theoretical numerical results, to ensure that the assumptions of the numerical model are representative of real life conditions.

Numerical methods provide algebraic expressions of real world situations and scientific concepts (Strand 7 verification manual, 2013). Research in the undergraduate dissertation "Numerical modelling of the strains in a sand mass when undermined by a developing sub grade void" (Munian, 2010) focused solely on the use of finite element analysis in order to model the formation of a sinkhole. Literature indicated that alternative methods to FEA can be considered, e.g. discrete element methods, finite difference method.

2.3.1 Finite Element Analysis

"Finite element analysis is a numerical method that is used in complex engineering applications where the solution would otherwise have been difficult to obtain" Lee et al. (2006). According to Potts & Zdravkovic (1999) most engineering solutions are based on the solution of the following equations.

1) Equilibrium equations

The equilibrium equations describes the transfer of forces throughout the soil body, this is done by analysing the variation of stress throughout the soil in the x, y and z plane.

$$\frac{\partial \sigma_x}{\partial x} + \frac{\partial \tau_{yx}}{\partial y} + \frac{\partial \tau_{zx}}{\partial z} = 0$$

$$\frac{\partial \tau_{xy}}{\partial x} + \frac{\partial \sigma_y}{\partial y} + \frac{\partial \tau_{zy}}{\partial z} = 0$$

$$\frac{\partial \tau_{xz}}{\partial x} + \frac{\partial \tau_{yz}}{\partial y} + \frac{\partial \sigma_z}{\partial z} + \gamma = 0$$

Where σ_x, σ_y, σ_z, τ_{xy}, τ_{xz}, τ_{zy} are the vector components of stress and γ is the unit weight of soil in the z-direction (Potts, 2007).

2) Compatibility equations

This is the strain - displacement relationship, the strain is considered to be the differential of the displacement. The compatibility equations accounted for the relationship between the strains in the soil mass and the displacement that the particles undergo (Potts & Zdravkovic, 1999).

$$\varepsilon_x = \frac{-\partial u}{\partial x}, \varepsilon_y = \frac{-\partial v}{\partial y}, \varepsilon_z = \frac{-\partial w}{\partial z}$$

$$\gamma_{xy} = -\frac{\partial v}{\partial x} - \frac{\partial u}{\partial y}, \gamma_{xz} = -\frac{\partial w}{\partial x} - \frac{\partial u}{\partial z}, \gamma_{xy} = -\frac{\partial w}{\partial y} - \frac{\partial v}{\partial z}$$

Where *u, v, w* represent the displacement components in the *x, y, z* direction and ε_x,ε_y, ε_z, γ_{xy}, γ_{xz}, γ_{zy} are the vector components of strain (Potts, 2007).

3) Constitutive behaviour

The material behaviour of a structural body is mathematically characterised by its constitutive equations or material laws (University of Colorado, 2012).

The relationship between the stress and strain effectively describes the Young's Modulus of the soil, i.e.

$$E = \frac{\sigma}{\varepsilon}$$

Young's Modulus = Stress/ Strain (for 1 D cases)

And Poisson's ratio (ν) = lateral strain/axial strain

For 2D applications the Young's Modulus takes Poisson's ratio into account and is modified to

$$E_{mod} = \frac{E}{1 - v^2}$$

For 3D applications, the Young's modulus is dictated by Poisson's ratio and is modified to:

$$E_{mod} = \frac{E}{(1 - 2v)(1 + v)}$$

The 1D expression for Young's modulus was then modified to take into account material behaviour of the system:

$$\{\Delta\sigma\} = [D]\{\Delta\varepsilon\}$$

Where D represents the matrix that describes the material properties of the soil, or in finite element analysis terms, the stiffness matrix.

4) Boundary conditions

The boundary conditions in terms of the force and the displacement must be defined. The Neumann boundary in the model is where normal stresses are given a value, and the Dirichlet boundary is where the displacement are given data (Sayas, 2008).

2.3.1.1 Finite element analysis process

The process of finite element analysis follows 3 general steps:

A) Pre-processing

The input of the models geometry, generation of the mesh and discretization of the boundary and specification of boundary conditions.

- Discretization:

FEA is based on the principle of reducing complex problems by dividing them into smaller problems and solving each one separately (Strand 7 verification manual, 2013). During element discretization, the problem domain is divided into small regions called finite elements. Elements are defined by nodes. Elements with nodes at the corners are straight, while the presence of mid-side nodes allows the elements to be curved. The various types of elements and their nodal positions are shown in Figure 2.1 below:

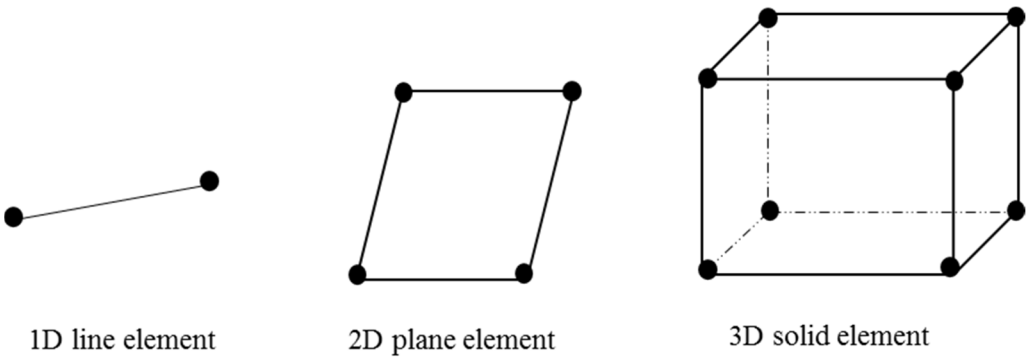

Figure 2.1: FEA element types

Looking at the example of a simple beam, a beam can bend in an infinite number of ways, by discretizing the boundary, it is assumed that the beam can only deform into a particular shape, limiting the variables and thus simplifying the problem.

The FEA pre-processing steps are as follows:

- Define the geometry of the model
- Define the type of elements being used
- Define the connectivity of the elements (define the mesh)
- Define the restraints/boundary conditions of the nodes

B) Analysis

Specifications of material properties and loading conditions.

- Define the material properties of the elements, e.g. Tensile strength, Young's modulus
- Define the loading conditions (gravity etc.)

The analysis process involves the selection of the primary variable. Potts (2007) states that most FEA programs select the displacement for this. Secondary quantities, like stress and strain are expressed in terms of the primary displacement quantity (Hutton, 2004). A set of algebraic equations to solve for the displacement are then developed. The deformation behaviour of the elements can be derived from the principle of minimum potential energy where "the static equilibrium position of a loaded linear elastic body is the one that minimises the total potential energy" Potts (2007). These leads to the following expression for the stiffness of the specific element:

$$[K_E]\{\Delta d_E\}_n = \{\Delta R_E\}$$

Where $[K_E]$ is the element stiffness matrix, $\{\Delta d_E\}_n$ is the vector of incremental element nodal displacements, and $\{\Delta R_E\}$ is the vector of incremental element nodal forces (Potts, 2007). The stiffness matrix represents the resistance of the element to change when subjected to external influences (Hutton, 2004).

In linear materials the element equations are then combined to form global equations:

$$[K_G]\{\Delta d_G\}_n = \{\Delta R_G\}$$

Where $[K_G]$ is the global stiffness matrix, $\{\Delta d_G\}_n$ is the vector of all incremental nodal displacements, and $\{\Delta R_G\}$ is the vector of all incremental nodal forces (Potts, 2007). The global equations are solved using Gaussian elimination and matrix decomposition (Potts, 2007).

C) Post processing

Analysis of results

FEA provides approximate solutions for the system, the accuracy of which depends on the convergence of the equations and the simplification assumptions made. The exact solution to the problem is solved by the program using the partial differential equations stated earlier. FEA will then produce and approximation of the exact solution. When the approximation converges on the exact solution, the computational process is complete. The actual convergence process is brought about by either altering the size of the elements or the order (magnitude) of the matrix. By changing the size of the element, the mesh is being constantly redefined and a more accurate solution can be obtained.

2.3.1.2 Limitations of the finite element analysis method

The process of flow of granular materials is difficult to model using the finite element method, due to the disfiguring of the mesh because of large soil deformations (Wieckowski, 2003). One of the main problems associated with modelling of flow conditions in finite element analysis is modelling the surface from which the soil is flowing. An entirely free surface, with a wide opening will cause free flow conditions in the soil mass, under these conditions the iterations do not converge and the points in the sand mass are in failure. In order to overcome this problem Sanad et al. (2001) initially modelled the discharge boundary as restrained in both the x and y direction. By releasing the restraint on the boundary and providing a downward displacement to the row of nodes in direct contact with the aperture boundary, initial flow conditions could be modelled.

2.3.2 Discrete element analysis

This numerical method is used for dynamic applications and accounts for motion of soil particles. The discrete element method can be used in order to model the motion of granular material as separate particles (Coetzee, et al., 2006). The program functions using Newton's second law and has the advantage of allowing for simulation of flow in a silo, when the boundary conditions are free. The discrete element code is a medium by which the "inter-particle contact parameters" in the soil structure can be investigated (Gallego, et al., 2010). When the void is formed, the soil particles are mobilized and hence undergo changes in displacement, shear strength and strength of contact bonds. According to Caudron et al. (2006) the soil properties that govern the particle interactions are:

- The frictional angle of the soil
- The degree of stiffness between contact particles
- The strength of the bond between contact particles

Some of the benefits of using a computer program to predict soil movement as opposed to practical laboratory methods is that in the modelling process all grain displacements and contact forces are known. Also, a specific sample can be tested multiple times and no heavy equipment is required (Van Baars, 1995).

The computational times for this method were however found to be excessive, due to the number of particles. Each particle undergoes a specific displacement and bonds that form between particles can change throughout the interactions. In order to limit computational time, a restriction on the number of soil particles was proposed by Van Baars (1995) where the number of particles would be limited to "no more than a few tens of thousands". By using discrete element analysis where the actual grain structure is simulated, it was anticipated that results would be more accurate.

In DEM when the particles undergo deformations, grains can break and new contacts will be formed. One of the main considerations in the modelling process is whether to use 2-D or 3-D modelling. 3-D models were found to be time consuming and required very powerful computer software; 2-D methods were more simplistic and yielded similar results. The physical modelling of the granular nature of the particles depends on the creation of particles and the formation of boundary conditions.

After performing the investigations, Van Baars (1995) concluded that models using equilibrium equations (FEM) yielded the same results as models based on equations of motion (DEM) but only when soil is in a quasi-static state and motion is minimal. FEM provides quicker convergence but for completely dynamic applications, DEM must be used. The main limitation in modelling using DEM is the restriction on the number of particles; hence any models performed will only illustrate laboratory models of a small scale.

2.4 Soil Properties

One of the objectives of the study was to investigate the behaviour of a soil fill layer when undermined by a subgrade void. Before the investigation was performed an understanding of the various parameters that govern soil behaviour must be obtained.

2.4.1 Coefficient of earth pressure

To describe the coefficient of earth pressure at rest consider a mass of soil confined by a frictionless wall. When the wall is in a state of static equilibrium, i.e. does not move left or right, the coefficient of earth pressure at rest is said to be the ratio of effective horizontal stress to effective vertical stress.

$K_0 = \sigma_h'/\sigma_v'$ (Das, 2006)

For granular non-consolidated soils, the coefficient of earth pressure at rest is described by Jakys formulae:

$K_0 = 1 - \sin(\varphi)$, where φ = Angle of internal friction

Sherif's 1984 study (cited in El Emam 2011) states that Jakys formulae is the accepted horizontal-to-vertical stress ratio in loose sand and normally consolidated soil. In the laboratory investigation, the soil fill retained in the concrete ring structure is in a state of equilibrium until a loss of support was induced. The soil used was loose sand hence the coefficient of earth pressure at rest was calculated using Jakys formulae.

CP Worth's 1972 (cited in El Emam 2011) proposed the following modification to Jakys formulae when soil is over consolidated:

$$K_0 = (1 - sin\varphi')OCR - \left\{\frac{\mu}{1-\mu}\right\}(OCR - 1)$$

Where the Poisson's ratio is 0.1 – 0.3 for loose sand and 0.3 – 0.4 for dense sand.

2.4.2 Young's Modulus

The Young's modulus provides as indication of the soils stiffness and the degree of settlement that a soil fill will undergo when subjected to static load. The elastic behaviour of the soil is governed by the Young's Modulus and the Poisson's ratio. At the onset of plastic deformation the soils behaviour is described by Mohr-Coulombs failure envelope. In previous studies performed by Mifsud (2005) and Potts (2007) the soils Young's modulus was varied in a parametric investigation to determine the influence it had on the FEM results.

2.4.3 Mohr-Coulomb failure criterion

Mohr theory states that when failure takes place in a soil mass it is due to a combination of the shear stress and the normal stress at a critical state. The shear strength is approximated by the following equation:

$\tau_f = c + \sigma \tan(\varphi)$ (Mohr-Coulomb equation)

c = cohesion

φ = Angle of internal friction

σ = Normal stress on the failure plane

τ_f = Shear strength

In the laboratory model, when the soil undergoes a loss of support it is expected that the soil behaves in a plastic manner as it will be suddenly forced into failure. The failure envelope that occurs is governed by the Mohr-Coulomb yield criterion. In the FEM program the soil elements were modelled as elastic-perfectly plastic materials with the Mohr-coulomb failure criterion.

2.4.4 Angle of internal friction

The angle of internal friction provides an indication of a soils ability to withstand shear force. The angle of internal friction as well as the angle of dilation should have an effect on the geometry of the surface trough and the deflected shape of the geosynthetic.

2.4.5 Density of soil

Compaction increases the shear strength of the soil. In previous studies performed by Potts (2007), the behaviour of dense and loose geosynthetically reinforced soil when subjected to a subgrade void was considered. Potts (2007) concluded that denser soil tended to dilate more due to the increased angle of shearing resistance and provided an overall decrease in soil settlements. Potts (2007) also concluded that in looser fill, adding, reinforcement had a greater effect on the surface settlement than adding reinforcement to a compacted soil fill layer.

2.4.6 Soil arching

Soil arching is defined as "The transfer of forces between a yielded mass of soil and adjoining stationery members" Terzagi (1943). Classical arching theory states that when the vertical support at some part of a soil mass is lost, the soil mass will want to move downward due to self-weight. The mass that moves downward will shear along a boundary between itself and the soil that remains stationary. The shearing resistance along this boundary opposes the downward motion and results in a redistribution in some of the stresses. This has an effect in reducing the pressure on the yielding area (vertical stresses) and increases the pressure in the stationary soil (horizontal stresses) (Potts, 2007). The occurrence of soil arching is indicated by the shear strength of the soil being larger than expected, due to the soil supporting itself over a certain area.

Various factors have been identified to effect the occurrence and degree of soil arching. Giroud et al. (1990) theorises that the H/D ratio has a significant influence on whether soil arching takes place. Other factors identified were the properties of the fill material, density of the fill and the number of reinforcement layers used.

The earliest recorded occurrence of soil arching was discovered in the 1800's (Smith, 2014). After the construction of a silo, it was found that the forces being applied to the base of the silo was less than the anticipated weight of fill within the silo. This was due to the fact that the sidewalls of the silo carried some of the fill weight due to the transfer of forces to the sidewalls of the silo structure. The soil tends to "arch over the yielded part of the support" Terzagi (1943).

Arching theory also plays a role in the initial formation of the sinkhole. Sinkholes are generally formed due to voids in the soil-rock interface, as the void gets larger; the soil above the void is

unsupported. The soil will arch until a point where the arch across the cavity is incapable of handling the overburden, after which collapse will occur. Potts (2007) concluded that there is a correlation between soil arching and the ratio of the overburden height to the depth of soil deflection. The larger the H/D ratio, the greater the chance of soil arching taking place.

2.4.7 Soil dilation

The angle of dilation "controls an amount of plastic volumetric strain developed during plastic shearing and is assumed constant during plastic yielding" (Bartlett, 2012). When a soil undergoes deformation while in shear, and the volume of the material is preserved, the angle of dilation of the soil is said to be zero. The dilation of the soil depends on the soil type, degree of compaction and the movement of the soil. Figure 2.2 shows the relationship between stress, strain and rate of volumetric change. The peak stress corresponds to the development of dilation in dense soil. Beyond this point the soil will continue to dilate until a critical state is reached. At the critical state the soils volume will remain constant as it shears (Bolton, 1986).

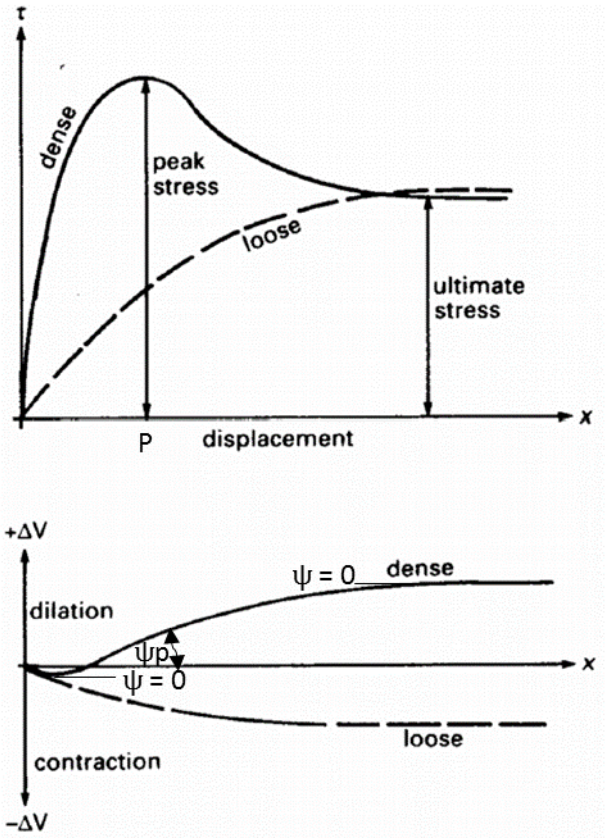

Figure 2.2 Diagrammatic representation of widely adopted concepts of the relationship between shearing and dilation as expressed in Schofield & Wroth (1986)

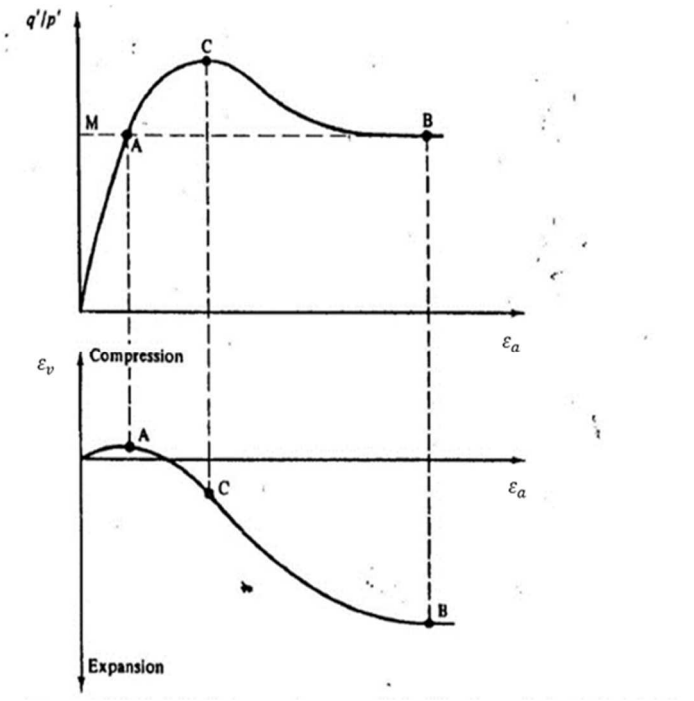

When constant volume deformation takes place and there's no dilation ($\frac{\delta\varepsilon_v}{\delta\varepsilon_a}$ = 0), $\frac{q'}{p'}$ = M. When strain < A the soil sample will contract and $\frac{\delta\varepsilon_v}{\delta\varepsilon_a}$ is a positive value. The sample undergoes expansion from $\frac{q'}{p'}$ = A to $\frac{q'}{p'}$ = B, and point C represents the point where the maximum rate of dilation occurs at some point C. Atkinson (1981) thus concluded that there is a

Figure 2.3: Typical $\frac{q'}{p'}$ vs ε_a and $\varepsilon_v$vs ε_a relationships for a drained triaxial test on dense sand where $\frac{q'}{p'}$ = stress ratio and $\frac{\delta\varepsilon_v}{\delta\varepsilon_a}$ = rate of dilation Atkinson (1981).

direct link between the shape of the ε_v: ε_a and $\frac{q'}{p'}$: ε_a curve.

According to Bartlett (2012) the angle of dilation for sands depends on the angle of shearing resistance. In non-cohesive soils like sand and gravel, when the angle of shearing resistance is greater than 30^0, the angle of dilation can be estimated as equal to 30^0 (Bartlett, 2012). Bartlett (2012) further states that soil contraction (negative dilation) is more likely to take place in loose sands. When performing an FEA involving soil in motion, the possible dilation of the soil must be accounted for. The Strand 7 program used for the FEA analysis regarded the angle of dilation as equal to the angle of shearing resistance. The angle of soil dilation cannot be altered independently from the shearing resistance hence the Strand 7 system may overestimate the predicted angle of dilation, especially in cases where the soil is in a loose state and is more likely to contract.

2.5 Current reinforcement techniques

The formation of voids in a soil substrate can result in collapse of the overlying soil, massive deflections and damage to any surface structures. In order to stabilise the soil above the sub grade void, different reinforcement techniques were considered historically:

a) Cement stabilisation
b) Grouting
c) Geosynthetic reinforcement

Previously pressure grouting and cement stabilization were used as a means of reinforcement against sinkhole formation. Generally speaking grouting is an expensive exercise and will be justified depending on the scale of the project (filling the void with grout may be an expensive application depending on how large the void is). An alternative would be to minimize the surface deflections by using geosynthetic reinforcement. Jaros et al. (2009) states that geosynthetic reinforcement provided technical advantages and was a more cost effective option for this particular problem.

For the purpose of this investigation, geosynthetic reinforcement will be used to span the sub grade void and provide temporary support to the soil mass. Within the subsection of geosynthetic reinforcement, various factors must be considered before the actual reinforcement takes place. Basal reinforcement is a commonly used option; this involves using a single layer of geosynthetic fabric of sufficient strength to minimise soil surface deflections.

2.5.1 Cement stabilisation

Studies performed by Alexiew et al. (2002) and Gooding's & Abdulla (2002) used a combination of soil stabilisation and geosynthetic reinforcement for a cost effect means of reinforcing large areas against subgrade voids. Cement stabilization is performed by combining the soil fill/aggregate with cement and water and compacting the material until the required strength parameters are met.

For rail and roadway conditions specifically, the Transnet Freight Rail S413 specification provides a design guide. Materials such as unslaked lime, Portland cement and slag are used as cementitious material. Stabilisation of sub-ballast layers is a common practice and is performed onsite during construction or for maintenance purposes during the tamping process. Cement

stabilisation is seen as a relatively cost effective means of reinforcing long stretches of sub-ballast layers when the support provided by the formation is insufficient.

2.6 Geosynthetics

The general definition of geosynthetic reinforcement is “A planar, polymetric (synthetic or natural) material used in contact with soil/rock and/or any geotechnical material in civil engineering applications” (Muller & Saathoff, 2015). Geosynthetics are basically sheets of woven materials used for reinforcement, separation, drainage etc. Geosynthetics also provide added stiffness if sufficient interlocking of soil particles takes place when support is lost. Geosynthetics are manufactured from polymeric materials (the synthetic) used with soil, rock, or other geotechnical- related material (the geo) as part of a civil engineering project or system (Kae, 2003). Geosynthetics are made from synthetic polymers such as polypropylene, polyester, polyethylene, polyamide, PVC (Kae, 2003) . Geosynthetics are generally categorized into two main sections: Natural and synthetic. It can be permeable or impermeable, depending on the application (Rajagopal, n.d.).

Geosynthetic products can be geocells, geotextiles, geomembranes or geogrids (Kae, 2003).

- Geocells: Are 3D honeycomb structures generally used for support and erosion control. Are also used to provide tensile reinforcement and shear resistance to increase the effective bearing capacity of the subgrade.
- Geotextiles: Used for reinforcement and are used for separation and filtration to prevent contamination of the ballast and provide quick relief of pore water pressures in rail applications.
- Geogrids: are used to provide tensile reinforcement and shear resistance to increase the effective bearing capacity of the subgrade. They are also used to interlock with and confine the ballast, increasing its resistance to both vertical and lateral movement in rail applications.
- Geomembranes: Are used as fluid barriers due to their low permeability.

The investigation will consider the application of geosynthetics as soil reinforcement. Geogrids and geotextiles are generally used for these applications and provide interlocking of soil fill.

The interactions between the soil and the geotextile interface results in the transfer of shear stress from the soil to the geotextile (Pinto, 2003). Using geosynthetic fabric as soil support over the cavity requires investigation into the load transfer ability of the material.

2.6.1 General principles:

The inclusion of geosynthetic reinforcement in the soil mass increases the bearing capacity of the fill layer. Geosynthetic reinforcement is based on the transfer of stresses between the soil and the reinforcement under tension. The stress is transferred to the geosynthetic by friction, the interlocking between the soil and the reinforcement causes this friction to occur.

Some of the key geosynthetic design factors are the required tensile strength, the depth at which the reinforcement must be installed and the number of layers that must be used. Geosynthetics are traditionally installed as basal reinforcement, where one layer of high tensile strength is placed at the required depth in the soil fill. A more comprehensive overview of the use of basal geosynthetic reinforcement is recorded in section 2.6.4.

2.6.2 Use of geosynthetics as reinforcement:

Geosynthetics are mainly used for the following purposes according to Han (n.d):

- Drainage
- Separation
- Reinforcement
- Erosion protection

2.6.2.1 Drainage

- Facilitate the flow of liquids or moisture
- Increased porosity to facilitate liquid movement

2.6.2.2 Separation

- Provide retention and prevent stones from punching through into soil
- Prevent soil fines from travelling into upper ballast or track (in rail applications)

2.6.2.3 Reinforcement

- Increase the interlocking between the soil and the reinforcement to increase the shearing resistance of the soil
- Increase the stiffness in the formation and minimise the formation settlements and deformations

2.6.2.4 Erosion protection

- Protect soil surfaces from erosion by rainfall/wind
- Retain the soil surface and minimise surface erosion

2.6.3 Geosynthetic characteristics:

The geosynthetic fabric characteristics vary in terms of the tensile strength, durability, and hydraulic properties (Han, n.d.).

2.6.3.1 Physical properties

Mainly for quality control and assurance

- Type of material (Polymer, polyester etc)
- Roll length, width, diameter (mm)
- Thickness (mm)
- Mass per unit area (g/m^2)

2.6.3.2 Hydraulic properties

The ability to provide drainage, containment, protection from fluid ingress, separation and containment.

- Opening characteristic, size of opening.
- Permeability
- Porosity
- In-plane flow capacity

2.6.3.3 Mechanical properties

This covers the strength requirements for geosynthetic reinforcement

- Tensile strength
- Creep resistance
- Penetration resistance

2.6.3.4 Durability properties

Long term quality assurance

- UV resistance
- Chemical resistance

Geosynthetic properties were selected based on the function required of the geosynthetic. Since the application considers geosynthetic design to span subgrade voids, the mechanical properties of the geosynthetic formed the main design criteria. The basal reinforcement design properties were further considered in section 2.6.4 below.

2.6.4 Basal reinforcement

In the British Standard BS 8006:1995 the use of basal reinforcement is extensively covered. The purpose of basal reinforcement is to prevent upward propagation of the sinkhole. Basal reinforcement was used in an investigation by Villard et al. (2009) as a safety measure to limit the deflections in the event of a sinkhole until the void material can be properly repaired.

Jaros et al. (2009) found that it is impractical to use basal reinforcement for applications where the diameter of the sinkhole is greater than 5m. This is because the strength and stiffness requirements for the geosynthetic in this application would be far too large hence a more economical option would be the use of multiple layers of geosynthetic reinforcement. In the case that basal reinforcement is used for this application, a supporting U-beam would still be required hence the less expensive multi-layered geosynthetic reinforcement must be considered.

2.6.5 Geosynthetic applications

In the case studies considered in chapter 2, geosynthetic reinforcement was used for various design situations, e.g. reinforcement for an embankment over soft clay (Bangkok), used in combination with cement stabilization (Germany, Kuwait, and U.S.A) to prevent collapse due

to void formation. The primary applications of geosynthetics in soil reinforcement considered in this investigation were for reinforcing embankments on soft soils and as a bridging system over sub grade voids.

2.6.5.1 Embankments on soft soil

Embankments constructed over soft soil face the threat of excessive settlement, due to the consolidation that the base layer undergoes. The basal reinforcement technique is generally used to prevent excessive settlements. Reinforcing it in this manner does not prevent settlement from taking place; instead it minimises the settlement and makes it more uniform.

2.6.5.2 Bridging of sub-grade voids

The German design guide EBGEO: 2011 regards two forms of geosynthetic stabilization:

a) Complete stabilization

The stability of the fill is guaranteed for the entire design working life, this is usually a geosynthetic used in combination with another type of reinforcement (e.g. cemented soils).

b) Partial stabilization

This is when local subsidence is allowed but it must not exceed the design limit. This is a temporary reinforcement technique used to prevent catastrophic collapse and maintain serviceability until a more permanent means of soil reinforcement can be installed.

2.6.6 Modelling of geosynthetic reinforcement

In order to model the geosynthetically reinforced fill an investigation into the current FEM geosynthetic design techniques was performed. In both Potts (2007) and Mifsud (2005) the geosynthetic layer is modelled as “special” membrane elements, specific to the ICFEP FEA program that was used. These were infinitesimally thin elements that allow stress to develop in their plane but not perpendicular to it (Mifsud, 2005). The reinforcement-soil interface was modelled as six-noded isoperimetric interface elements. The interface elements were put in place to prevent the reinforcement pulling-out from the soil fill.

In the laboratory model, the friction that occurs between the soil particles and the geotextile surface can result in variation of results and interlocking of soil grains. Messafer (1996) used a

combination of boundary element methods and discrete element analysis. The actual modelling of the geotextile was performed using a combination of a fabric surface and interface elements. Importing the surface as a fabric represents the fabric strength of the geotextile. The interface elements account for the bonding and shear between the membrane and the soil.

In Ling & Lui (2003) a 2D model of a geosynthetically reinforced roadway was developed. The geosynthetic reinforcement was modelled as 3-node non-compression bar elements with linear elastic properties. In Bohagr (2013) the geosynthetic layer was modelled as an 8-noded axisymmetric element. In Perkins (2001) the interaction between the soil and the geosynthetic layer was modelled as nonlinear spring elements.

In this investigation the FEM modelling was performed using Strand7 FEM software, for the 2D analysis, the geosynthetic reinforcement is modelled as a 2-noded beam element and the 3D analysis, the geosynthetic is modelled as a 3D membrane element.

2.7 Previous experimental models

The objective of the investigation is to prove that numerical FEM modelling can be used to predict the behaviour of a reinforced fill layer when undermined by a subgrade void to a sufficient degree of accuracy. In order to validate the FEM modelling results, experimental laboratory models are developed. This stage of the literature review covers an investigation into the different laboratory models developed.

Villard et al. (2009) used a laboratory model with balloons placed as support in the area of void formation and progressively deflated them to model the void condition (overburden height = 0.5m). The experiment took place over a 5 month timeframe. In the laboratory model used at The University of Kwa-Zulu Natal, a piston and hydraulic jack system was developed to perform the same function as the balloons.

Coetzee et al. (2006) used a laboratory silo model, similar to the one used in the UKZN laboratory. The model was 310mm wide and 600mm high. An opening is created at the base of the silo to cause a loss of support. The length of the opening was varied in order to investigate the soil discharge patterns under different flow conditions. Materials of different colour but the same consistency were used in order to determine the soil flow patterns.

In a laboratory model undertaken by Craig (2001) two model scenarios were developed to determine the failure pattern of the soil. Both tests involved the use of a soil sample containing two layers of clay, with a cylindrical cavity opened underneath it. For the first test, failure was induced by gradually increasing the overburden height of the soil. The second test involved extraction of sand below in order to form a void underneath the clay layers. The height to depth ratio (height of fill/depth of surface deflection), was found to correlate between the two experiments.

In laboratory testing undertaken by RAFAEL (a French research program that investigated the use of geosynthetic reinforcement as a support for embankment fills) (Blivet, et al., 2002). A localized sinkhole of diameter 2 - 4m was simulated by filling a void with clay beads. A circular void is created beneath an embankment and filled with circular clay beads. The clay beads are pumped from the cavity in order to model sinkhole conditions, and the strains, deformations and settlements of the fill layer above the sinkhole are recorded. The test was performed with

the inclusion of geosynthetic reinforcement, in order to determine whether multiple layers of geosynthetic effect the resulting sinkhole dimensions.

2.7.1 Conclusions of experimental models:

Caudron et al. (2006) concludes that numerical methods provide a better description of the volume of the settlement trough when compared to the semi-empirical estimation. The numerical method and experimental procedure did not yield the same results, due to the difference in collapse mechanisms between the two methods. In the experimental model only part of the sand collapsed into the cavity, due to cohesion in the soil.

Analysis of the results from both Villard et al. (2009) and Caudron et al. (2008) indicated that numerical methods produced the most accurate model of the soil structure interactions (when compared to the analytical model) because the membrane effect, friction, and sliding of the geosynthetic was accounted for.

Jaros et al. (2009) concluded that the difference in soil strain values and deflections calculated using plane strain and axisymmetric conditions were very similar. The results obtained from the laboratory model were acceptable but it "yielded little quantitative information."

Sanad et al. (2001) found a large discrepancy between FEM and DEM results. The discrete element analysis provided results that gave a satisfactory representation of the flow of particles through the aperture. The finite element analysis yielded results that were accurate with regards to the pressure formation within the silo but there was difficulty modelling the flow of the soil through the orifice.

The RAFAEL team performed experiments using basal and multi-layered geosynthetic reinforcement (Blivet, et al., 2002). RAFAEL concluded that the multi-layered reinforcement subsystem produced the same results as the basal layer model and that there was no obvious benefit to the multi-layered model (Blivet, et al., 2002). Results presented by Villard et al. (2009) indicated that for an H/D ratio of 0.75, stabilised arches tend to form. The lower the H/D ratio, the greater the chance of sudden collapse taking place.

2.8 Current design procedures

In addition to the experimental and numerical model, an analytical investigation into the current geosynthetic design techniques was performed. An analytical model where the theoretical soil surface settlements and geosynthetic deformation are calculated was developed. A theoretical investigation into the current design techniques was recorded below:

The following design procedures were investigated:

a) SANS 207/ BS8006: 1995
b) RAFAEL Design method
c) Girouds layer thickness analysis
d) Multi-layer method

2.8.1 SANS 207/BS8006:1995

SANS 207:2006 covers the design of a reinforced layer at the base of an embankment situated over a subgrade void. The design process in SANS 207 is the same as the British code BS 8006:1995. The role of the basal layer of reinforcement design in SANS 207 is to limit vertical settlement and maintain serviceability until a time when permanent reinforcement measures can be put in place. This is a temporary reinforcement measure to prevent ULS (collapse) from taking place.

When designing foundations over poor soil conditions the following factors are considered in SANS 207:

i. The maximum acceptable soil surface deformations for the structures requirements i.e. road, railway line, embankment

$\frac{d_s}{D_s}$ = [1 – 2%]. Depending on the expected traffic flow in the design area, 1% = high traffic flow, 2% = low traffic flow.

ii. Choosing a suitable soil void diameter

Survey of the ground conditions in the area and the geological history will help determine the diameter of the void that will be used. SANS 207 states that it is preferable to select a conservative value due to “uncertainties of future subsidence, and the consequent risks involved”.

iii. Determine the maximum strain allowable in the reinforcement

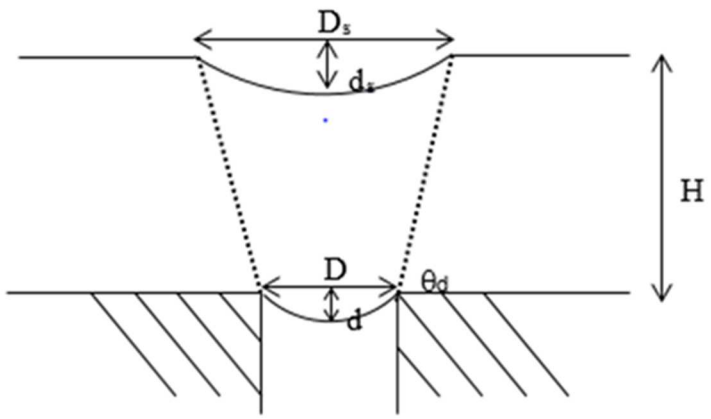

Figure 2.4: Upward propagation of void as assumed by SANS 207

As shown in Figure 2.4 above, SANS 207 assumes a void of diameter D forming beneath a fill layer, resulting in a deflection bowl developing at the surface of the fill. The symbols are defined as follows:

Ds = Diameter of surface settlement trough (mm)

ds = Vertical settlement at surface of fill layer (mm)

H = Height of fill layer (mm)

D = Design diameter of void (mm)

d = deflection of geosynthetic reinforcement (mm)

θ_d = Angle of draw/angle of void propagation

The shape of the deflected geosynthetic layer is assumed to be parabolic by SANS 207. The vertical forces the geosynthetic are due to weight of the soil and any addition surcharge loading. All loading is regarded as vertical and uniformly distributed.

The parabolic shape of the deflected geosynthetic is shown in Figure 2.5 below:

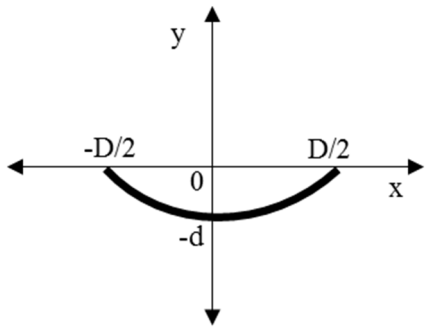

Figure 2.5: Shape of deflected geosynthetic fabric as per SANS 207 specifications

The parabolic equation describing the vertical deflection of the geosynthetic then becomes:

$$y = \frac{4dx^2}{D^2} - d$$

Using the extended length of the geosynthetic, the reinforcement strain is derived in Steinman (1957):

$$\varepsilon_{max} = \frac{8d^2}{3D^2}$$ (Steinman, 1957)

SANS 207 assumes that no volumetric change takes place in the soil mass, hence the soil volume displaced at geosynthetic level = the volume of the surface settlement trough. The volume of the settlement trough subsequently depends on the shape of the void that forms. Two void shapes are considered, an axisymmetric void (circular in shape) and a longitudinal void (in the shape of a long trench).

The volume of soil displaced due to these void shapes is as follows:

1) Longitudinal void: V =

$$\frac{2\,dD}{3} = \frac{2d_sD_s}{3}$$

2) Circular void: V =

$$\frac{dD^2}{3} = \frac{d_sD_s^2}{3}$$

The mass of soil effected by the formation of the void is in a funnel-like shape which is governed by the angle of void propagation θ_d.

Given this information, an expression can be written for the settlement trough diameter:

$$D_s = D + \frac{2H}{tan\theta_d}$$

Substituting the expressions for d and D in the ε_{max} equation the following is obtained for circular voids:

This is done using the formulae ε_{max}:

$$\varepsilon_{max} = \frac{8\left(\frac{d_s}{D_s}^2\right)(D+\frac{2H}{tan\theta_d})^6}{3D^6}$$

iv. Determine the tensile properties of the reinforcement needed for design

T_{rs} is the tensile load in extensible geosynthetic fabric. This is calculated by apply safety factors to the maximum stress in a cable as per Steinman (1957):

$$T_{rs} = 0.5\lambda\ (f_{fs}\gamma H + f_q w_s)\ \mathrm{D}\ \sqrt{1 + \frac{1}{6\varepsilon}}$$

T_{rs} = Tensile load in the reinforcement per m run

λ = Load distribution coefficient. (Axisymmetric = 0.67; plane strain longitudinal voids = 1)

f_{fs} = Partial load factor for soil unit weight, ffs = fq = 1.3 (ULS), ffs = fq =1.0 (SLS).

γ = Soil unit weight

H = Embankment height

f_q = Partial load factor for embankment loading

w_s = Embankment surcharge

D = Selected void diameter

ε = Reinforcement strain (< εmax)

For inextensible reinforcement SANS 207 states that alternate measures should be considered.

v. Determine the reinforcement bond length

The reinforcement bond length is the length of geogrid required for anchorage to take place, ensuring that no slippage takes place at the base of the embankment. This is based on activating soil friction and requires interlocking between the soil particles and the geogrid mesh. The minimum bond length required to carry the load of T_{rs} is:

$$L_b \geq \frac{f_n f_p T_{rs}}{\gamma H \left(\frac{\alpha_1 \tan \varphi' cv1}{f_{ms}} + \frac{\alpha_2 \tan \varphi' cv2}{f_{ms}}\right)}$$

fn = Partial factor governing the economic ramifications of failure (*fn* = 1 for embankments and soil, *fn* = 2 for structures of larger monetary value)

fp = Partial factor applied to the pull-out resistance of the reinforcement.

H = Average height of fill over the bond length of the reinforcement;

γ = Unit weight of the embankment fill;

α_1 = Interaction coefficient relating the soil/reinforcement bond angle to tan φ'cv on one side of the reinforcement;

α_2 = Interaction coefficient relating the soil/reinforcement bond angle to tan φ'cv on the opposite side of the reinforcement; *fms*

fms = Partial material factor applied to $\tan \varphi'$ (*fms* = 1 for both ULS and SLS)

vi. SANS 207 design assumptions

SANS 207 calculates the expected soil surface deflections and geotextile strain by using volumetric change calculations. It assumes that the volume of soil contained in the basal layer when a loss of support takes place is the same as the volume of soil in the surface displacement trough. No volumetric change is accounted for, hence SANS 207 does not account for any soil dilation due to shearing. The soil is also assumed to be cohesion less. When tensile forces are activated in the geosynthetic layer after soil collapse has taken place, SANS 207 assumes that the geogrid layers deflected shape is parabolic.

The second analytical method considered was developed by the RAFAEL team (Renforcement des Assises Ferroviaires et Autoroutières contre les Effrondrements Localisés – reinforcement of railway and motorway foundations against localised subsidence) (Blivet, et al., 2002).

2.8.2 RAFAEL design method

The RAFAEL team consisting of Gourc, Blivet, and Villard conducted investigations on the use of geosynthetic reinforcement as a means of sinkhole prevention beneath an embankment. Several tests were performed, using embankments beneath roadways and railway lines, single basal reinforcement and a two layered geogrid system was considered. The development of the sinkhole was simulated by pumping clay beads out of a dug out void in the formation level. The results measured were the geogrid strain and deformation, the soil movement and surface settlement.

It was found that soil arching took place when the ratio of embankment height (H) to void size was sufficiently high. The RAFAEL method of analysis assumes that the area affected by subsidence is limited to the soil directly above the void, in a cylindrical shape (Blivet, et al., 2002). The design method suggested in both SANS 207 and the RAFAEL method assumes that the load on the geogrid is uniformly distributed and that the shape of the geotextile is parabolic for design simplification.

The analytical methods developed based on the experimental results take into account soil arching and soil dilation. This differs from the method suggested in SANS 207, both analytical methods will be considered and differences in the results will be noted with respect to:

- Soil surface settlements
- Soil collapse zone geometry
- Deformed geogrid geometry

Using the analytical model developed by RAFAEL the load in the geogrid layer can be calculated, as well as the maximum strain that the reinforcement layer can handle and the soil surface deflections.

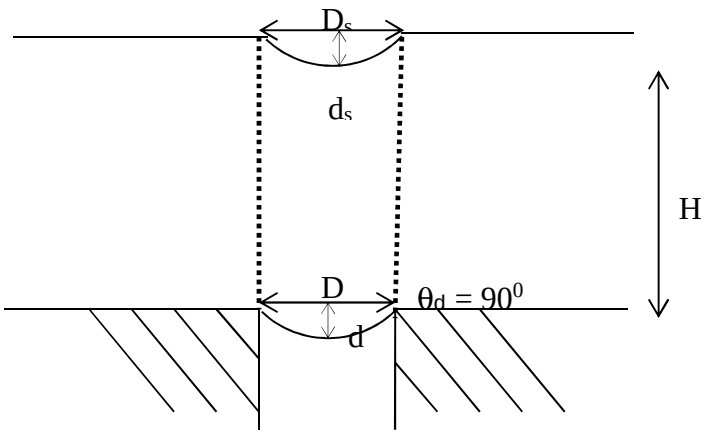

Figure 2.6: Soil movement in the event of a subgrade void as assumed by RAFAEL

i. Load (P) in geogrid layer:

The RAFAEL methodology assumes that the area of movement is limited to the cylinder of soil directly above the void alone. The soil is assumed to be cohesion less. The load acting on the geosynthetic reinforcement was derived by the RAFAEL team and was assumed to be vertical and uniformly distributed and is shown in the equation below (derived from Steinman's equation for stress in the geotextile:

$$\rho = \frac{\gamma D}{4Ktan\varphi}\left[1 - e^{\frac{-4KHtan\varphi}{D}}\right] + w_s e^{\frac{-4KHtan\varphi}{D}}$$

γ = unit weight of the fill

K = coefficient of lateral earth pressure

φ = angle of internal shearing resistance of the fill

w_s = surcharge intensity on top of the fill layer

ii. Maximum strain in geogrid:

The shape of the geosynthetic is assumed to be parabolic, as it is in the SANS 207. The expression for maximum strain from Steinman (1957) is used:

$$\varepsilon_{max} = \frac{8d^2}{3D^2}$$

ε_{max} = Maximum strain that can developed in the geogrid before ULS

iii. Tensile force

The maximum tensile force that can be sustained by the geosynthetic was derived by RAFAEL and is shown in the equation below:

$$T_{max} = \frac{\rho D}{2}\sqrt{1 + \frac{1}{6\varepsilon_{max}}}$$

T_{max} = The maximum tension the geogrid can develop before ULS

iv. Soil surface settlement:

RAFAEL assumes that as the soil is undergoing de-compaction when the void forms, it dilates. RAFAEL then assumes that "the volume of the settlement trough and the displaced volume at geosynthetic level are paraboloids of revolution." Potts (2007). This leads to the derivation of the following relationship:

$$d_s = d - 2H(C_e - 1)$$

Where d is the deflection in the geogrid layer.

C_e is the ratio of the dilated soil volume to the initial soil volume before de-compaction.

Villard et al. (2000) provided the following equation for C_e:

$$C_e = \frac{V_{se}}{V_s}$$

Where V_{se} = the de-compacted soil volume (m^3)

V_s = soil volume prior to de-compaction (m^3)

Analytical calculations will be performed using both the SANS 207 and the RAFAEL design method and will be compared to the laboratory and FEM model.

2.8.3 Girouds layer thickness analysis

Giroud's method is a limiting equilibrium method where the deflected shape of the geosynthetic is approximated as a circular arch (Giroud, et al., 1990). This method takes into account the tension membrane action of the geotextile and the effect of soil arching on the shear strength of the soil.

This method however does not take into account the shear stresses at the soil-geotextile interface. Apart from assuming a circular shape for the geotextile, the strain within the geotextile is regarded as uniform.

This particular method of analysis is only applicable for basal reinforcement systems. Wang et al (1996) proposes a modification to Giroud's design that will allow for the design of multi-layered geosynthetic reinforcement. As with Giroud's method, this modification does not take into account the soil- geosynthetic interface shear stresses and it neglects the presence of interlayer soil.

In Giroud's method the strain within the geotextile is calculated using the following equation:

$$\varepsilon = 2\Omega sin^{-1}\left\{\frac{1}{2}\Omega\right\} - 1$$

$$\Omega = \frac{1}{4}\left[\frac{2d}{D} + \frac{D}{2d}\right]$$

Where $D/d \leq 0.5$

Where D = diameter of sub grade void

d = the deflection of the geosynthetic

This is an adaptation of the tensioned membrane theory (the loading force was regarded as perpendicular to the geotextile, the geotextile deforms in a circular arch).

In order to calculate the tension value that the geosynthetic is required to support the following equation is used:

$T = \sigma_v' D\Omega$

Where σ_v' can be represented as the weight/m^2 of the soil fill and the surface loads (if any), or σ_v' takes into account soil arching and uses the following equation:

$\sigma_v' = \frac{\gamma D}{K\ tan\phi'}\left[1 - e^{Ktan\phi'\frac{-z}{d}}\right] + qe^{Ktan\phi'\frac{-z}{d}}$ Terzaghi (1943)

More accurate results will be obtained by using the equation above because the decrease in tension on the geosynthetic due to soil arching is taken into account. The soil arching equation depends mainly on the computation of the earth pressure coefficient *K*.

$K = 1.06(cos^2\theta + K_a\ sin^2\theta)$

Where:

$K_a = tan^2(45^0 - \frac{\phi'}{2})$

$\theta = 45^0 + \frac{\phi'}{2}$

Giroud et al. (1990) proposes that Jakys equation for the coefficient of earth pressure at rest is also applicable.

$K = 1 - sin\phi'$

When z = the overburden height, then the vertical stress equation can be modified to:

$\sigma_v' = 2\gamma D\left[1 - e^{\frac{-z}{2D}}\right] + qe^{\frac{z}{2D}}$

Where K and θ are not taken into account.

2.8.4 Multi-layer method:

In this method the decrease in net downward vertical pressure is taken into account in each preceding layer due to the occurrence of soil arching. Soil arching results in a redistribution of forces, resulting in an increase in horizontal stress in the soil mass and a subsequent decrease in vertical stress.

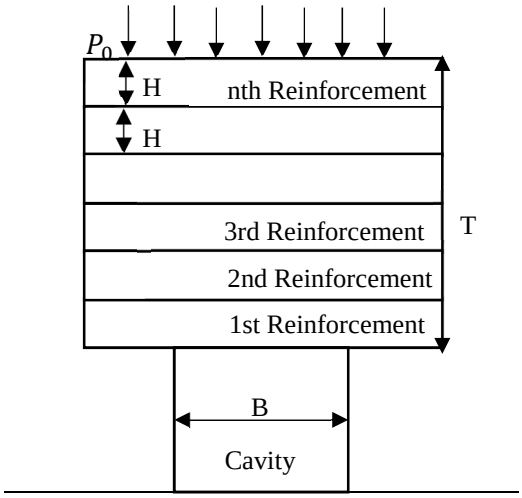

Figure 2.7 Multi-layered geosynthetic reinforcement (Wang, et al., 1996).

Figure 2.7 above illustrates the use of multi-layered geosynthetic reinforcement when subjected to pressure loading. The proposed multi-layered method shows the change in tension in the geotextile with depth, i.e. the forces will decrease lower down in the fill, the equilibrium equations account for this. (Wang, et al., 1996)

The multilayer method takes into account the pressure force P (loading force), the upward reaction force (R) and the self-weight.

The force interactions in the system are illustrated as follows:

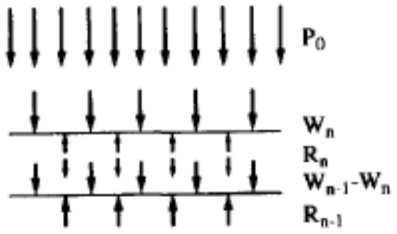

Figure 2.8: Multi-layered reinforcement distribution of forces (Wang, et al., 1996)

For the uppermost layer, the tension in the geotextile can be analytically calculated using the following equation:

$$p_0 + W_n - R_n = \frac{t_n}{[B_n f_n(y)]}$$

The tension in the preceding layers is described using the following equation:

$$R_n + (W_{n-1} - W_n) - R_{n-1} = \frac{t_{n-1}}{[B_{n-1} f_{n-1}(y)]}$$

(Wang, et al., 1996)

p_o = Uniform surface pressure

W_{n-1} - W_n = downward pressure due to weight at the lst-nth geosynthetic layer with a consideration of soil arching effect

R_n = The upward reaction force on the geotextile (From the 1st layer to the nth layer)

T_n = The tensile force per unit width of the geotextile

B_n = Horizontal distance of deflected geotextile (From the 1st layer to the nth layer)

f_n = Dimensionless vertical displacement function

The British design guide has little information on the use of multi-layered geosynthetic reinforcement, stating that "The analysis of this technique is complex and is not covered further in this code", (British Code BS 8006, 1995).

2.9 Case Studies

2.9.1 Case Study: Geosynthetic reinforced railway embankments: Design concepts and experimental tests results. (Montanelli & Recalcati, n.d.).

In this case study the use of geosynthetic reinforcement in minimizing the vertical deflections and the horizontal strains was investigated. Design guides cover the use of basal geosynthetic reinforcement to some detail, the optimal positioning of the reinforcement however is still to be determined. The aim of the study was thus to analyse the performance of geosynthetic reinforcement installed at different locations in a track structure specifically.

The track components function was to convert the wheel load into a relatively even load on the subgrade. Previous investigations performed by Montanelli & Recalcati (n.d) had yielded a positive result when geosynthetic layers are placed at the base of railway embankments, within the fill layers and at the sub ballast level.

Geotextiles provided the following benefits in the railway embankment:

- The geotextile creates a stiff platform where horizontal strains and the settlements are controlled and minimized in the overlying materials and the geotextile undergoes deformation.
- Increase the bearing capacity of the formation, thus minimizing formation stresses
- Increasing the soil fill stiffness and apparent long term cohesion under dynamic loading.
- Provides reinforcement, separation and a soil filter.

Due to uneven formation deflection, the wear on the rail itself will be increased and non-uniform, resulting in the design life of the rail being compromised. In order to prevent the uneven wear and subsequent track problems, the upper formation layers must be reinforced. In normal track applications, measures like increasing the depth of the sub ballast/ballast layer can be employed in order to improve subgrade strength. This is an expensive technique in that re-constructing the sub-ballast layer is time consuming and may result in closure of the rail line during construction. These delays may result in loss of tonnages and inefficiency of the line. The case study investigated the use of geosynthetic fabrics in strengthening the upper SSB formation layers. The use of the reinforcement allows a decrease in the depth of the excavated soil without compromising the strength of the upper layers.

The case study presents a rehabilitation technique for the Foligno-Terontola line in Italy, the embankment that the line was founded on is almost a century old, and was undergoing settlement due to the repeated loading and the silty sub-grade. The design solution involved the use of a TENAX geosynthetic-geotextile composite within the sub-ballast layer at a depth of 0.3m and the replacement of the first 0.7m of silty subgrade with free-draining granular fill. The geosynthetic-geogrid composite had a tensile modulus of 30kN/m. The rehabilitation took place at night to ensure the traffic on the line would not be disturbed, the upper and lower geotextile surfaces were instrumented with strain gauges for data capturing. The deflection settlement of the line showed an improvement with the inclusion of the geosynthetic reinforcement and the strains measured at geosynthetic level were deemed to be sufficiently low by the authors. The figure below illustrates the reinforcement placed in the rail lines subgrade.

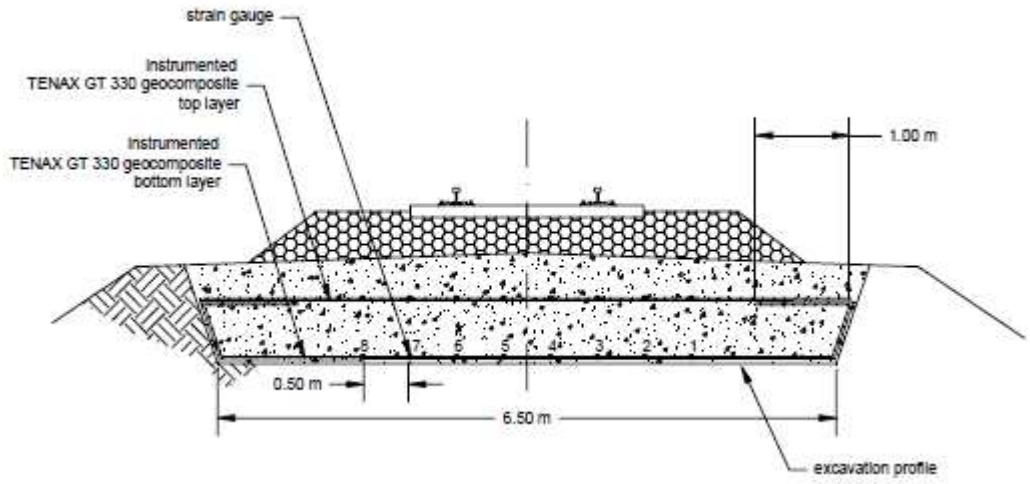

Figure 2.9: Railway earthworks cross section (Montanelli & Recalcati, n.d.)

The case study then considered a comparison between a single and multi-layered geosynthetically reinforced embankment. A full scale laboratory model was developed in which the vertical train load was applied by means of a dynamic actuator. A single and multi-layered instrumented geosynthetic system was constructed under the 13m section railway line. The TENAX geosynthetic range was again used, with a tensile strength of 30kN/m. Comparison between the unreinforced model, the single geosynthetic layer and 2 reinforcement layers showed a 20 - 40% and a 30 – 60% reduction in dynamic load respectively at a depth of 0.9m.

The study concluded that the following factors affected the efficiency of the geosynthetic design:

- Type of reinforcement used
- Number of layers of reinforcement
- Spacing between reinforcement
- Distance between the ballast and first layer of reinforcement
- Type and placement of the fill layer

From the investigation it was concluded that the use of geosynthetic reinforcement improves the bearing capacity of the soil and decreases the settlements. Geosynthetics also decrease the formation/excavation depth required in railway lines, studies performed by Kae (2003) similar conclusions were drawn that geosynthetics decrease the required depth of formation excavation.

2.9.2 Case Study: The use of geosynthetics as reinforcement in formation layers (Kae, 2003)

2.9.2.1 Investigation overview:

Investigations into the quality of geocells, geotextiles and geogrid products took place at Transnet's track testing centre. The aim of the investigation was to determine the influence that difference geosynthetic products had on the stress state of a track formation. The reinforcement was placed at a depth of 200mm below the pavement/ballast layer. The investigation will determine whether the stiffening effect that the reinforcement provided to the upper formation would allow a reduction in the number of formation layers required as well as a reduction in the formation layer depth.

2.9.2.2 Laboratory testing:

A 2.4 x 2.4m steel box was filled with earthworks, the earthwork layers were constructed to Transets S410 specification (Specification for railway earthworks) and compacted. Pressure transducers P1 – P6 were placed at various depths in the soil.

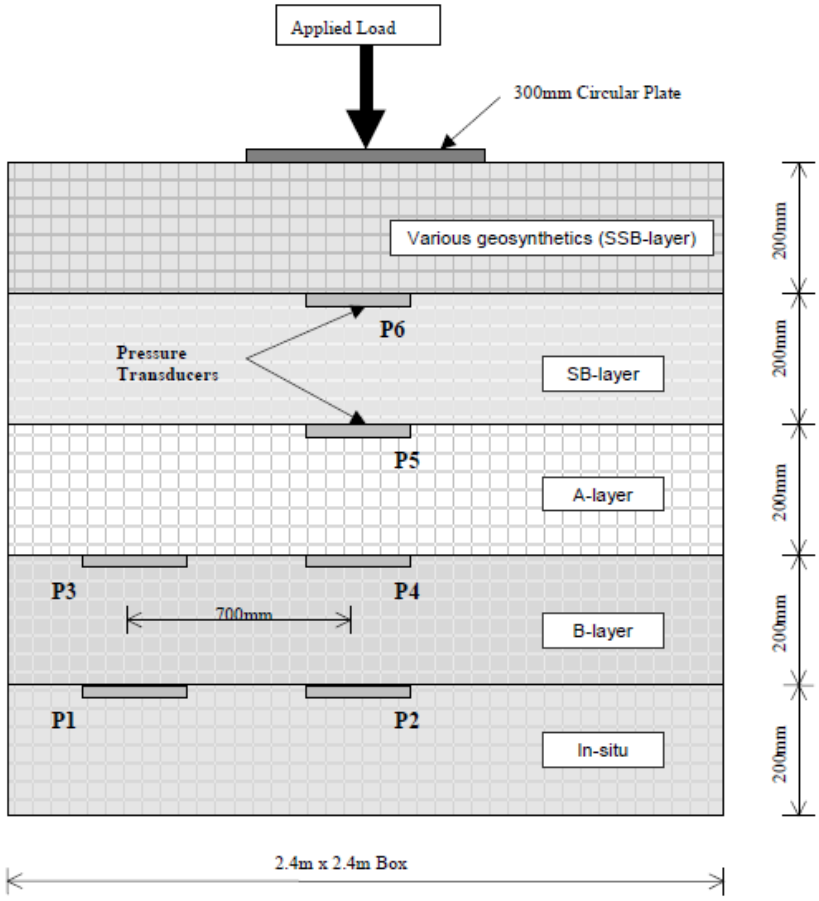

Figure 2.10: Experimental model cross section (Kae, 2003)

Figure 2.10 above shows the various layer work depths as well as the placement of the pressure transducers and loading conditions.

Table 2.1 shows the properties of the layer works as well as the degree of compaction. All layers complied with the limits as set out in Transnet's S410.

Table 2.1 Earthwork properties (Transnet Limited S410, 1990)

Layer	Minimum Grading Modulus	PI	%<0.075	CBR	Minimum Compaction % Modified AASHTO Density
SSB	2.18	SP	14	98	96
SB	2.12	10	18	30.8	95
A	2.12	10	18	30.8	95
B	1.73	11	16	-	93
In-situ	1.73	11	16	-	90

The various geosynthetic products are placed at a depth of 200mm, a 14kN load was applied to the formation using a 300mm diameter actuator plate as shown in Figure 2.11 below:

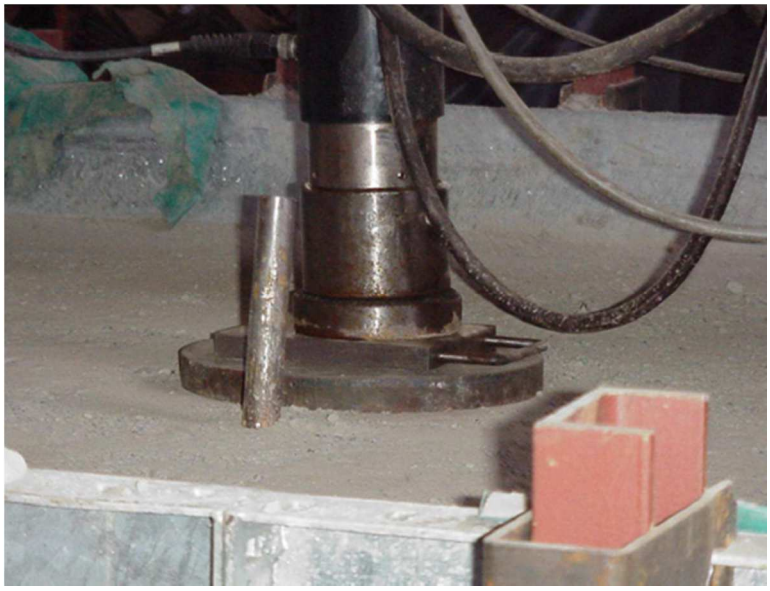

Figure 2.11 Actuator with steel plate for the application of loading

The geosynthetic products used during the investigation and their properties are shown in Table 2.2 below:

Table 2.2 Range of geosynthetic products and properties considered during investigation by Kae (2003).

GEOSYNTHETIC PRODUCT NAME							
Property	***Units***	***Multicell***	***Ecocell***	***Geoweb (textured)***	***Geoweb (perforated)***	***Greencell***	***Test Method***
DIMENSIONS							
Weld Spacing	mm	-	330	-	-	-	-
Cell Dimensions	mm	-	245 * 205 (max.)	244 * 203 (max.)	244 * 203 (max.)	244 * 203 (max.)	-
Cell Depth	mm	150	150	152	152	150	-
POLYMER PROPERTIES							
Polymer Type	-	Polypro-pylene, PVC laminate coating	HDPE	Polyethylene (1.5% C. black)	Polypropylene polyethylene coated	Polypropy-lene, polyethy-lene coated	-
Density	g/cm^3	-	0.945 – 0.96	0.935 – 0.96	0.935 – 0.96	0.935 – 0.96	ASTM D 792
Sheet Thickness	mm	-	1.2	1.25	1.25	-	ASTM D 3767
STRENGTH							
Seam Strength	N/100 mm	-	1600	1420	1420	1420	AS 3706.2

GEOSYNTHETIC PRODUCT NAME							
Property	***Units***		***Polytex (PT715)***	***Polyforce (PE4530/200)***	***Geomesh (BSP262)***	***Tensar (SS30)***	***Test Method***
DIMENSIONS							
Mass	g/m^2		310	400	190	300	-
Roll Length	m		200	Av. on request	100	30	-
Roll Width	m		5	Av. on request	1.6	4	-
POLYMER PROPERTIES							
Polymer Type	-		Polypropy-lene	100% Polyester	Polyester PVC Coated	Polypropy-lene	-
Sheet Thickness	mm		1.3	2.5	0.45	2.2	ASTM D 3767
STRENGTH							
Tensile Strength	KN/m	Warp	50	45	35	30	SABS 0221-88
	KN/m	Weft	55	30	35	30	

The pressure at various depths was measured and recorded using the pressure transducers. The theoretical pressure at each depth is calculated using Boussinesq's equation:

$\delta_z = q(A + B)$

Where, δ_z = Pressure at a depth z

q = Surcharge loading

A&B = Partial influence factors

The results obtained after all geosynthetic products were tested showed the soil pressure decreased from the reference value of 77kPa to a minimum of 35kPa at a depth of 200mm.

Table 2.3: Soil pressure at various depths in the fill layer

Products	Depth (mm)			
	200	400	600	800
Boussinesq equation	73	32	13	8
G4 (reference product)	77	31	12	6
Geotextiles				
Geotextile_1	99	31	6	2
Geotextile_2	38	12	2	0
Geotextile_3	60	15	2	0
Geogrids				
Geogrid	35	20	4	0
Geocells				
Geocell_1	76	26	0	0
Geocell_2	83	42	13	3
Geocell_3	120	47	8	5
Geocell_4	85	30	0	0
Geocell_5	58	29	9	3
Geocell_6	58	29	2	0
Geocell_7	51	14	1	0

From the laboratory experiment it was concluded that geosynthetic products have the ability to reduce pressure in the formation level at different depths. Certain products reduce the pressure better at a higher level (200mm depth) while other products successfully reduce the pressure with depth.

2.9.2.3 Finite element analysis:

A formation model was developed using the Strand 7 finite element analysis program in order to model the stiffening effect that geosynthetic products have on the formation layers. A linear axisymmetric analysis was used, the Young's modulus in the initial 200mm layer was varied in

the program to simulate the increased stiffness in the soil due to the inclusion of the geosynthetic product.

The Young's modulus was varied until the pressure measurement in the subsequent soil layers matched the pressure measurement in the laboratory experiment in order to give an indication of the increase in stiffness that the geosynthetic product has on the formation layer.

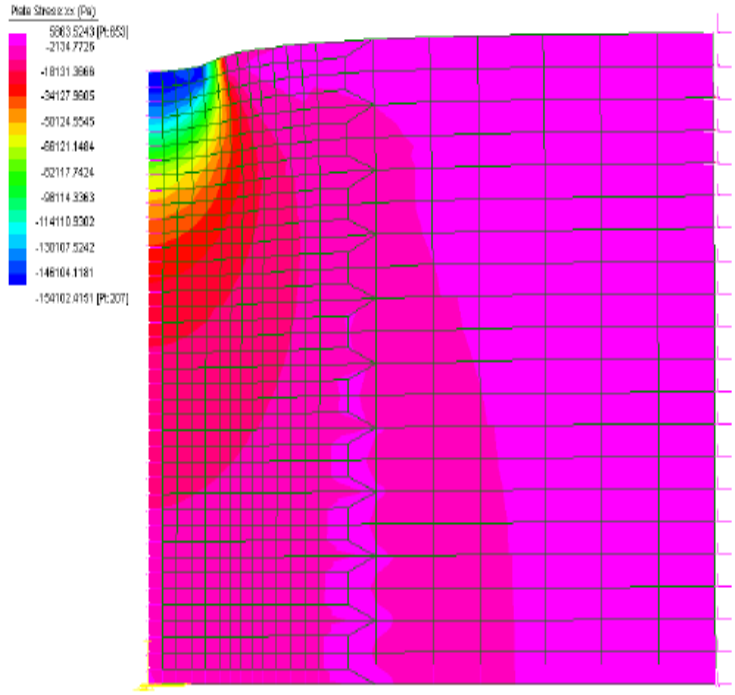

Figure 2.12: Strand 7 plate stress contours

The soil characteristics used in the formation layers were in accordance to Transnet's S410 specification. The soil was modelled as 2D plate elements, symmetrical about the y-axis, with an increased mesh density in the vicinity of the load application.

The soil stress and deformation were observed at various depths and compared with the laboratory results.

The soil pressure generated by the FEM program at various depths were compared to the laboratory model and the results were accurate and within the range of the experimental model.

Table 2.4: Strand 7 FEA predictions vs measured data

Depth	FEA (kPa)	Measured Pressure (kPa)
200	57.2	58.2
400	22.5	29.4
600	12.8	9.08
800	9.7	2.9

2.9.2.4 Case study conclusions:

From the laboratory experiment it was observed that geosynthetic products are capable of decreasing the applied pressure along the entire depth of the formation layers. Certain geosynthetic products provided better pressure reduction in the upper formation layers while other products provided a more significant pressure decrease at a depth in the fill.

The Tensar (SS30) and Polytex (PT715) range exhibited the largest overall reduction in pressure in the soil layers of approximately 50%. The geotextile, Polyforce (PE4530), geocells, Geoweb and Greencell produced a 22- 34 % reduction in pressure in the upper 200mm. The Geomesh (BSP 262) and multicell product did not produce a large reduction in pressure within the upper 200mm, but rather decreased the pressure more significantly at a depth of 400mm. The Ecocell products however did not provide a significant pressure decrease at any level in the fill.

It was thus concluded that use of geosynthetic products in the formation layers increased the bearing resistance of the formation and helped reduce the required formation depth and subsequently decreased excavation costs. The FEM analysis proved that the Strand 7 Finite element analysis software can be used to model a geosynthetically reinforced fill layer.

The pressure values obtained from the FEM and laboratory model were within the same range when the stiffness in the upper 200mm was increased by 30%. This indicates that the geosynthetic product increases the formation stiffness by up to 30%.

2.9.3 Case Study: FEM analysis and dimensioning of a sinkhole overbridging system for high speed trains at Groebers in Germany: (Alexiew, et al., 2002).

The case study identified that the design guides and analytical procedures currently present were inaccurate and only applicable under certain circumstances. Due to this numerical procedures were employed in order to investigate the behaviour of a cement stabilised railway bed with a layer of geosynthetic reinforcement present on the LeipZig-Halle line. The high-speed rail link LeipZig-Halle travels at up to 300km/h, facilitating the transport of both passengers and heavy cargo. The 800m long and 120m wide railway section was constructed over a post-mining area in the Groebers region of Germany. The whole area was prone to subsidence with sinkhole diameters of less than 4m occurring. The collapse in the area was

attributed to “sub-ground excavations” in karstic regions. In order to reinforce the soil embankment against collapse various methods were considered (e.g. deep foundation on piles, stiff reinforced concrete plate, and dynamic compaction after deep excavation). The methods generally employed in this region are spanning the void with concrete slabs or backfilling. These methods of reinforcement were not sufficiently cost-effective, due to the vast area that the rail-line covers. Geosynthetic reinforcement was a more economical method and was used for the project. High strength basal reinforcement was used extensively in Great Britain for the similar purpose of bridging voids. The design was based on two fundamental concepts, ensuring serviceability for a given period of time after a void forms and a sinkhole detection warning system. In the event of a sinkhole taking place, the speed of the trains of the line were limited until the void can be filled and the fill rehabilitated so that the stability of the line will not be compromised.

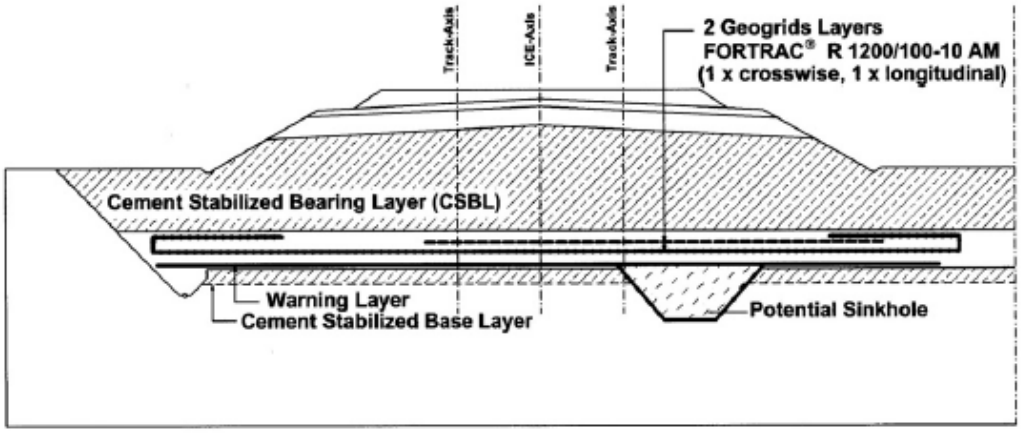

Figure 2.13 Cross section of the embankment including the stabilized layer, the placement of the geosynthetic reinforcement and sinkhole detection system.

Figure 2.13 above shows the embankment considered, with the basal reinforcement placed above the potential sinkhole

2.9.3.1 Soil reinforcement:

The investigation used a combination of cemented soils, high strength geosynthetic reinforcement and a warning system. A cement stabilized bearing layer made from cohesive soil, a mixture of cement and soil and a thin layer of gravel was used above the geosynthetic

reinforcement layer. An electronic warning system was integrated into the geosynthetic reinforcement; this consisted of insulated and embedded wires. Rupture of the geosynthetic results in a change in the electrical resistance of the wires. The systems design life spans 60 years, with a serviceability limit of a month to rehabilitate the fill after the void forms.

The specialized method developed within the project is the use of the CSBL (Cement stabilized bearing layer). When collapse occurs, a stable arch must form in the CSBL layer to ensure serviceability until permanent reinforcement can be placed. In order to ensure serviceability, the train speed was decreased from 300km/h to 100km/h (and the sinkhole must then be backfilled).

The design limitations identified were as follows:

- Due to the high speed of the trains on the line, the specified serviceability life of 30 days was too high
- Analytical methods provide a guide for design when non-cohesive soils are present, even then the guides are not sufficiently accurate. No guidance at all exists for a bridging system designed in cohesive soils
- The position of the sinkhole cannot be predefined in this 120m wide track (spans about 8 tracks)

Subsequent to these limitations, the design cannot be performed without a numerical analysis, the FEM technique.

2.9.3.2 Experimental procedure:

The two design conditions considered were:

a) Low coverage, where the overburden height of soil was small hence the geosynthetic deflection was equal to the soil surface deflection.
b) In the second case the maximum allowable tension of the geotextile was reached.

The analysis of the design factors, stress, strain, deflections, arching in the cement stabilised layer and the diameter of the resulting surface depression were all estimated by a combination of the finite element method and analytical methods. The design calculations for the ultimate

and serviceability deflection level of the geotextile was performed using the German codes for geotechnical structures.

2.9.3.3 Finite element method:

FEM was performed on the PLAXIS software, the FEM process was found to be inefficient in the post-failure analysis. In order to gain a better understanding of post-failure stress and strains, analytical procedures were used. The model used was a linear elastic perfect-plastic Mohr-Coulomb model.

The finite element method was performed successfully but it was found that the FEM-calculations would be insufficient for the complexity of the problem. This problem was also experienced in Jaros et al. (2009) and Munian (2010) where soil collapse caused convergence problems within the finite element model.

2.9.3.4 Geosynthetic:

The analysis of the geosynthetic reinforcement was simplified in that it took into account the membrane effect of the reinforcement alone (any occurrence of soil arching was localized to the cement stabilised layer). The membrane effect is generally used when considering geotextiles and only takes into account the vertical loading/surcharge forces and not the upward reaction of the soil. A sufficient cover distance was required in the geotextile so that the pull-out resistance of the soil can be calculated. The geogrid was modelled as a linear elastic liner. The ultimate tensile strength of the geosynthetic was between 1200 – 1400 kN/m with low creep capacity. One of the limitations in the geosynthetic modelling procedure was the post failure analysis of the geosynthetic. The tensile modulus J was measured in kN/m (J =force, kN/m / strain). Alexiew et al. 2002 stated that “theoretically the reinforcement can strain infinitely mobilizing a never ending force and can never fail, which is not correct”. According to Alexiew et al. 2002 this makes it difficult to test the reinforcement to failure, because the tensile force within the reinforcement must be monitored after each simulation to determine whether it exceeds the ultimate tensile strength of the reinforcement.

2.9.3.5 Case study conclusions:

The propagation of the sub-grade void can be successfully modelled using finite element analysis PLAXIS software, until the point where collapse occurs. In order to obtain more

accurate results for the post failure analysis, analytical methods were used. The analytical solution solved for the critical tension in the geotextile. The analysis of the cement stabilised layer is a relatively new concept and arching was expected in the highly cohesive soil block.

2.9.4 Case Study: Stability charts for predicting sinkholes in weakly cemented sand over Karst limestone (Goodings & Abdulla, 2002)

This study was motivated due to the formation of sinkholes in a housing development in Kuwait City. The diameters of the sinkholes were found to vary from 4-8m with a maximum diameter of 15m and a corresponding depth of 3m.

Similarities can be drawn between the soil profiles in the Kuwait area to the South African case. The bedrock consists of karst limestone, overlain with weakly cemented sand and completely uncemented sand. If the ground water (with the dissolved minerals) is pumped above the water table level and then evaporation takes place, the mineral residue is left behind. This sticks together resulting in the partial cementation of the soil.

2.9.4.1 Experimental Procedure:

The experimental models considered in this case study cover the effect of void formation on a weakly cemented fill layer. Two types of experiments were performed, in the first the weakly cemented fill was placed above the void alone. In the second set of testing a weakly cemented fill layer was overlain with uncemented material (Ottawa sand was used for both the cemented and uncemented soil), and a void was formed beneath the cemented layer. The degree of cementation was varied in the weakly cemented layer between 2 – 4% Portland cement. All models were tested in a centrifuge and brought to failure under self-weight.

2.9.4.2 Case study conclusions:

The various failure shapes the cemented material underwent is shown in Figure 2.14 below:

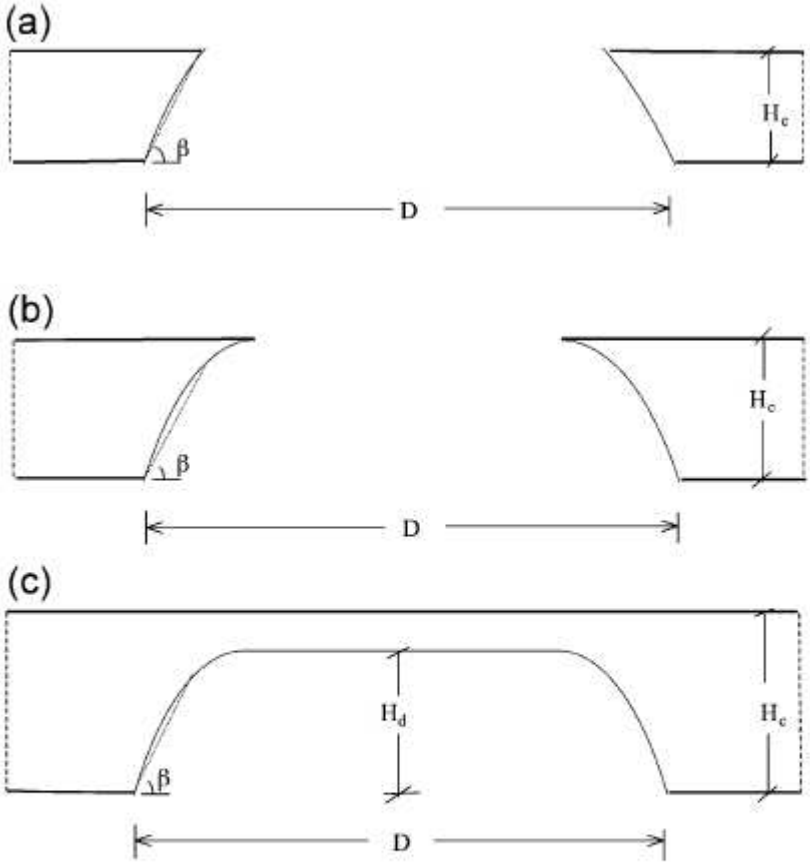

Fig. 1. (a) Shape of failure in the cemented sand layer for $H_c/D<0.25$. (b) Shape of failure in the cemented sand layer for $H_c/D=0.25$. (c) Shape of failure in the cemented sand layer for $H_c/D>0.31$.

Figure 2.14 a) Shape of failure in the cemented sand layer for Hc/D < 0.25

b) Shape of failure in the cemented sand layer for Hc/D = 0.25

c) Shape of failure in the cemented sand layer for Hc/D > 0.31

(Goodings & Abdulla, 2002)

It was found that for lower Hc/D < 0.25 ratios, the soil "plug" that falls out from the cemented layer during sinkhole formation tended to propagate to the top of the layer.

When Hc/D = 0.25, a similar result was obtained, with a smaller plug collapsing.

When Hc/D > 0.31 however, the collapsing soil plug does not propagate to the surface of the cement layer. The layer forms an arch where the surface of the model is not affected by the void. A similar condition was found in the case study 1, for the German link rail LeipZig-Halle, where some of the load transfer was taken up by the formation

of a stable arch within the cemented sand. The ratio of the overburden height to the diameter of the sinkhole are similar to those found in Terzaghi's experiment in 1943.

The following factors were found to affect the critical failure of the soil mass:

a) The unit weight of the cemented sand
b) The overburden height of the soil
c) The diameter of the void in the underlying karstic rock

By combining the method of cement stabilization and geosynthetic reinforcement, a more economic and equally stable solution was obtained.

2.9.5 Case study: Potts (2007)

The Potts (2007) investigation considered a vast range of geosynthetic design scenarios and applications. For the purpose of the case study, only Potts laboratory model and the FEM validation of it was considered. The experimental model consisted of a basally reinforced soil layer, which was undermined by a subgrade void of varying dimensions. Potts (2007) thus developed an FEM model describing the experimental test and compared both sets of results.

Potts (2007) case study considered the use of basal geosynthetic reinforcement alone with variations in the H/D ratio (H = fill height, D = void diameter). The de Lange (2016) laboratory model (covered in Chapter 3) differed from the Potts (2007) model in that it considered multi-layered reinforcement in addition to basal reinforcement as well as a variation in the H/D ratio.

The case study provided both experimental and numerical data which was used for comparative purposes. The sets of data and design scenarios considered are shown in Table 2.5 below.

Table 2.5: Summary of results from Potts (2007) case study

Potts (2007) Case study data	
Experimental results	**Numerical results (ICFEP)**
Unreinforced model	Reinforced model
Reinforced model	H/D = 1
	H/D = 0.5
	H/D = 3

H* = Soil height (mm)

D* = Void diameter (mm)

2.9.5.1 Model overview

The model was developed using a strongbox with a moveable platform that allowed the void to form at the base of the box. The soil was loosely poured into the strongbox using a hose and a funnel. LVDT's were placed along the soil surface in order to measure the soil surface deflections resulting from the void formation.

It should be noted that the experimental model employed by Potts (2007) did not take place in a geotechnical centrifuge. Potts (2007) states that when future laboratory experiments are performed, the use of a centrifuge will be considered.

2.9.5.2 Model geometry

The height of soil considered in the laboratory tests varied from 40, 80, 160, 240, 320, 400mm. The void diameter values were 80, 160mm. The moveable platform was positioned at the base of the structure and moved downward a distance of 25mm. This allowed the polythene layer to support the soil resulting in subsequent soil surface deflections.

2.9.5.3 Material characteristics:

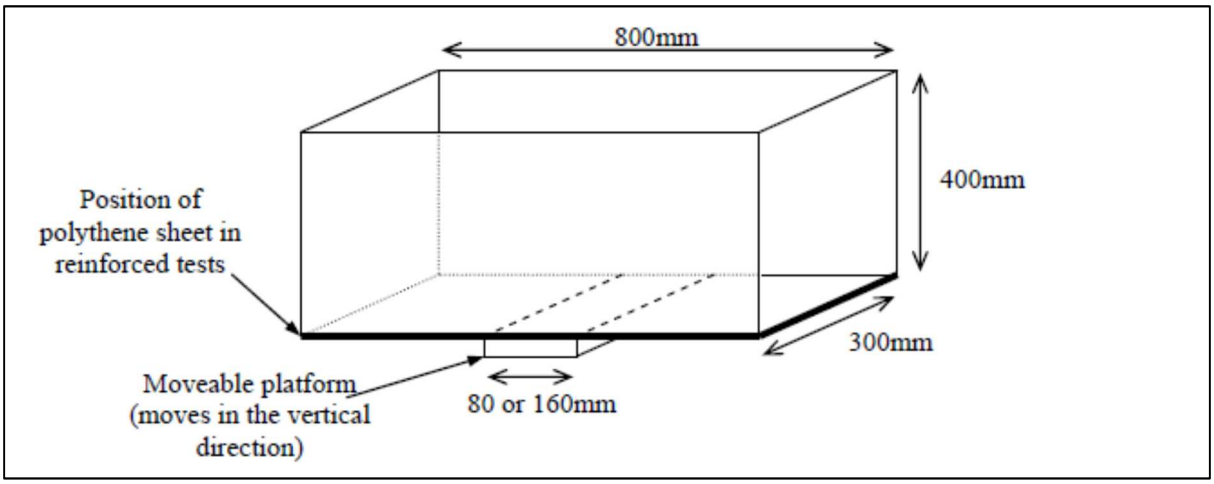

Figure 2.15: Experimental model geometry (Potts, 2007)

The soil fill layer used in Potts (2007) was fine gravel with some medium coarse sand. The soil density and angle of shearing resistance were tested and are shown in Table 2.6 below. A continuous polythene sheet was used as a geotextile layer.

Table 2.6: Material properties used in Potts (2007) experimental model

Material	Parameter	Recommended value
Fill	γ_{loose}	15.5 kN/m^3
	$\phi'_{fill\ loose}$	35^0
	E	20 MPa
	μ	0.3
	K	0.4285
	e	0.2
Polythene sheet	J	11 kN/m/m
	T_{ult}	0.11 kN
	μ	0.2

2.9.5.4 Results:

Section 2.9.5.5 covers the results obtained by Potts (2007) when the soil mass was unreinforced. In section 2.9.5.7 a comparison between the unreinforced and reinforced results took place. The subsection concludes with 2.9.5.8 in which Potts (2007) FEA results are compared to experimental data.

2.9.5.5 Soil surface deflections: Unreinforced model

Figure 2.16 below shows the soil surface deflections for varying soil heights when the void diameter = 80mm in an unreinforced soil mass. The graph shows the soil surface deflections decrease with increasing soil height, the results for the maximum soil surface deflections for the varying soil heights are shown in Table 2.7.

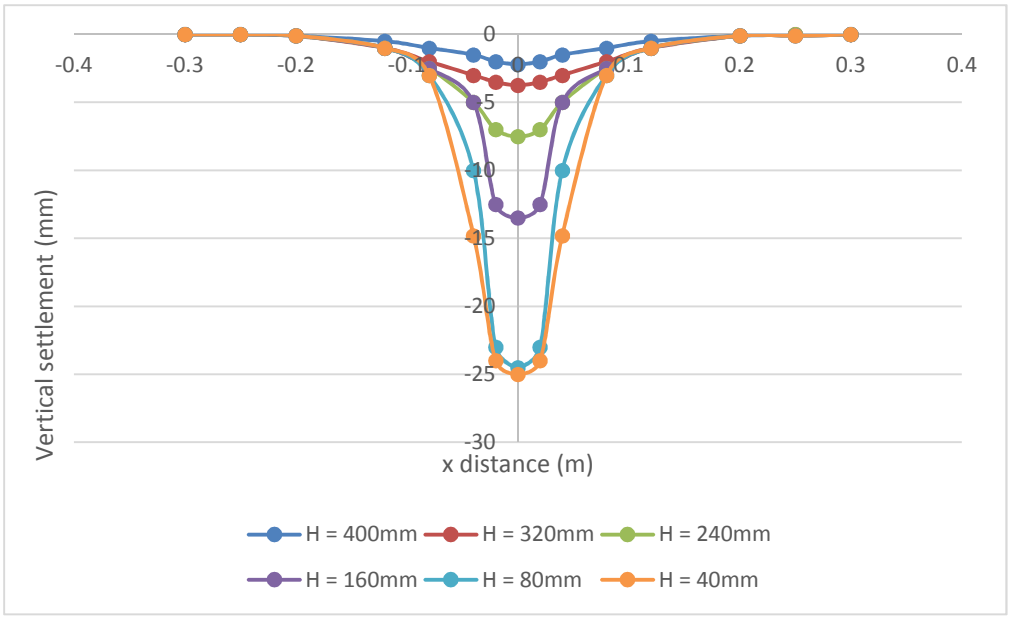

Figure 2.16: Vertical soil surface deflections obtained from the unreinforced laboratory experiment performed in Potts (2007), soil fill height (H) is varied while void width (D) is constant at 80mm

A summary of the maximum surface deflections are shown in Table 2.7 below.

Table 2.7: Maximum soil surface deflection from Potts (2007) unreinforced experimental model

Height of fill, H (mm)	Void width, D (mm)	H/D	Maximum surface deflection, d_s (mm)
400	80	5	2.241
320	80	4	4.043
240	80	3	7.501
160	80	2	13.504
80	80	1	24.501
40	80	0.5	25.012

The soil surface deflection increased as the H/D ratio decreased, as expected due to a smaller volume of soil undergoing a larger displacement. The results presented in Figure 2.16 are for an unreinforced model, the platform was lowered a full 25mm.

2.9.5.6 Diameter of soil settlement trough

Some inaccuracies were observed in measuring the surface settlement trough diameter, the LVDTS were not necessarily placed at the exact position where the trough began.

From Figure 2.16 a slight increase in the trough diameter with an increase in soil fill height was observed. The conclusion made at this stage was that a larger H/D ratio resulted in a shallower wider soil settlement trough.

2.9.5.7 Comparison: Unreinforced vs reinforced

The previous section illustrated the increase in soil surface deflection in an unreinforced soil layer with an increase in the H/D ratio. This also provided an initial reference point for the deflections that took place when no reinforcement was present. In this part of Potts (2007) experimental study, the polythene sheet representing the geosynthetic reinforcement was placed at the base of the model. When the void was created at the base of the model, the polythene sheet retained the soil and subsequently minimised the soil surface defections.

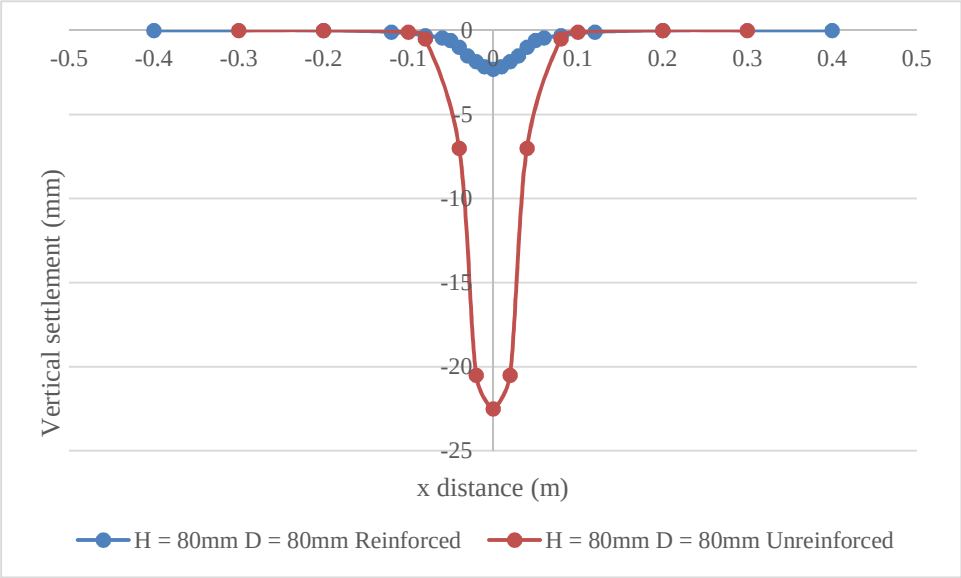

Figure 2.17 Comparison between vertical soil surface deflections obtained from the laboratory experiment performed in Potts (2007) between reinforced and unreinforced fill layers.

The inclusion of the basal polythene layer resulted in a decrease in the soil surface settlement as expected. There was no discernible change in the diameter of the soil settlement trough. This validated the conclusion that the inclusion of geogrid reinforcement does indeed decrease the soil surface settlement.

2.9.5.8 Soil surface deflection: FEM Reinforced

Once it was concluded that the inclusion of the geogrid layer effectively decreased the expected soil surface settlement values, an investigation into the accuracy of FEA as a means of analysis was carried out. The following soil fill heights and diameters were considered:

A) H = 80 mm, D = 80 mm

B) H = 80 mm, D = 160 mm

C) H = 240 mm, D = 80 mm

Conclusions were drawn from a comparison between A & B and A & C as only one parameter was altered, the D and H respectively.

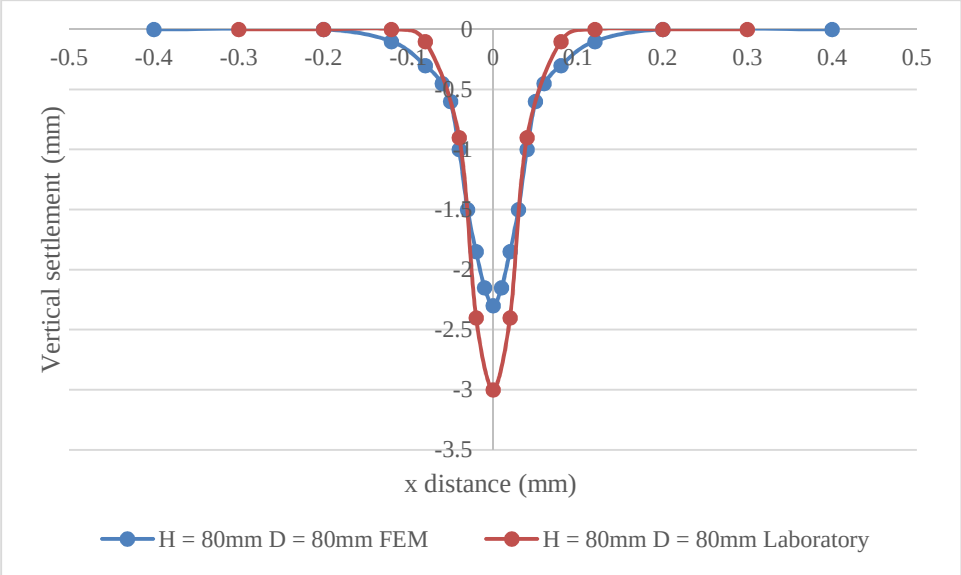

Figure 2.18: Comparison between vertical soil surface deflection values generated by Potts (2007) ICFEP FEA program and the experimental laboratory data

Figure 2.18 above compares experimental data to the FEM model generated by Potts (2007). The FEA deflections are smaller than the actual results obtained for an H/D = 1. Similar results were obtained for H/D = 0.5. Table 2.8 below provides a summary of the maximum soil surface deflections for the various H/D ratios.

Table 2.8: Laboratory vs FEM comparison

H/D	Soil surface deflection laboratory (mm)	Soil surface deflection FEM (mm)
0.5	14.014	10.022
1	2.981	2.314
3	0.651	1.201

In Figure 2.18 the settlement trough predicted by the FEM program was smaller for cases where the H/D was 1 and 1.5; and where H/D = 3 the FEM program over predicts the surface settlement. Potts (2007) concluded that the soil surface settlement predicted using the FEM program ICFEP was not highly accurate but the values were at least in the same order of magnitude as the laboratory results. Potts (2007) also concluded that the FEM model results can be improved by adjusting the material properties of the model.

The loading in the model was from gravity and self-weight of the soil alone. Due to the size of the model, the load applied to the geosynthetic would be too small to generate significant stresses. To get a more accurate representation of the stress-strain behaviour of the soil fill, Potts suggests that further investigation takes place using a centrifuge.

In order to further investigate the effect of a loss of support on a reinforced soil mass, a laboratory experiment was performed by de Lange (2016). In later chapters an FEM model describing the laboratory experiment is developed.

3. CHAPTER 3: PREVIOUS STUDIES

3.1 Rationale

The FEA models have been related to data obtained from laboratory model tests conducted at UKZN by H de Lange (2016) (MSc thesis currently in draft). This chapter describes the development of said physical laboratory models.

3.2 Experimental model: de Lange (2016).

The experimental laboratory work performed by de Lange involved the monitoring of a cohesion less sand fill undermined by a developing void. The model comprised a stack, height H, of sand filled concrete manhole ring standing on horizontal base-board with a concentric circular trapdoor of diameter D. Controlled lowering of the trapdoor simulated the development of a void at the base of the sand. The tests were performed with and without horizontal sheets of mosquito netting embedded in the sand to assess the benefits of reinforcement in controlling subsidence and soil settlements. A series of tests were conducted varying the H/D ratio, and the number of geosynthetic layers. The models used by de Lange were a 1:10 scaled axisymmetric development of the 2-dimensional "proof of concept" field experiment performed by Jaros et al. (2009).

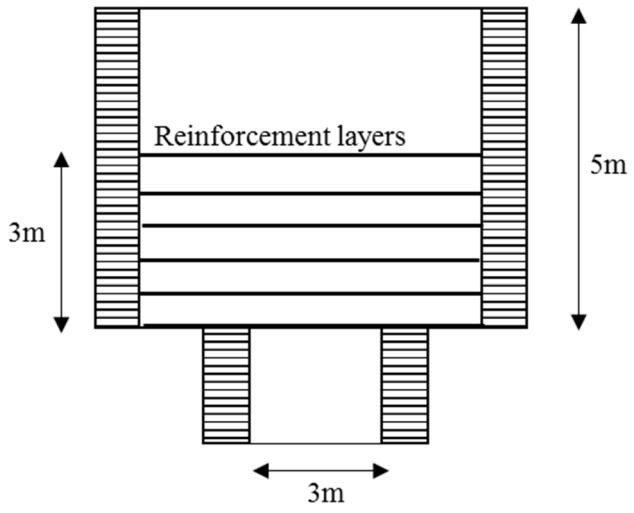

Jaros' model was a $9m^2$, 5m high embankment with a 3m longitudinal void formed beneath its base. The bottom three meters of the embankment were reinforced with horizontal layers of geosynthetic fabric.

Figure 3.1: Schematic of field test performed by Jaros et al. (2009)

3.3 Experimental model setup:

In the initial model tests conducted by de Lange the sand was unreinforced and vertical deflections at the upper surface of the sand were read visually from an array of mechanical dial gauges. For subsequent tests on sand with multiple layers of reinforcement, vertical deflections at the upper surface and at the reinforcement levels within the sand were logged using LVDT transducers.

3.3.1 Unreinforced Model

A sand mass was placed inside the concrete rings over the base board with concentric trapdoor section. The lowering of the trapdoor was controlled by the use of a piston and jack; this allowed a simulation of the loss of support in a controlled manner. The vertical deflections of the sand at the surface as the trapdoor was lowered were then observed using the dial gauges. The laboratory model provided a platform to observe the soil movement patterns and soil surface deflections when support was lost.

3.3.1.1 Test methodology: Unreinforced model

Test apparatus:

- Stacked concrete rings with a 100mm height and 900mm diameter
- Dry uncompacted sand, filled loosely to a 600mm height within the concrete rings
- Dial gauges set at various distances along the sand surface to measure sand deflection
- Piston and jack to represent the trapdoor by which the loss of soil support will be simulated.

Test setup

- The circular rings were stacked on top of one another and used to build a hollow cylindrical concrete structure (See Figure 3.3 below)
- The structure was filled with sand
- Dial gauges were set up at varying distances along the soil surface to measure vertical soil surface displacement.
- A 300mm void was cut into the board at the base of the model, the piston was aligned with the void. The jack was setup such that it lowers the 300mm trapdoor section.

- The soil within the concrete section was allowed to settle by lowering a piston at the base of the concrete structure in increments of 10mm ranging from 10 – 50mm.

In later experiments when reinforcement was present, the laboratory model was refined further. The trapdoor system by which the void was simulated was altered so that the diameter of the void could be changed. This allowed a variation in the H/D ratio of soil height to void diameter.

Figure 3.3: 600mm height unreinforced model de Lange (2016)

Figure 3.2: Placement of dial gauges at soil surface in de Lange (2016) experimental model

Figure 3.3 shows the model setup, the unreinforced model an overburden soil height of 600mm. Dial gauges were positioned as indicated above. The unreinforced model considered a range of overburden heights, 200, 300, 400, 600mm. The results presented below were for an overburden height of 300mm, the void diameter was kept constant at 300mm.

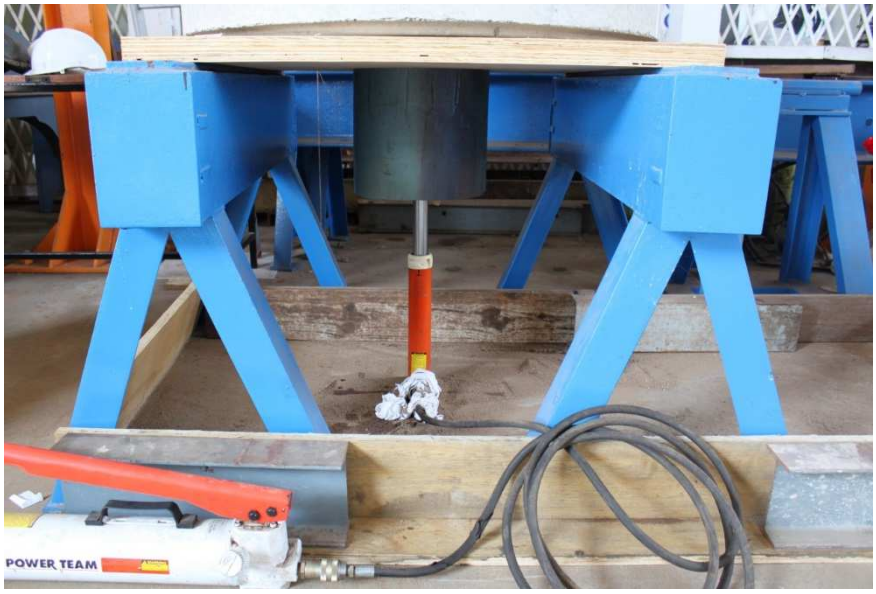

A hydraulic jack was used to lower the piston in increments of 10mm from 10mm – 50mm, in order to observe the soil surface deflections resulting from the loss of support. The soil remained in the 300mm diameter circular piston sheath as the piston was lowered.

Figure 3.4 Hydraulic jack and piston system

The unreinforced model formed a platform to observe the soil movement patterns when support was lost.

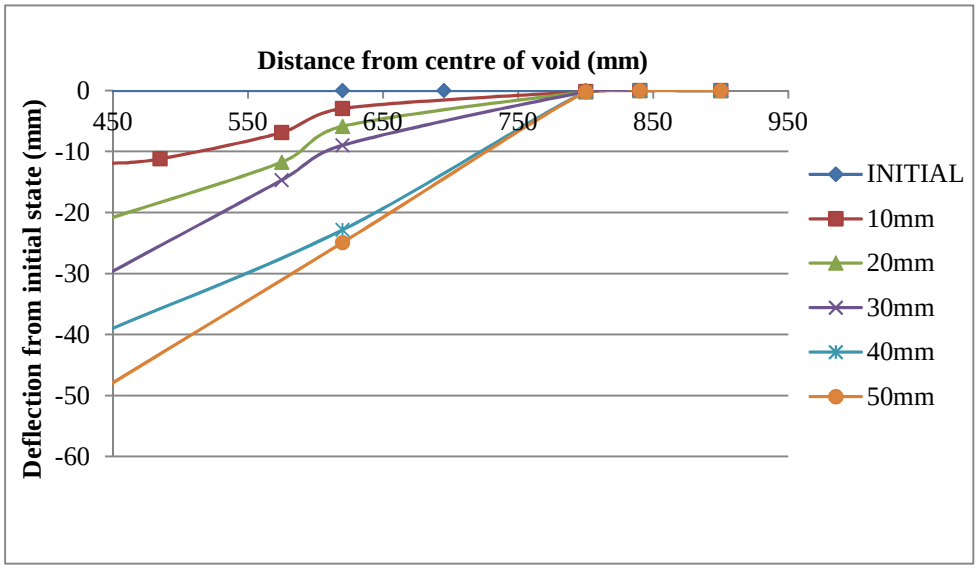

The 10mm increment stated in the legend represented the distance the piston was dropped. The overburden height

Figure 3.5: Surface deflection obtained during the laboratory experiment on an unreinforced soil fill with a fill height of 300mm and a void diameter of 300mm.

considered was 300mm and the void diameter is 300mm, hence H/D = 1. The results from the unreinforced model in terms of the soil surface deflection are presented in Figure 3.5 and are summarised in Table 3.1.

Table 3.1: Summary of soil surface deflection results for an unreinforced soil fill

H/D	Piston drop (mm)	Maximum surface deflection (mm)
1	0	0
	10	11.951
	20	20.904
	30	29.851
	40	39.152
	50	47.951

As the distance the piston drops increased the soil surface deflection increased. To establish that geosynthetic reinforcement had a positive effect in minimising soil surface deflections, a reinforced model with the same overburden height and void diameter was tested. The results obtained from the reinforced and unreinforced model were compared in Figure 3.6 below.

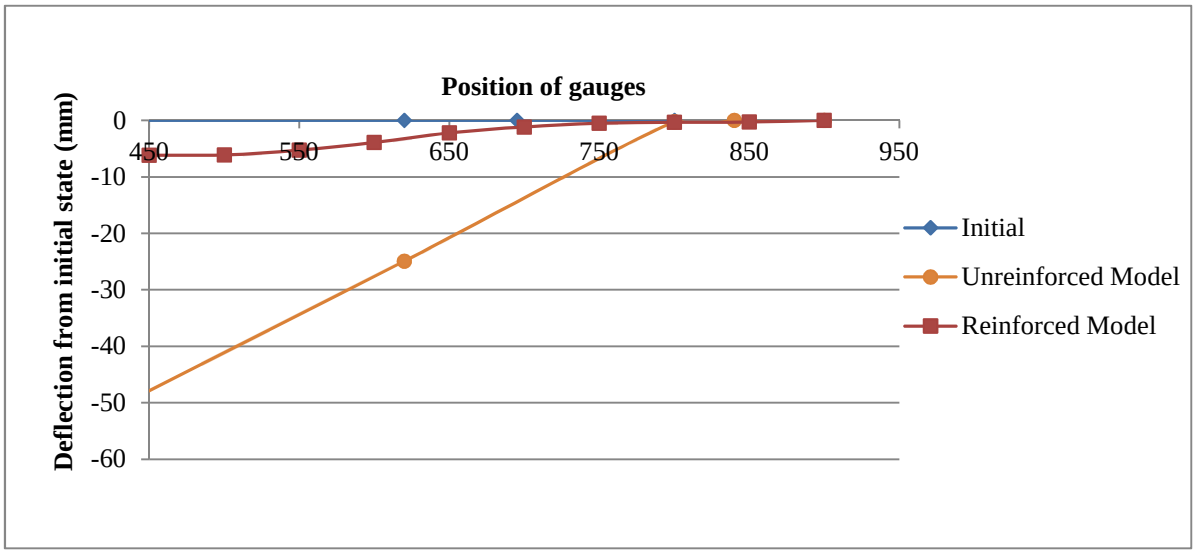

Figure 3.6 Comparison between soil surface deflection results for an unreinforced soil fill mass and a basal reinforced soil mass with a 300mm height and 300mm diameter.

As shown in Figure 3.6, the soil surface deflection decreased when reinforcement was present, indicating that the reinforcement had a positive effect in minimising the soil surface deflections.

3.3.2 Reinforced model

Now that it's been established that geosynthetic reinforcement helps minimise soil surface deflections, tests using basal and multiple layers of geosynthetic reinforcement were undertaken.

3.3.2.1 Rationale

The British code BS8006:1995 and subsequently SANS 207:2006 provided a design approach on the use of basal geosynthetic reinforcement as a means of sinkhole and mining subsidence protection. Investigations into the use of multilayer geogrid reinforcement however have been less frequent and there are no existing design guides on it. The British code states that "The analysis of this technique (Multi-layered geogrid reinforcement) is complex and is not covered further in this code", (British Code BS 8006, 1995). The gap in knowledge identified lead to de Lange (2016) developing the multi-layered model. The objective of the laboratory tests was to relate the soil surface deflection to the height of the soil, the number of geogrid layers used as well as the diameter of the void.

3.3.2.2 Test methodology: Reinforced

Test apparatus:

- 3 x concrete rings with a 100mm height and 900mm diameter
- Dry uncompacted sand, poured loosely to a 300mm height within the concrete rings
- LVDT's were set at various distances along the sand surface and on the reinforcement basal layer to measure displacement.
- Three trapdoor disks with a diameter of 150, 200, 300mm

Test setup

- The circular rings were stacked on top of one another and used to build a hollow cylindrical concrete structure.
- The sand was loosely filled into the rings to a height of 300mm

- A trapdoor disk was present at the base of the concrete ring structure. This trapdoor was gradually lowered in 10mm increments then removed completely in order to simulate a loss of support.
- The diameter of the trapdoor (representative of the sinkhole) was 150, 200, and 300mm.
- LVDT's (linear variable differential transformers) were placed at the sand surface and base in order to measure sand deflections.
- To simulate the geogrid reinforcement a layer of polyester mosquito mesh was placed at the base of the model and at 50mm intervals.
    - The polyester mesh was used instead of a geogrid layer due to the small scale of the experiment. The tensile strength provided by an actual geogrid layer would be too high and result in little to no soil surface deflections.
    - The polyester mesh was fine enough to prevent soil falling through the mesh apertures but coarse enough to allow particle interlock between the soil and the mesh.
    - The anchorage of the mesh layer to the concrete rings is explained further below

Figure 3.7: Reinforced model with LVDTs

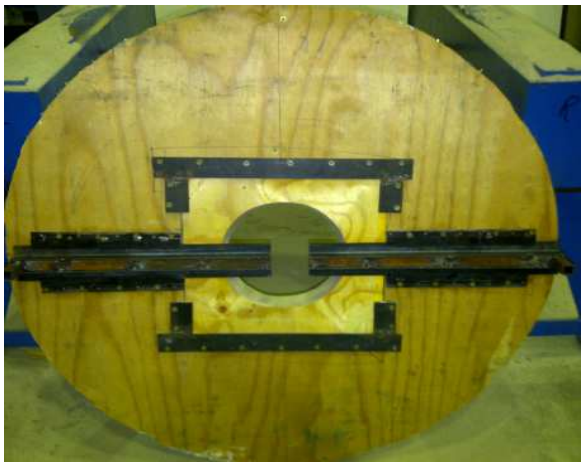

Figure 3.8: Trapdoor disk

Figure 3.9: Placement of reinforcement mesh layer

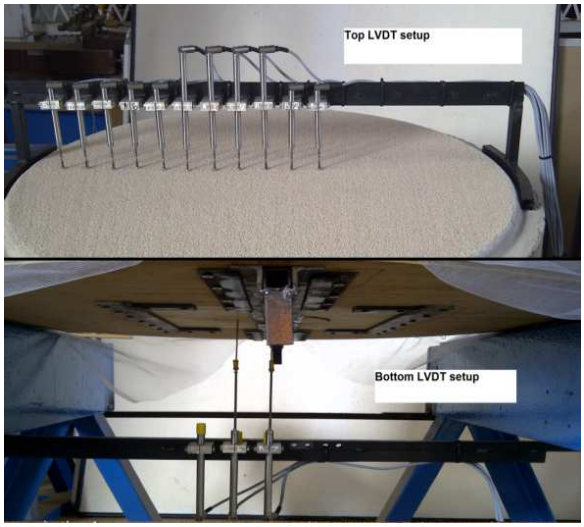

Figure 3.10: Placement of LVDT's at 50mm spacing

Figure 3.8 shows the adjustable trapdoor disk used to simulate the 150, 200 and 300mm void. Figure 3.10 and Figure 3.9 show the placement of the reinforcement in the circular concrete rings as well as the position of the LVDT's (de Lange, 2016). The position of the geosynthetic reinforcement and the general layout of the model is shown in Figure 3.11.

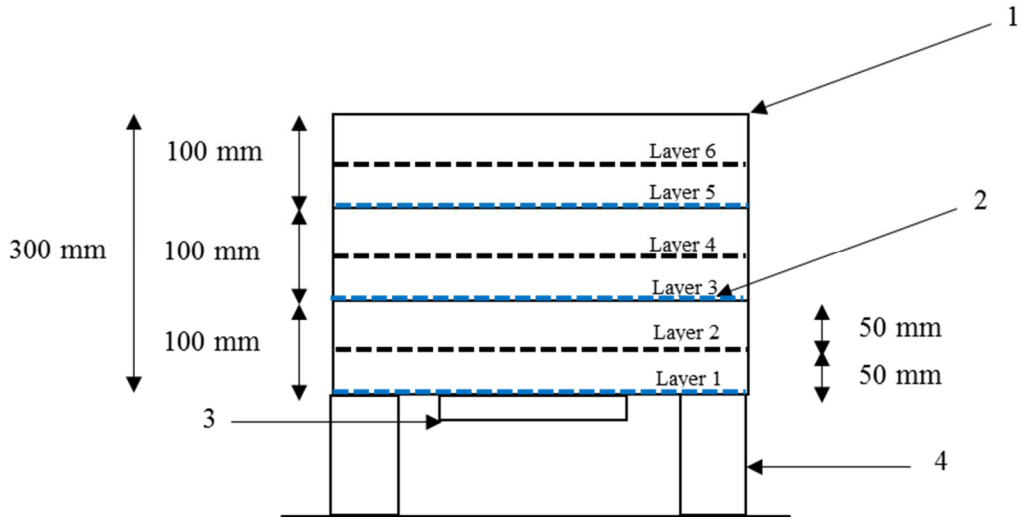

Figure 3.11: Sketch of test setup (de Lange, 2016)

1 = Concrete rings

2 = Geogrid layers anchored every 50mm*

3 = Trapdoor section

4 = Concrete ring stand

* The geogrid layers displayed in blue are anchored between the concrete rings layers, the layers displayed in black are anchored as shown in Figure 3.12 below.

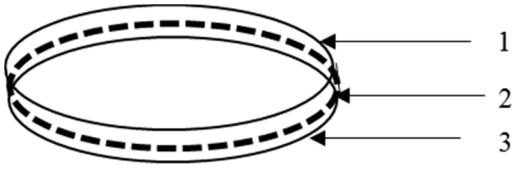

Figure 3.12: Timber ring used for geogrid anchorage

1 = Upper timber ring

2 = Geogrid layer

3 = Lower timber ring

The geogrid was glued between two timber rings and placed within the concrete rings at 50mm increments. The anchorage conditions prevented the fabric from slipping into the void when it formed. de Lange (2016) postulated that in field conditions interlocking between the geosynthetic and the soil as well as the overlap and anchorage lengths used onsite, would prevent the geosynthetic layer from slipping into the void. The anchorage conditions imposed on the geosynthetic were to prevent the said slippage of the geosynthetic occurring, and to model the anchorage effects provided onsite by frictional interlocking to a smaller scale.

Material tests undertaken to determine the properties of the fill layer and geosynthetic reinforcement are presented in Appendix B. The sand was poured in loosely, and uncompacted.

Madabhushi (2011) stated that soil behaves in a nonlinear and plastic manner. Due to soil being nonlinear, it cannot simply be modelled at a small scale. In a centrifuge, a gravitational acceleration is applied to the soil sample, to increase the stress/strain within the soil mass and provide more accurate results. de Lange (2016) states that "To generate significant stresses in the reinforcing fabric and it is planned to repeat these tests in a centrifuge in order to increase the stress levels. However, displacements under normal gravity were measured to an accuracy sufficient to provide useful information." At this stage, testing using a centrifuge is still to be performed and is planned as future research.

3.3.2.3 Results: soil surface deflection

The experimental model results from (de Lange, 2016) are presented in section 3.3.2.3 below. Three different design geometries are considered, the sand height remained constant at 300mm while the diameter of the void increases from 150, 200, 300mm. The number of layers of geosynthetic reinforcement used was increased from 1 – 6 layers.

i. D = 150mm, H/D = 2

Table 3.2: Experimental model soil surface deflections H/D = 2

D = 150mm						
Distance from centre of void (mm)	**Vertical deflection (mm)**					
	1 Layer	**2 Layers**	**3 Layers**	**4 Layers**	**5 Layers**	**6 Layers**
0	-2.023	-1.754	-1.205	-1.153	-1.205	-1.103
50	-1.851	-1.652	-1.153	-1.011	-1.153	-1.072
100	-1.68	-1.512	-1.021	-0.753	-0.755	-0.751
150	-0.914	-0.902	-0.654	-0.451	-0.404	-0.405
200	-0.521	-0.431	-0.422	-0.283	-0.272	-0.253
250	-0.133	-0.121	-0.126	-0.112	-0.113	-0.112
300	-0.124	-0.103	-0.091	-0.091	-0.093	-0.081
350	-0.112	-0.091	-0.081	-0.082	-0.064	-0.052
400	0	-0.081	-0.06	-0.05	-0.05	-0.04
450	0	0	0	0	0	0

Table 3.2 above shows the soil deflection measured using dial gauges at various positions along the soil surface (x).

From Figure 3.13 a slight decrease in soil deflection with the addition of the second layer of reinforcement was observed.

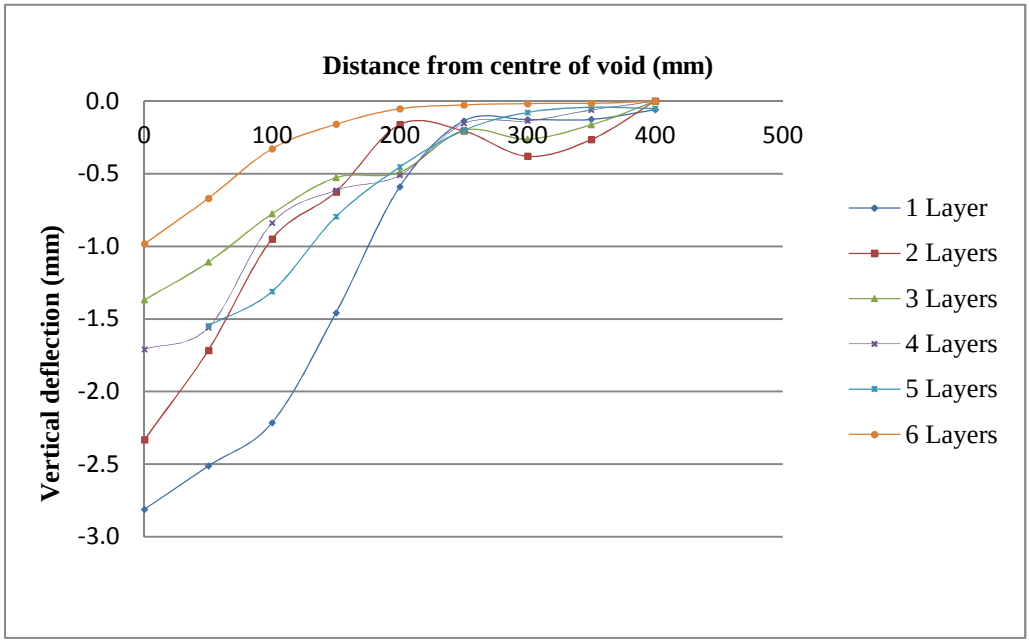

Figure 3.13: Vertical soil surface deflection obtained from experimental model for an H/D = 2

The addition of the 3rd and 4th layer created a considerable decrease in soil deflection. There was a slight increase in deflection with the addition of the 5th layer of reinforcement and again an expected reduction with the inclusion of the 6th layer. The general trend observed is a decrease in settlement with an increase in the number of reinforcement layers used.

ii. D = 200mm, H/D = 1.5

The void diameter is increased to 200mm and the results of which are tabulated in Table 3.3

Table 3.3: Experimental model soil surface deflections H/D = 1.5

D = 200mm						
Distance from centre of void (mm)	**Vertical deflection (mm)**					
	1 layer	**2 layers**	**3 layers**	**4 layers**	**5 layers**	**6 layers**
0	-2.812	-2.333	-1.370	-1.711	-1.547	-0.983
50	-2.513	-1.717	-1.109	-1.560	-1.311	-0.670
100	-2.215	-0.950	-0.777	-0.839	-0.796	-0.328
150	-1.459	-0.625	-0.527	-0.614	-0.454	-0.159
200	-0.590	-0.161	-0.489	-0.511	-0.201	-0.052
250	-0.137	-0.205	-0.201	-0.155	-0.078	-0.026
300	-0.126	-0.380	-0.261	-0.136	-0.041	-0.016
350	-0.126	-0.265	-0.163	-0.061	-0.051	-0.014

400	-0.059	0	0	0	0	0
450	0	0	0	0	0	0

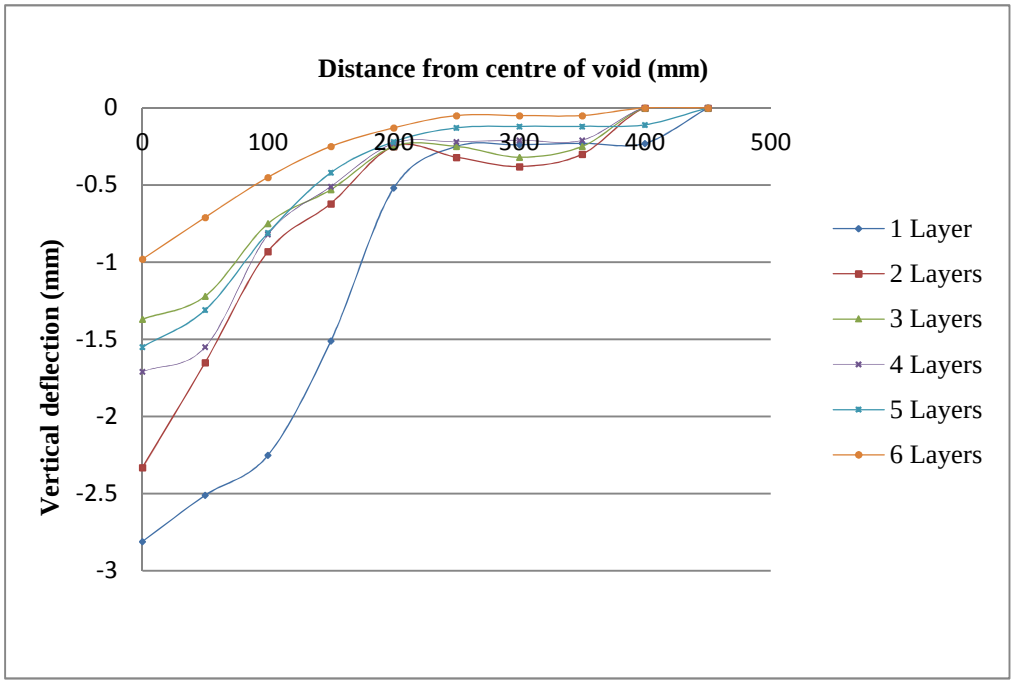

Figure 3.14: Vertical soil surface deflection obtained from experimental model for an H/D = 1.5

In Figure 3.14 a gradual reduction in the soil surface deflection with the addition of the 2nd and 3rd layers was observed. The inclusion of the 4th layer of reinforcement showed an unexpected increase in surface deflection. There was once again a gradual decrease in deflection with the addition of the 5th and 6th layer. In previous studies performed by Blivet et al. (2002) similar variances in the soil surface deflection were observed with the inclusion of multi-layered reinforcement. This unexpected result was attributed to the occurrence of soil arching. When support of some part of the soil mass is lost, the soil will want to move downward due to self-weight. The shearing between the soil in motion and the unaffected stationary soil opposes the downward motion. This results in a redistribution of some of the vertical stresses to horizontal stress, creating the soil arching effect.

If the redistribution of stress takes place at a particular soil height and the soil at this level is disturbed (in this case by the inclusion of a geogrid layer) at the critical height, the arching mechanism will break down. de Lange (2016) attributed the sudden increase in deflection when

the 4th layer was placed to a breakdown of the soil arching as the geogrid added a horizontal plane of weakness and negated the effect of soil arching as a load transfer mechanism.

iii. D = 300mm, H/D = 1

The void diameter was increased to 300mm and tabulated in Table 3.4.

Table 3.4: Experimental model soil surface deflections H/D = 1

D = 300mm						
Distance from centre of void (mm)	**Vertical deflection (mm)**					
	1 Layer	**2 Layers**	**3 Layers**	**4 Layers**	**5 Layers**	**6 Layers**
0	-6.151	-6.133	-3.864	-3.661	-3.642	-3.612
50	-6.112	-6.124	-3.654	-3.452	-3.431	-3.411
100	-5.284	-5.513	-3.125	-2.922	-2.837	-2.811
150	-3.912	-3.922	-2.131	-1.933	-1.823	-1.812
200	-2.213	-2.254	-1.213	-1.011	-0.841	-0.821
250	-1.153	-1.134	-0.512	-0.314	-0.333	-0.322
300	-0.521	-0.514	-0.252	-0.051	-0.052	-0.041
350	-0.331	-0.323	-0.213	-0.011	0	0
400	-0.284	-0.272	-0.181	0.023	0	0
450	0	0	0	0	0	0

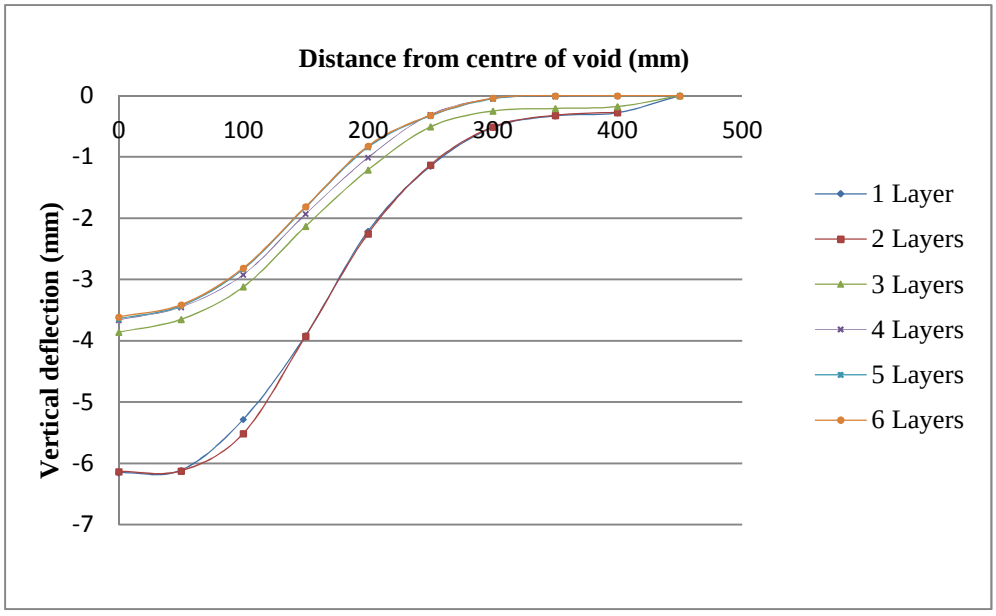

The addition of the second layer of reinforcement 50mm above the basal layer showed no significant difference in the surface deflection.

Figure 3.15 Vertical soil surface deflection obtained from experimental model for an H/D = 1

This was similar to the results obtained in Figure 3.13 (D=150mm). As the 3rd and 4th layers were added there was a marked difference in the surface deflection. Layers 5 and 6 did not cause any noticeable effect in decreasing the soil deflection further.

3.3.2.4 Experimental model results with increasing void diameter:

The results presented below are a comparison between the soil surface deflections obtained when the void diameter was increased.

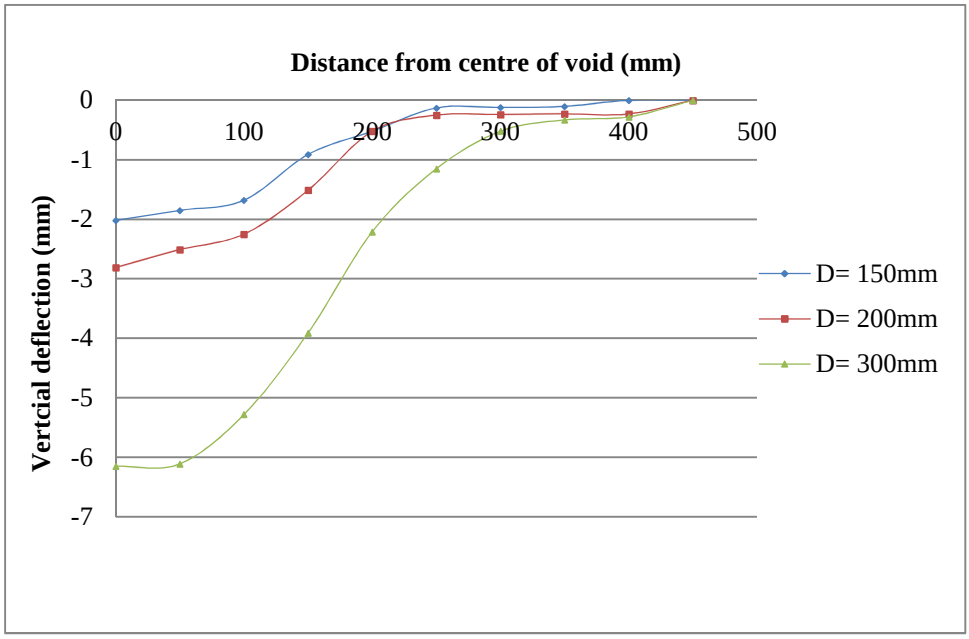

Figure 3.16: Effect of increasing void diameter on vertical soil deflection with a single layer of geosynthetic reinforcement present.

The soil surface deflection shows an increase with increasing void diameter. The diameter of the settlement cone was the same when the void diameter was 150 and 200mm. The settlement cone diameter increases when the void diameter was increased to 300mm.

Similar results were observed when multi-layered geosynthetic reinforcement was used as shown in Figure 3.17 below.

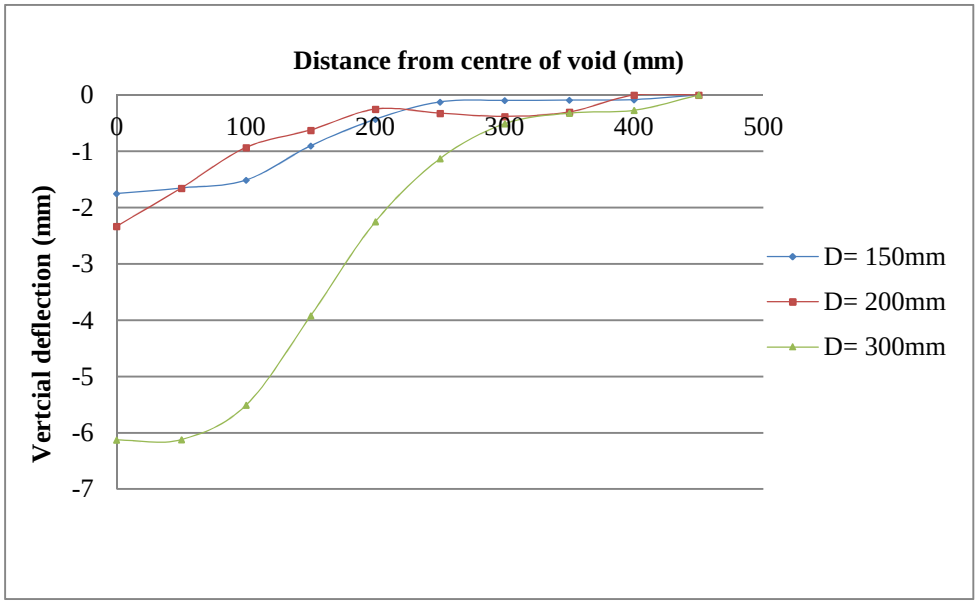

The general trend was an increase in soil surface deflections with increasing void diameter as would be expected

Figure 3.17: Effect of increasing void diameter on vertical soil deflection with 2 layers of geosynthetic reinforcement present

3.3.2.5 Summary of results

Figure 3.18 below is the ratio of surface deflection to embankment height for the 3 H/D ratios.

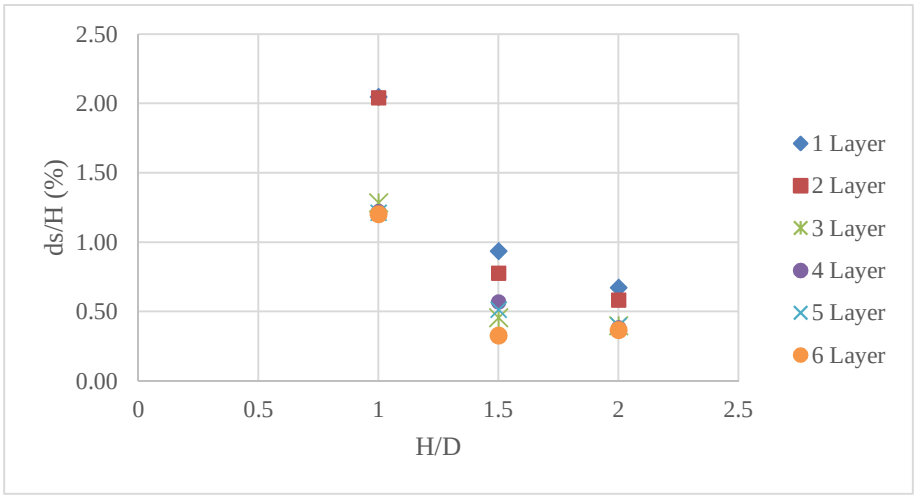

The ratio of surface settlement to embankment height halves when H/D is increased from 1 to 1.5. Beyond H/D = 1.5, the settlement decrease is less apparent.

Figure 3.18: Maximum vertical deflections along the centreline at the 3 H/D ratios

3.3.2.6 Summary of findings:

From the laboratory model it was evident that the presence of geosynthetic reinforcement in a soil mass helped minimise soil surface deflections. The degree to which the deflections are minimised however depended on various factors, e.g. soil arching, H/D ratio, number of reinforcement layers used. Theoretically increasing the number of geosynthetic layers should decrease the soil surface deflections. In most cases of the laboratory experiment this theoretical assumption holds true. However, in some cases the results were unpredictable when multiple reinforcement layers are introduced. The propensity of the soil towards arching affected the outcome of the test results, causing variations.

When H/D = 1, reinforcing the model above mid-height did not result in any further improvement in relative settlement, and no soil arching was observed at the lower H/D ratio. When H/D $\geq$ 1.5, the soil fill exhibited arching behaviour, that tended to be disrupted when multiple layers of reinforcement were present. de Lange (2016) postulates that when multiple reinforcement layers are present, the occurrence of soil arching was minimised as the reinforcement layers caused discontinuities in the soil mass.

The diameter of the settlement cone tended to increase with an increase in void diameter, as expected. The angle of draw that dictated the diameter of the soil surface cone is approximately 60^0. SANS 207 assumes that the angle of void propagation is equal to the angle of shearing resistance of the soil (41^0, refer to Table 5.1 in Chapter 5) while the RAFAEL method assumes the angle to be perpendicular. From the results obtained it was observed that neither of these assumptions hold true, the analytical calculations are further investigated in Chapter 4. The laboratory results were used to validate the numerical model in the ensuing chapters.

4. CHAPTER 4: COMPARISON OF MODEL DATA WITH CURRENT DESIGN METHODS FOR BASAL REINFORCEMENT

The existing guide for designing geosynthetic reinforcement as basal geosynthetic reinforcement in the South African environment is SANS 207: 2006. The preceding chapters have covered actual laboratory simulations, given this real life data, the SANS 207 calculations were performed and compared to the laboratory data. This serves to test the validity of the SANS 207 assumptions. Section 2.8.1 provided an overview of the design techniques employed in SANS 207. In addition to SANS 207, the design approach developed by the RAFAEL team was also considered.

4.1 Analytical investigation: Reinforced model

In the reinforced experimental model developed in de Lange (2016) the soil surface deflections and geogrid deflections were calculated using the analytical design method stated in SANS 207 as well as the RAFAEL method. This could only be performed for the basal layer, as multiple layers of reinforcement are not considered in either design methodology.

4.1.1 SANS 207:2006

Figure 4.1 shows the manner in which the void is assumed to propagate when determining the tensile strength required for a basal layer of reinforcement according to SANS 207: 2006.

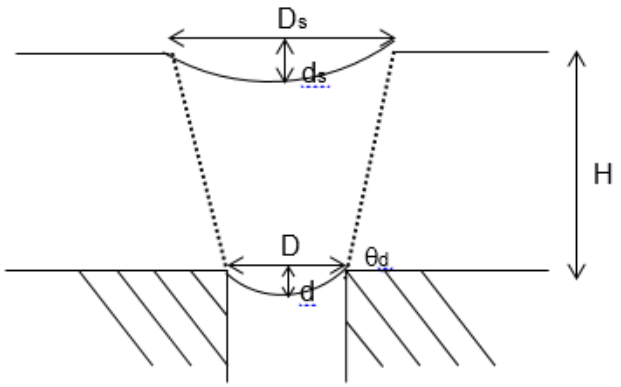

Figure 4.1: Propagation of subgrade void assumed geometry in a basally reinforced soil fill layer (South African National Standard SANS 207, 2006)

de Lange (2016) used a laboratory scale model of cohesion less sand to assess geometrical influences on the “angle of draw”.

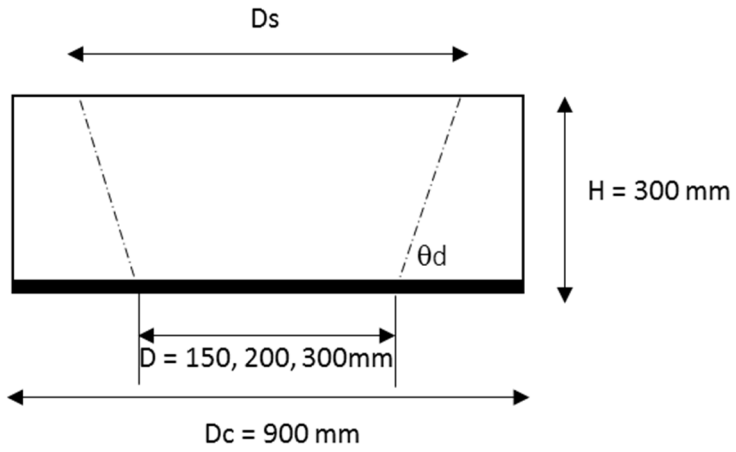

Figure 4.2 Schematic representation of the experimental model performed by de Lange (2016) with a variation in void diameter.

H = 300mm

D = 150, 200, 300mm

*θ_d = Angle of draw = soil friction angle (41^0)

Dc = Inside diameter of concrete rings = 900mm

d = Unknown

d_s = Unknown

D_s = Unknown

A void diameter of 300mm was used in the calculations presented below. The same calculations were performed for 150, 200mm voids and tabulated.

*SANS 207 assumed that the angle of draw was equal to the soils angle of shearing resistance (Refer to section 2.8.1). In triaxle tests performed by Sparks (2012), the sand used in de Lange (2016) experimental model was tested and yielded an average angle of shearing resistance of 41^0 (See appendix B).

i. Calculating D_s:

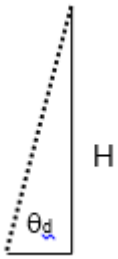

If it is assumed that the angle of draw = the angle of shearing resistance then:

$D_s = 2*\frac{H}{tan\theta d} + D$

D_s = 986mm

The diameter of the concrete rings containing the sand was 900mm, the settlement cone diameter is thus too large as it surpassed the 900mm limit. This in turn indicated that the selected angle of draw according to the design method set out in SANS 207 was incorrect.

de Lange (2016) used his model data to assess the value of the angle of draw which he found to be larger than the angle of shearing resistance and within the small range investigated, relatively insensitive to H/D.

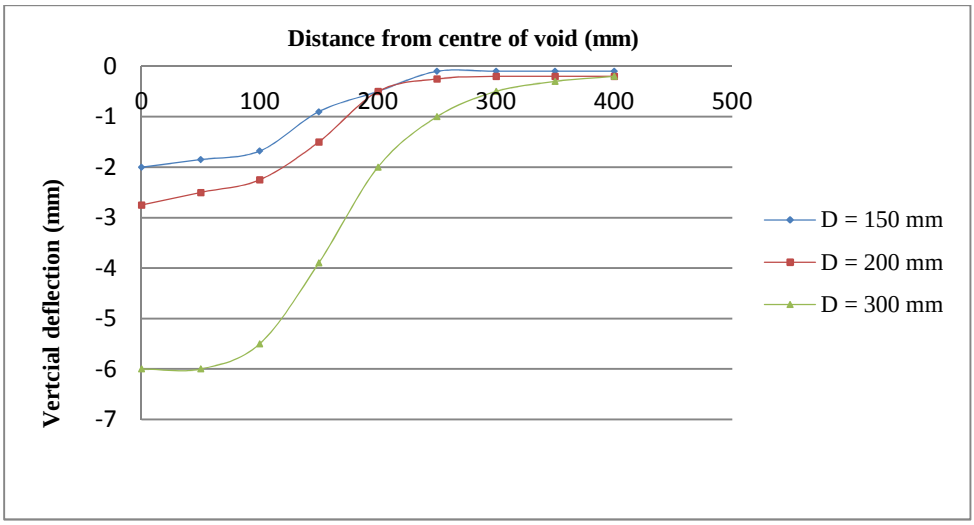

Figure 4.3 Laboratory results: Vertical soil surface deflection with basal reinforcement present for a varying void diameter de Lange (2016).

The results from Figure 4.3 in terms of the settlement cone diameter were summarised and presented in Table 4.1 below.

Table 4.1: Diameter of settlement cone according to laboratory data and the subsequent angle of draw

D (mm)	Ds (mm)	θ_d
150	500	59.74
200	500	63.43
300	700	56.31

ii. Calculating ds:

The equation describing the maximum geosynthetic strain in SANS: 207 is shown below:

$$\varepsilon_{max} = \frac{8\left(\frac{d_s}{D_s}^2\right)(D+\frac{2H}{tan\theta_d})^6}{3D^6}$$

The geosynthetic fabric used in de Lange (2016) underwent testing in Kaytech's geosynthetic laboratory facility (An ISO 17025 accredited laboratory). The strain at the maximum force in the geogrid layer was tested in Geosynthetics Laboratory and yielded the following results:

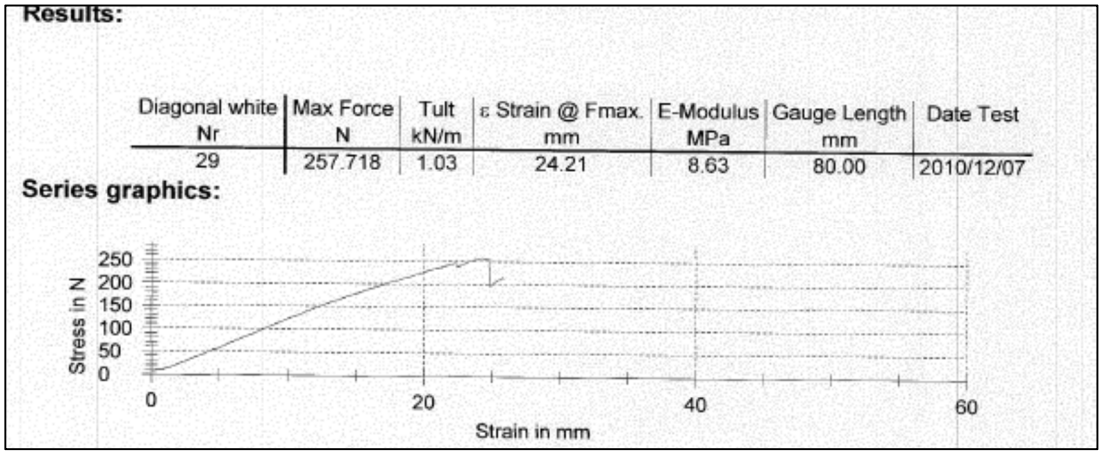

Figure 4.4: Geosynthetic testing results obtained from Geosynthetic Laboratory

(See Appendix A for full results page)

Using the results for the maximum strain before rupture, the surface settlement of the deflection cone was calculated:

ε_{max} = Elongation/ Gauge length

ε_{max} = 24.21/80

= 0.3026

Substituting into equation:

$0.3026 = [8*(\frac{ds^2}{700^2})*(700.15)^6]/3*300^6$

$6.617*10^{14} = 1.923x10^{12}*d_s^2$

d_s = 18.551 mm

iii. Calculating d:

$$\varepsilon_{max} = \frac{8d^2}{3D^2}$$

$0.3026 = (8*d^2)/ (3*300^2)$

d = 101.062 mm

The complete results including the range of void diameters was drawn up in Table 4.2

Table 4.2: Expected vertical surface settlements using SANS 207 design method

SANS207	D (mm)		
	150	**200**	**300**
Ds (mm)	500	500	700
ds (mm)	-4.546	-10.776	-18.551
d(mm)	-50.529	-67.374	-101.062

4.1.1.1 Soil surface deflection: SANS 207

Using the results obtained in Table 4.2, a graph representing the soil surface deflection patterns estimated by SANS 207 was drawn up and shown in

Figure 4.5. SANS 207 assumes that the surface deflection is parabolic, using this assumption the soil surface deflection points were estimated and plotted using the equation:

$$y = \frac{4d_s x^2}{{D_s}^2} - d_s$$

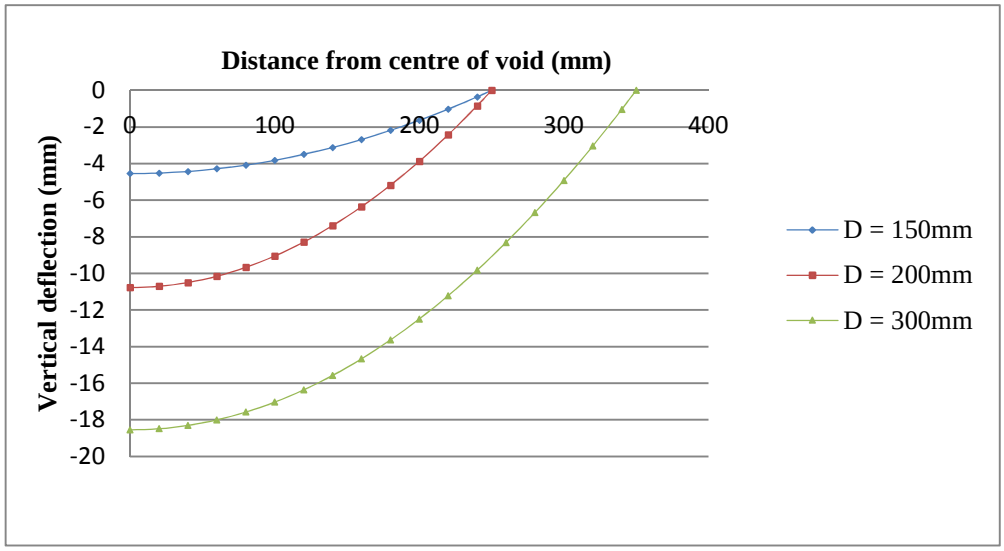

Figure 4.5: Vertical soil surface deflection calculated using SANS 207

4.1.1.2 Deflected shape of geogrid:

SANS 207 assumes the deflected shape of the geosynthetic fabric is parabolic. Table 4.2 results in terms of maximum geosynthetic deflection were used to develop Figure 4.6 below.

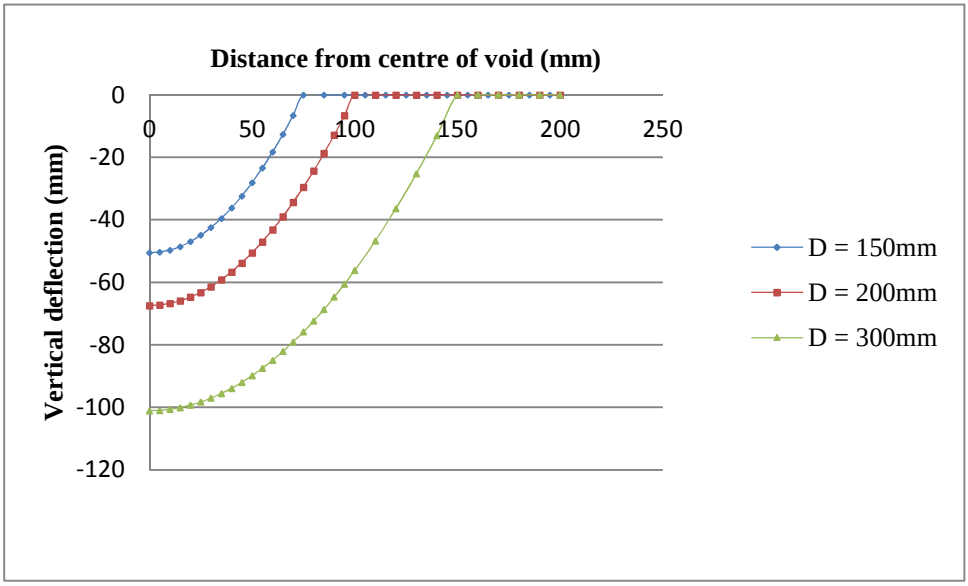

Figure 4.6: Vertical geogrid deflection calculated using SANS 207

The equation governing the shape of the geogrid deflection was as follows:

$$y = \frac{4dx^2}{D^2} - d$$

4.1.2 RAFAEL Method:

In the RAFAEL approach, it is assumed that the diameter of the soil surface deflection cone is the same as the diameter of the void, i.e. the angle of void propagation is 90^0.

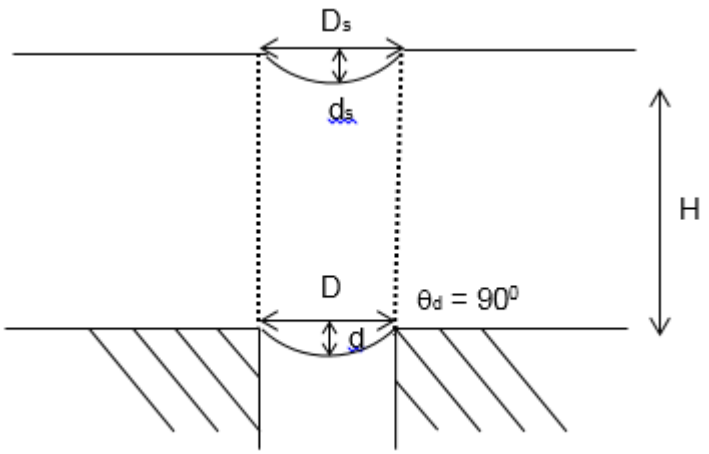

Figure 4.7 Propagation of subgrade void assumed by RAFAEL

The laboratory model geometry was considered

H = 300mm

D = 150, 200, 300mm

d = Unknown

d_s = Unknown

D_s = D (void diameter represents the diameter of the settlement cone due to the angle of void propagation being 90^0)

For the calculation a void diameter of 150mm was considered, the same calculations were performed for 200, 300mm voids and tabulated.

i. Calculating Ds:

For the RAFAEL investigation it was postulated that the failure zone in the supported soil takes the form of a cylinder directly above the void.

From this assumption D = Ds

Consider the model with D = 300mm

Ds is subsequently equal to 300mm

ii. Calculating d:

Section 2.8.2 provided an overview of the RAFAEL approach. The equation for maximum geosynthetic strain assumed by RAFAEL is the same as SANS 207, hence the shape of the deflected geosynthetic was the same from both design approaches.

Using equation:

$$\varepsilon_{max} = \frac{8d^2}{3D^2}$$

$0.302 = (8*d^2)/ (3*300^2)$

d = 101.062 mm

iii. Calculating d_s:

Using equation:

$$d_s = d - 2H(C_e - 1)$$

Where C_e is the coefficient of soil expansion.

Villard, et al., (2000) provided the following equation for C_e:

$$C_e = \frac{V_{se}}{V_s}$$

Where V_{se} = the de-compacted soil volume (m^3)

V_s = soil volume prior to de-compaction (m^3)

According to Potts (2007) the coefficient of soil expansion is 1.15 for granular fill layers

$d_s = 50.531 – (2*300)*(1.15-1)$

= -39.469 mm (Upward heave)

The experimental data does not show any such heave taking place, indicating that the selected coefficient of soil expansion was too high. A revised value for C_e was selected based on recommendations from the German design guide EBGEO: 2011 which states that:

C_e = 1.03 for round grained material, C_e = 1.05 for crushed aggregate

d_s = 50.531 – (2*300)*(1.03 -1)

d_s = 32.531 mm

The complete results including different void diameters was drawn up in Table 4.3

Table 4.3: Expected vertical soil surface deflection using RAFAEL design method

RAFAEL	D (mm)		
	150	**200**	**300**
Ds (mm)	150	200	300
ds (mm)	-32.531	-49.374	-83.062
d(mm)	-50.531	-67.374	-101.062

4.1.2.1 Soil surface deflection: RAFAEL

RAFAEL assumed that the surface deflection was parabolic. The equation governing the shape of the soil surface deflection was as follows:

$$y = \frac{4d_s x^2}{{D_s}^2} - d_s$$

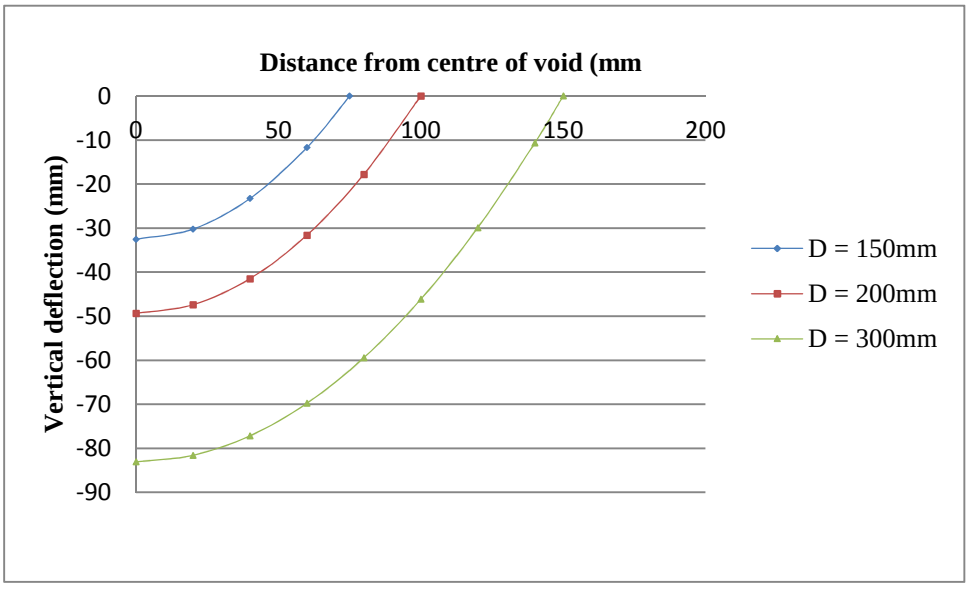

Figure 4.8: Vertical soil surface deflection representing de Lange (2016) experimental test calculated using RAFAEL assumptions.

4.1.2.2 Deflected shape of geogrid RAFAEL:

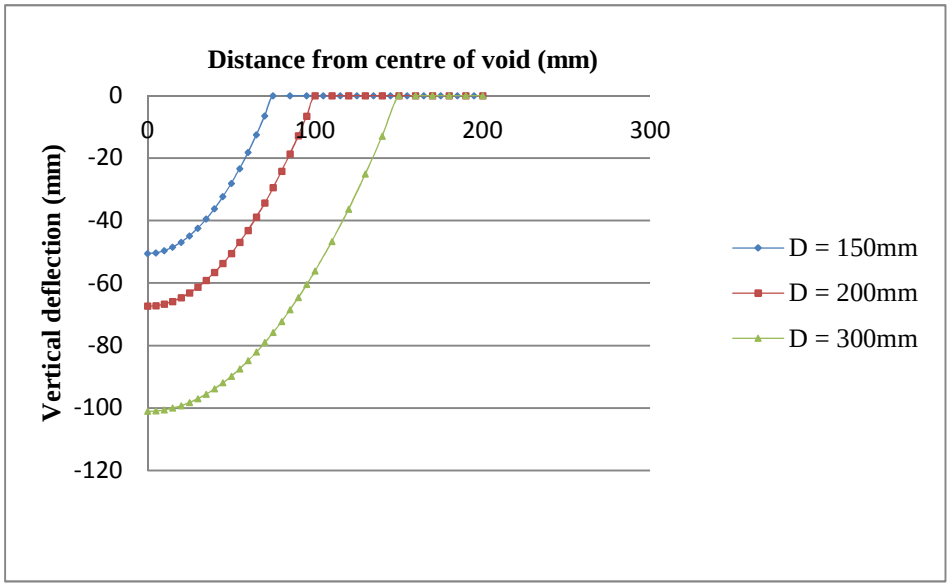

RAFAEL assumed that the geogrid deflection was parabolic or circular.

Figure 4.9 Geogrid deflection representing de Lange (2016) experimental test calculated using RAFAEL assumptions.

The equation governing the shape of the geogrid deflection is as follows:

$$y = \frac{4dx^2}{D^2} - d$$

4.2 Comparison between analytical methods and laboratory data

The RAFAEL method of estimating soil/geogrid deflections differs from the SANS 207 methodology in that it takes soil dilation into account and the angle of draw differs. The angle of sinkhole propagation is assumed to be 90^0, and only the cylinder of soil directly above the void experiences displacement. SANS 207 assumes that the void causes a deflection cone governed by an angle of propagation (Taken as the soils angle of internal friction).

Figure 4.10 below illustrates a comparison between the soil surface deflection profiles estimated using the SANS 207 and RAFAEL methodology. The soil surface deflection estimations from both the analytical methods differ. The RAFAEL assumptions tend to be larger surface deflections concentrated over a small diameter (D = D_s). The SANS 207 assumptions provide a shallower wider area of effect.

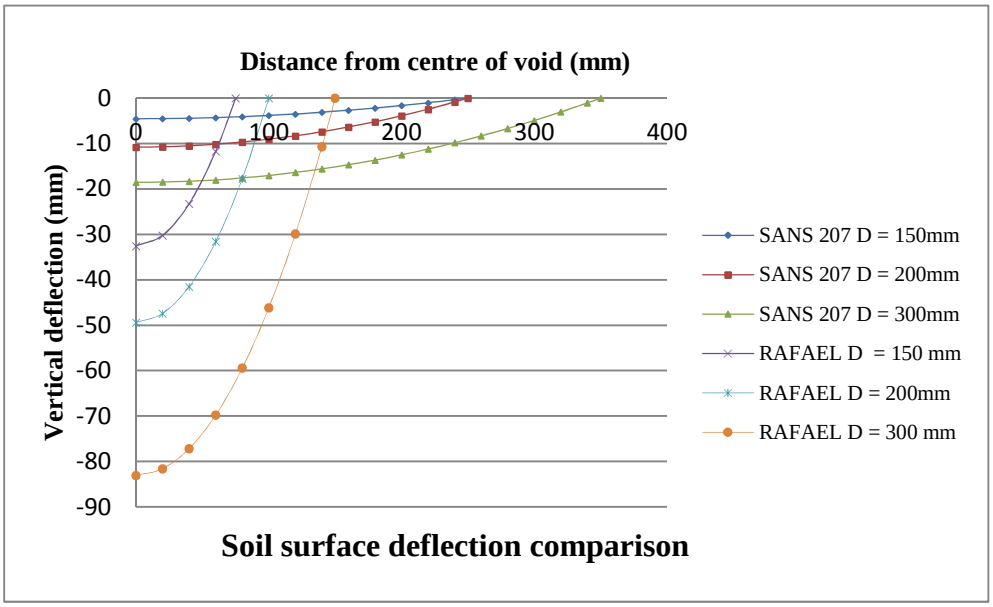

Figure 4.10 Vertical soil surface deflection comparison between SANS 207 and RAFAEL design methodology

4.2.1 Analytical results: SANS 207 vs Experimental data

The previous calculations indicated that SANS 207 overestimated the diameter of the soil surface settlement cone. This was due to the low angle of draw (θ_d) assumed by SANS 207 (θ_d= Angle of internal friction = 41^0). Consider the model where Ds = 300 mm. The laboratory results of de Lange (2016) suggested an angle of draw of about 60^0.

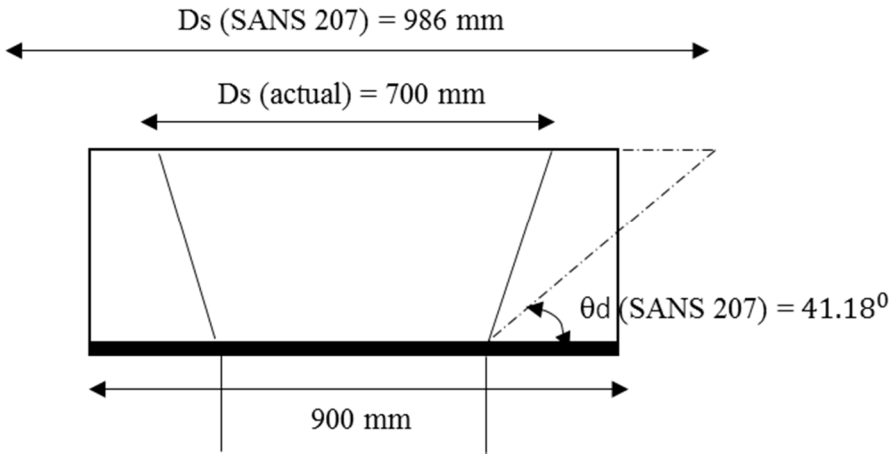

Figure 4.11: Schematic of laboratory test set up by de Lange (2016) showing SANS 207 estimations of the settlement cone diameter

Figure 4.11 above showed the overestimation of the soil settlement cone from the SANS 207 methodology. This indicated that SANS 207 overestimates the area of effect the sinkhole had on the soil surface. When the actual cone diameter was used, the following results were plotted against the de Lange (2016) laboratory results and shown in Figure 4.12 below.

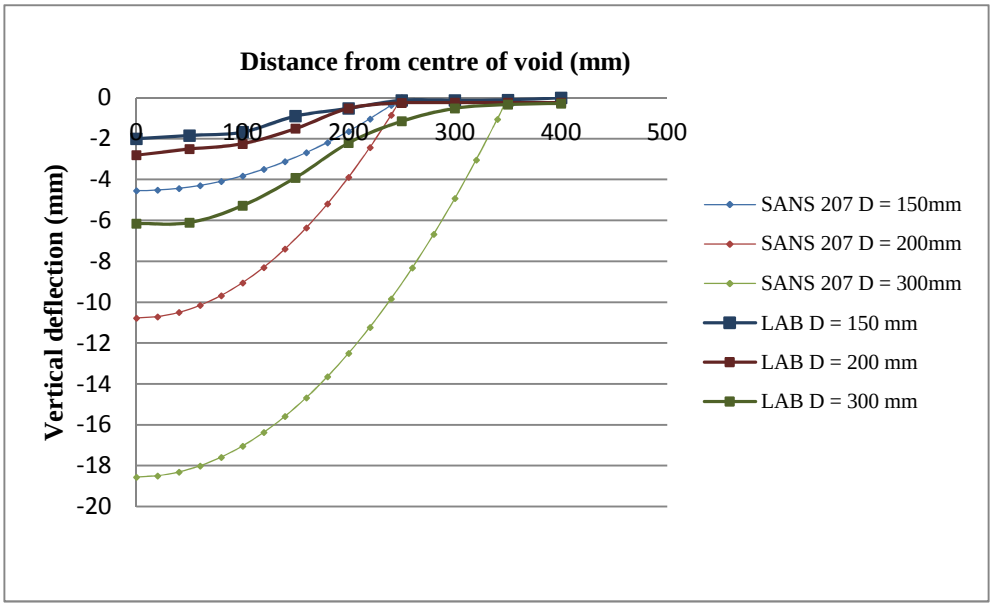

Figure 4.12 Vertical soil surface deflection comparison between de Lange (2016) experimental results and SANS 207 calculations.

SANS 207 assumed that the volume of soil displaced at the level of the geosynthetic layer was equal to the volume of the soil settlement cone at the soil surface, as shown in Figure 4.13 below ($V_1 = V_2$)

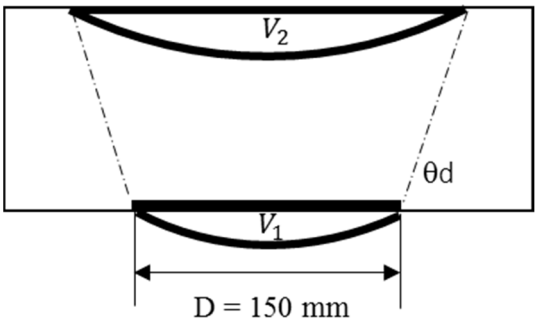

For the volumes to be the same, no soil dilation or arching must take place. In Figure 4.12 the actual laboratory data exhibits lower soil surface settlements, indicating that soil dilation and/or arching has taken place.

Figure 4.13: Schematic of de Lange (2016) experimental model test showing the deflected shape of the geosynthetic and surface settlement cone.

This lead to the conclusion that SANS 207 overestimates the surface area affected by a subgrade void and does not take into account soil dilation or arching, which compromised the accuracy of the results.

4.2.2 Analytical results: RAFAEL vs Experimental data

The RAFAEL method differed from SANS 207 in that it took soil dilation into account. It also assumed that the void did not propagate outward, but caused a tunnel like soil surface collapse i.e. $\theta_d = 90^0$. Comparison between the RAFAEL results and actual laboratory data yielded the following results:

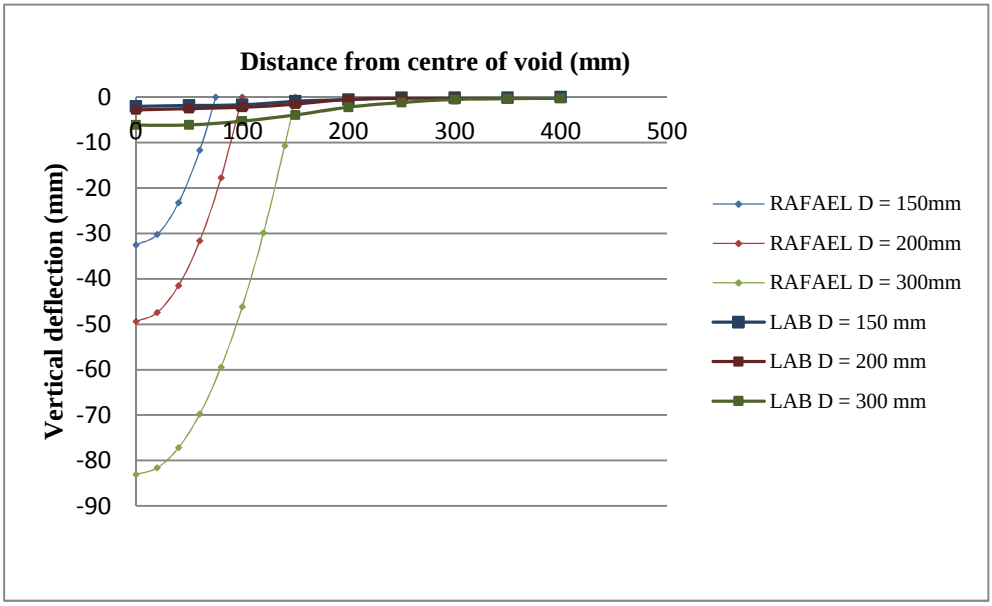

Figure 4.14 Vertical soil surface deflection comparison between de Lange (2016) experimental results and RAFAEL calculations.

The cone diameter estimated by RAFAEL was too small, the method underestimates the area affected by the subgrade void. RAFAEL estimates larger soil surface settlements, due to the void affecting a smaller more concentrated area. The settlement results estimated when using the German design guides EBGEO: 2011 coefficient of expansion was still inaccurate, as the defections were now largely over predicted. Using de Lange (2016) experimental data, the coefficient of expansion can be calculated:

$$d_s = d - 2H(C_e - 1)$$

For H/D = 1.5, ds = -2.81 mm and d = -7.39 mm.

Hence C_e = 1.0076, which is lower than the expansion coefficient assumed by both Potts (2007) and the German design guide EBGEO: 2011 for granular fill layers.

$$C_e = \frac{V_{se}}{V_s}$$

Where V_{se} = the de-compacted soil volume (m^3)

V_s = soil volume prior to de-compaction (m^3)

Hence soil expansion/dilation does take place in the experimental model, the degree to which expansion occurs however is over predicted by the Potts (2007) and German code design assumptions. The degree of expansion however must be further investigated as meaningful conclusions with regard to the $C_e$value of the soil cannot be made based on one available set of data.

4.2.3 Comments:

Both analytical design methods had limitations when estimating the diameter of the soil surface settlement cone. SANS 207 tended to overestimate while RAFAEL underestimates D_s. SANS 207 did not take soil dilation into account, this leads to a larger settlement value. Although RAFAEL accounted for soil dilation, the deflection values estimated were still too high when compared to the laboratory data. This was due to the concentration of the surface settlements to directly above the void. The degree of soil dilation depended on the coefficient of expansion C_e. A coefficient of expansion of 1.15 used in Potts (2007) for granular soil was too high and resulted in the soil heaving upward. The revised value for C_e of 1.03 used in the German design guide EBGEO: 2011 resulted in a significant increase in the soil surface deflections but the deflections calculated were far higher than the actual laboratory results. In order to determine the actual C_e further laboratory tests and investigations must take place.

5. CHAPTER 5: NUMERICAL MODEL DEVELOPMENT

5.1 Numerical model:

5.1.1 Rationale:

In order to perform the numerical analysis, the Strand 7 finite element analysis program was used. In previous investigations performed by Kae (2003) and Grabe (2003), Strand 7 was used in geotechnical applications showcasing the benefits geosynthetic reinforcement provided to a railway formation in terms of stress reduction. Numerical modelling was beneficial in that various model parameters were altered with relative ease. Performing similar parameter changes to a laboratory model would be more time consuming.

5.1.2 Basal reinforcement:

The development of the FEM model required the following general steps:

- Selection of type of element
- Selection of type of model analysis
- Input of model geometry
- Selection of model mesh structure
- Input of restraint conditions
- Input of loading conditions
- Selection of material characteristics for sand fill and geosynthetic
- Setting model staging

5.1.3 Type of element

The soil was modelled using 8-noded quadratic plate soil elements as shown in Figure 5.1:

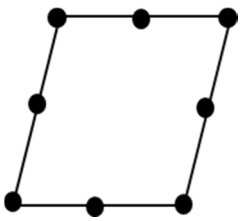

The presence of the mid-side nodes allowed the elements to be curved. For the sake of simplicity and to decrease computational time, 2D analysis was used. The type of element selected should effectively represent the 3D nature of the laboratory model in 2D. The soil was modelled using 2D plate

Figure 5.1: 8-noded quadratic elements representing the soil fill layer

elements, which represented the solid soil elements in 3D. The geogrid was modelled as 1D

truss elements (that can only carry tensile forces), and represent membrane elements in 3D, Grabe (2003).

5.1.4 Type of model analysis

The laboratory model was rotationally symmetric about the y axis hence was regarded as axisymmetric. Axisymmetric analysis was thus selected but plane strain conditions were also modelled for comparative purposes.

5.1.5 Model geometry

Overburden height = 300mm, void diameter = 150, 200, 300mm

A half model was used with symmetry along the y-axis

5.1.6 Model mesh structure

The soil fill was discretized as shown in Figure 5.2 below. The density of the mesh directly above the void was increased to improve the accuracy of the results in the area directly above the void.

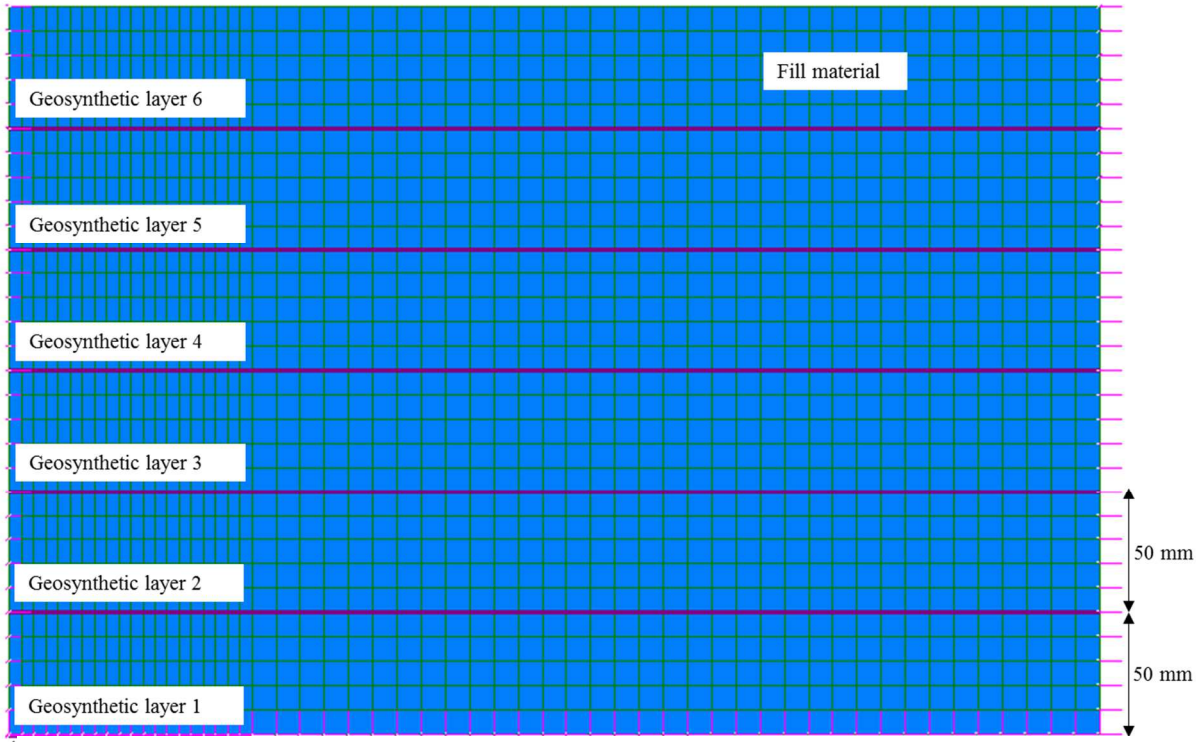

Figure 5.2: Mesh structure used in FEM analysis of de Lange (2016) experimental model

5.1.7 Restraint conditions

In order to simulate the formation of the void, the restraint conditions of the model were changed. Initially, the geosynthetic layer was fully restrained (closed), and no vertical movement was allowed. This first stage in the model represented the laboratory conditions where the void had not been formed yet. The second restraint condition (open) modelled the formation of the void itself. The restraints on the geosynthetic layer were released and the geosynthetic was allowed to deform due to the weight of the soil fill above it.

i. Closed

The vertical concrete ring walls were unrestrained in the y-direction for soil movement to take place. The basal geotextile layer is fully restrained. This represented the initial conditions with no subgrade void and the movable base still in place.

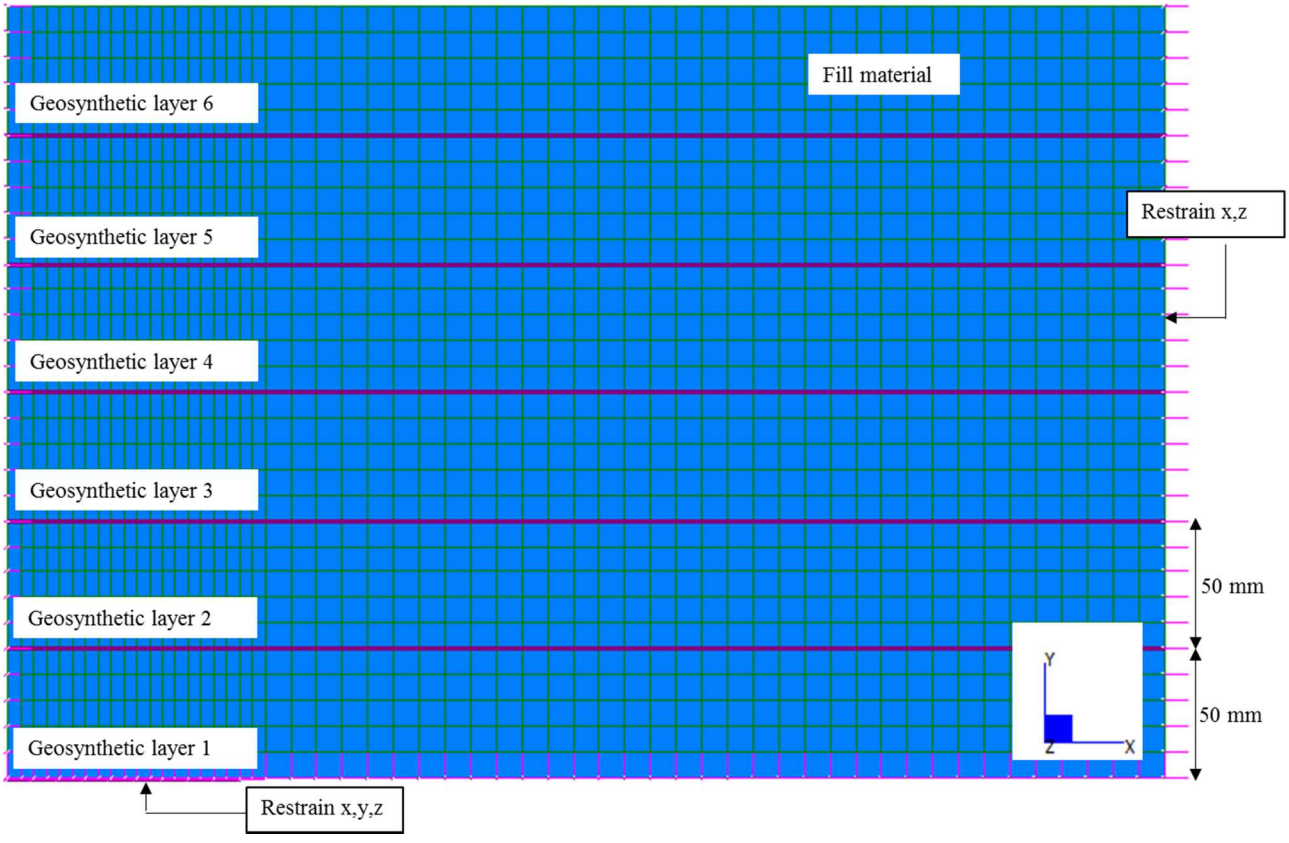

Figure 5.3 Restraint conditions in the FEM model when the void has not formed

ii. Open

In Figure 5.4 below the restraints on the geosynthetic layer were released to simulate the formation of the void. Removing all boundary restraints from the geosynthetic layers allowed for the nodes to be free to move. This resulted in soil movement, and downward deflection of the geosynthetic layer due to the weight of the soil above it.

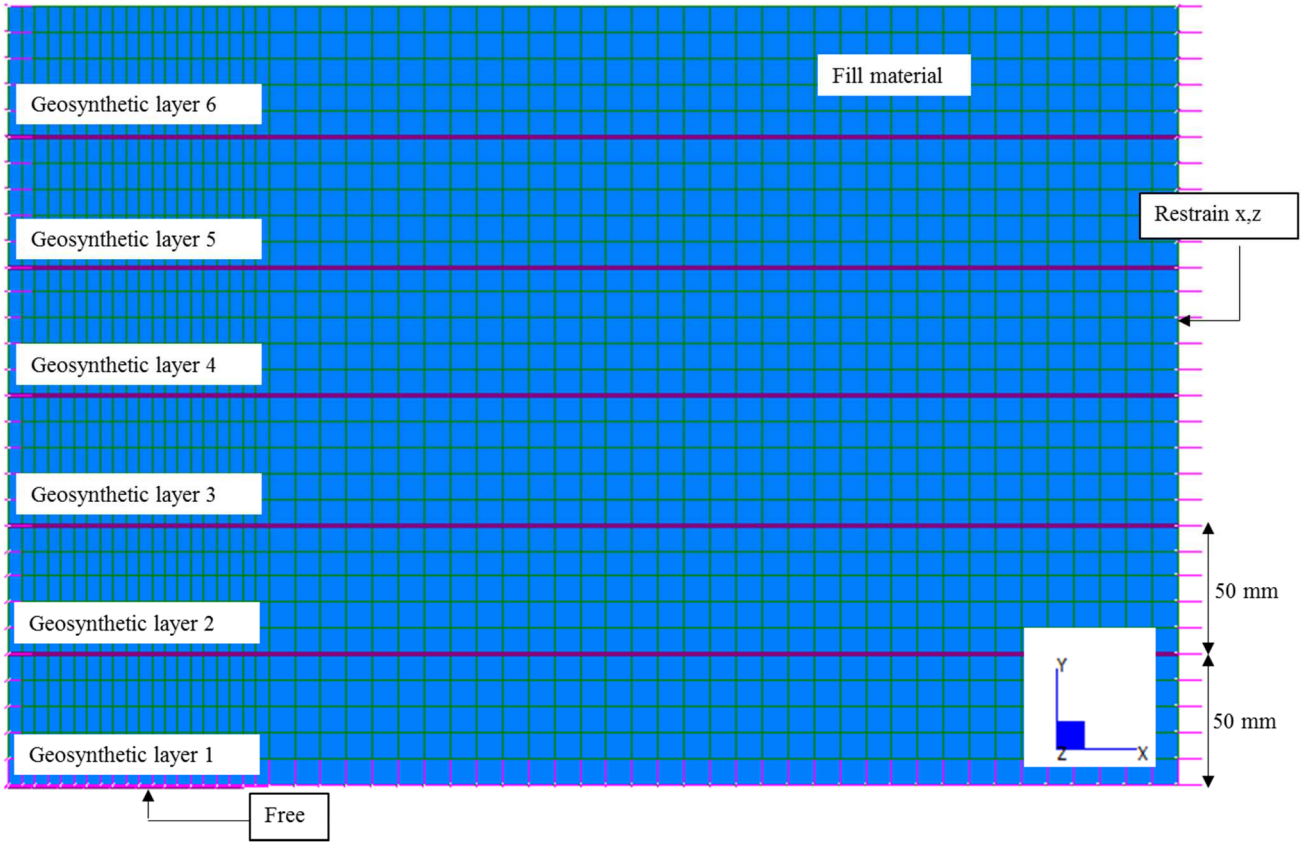

Figure 5.4 Restraint conditions in the FEM model when the void has formed

5.1.8 Loading conditions

No surface loads were imposed on the laboratory model, the soil moved downward by self-weight due to gravity. Gravity acting in -y direction, gravitational acceleration = 9.8m/s^2

5.1.9 Material characteristics

The material characteristics for the soil and geosynthetic used are given in Table 5.1 below.

Table 5.1: Soil and geosynthetic properties used in FEM model

Material	Young's Modulus (MPa)	Tensile strength (N/m)	Poisson's Ratio	Density (kN/m^3)	Cohesion (kPa)	Friction Angle (deg)
Soil	20	_	0.3	16.96	1	41
Geogrid	_	8.63	0.25	10	_	_

The geosynthetic properties in terms of the tensile strength were calculated from Table 5.1 using a 1mm geosynthetic thickness. de Lange (2016) used "washed silica sand" during the laboratory tests and performed a sieve analysis on the soil.

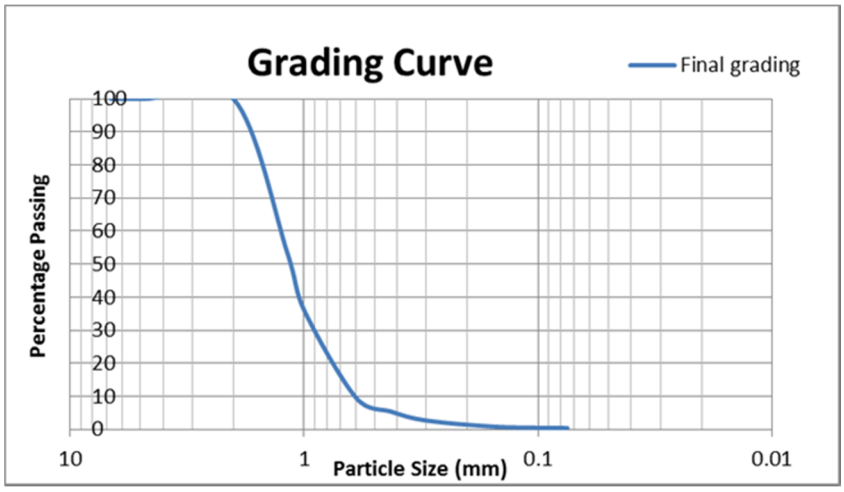

Figure 5.5: Grading curve for soil used in experimental model in de Lange (2016)

The grading curve yielded that the soil was uniformly graded sand with no cohesion. The soil was poured into the concrete rings loosely with no compaction. Triaxle tests performed on the soil in Sparks (2012) yielded an average soil friction angle of 41° and a dry density of 16.96 (Results shown in Appendix B). The general Young's modulus for loose sand was taken from Geotech data information (2013). A minimum cohesion of 1 kPa was used as the FEM model experienced difficulty in convergence with a cohesion value of zero.

5.1.10 Numerical analysis

A non-linear staged analysis was used. Non-linear models analyse the elastic-plastic soil deformation hence is used when the expected displacements in elements of the model are large (Strand 7 verification manual, 2013). The staging took place by changing the restraint conditions of the geosynthetic fabric as shown in section 5.1.7. "Freeing" the restraints in the

geosynthetic layer resulted in movement of the soil and geosynthetic layer downward. The results obtained for all three H/D ratios were compared in terms of the soil surface and geosynthetic deflections in Chapter 6.

6. CHAPTER 6: NUMERICAL MODEL RESULTS

6.1 Introduction:

The numerical models performed in Chapter 6 represent the laboratory experiments performed in both de Lange (2016) and Potts (2007). Both experimental models followed a similar principle, a void formed beneath the geosynthetically reinforced fill layer resulting in soil deflections. The difference was in that de Lange (2016) considered the use of both multi-layered and basal reinforcement as opposed to basal reinforcement alone. Both experimental models were reproduced using the FEM program Strand 7 and the results were compared.

6.2 Numerical model results Potts (2007):

An overview of the laboratory experiment performed by Potts (2007) was covered in the case study in section 2.9.5. The results of the case study are presented below. Strand 7 was used to model the laboratory simulations. The aim was to establish that Strand 7 was capable of generating results of the same order of magnitude as the laboratory experiment. The method followed in developing the FEM model is covered in Chapter 5, the methodology section. The material characteristics of the soils and the geogrid layer taken from Potts (2007) are shown in Table 6.1 below.

Table 6.1: Material characteristics used in Potts (2007) laboratory experiment

Material	Parameter	Recommended value
Fill	γ_{loose}	15.5 kN/m^3
	$\phi'_{fill\ loose}$	35^0
	E	20 MPa
	μ	0.3
	K	0.4285
	e	0.2
Polythene sheet	J	11kN/m/m
	μ	0.2

6.2.1 Soil surface settlement

The results of the FEM analysis using Strand 7 are presented below. The FEM results in Figure 6.1 illustrated that the soil surface deflection decreased with an increase in the H/D ratio.

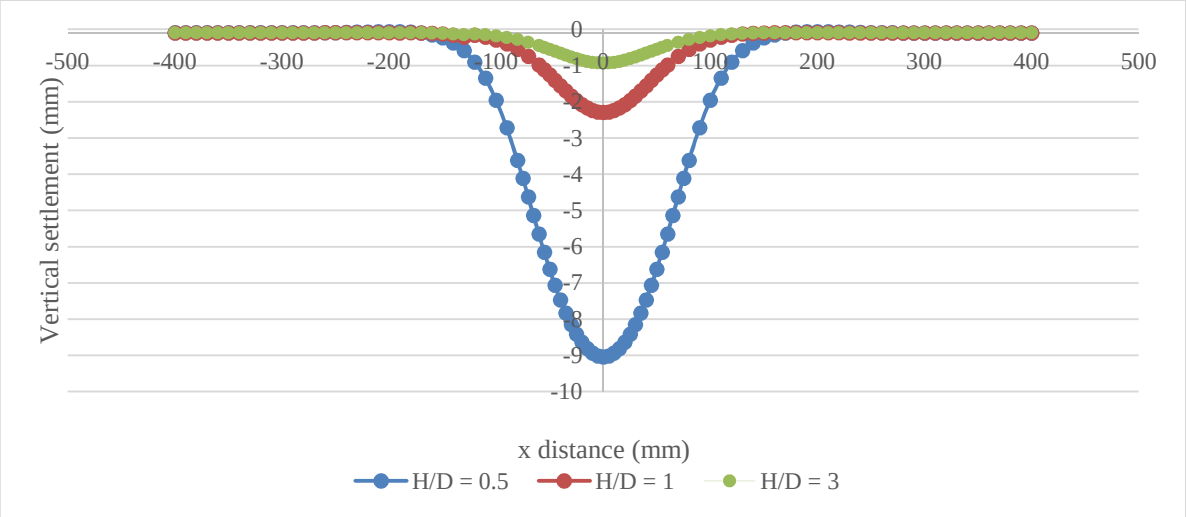

Figure 6.1: The soil surface deflections generated using Strand 7 FEM software to model Potts (2007) laboratory experiment with a change in H/D ratio.

The laboratory results in Figure 6.2 showed a similar decrease in soil settlement with an increase in the H/D ratio.

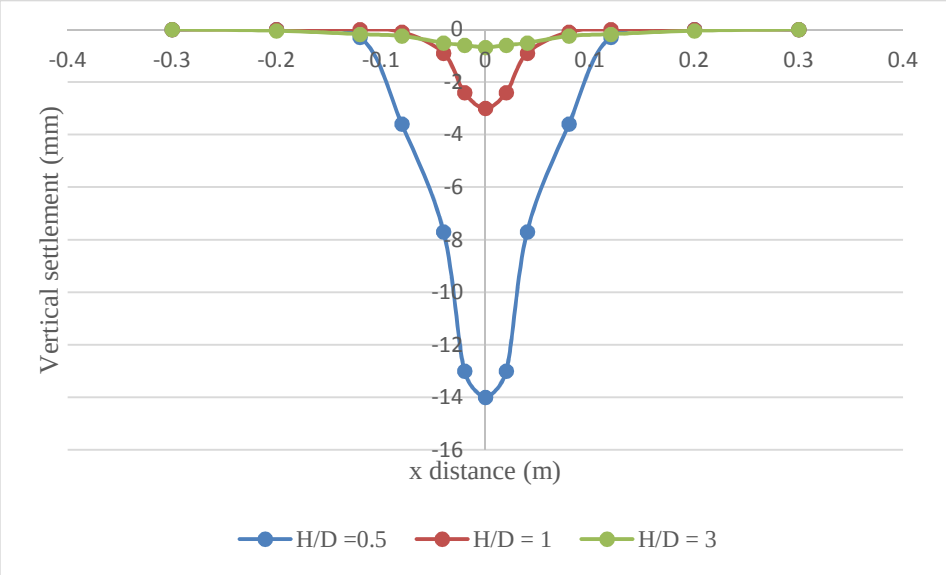

The results from both Potts (2007) and Strand 7 FEM simulations are similar to the laboratory experiment in terms of the inversely proportional

Figure 6.2: The soil surface deflections from Potts (2007) with an increasing H/D ratio

relationship that existed between the settlement and H/D ratio.

6.2.2 Magnitude of soil surface deflection:

A comparison between the Potts (2007) laboratory, FEM results and the Strand 7 FEM results in terms of the maximum soil surface deflections was summarised in Table 6.2.

Table 6.2: Maximum vertical soil settlement comparison between the maximum soil surface settlements obtained from the laboratory experiment, and the FEM model developed by Potts (2007) and Strand7.

Soil fill height/void diameter		**Maximum soil surface settlement, d_s (mm)**		
H/D	**Description**	**Potts laboratory results**	**Potts FEM (ICFEP)**	**Strand 7 FEM**
0.5	H = 80mm D = 160mm	14.014	10.022	8.938
1	H = 80mm D = 80mm	2.981	2.314	2.194
3	H = 240mm D = 80mm	0.651	1.201	0.836

The percentage difference between the laboratory data and the Strand 7 model were calculated and presented in Table 6.3.

Table 6.3: Maximum soil surface settlement comparison between the maximum soil surface settlements obtained from the laboratory experiment, the FEM model developed by Potts (2007) and Strand7 and the percentage difference.

		Maximum soil settlement (mm)		
H / D	**Details**	**Potts laboratory results**	**Strand 7 results**	**% Difference**
0.5	H = 80mm D = 160mm	14.014	8.938	36.220
1	H = 80mm D = 80mm	2.981	2.194	26.386

3	H = 240mm D = 80mm	0.651	0.836	28.488

		Maximum soil settlement (mm)		
H / D	**Details**	**Potts laboratory results**	**Potts FEM (ICFEP)**	**% Difference**
0.5	H = 80mm D = 160mm	14.014	10.022	28.486
1	H = 80mm D = 80mm	2.981	2.314	22.375
3	H = 240mm D = 80mm	0.651	1.201	45.795

The FEA results generated from both the ICFEP and Strand 7 were not highly accurate but were at least of the same order of magnitude as the laboratory results.

6.2.2.1 H = 80mm D = 160mm

Figure 6.3 below provided a visual representation of the comparison between the laboratory and two FEM model data for the H/D = 0.5.

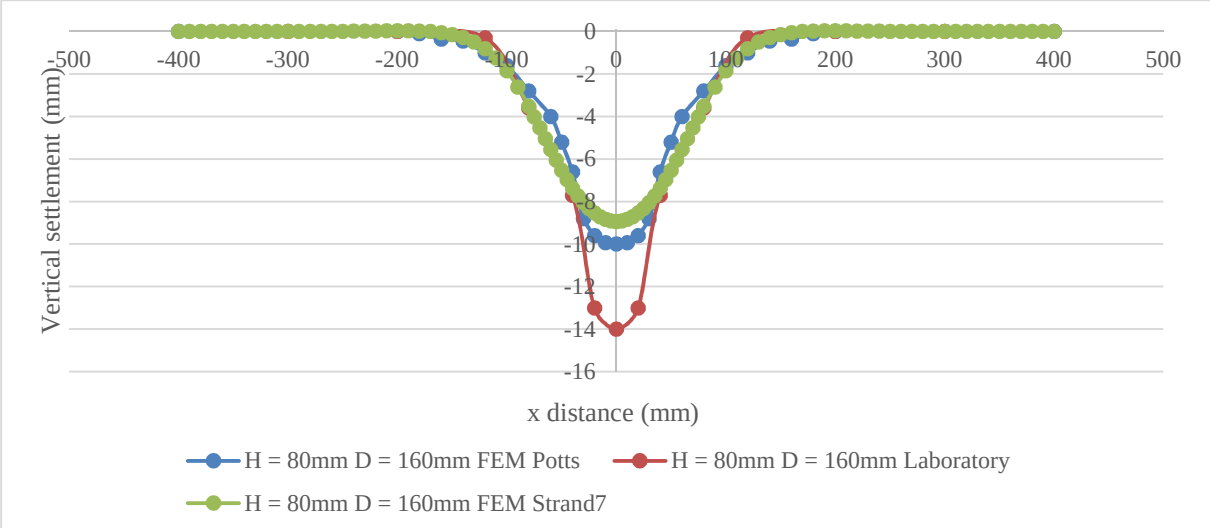

Figure 6.3 Soil surface deflection comparison between Potts (2007) laboratory and FEM model and the FEM model generated using Strand 7

Both FEM programs under predicted the settlement to a different degree. Potts (2007) attributed the under prediction of settlement to current material properties used in the FEM model. Improvement in the accuracy of the material properties should increase the accuracy of the results particularly in the case of the soil settlement. The same material properties were used in the Strand7 model, the results obtained are similar to those of the Potts (2007) FEM prediction and are lower than the actual laboratory values. The diameter of the cone is relatively constant in both the FEM models and the laboratory model.

6.3 Observations:

Potts (2007) concluded that the soil surface settlement predicted using the FEM program ICFEP was not highly accurate. The values were however at least in the same order of magnitude as the laboratory results. The FEM model results can be improved by adjusting the material properties of the model.

The material properties used in the Strand7 model were the same as the ICFEP model for consistency. A discrepancy between the laboratory predictions and the Strand7 model to about the same degree as the ICFEP model would thus be expected. After further tests Potts (2007) drew the conclusion that the ICFEP program tended to over predict the settlement for H/D ratios larger than 1. For smaller H/D ratios the program tended to under predict settlement values.

From the Strand7 model both the settlements and the resulting settlement cone diameter were under predicted. One factor that accounted for the under prediction of the soil surface deflection would be the occurrence of dilation in the soil mass modelled by Strand 7. Dilation is the change in volumetric strain with respect to the change in shear strain (Craig, 2004). In Section 2.4.7, the concept of dilation in soils was investigated. When shearing took place due to soil movement, the soil mass could either dilate or contract. This depended on how loose or dense the soil initially was. Hence dense soil will have the tendency to dilate/expand upon shearing. The soil used in Potts (2007) laboratory model was poured in loosely. Strand 7 automatically took soil dilation into account, by assuming that the angle of soil dilation is equal to the angle of shearing resistance. The degree of dilation assumed by the program may not necessarily be indicative of the actual dilation that occurred. The under prediction on the soil surface settlements was thus attributed to an over estimation of the amount of dilation that occurs in the soil mass by the program.

At this stage of the investigation it was concluded that Strand7 could be used to predict soil surface settlements when the soil experiences a void and was supported by a geogrid layer. The accuracy of the results however depended on the nature of the soil being modelled (dilative or non-dilative). Based on the conclusions obtained from the Potts (2007) case study, FEM modelling using Strand 7 continued and the de Lange (2016) laboratory experiment was investigated.

6.4 Numerical model results (de Lange, 2016)

Numerical models representing the laboratory tests described in Chapter 3 was developed using Strand 7. The experimental model provided information about the pattern of soil surface settlements. So in order to validate the numerical model, it was necessary to reproduce the deflection patterns as closely as possible. The numerical model only considered the experiments performed when reinforcement was present in the soil mass, as a fully unreinforced model resulted in convergence problems.

6.4.1 Finite element analysis simulation: Reinforced model

The inclusion of 1-6 geogrid layers were added to each H/D ratio of 1, 1.5 and 2 respectively. The method followed in developing the numerical model was covered in Chapter 5.

6.4.1.1 Results: Soil surface deflection: D = 150mm, H/D = 2

Figure 6.4 below shows the soil surface deflections predicted using FEA with 1 – 6 layers of reinforcement present.

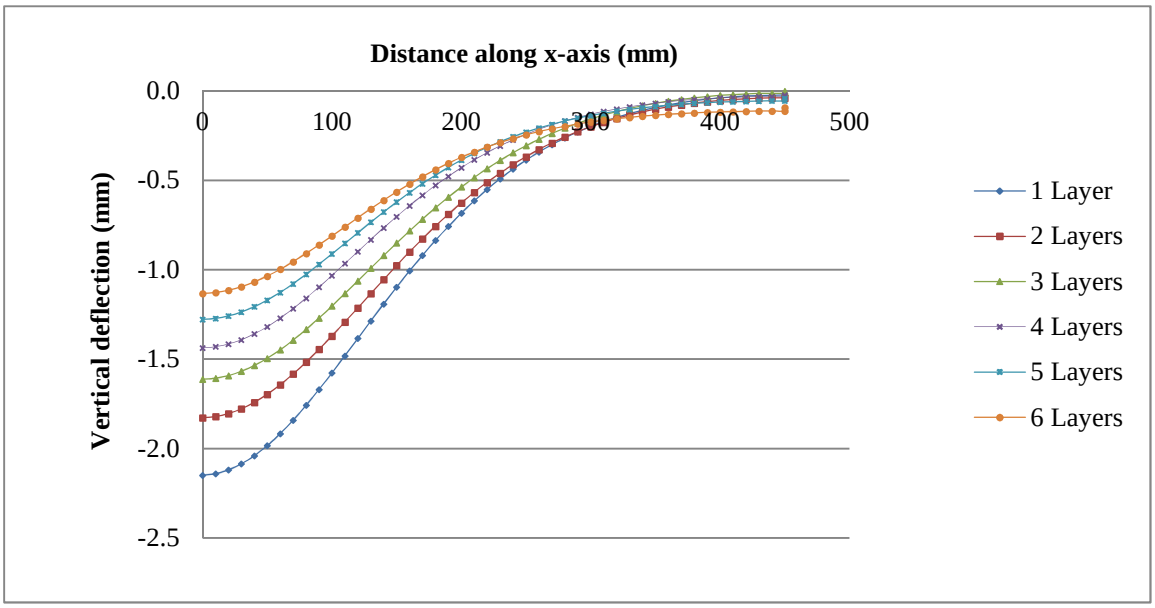

Figure 6.4: FEM simulation results for vertical soil surface settlements for an H/D = 2 with the inclusion of 1 – 6 layers of geosynthetic reinforcement.

As the number of reinforcement layers increased the surface deflection decreased to a smaller degree. The shape of the displacement cone was consistent throughout the inclusion of more geogrid layers, the settlement cone just became shallower.

6.4.1.2 Soil surface deflection: D = 200 mm, H/D = 1.5

Figure 6.5 shows the soil surface deflections obtained when the void diameter was increased to 200mm. The largest decrease in defection was seen when the second geogrid was placed. Each subsequent layer had a slightly diminished effect in decreasing the soil surface deflection.

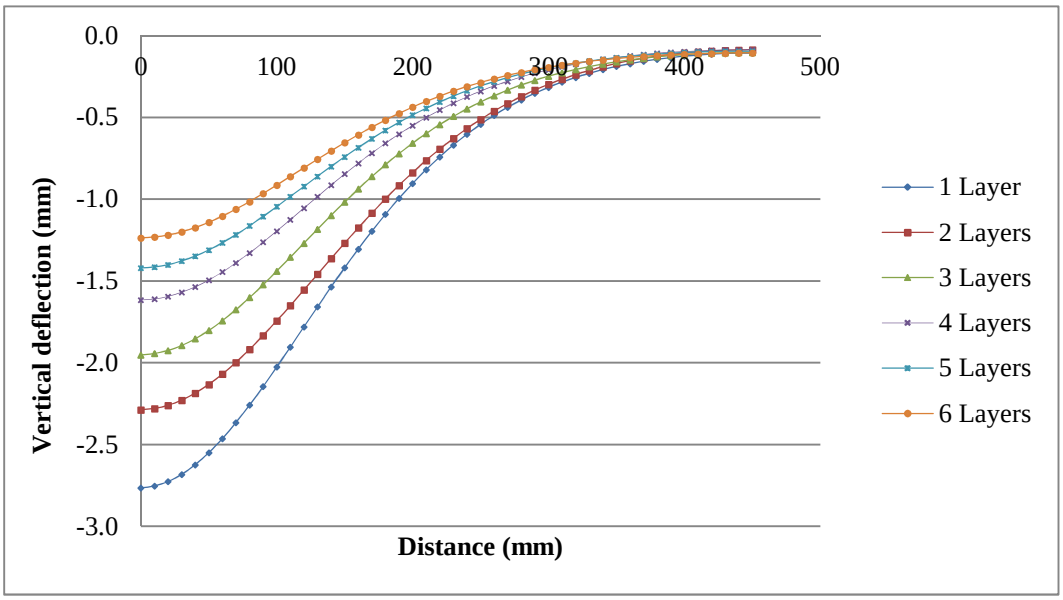

Figure 6.5: FEM simulation results for vertical soil surface settlements for an H/D = 1.5 with the inclusion of 1 – 6 layers of geosynthetic reinforcement.

The shape of the deflection cone again remained consistent throughout the simulation, while the cone became shallower.

6.4.1.3 Soil surface deflection: D = 300mm, H/D = 2

The diameter of the void was increased to 300mm.

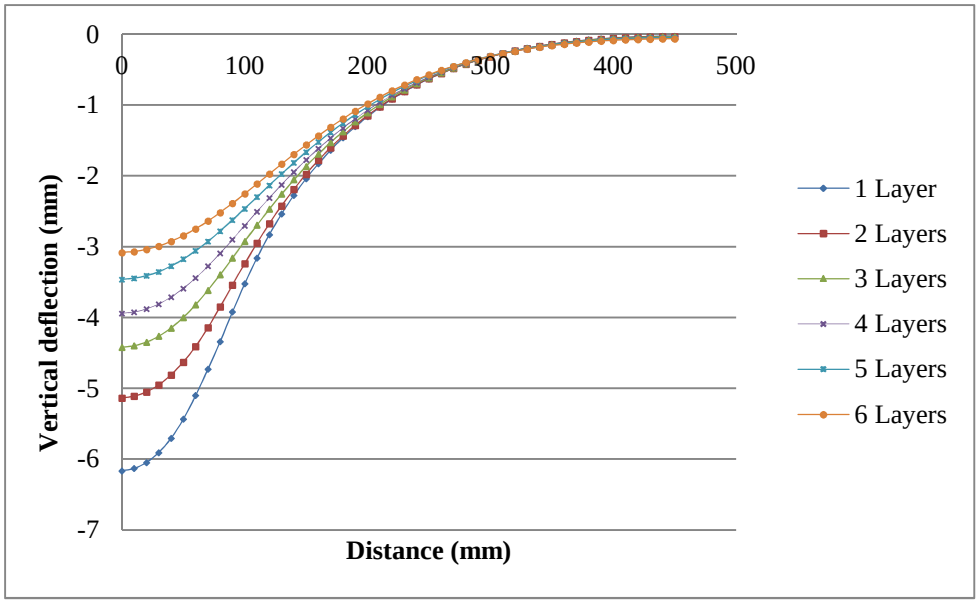

The deflection cone had the same shape in all three cases. Once again the 1st and 2nd layer had the largest affect in decreasing the

Figure 6.6: FEM simulation results for vertical soil surface settlements for an H/D = 2 with the inclusion of 1 – 6 layers of geosynthetic reinforcement.

soil surface settlements.

6.4.1.4 Soil surface deflections with an increase in void diameter

In this section the effect that the increasing void diameter had on the FEM soil surface deflections was considered. The soil surface deflections predicted by the FEM model increased with an increase in the void diameter as shown in Figure 6.7 below.

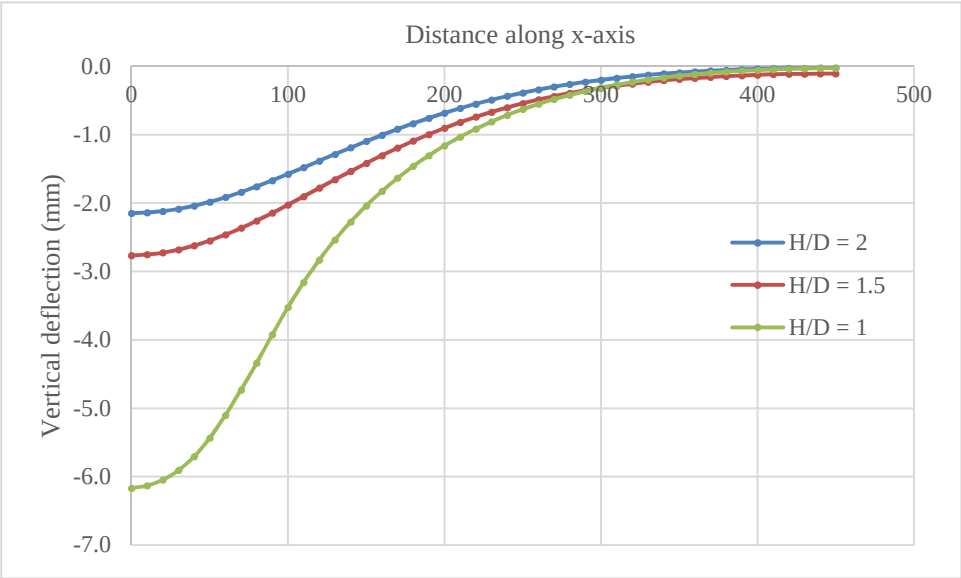

The diameter of the settlement cone appeared to be uniform but the cone became deeper with the increase in void diameter.

Figure 6.7: FEM soil surface deflection predicted using Strand 7 with change in the H/D ratio and a single layer of geosynthetic reinforcement

The trend in behaviour was the same as that observed in the experimental model, i.e. H/D increase resulted in a decrease in maximum surface settlement. Now that it's been established that the FEM model simulation behaved in a realistic manner, a comparison between the experimental data and numerical data took place.

6.5 Numerical model vs experimental model:

In section 6.5 the numerical model was compared to the experimental results in terms of the maximum vertical soil surface deflection as well as the shape of the settlement cone.

6.5.1 Soil surface deflection comparison

Figure 6.8 illustrated the soil surface deflections for both the numerical and experimental model, with 1 – 6 layers of geosynthetic reinforcement and an H/D = 1.5. The shape of the experimental model settlement cone was not uniform and varied when more reinforcement layers were placed. The FEM models settlement cone was parabolic throughout the simulation.

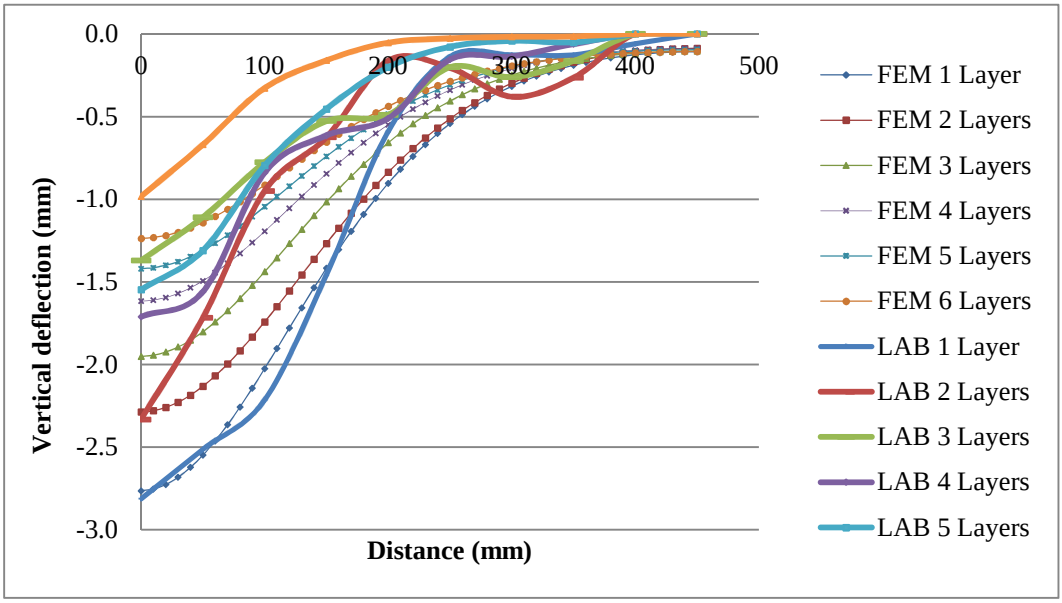

Figure 6.8: Vertical soil surface deflection of the numerical model compared to the experimental model with 1 – 6 layers of geosynthetic reinforcement and an H/D = 1.5 for de Lange (2016).

To get a better indication of the maximum soil surface settlements, the results for all H/D ratios were summarised in Table 6.4 below.

Table 6.4: Maximum surface deflection comparison between the numerical and experimental model with 1 – 6 layers of geosynthetic reinforcement de Lange (2016).

	Maximum surface deflection (mm) H/D = 2					
Number of layers	**1**	**2**	**3**	**4**	**5**	**6**
Laboratory	2.023	1.754	1.205	1.153	1.205	1.103
FEM	2.148	1.827	1.613	1.437	1.278	1.132
% Difference	6.199	4.186	25.276	19.742	5.715	2.656
Average %	**10.629**					
	Maximum surface deflection (mm) H/D = 1.5					
Number of layers	**1**	**2**	**3**	**4**	**5**	**6**
Laboratory	-2.812	-2.333	-1.370	-1.711	-1.547	-0.983
FEM	2.765	2.288	1.952	1.617	1.420	1.236
% Difference	1.612	1.822	29.806	5.760	9.146	20.729
Average %	**11.479**					
	Maximum surface deflection (mm) H/D = 1					
Number of layers	**1**	**2**	**3**	**4**	**5**	**6**
Laboratory	6.151	6.133	3.864	3.661	3.642	3.612
FEM	6.166	5.135	4.420	3.942	3.462	3.082
% Difference	0.257	16.225	12.663	7.153	5.156	17.143
Average %	**9.766**					

The maximum vertical soil surface deflection in the FEM model was smaller than the experimental model in most cases. There were various instances in which the experimental model did not behave as expected, and exhibited a sudden increase or decrease in maximum deflection with the inclusion of more geosynthetic layers. de Lange (2016) attributed this variation in results to the occurrence of soil arching in the experimental model. On average the numerical model shows a 10.624% variation when compared to the experimental data.

Figure 6.9 below shows the ratio of surface deflection to embankment height for all H/D ratios for the FEM model.

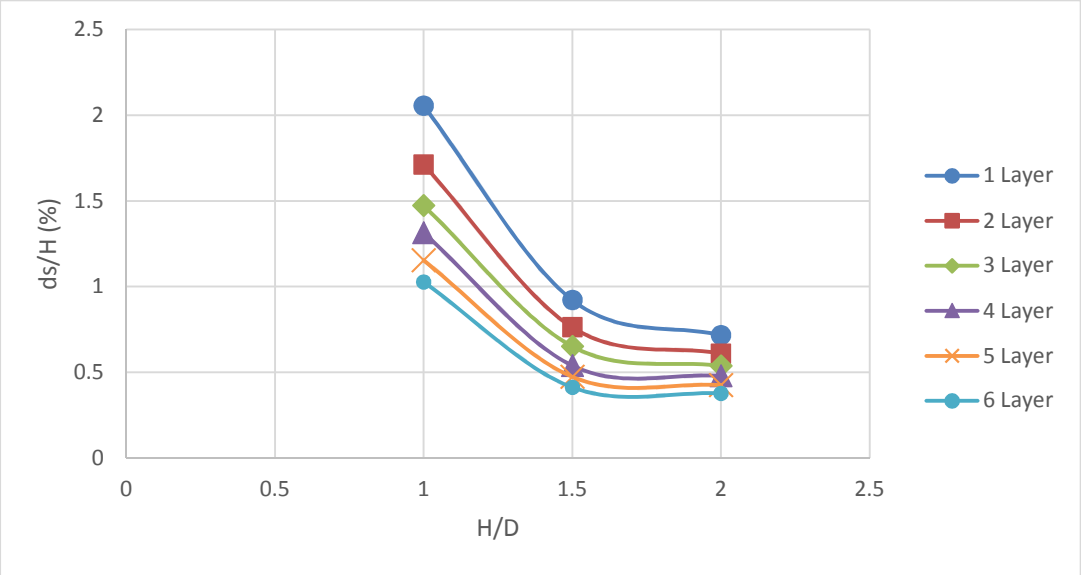

Figure 6.9 Maximum vertical deflections along the centreline at the 3 H/D ratios in the FEM model

When H/D = 1, the decrease in surface deflection with the inclusion of geosynthetic layers is most prominent, exhibiting a 50% reduction in settlements when multiple layers were present. For H/D = 2, the multiple layers of reinforcement are not as effective, and does not appear to provide any meaningful reduction beyond the third layer of reinforcement. This leads to the conclusion that multiple reinforcement layers have a more pronounced positive design effect in lower H/D ratios.

6.5.2 Deflection cone shape

No relationship could be drawn between the shapes of the deflection cone for the numerical and experimental model for this specific H/D ratio (1.5). To get a better indication of the settlement cone shape, Figure 6.10 below showed a comparison of results when H/D = 1. The experimental model in this case exhibited a parabolic cone no matter how many reinforcement layers were present. This cone shape was similar to that predicted by the FEM model.

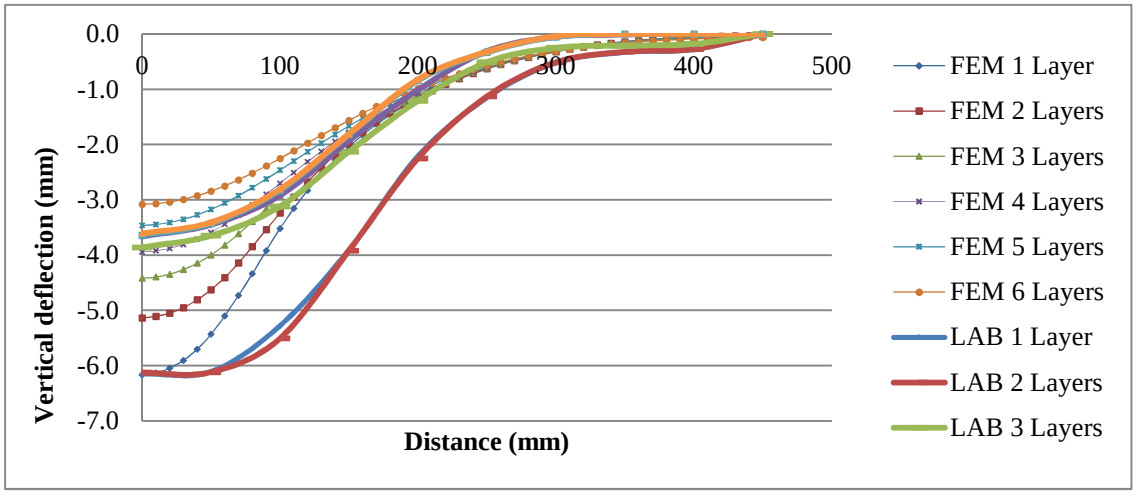

Figure 6.10: Vertical soil surface deflection of the numerical model compared to the experimental model with 1 – 6 layers of geosynthetic reinforcement and an H/D = 1 for de Lange (2016).

The angle of void propagation or angle of draw dictated the diameter of the soil surface settlement cone. This in turn played a role in selecting the dimensions of the geosynthetic reinforcement required on site and developing an economical design.

Table 6.5: Angle of draw comparison between numerical and experimental model with basal reinforcement

	Experimental model			
H/D	2	1.5	1	Average
D (mm)	150	200	300	
Ds (mm)	500	500	700	
Angle of draw (deg)	59.744	63.435	56.310	59.830
	Numerical model			
H/D	2	1.5	1	Average
D (mm)	150	200	300	
Ds (mm)	800	800	800	
Angle of draw (deg)	42.710	45.00	50.194	45.968

Table 6.5 above shows the angle of draw values for the numerical and experimental model, with a basal geosynthetic reinforcement layer. The numerical model predicted a wider and shallower deflection cone when compared to the experimental data.

6.5.3 Observations:

When comparing the experimental laboratory results with the FEA data it was observed that the FEM program under predicted the soil surface deflection in most cases. The exception being the outlying data points obtained when apparent soil arching took place in the experimental model. With the outlying data points taken into account the FEA soil surface deflection is on average 10.624% lower than the actual experimental soil deflection. The FEA results were of the same magnitude as the experimental data, but as stated earlier the soil deformations were under predicted to a certain degree. The shape of the settlement cone predicted by the numerical model was generally shallower and wider than the experimental result. This would result in a lower strength geotextile being used over a larger surface area in actual track conditions.

One of the limitations of using FEA as a means of soil movement prediction is that the flow of the soil particles when in motion was difficult to predict. The individual soil particles were shearing relative to one another, which could result in soil expansion/volumetric change. Similar to the results obtained from the Potts (2007) FEM model, the soil deflections were under predicted. This is again attributed to the over prediction of the soil dilation from the Strand 7 program.

It was observed at this stage that FEA could in fact be used to numerically model the behaviour of a reinforced soil fill layer undermined by a subgrade voids, the accuracy of the results however depended greatly on the parameters input in the system and the degree of soil dilation. In order to further investigate the effect that parametric changes had on the accuracy of the FEA predictions, certain model parameters were altered and the effect that the parameters had on the accuracy of the FEA results were observed.

6.6 Axisymmetric vs plane strain analysis

Axisymmetric analysis is used when the model is rotationally symmetric with respect to an axis, this provides a platform to model a 3D analysis as a 2D one. The previous FEM simulations used the axisymmetric analysis as this was the most appropriate means to model a circular void.

In plane strain analysis, it is assumed that the structures geometry is of infinite length normal to the plane section of the analysis. In order to investigate the behaviour of the model when subjected to a longitudinally shaped void, some of the models were analysed under plane strain conditions.

6.6.1 Results: Axisymmetric vs plane strain

In investigations carried out by Potts (2007) and Mifsud (2005) both plane strain and axisymmetric analysis were performed. The plane strain results predicted for the surface deflection as well as the geosynthetic strain/deflection were higher than the axisymmetric result. Potts (2007) then used plane strain conditions throughout the parametric modelling because plane strain analysis predicted the worst case scenario.

AXI = Axisymmetric, PS = Plane strain
Model used: H/D = 1 with single layer of reinforcement.

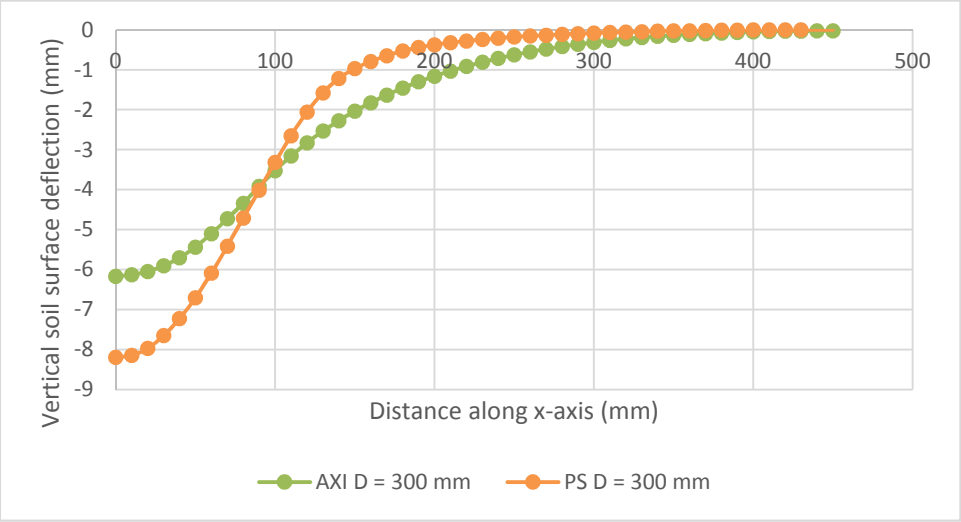

Figure 6.11: Comparison between soil surface deflections obtained when using both axisymmetric and plane strain analysis for a basally reinforced fill with an H/D ratio of 1.

In the FEM models plane strain analysis predicted a higher surface deflection than axisymmetric analysis, with a smaller deflection cone diameter

A similar result was

obtained when two layers of geosynthetic reinforcement were used. The general trend observed is that plane strain analysis tends to result in a deeper more concentrated soil settlement cone, which is more indicative of the actual cone obtained from the experimental model.

Table 6.6: Comparison between soil surface deflection values obtained for the experimental model, with axisymmetric and plane strain conditions.

Diameter of void (mm)	Maximum soil surface deflection (mm)		
	Experimental data	Numerical model	
		Axisymmetric	Plane strain
150	2.023	2.148	3.536
200	2.812	2.765	4.112
300	6.151	6.166	8.189

In

Table 6.6 the plane strain and axisymmetric results were then compared to the laboratory model. The plane strain model over predicts the surface deflection according to the laboratory model.

6.6.2 Conclusions: Axisymmetric vs plane strain

For this specific design the axisymmetric results were more accurate in terms of soil surface deflection predictions. In the previous FEM model performed in the Potts (2007) case study, plane strain analysis was used (as the Potts 2007 laboratory model geometry was more accurately described using plane strain conditions). In general plane strain analysis is used as it predicts a larger degree of soil deformation and failure is more likely to take place in a plane strain analysis than an axisymmetric one.

6.7 3D vs 2D FEM model

To this point plane strain and axisymmetric modelling have been represented in 2D simulations. A 3D model of the laboratory simulation was developed, using the same model characteristics as the 2D model and the results obtained from this analysis were compared. The 2D models provided a simplification of the actual 3D laboratory simulation. The aim of developing the 3D model was to confirm that the accuracy of results in the 2D analysis was not compromised by the assumptions made. It was expected that the 3D model generates the same results as the

axisymmetric model, as the axisymmetric model is a 2D representation of a rotationally symmetric 3D analysis.

6.7.1 Methodology: 3D Model

In the 3D model 8-noded hexahedron brick elements was used to represent the soil, and 3D membrane elements represented the geotextile layer. A cylindrical co-ordinate system was used with a radius of 450 mm. An H/D ratio of 1.5 was considered throughout the 3D analysis. The soil height was set in the z-direction as shown in Figure 6.12

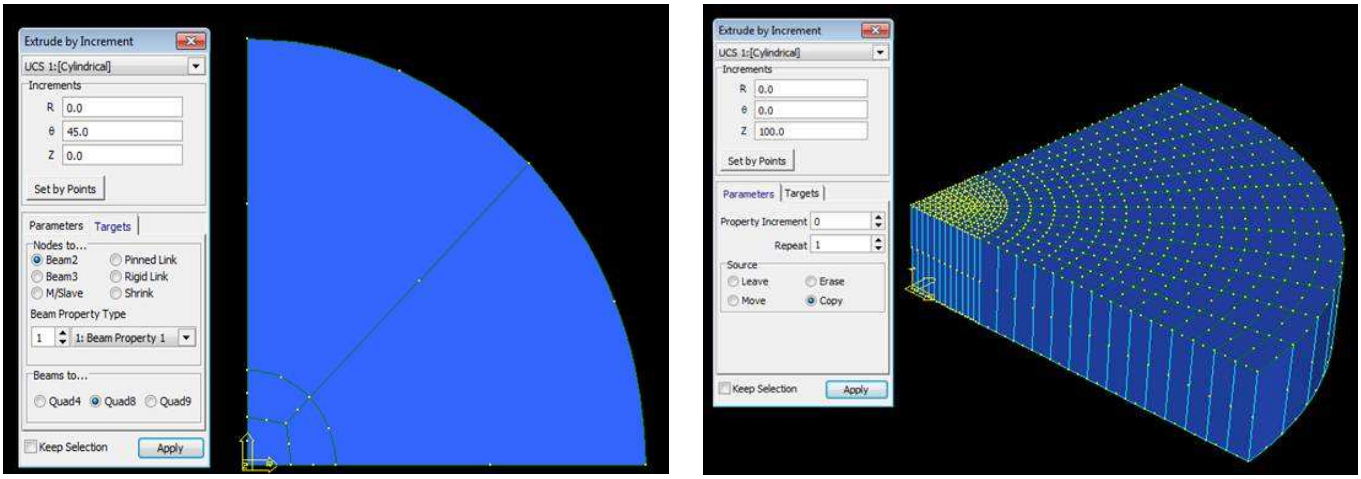

Figure 6.12: 3D model geometry representing the soil fill layer

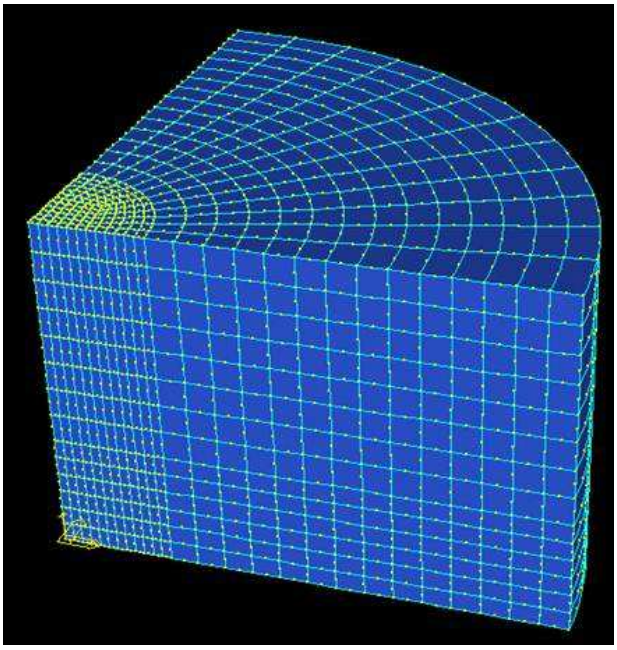

The restraint conditions were set and the soil material properties were input. The loading condition was set to gravitational loading

The geogrid and soil material properties were input into the program. Membrane elements were used to model geosynthetic reinforcement in Potts (2007) and Mifsud (2005).

Figure 6.13: Full 3D geometry

Geogrid layers were added into the 3D model to simulate multiple layers of reinforcement:

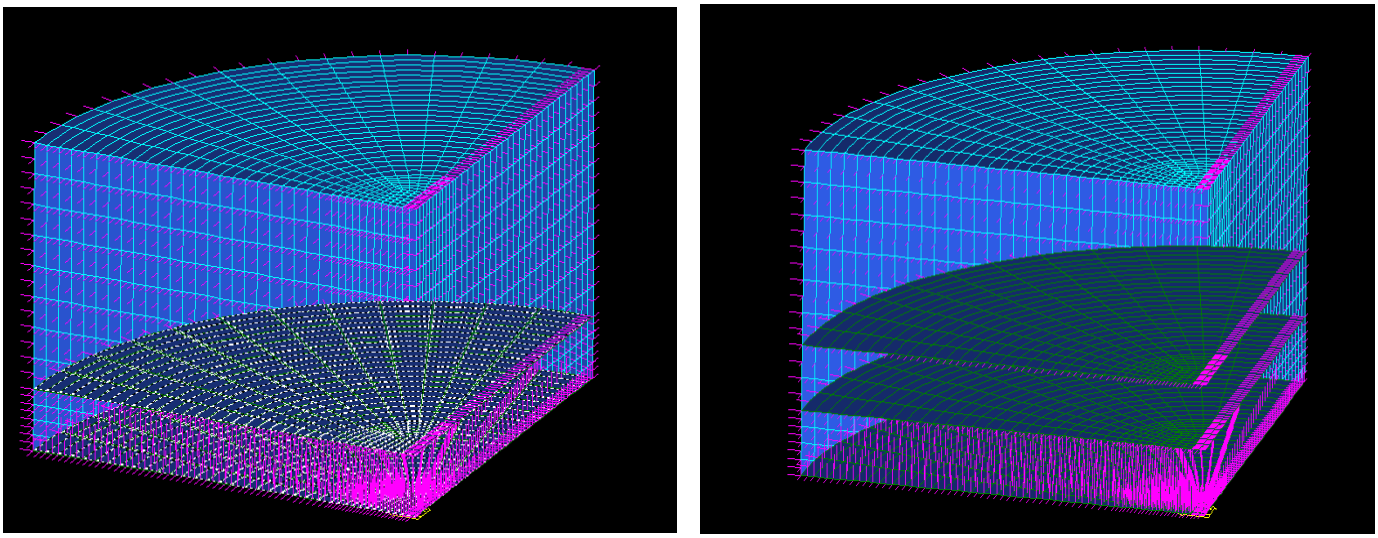

Figure 6.14: 3D model with geogrid reinforcement present

6.7.2 Results: 3D vs 2D Model

The maximum soil surface deflection obtained from the 2D and 3D analysis are compatible. The shape and diameter of the deflection cone also remained the same

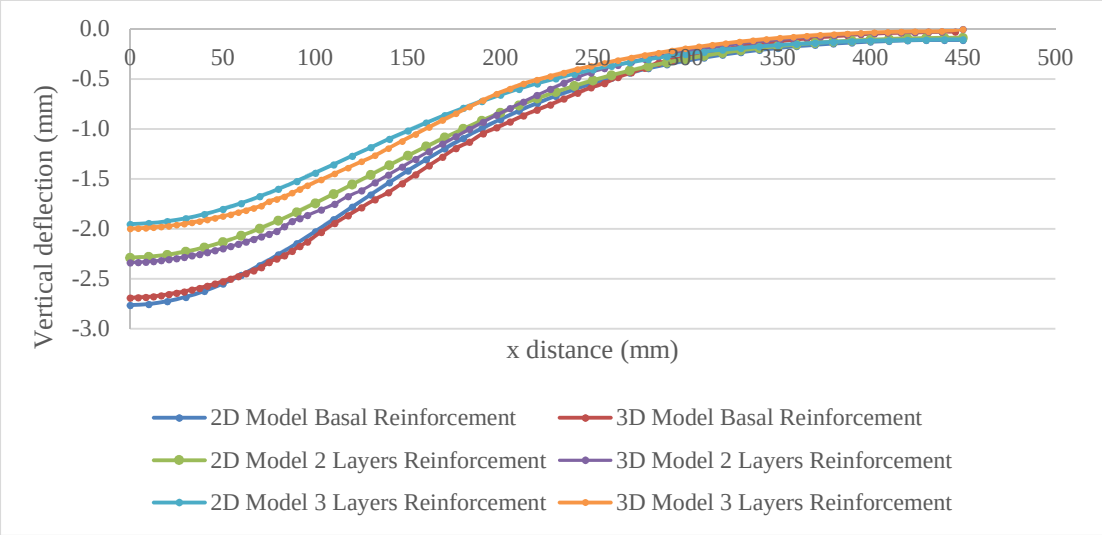

Figure 6.15 Comparison between soil surface deflection for a 2D and 3D model with 1- 3 layers of geosynthetic reinforcement and an H/D ratio of 1.5

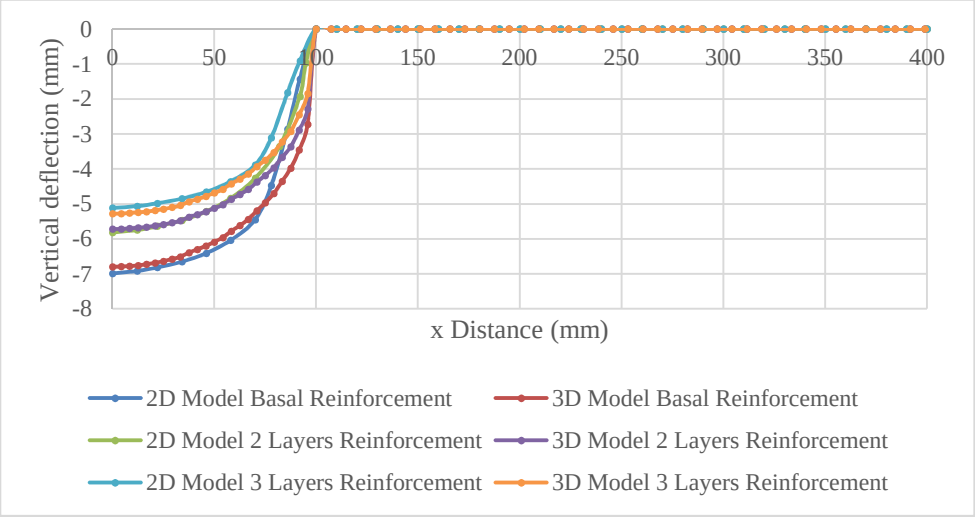

Figure 6.16 Comparison between geosynthetic deflection for a 2D and 3D model with 1- 3 layers of geosynthetic reinforcement and an H/D ratio of 1.5

The predicted geogrid deflection showed similar results. The deflected shape predicted in the 3D model was however slightly wider than the 2D model.

The magnitude of the geosynthetic displacement was the same in the 2D

and the 3D model, the geometry however differed slightly. The 3D model predicted a wider shape than the 2D model. The 2D vs 3D phase of the laboratory investigation proved that the 3D model can accurately predict geogrid and soil displacements. Further investigations with regard to 3D modelling took place in Chapter 7.

6.8 Summary of observations:

The results of the FEM representation and the experimental models demonstrated similar trends in behaviour. The deformed shape of the geosynthetic was parabolic, in keeping with the theoretical assumptions presented in SANS 207. The soil surface settlement tended to decrease with an increase in the H/D ratio, as similarly demonstrated in the experimental model. The maximum soil surface settlement values themselves were not highly accurate but were at least of the same order of magnitude as the experimental data. The results can be improved further by refining the material properties of the model. For our current purpose of validating FEM as a means of modelling a geosynthetically reinforced fill layer however the results were sufficiently accurate. The observations from the various models are summarised below:

- The FEM results showed a relatively uniform decrease in soil surface deflection with the addition of reinforcement layers. The decrease in deflection did however become less apparent when more geosynthetic layers were present.
- The FEM model tended to predict a shallower soil surface settlement cone acting over a larger area while the experimental data was more concentrated to the area directly above the void.
- The results predicted using plane strain analysis produced larger soil surface and geogrid deflections when compared to the axisymmetric analysis. The settlement cone geometry predicted used plain strain analysis was deeper and more concentrated to above the void alone, as predicted in the experimental model. This indicates that the plain strain conditions would provide a more accurate geometric representation of the deflection cone in future analysis.
- The soil surface deflections and geogrid deflections predicted were the same for 2D and 3D analysis, showing that the accuracy of results were not compromised in the simplified 2D model. The geogrid deflection shape was parabolic in both applications, the 3D models parabolic shape was however wider than the 2D models.

7. Chapter 7: APPLICATION TO VOIDS BELOW RAILWAY TRACKS

7.1 Introduction

Now that the use of FEM in modelling soil/geogrid systems has been validated, a parametric investigation took place. During the investigation various parameters in the FEM model were altered and the change that occurs to the results analysed and discussed. The theoretical behaviour of the soil mass when a change in certain parameters took place, e.g. frictional angle, Young's modulus can be predicted using soil theory. But the degree to which changing the parameters will affect the results obtained is unknown. The parametric stage of the investigation thus observed the effect that the following parameters had on the results produced by the FEM method.

7.1.1 Soil properties

- Young's modulus
- Soil frictional angle
- Coefficient of earth pressure

7.1.2 Geogrid properties

- Geogrid tensile strength
- Geogrid position
- Number of geogrid layers

7.2 Parametric model description:

The objective of this study was to develop a cost effective means of reinforcing a sand mass to prevent catastrophic collapse of a rail track when undermined by the development of a sinkhole. The study was conducted using a FEM numerical model of a rail track structure over a reinforced sand mass. The model structure was a standard South African heavy haul line as set out by Transnet's manual for track maintenance.

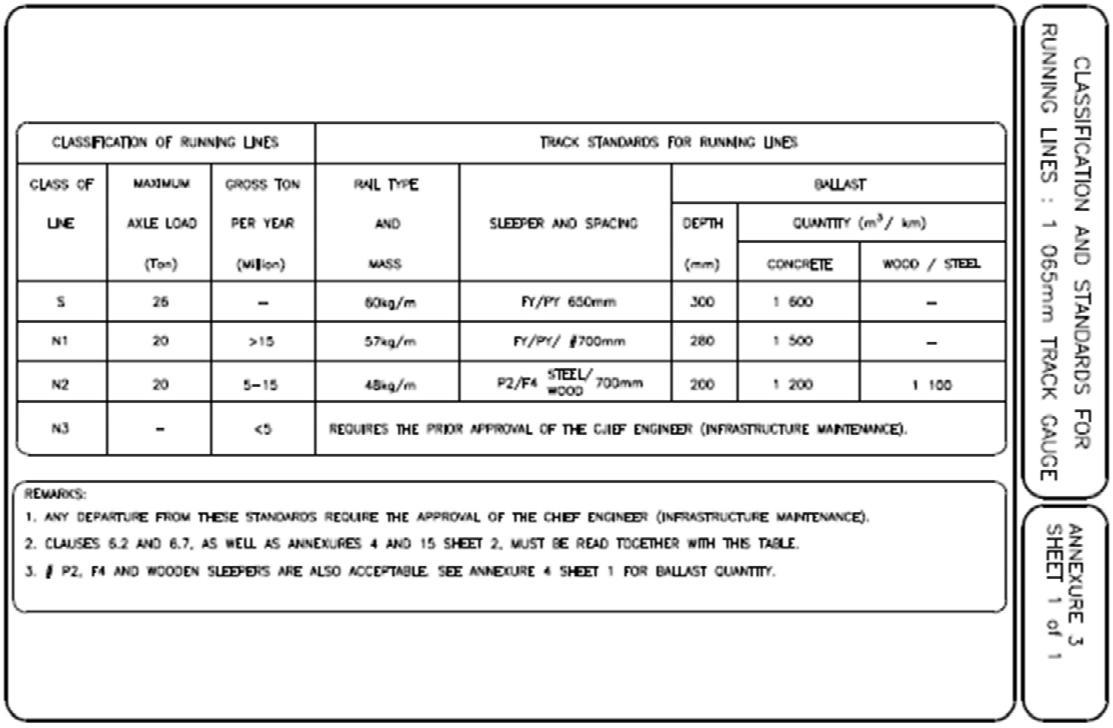

CLASSIFICATION AND STANDARDS FOR RUNNING LINES : 1 065mm TRACK GAUGE

ANNEXURE 3
SHEET 1 of 1

CLASSIFICATION OF RUNNING LINES			TRACK STANDARDS FOR RUNNING LINES				
CLASS OF LINE	MAXIMUM AXLE LOAD (Ton)	GROSS TON PER YEAR (Million)	RAIL TYPE AND MASS	SLEEPER AND SPACING	BALLAST		
					DEPTH (mm)	QUANTITY (m^3/ km)	
						CONCRETE	WOOD / STEEL
S	26	–	60kg/m	FY/PY 650mm	300	1 600	–
N1	20	>15	57kg/m	FY/PY/ #700mm	280	1 500	–
N2	20	5–15	48kg/m	P2/F4 STEEL/WOOD 700mm	200	1 200	1 100
N3	–	<5	REQUIRES THE PRIOR APPROVAL OF THE CHIEF ENGINEER (INFRASTRUCTURE MAINTENANCE).				

REMARKS:
1. ANY DEPARTURE FROM THESE STANDARDS REQUIRE THE APPROVAL OF THE CHIEF ENGINEER (INFRASTRUCTURE MAINTENANCE).
2. CLAUSES 6.2 AND 6.7, AS WELL AS ANNEXURES 4 AND 15 SHEET 2, MUST BE READ TOGETHER WITH THIS TABLE.
3. # P2, F4 AND WOODEN SLEEPERS ARE ALSO ACCEPTABLE. SEE ANNEXURE 4 SHEET 1 FOR BALLAST QUANTITY.

Figure 7.1: Transnet classification of rails as per the Track maintenance manual (Transnet Freight Rail BBB0481, 2012)

For a standard S-class line a 60 kg/m rail will be used paired with FY sleepers at a spacing of 650mm with a ballast depth of 300mm.

The axle loading used is 26T, the maintenance manual states that the maximum loading is 25T but the manual is currently under review and an updated value of 26 and 30T can be carried on 60kg rails.

7.2.1 Rail line characteristics:

Rail: 60 kg/m

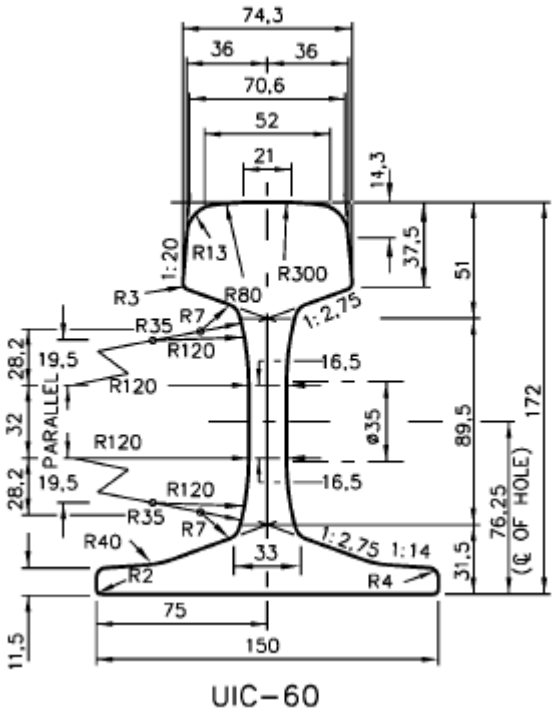

Figure 7.2 Cross section of UIC-60 Rail (Transnet Freight Rail BBB0481, 2012)

The structural properties of the rail section used in the FEM model were developed from the dimensions shown in Figure 7.2 above. Some approximation was necessary due to the complexity of the section.

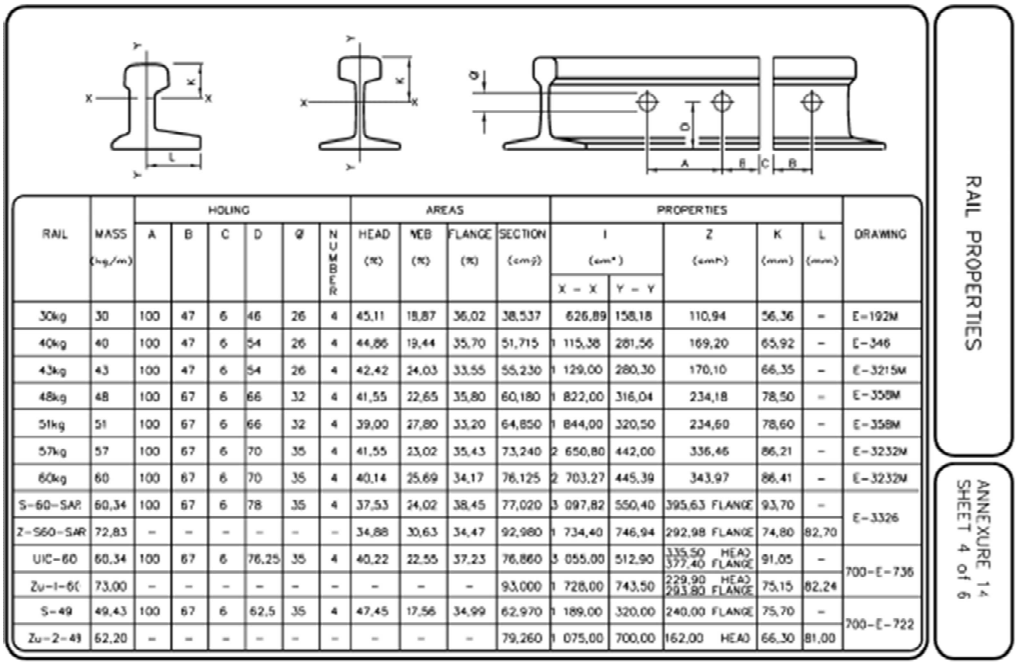

RAIL PROPERTIES

ANNEXURE 14
SHEET 4 of 6

RAIL	MASS (kg/m)	HOLING A	B	C	D	Ø	NUMBER	AREAS HEAD (%)	WEB (%)	FLANGE (%)	SECTION (cm²)	PROPERTIES I (cm⁴) X – X	Y – Y	Z (cm³)	K (mm)	L (mm)	DRAWING
30kg	30	100	47	6	46	26	4	45,11	18,87	36,02	38,537	626,89	158,18	110,94	56,36	–	E-192M
40kg	40	100	47	6	54	26	4	44,86	19,44	35,70	51,715	1 115,38	281,56	169,20	65,92	–	E-346
43kg	43	100	47	6	54	26	4	42,42	24,03	33,55	55,230	1 129,00	280,30	170,10	66,35	–	E-3215M
48kg	48	100	67	6	66	32	4	41,55	22,65	35,80	60,180	1 822,00	316,04	234,18	78,50	–	E-358M
51kg	51	100	67	6	66	32	4	39,00	27,80	33,20	64,850	1 844,00	320,50	234,60	78,60	–	E-358M
57kg	57	100	67	6	70	35	4	41,55	23,02	35,43	73,240	2 650,80	442,00	336,46	86,21	–	E-3232M
60kg	60	100	67	6	70	35	4	40,14	25,69	34,17	76,125	2 703,27	445,39	343,97	86,41	–	E-3232M
S-60-SAR	60,34	100	67	6	78	35	4	37,53	24,02	38,45	77,020	3 097,82	550,40	395,63 FLANGE	93,70	–	E-3326
Z-S60-SAR	72,83	–	–	–	–	–	–	34,88	30,63	34,47	92,980	1 734,40	746,94	292,98 FLANGE	74,80	82,70	
UIC-60	60,34	100	67	6	76,25	35	4	40,22	22,55	37,23	76,860	3 055,00	512,90	335,50 HEAD 377,40 FLANGE	91,05	–	700-E-736
Zu-I-60	73,00	–	–	–	–	–	–	–	–	–	93,000	1 728,00	743,50	229,90 HEAD 293,80 FLANGE	75,15	82,24	
S-49	49,43	100	67	6	62,5	35	4	47,45	17,56	34,99	62,970	1 189,00	320,00	240,00 FLANGE	75,70	–	700-E-722
Zu-2-49	62,20	–	–	–	–	–	–	–	–	–	79,260	1 075,00	700,00	162,00 HEAD	66,30	81,00	

Figure 7.3 Rail geometric properties as per Track maintenance manual (Transnet Freight Rail BBB0481, 2012)

According to the Manual for track maintenance the cross sectional area of a 60kg rail should be 76.125 cm^2. In the rail section developed for the FEM model the cross sectional area of the rail was 76. 673 cm^2, a 0.7% difference in cross sectional area.

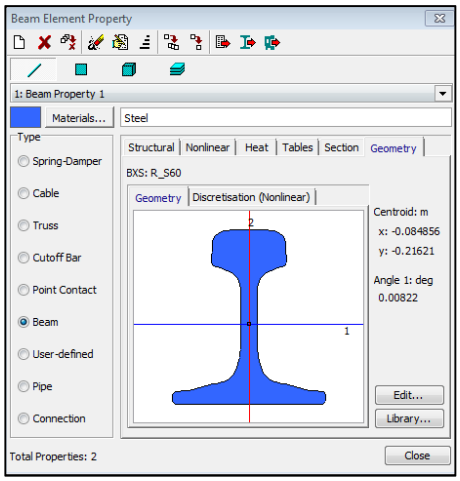

Figure 7.4: Rail cross section generated using Strand 7

7.2.2 Sleeper characteristics:

SLEEPER DETAIL : GENERAL

ANNEXURE 30
SHEET 1 of 7

SLEEPER	TYPE	LENGTH (mm)	WIDTH (mm)	HEIGHT (mm)	MASS (kg)	REFERENCE DRAWING
P2	CONCRETE	2 057	254	230	215	E-3303 SH 1
PY	CONCRETE	2 200	300	232	278	E-3318 SH 1
F4	CONCRETE	2 057	254	244	215	E-3303 SH 2
FY	CONCRETE	2 200	300	258	282	E-3318 SH 2
WOOD	LAMINATED	2 100	250	195	72	———
WOOD	LAMINATED	2 400	250	195	82	———
WOOD	LAMINATED	2 700	250	195	92	———
WOOD	LAMINATED	3 000	250	195	102	———
WOOD	LAMINATED	3 400	250	195	116	———
WOOD	LAMINATED	3 800	250	195	130	———
WOOD	LAMINATED	4 200	250	195	143	———
WOOD	LAMINATED	6 000	250	195	205	———
STEEL	———	2 060	260	87	63	E-3277
UNIVERSAL	CONCRETE	2 100	200			———
WOOD	HARD	2 100		150		———

Figure 7.5: Transnet standard sleeper detail (Transnet Freight Rail BBB0481, 2012)

A standard FY concrete sleeper, as sketched in elevation Figure 7.6 has an average estimated cross sectional area of the sleeper of 768700 mm^2.

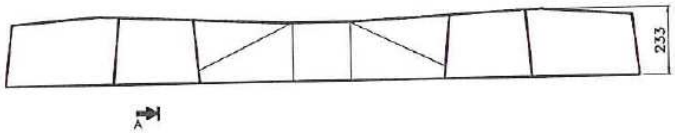

Figure 7.6: Standard rail transition sleeper

The rectangular section used in the FEM program has a height of 300mm and a width of 275mm. The cross sectional area of 82500 mm^2, was higher than the actual cross sectional area to preserve the similarity of the elastic characteristics of the prototype sleeper.

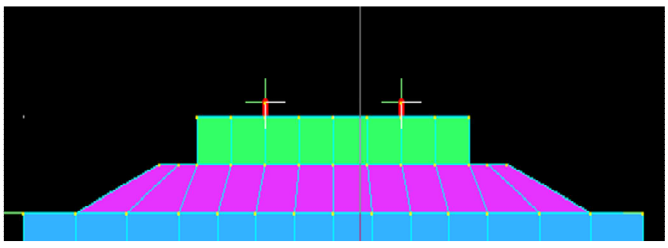

Figure 7.7: FEM cross section of sleeper, ballast and SSB layer

7.2.3 Parametric model properties:

The following material properties were used for the parametric study: (Refer to Table 7.3 for soil layer nomenclature). Values for the formation layers Young's modulus and Poisson's ratio were taken from past studies performed on Transnet lines by Grabe (2003).

Table 7.1 Parametric model properties of formation layers

Soil layer	Depth (mm)	E (MPa)	Poisson's ratio	Soil density (kg/m^3)
SSB	200	160	0.3	1900
SB	200	50	0.3	1950
A	200	20	0.3	1950
B	200	10	0.3	1950
BE	1200	5	0.3	1870
Ballast	200	200	0.35	1850

Table 7.2: Parametric model properties of superstructure

Track super-structure	E (MPa)	Poisson's ratio	Density (kg/m^3)	fc (MPa)
Sleeper	36000	0.2	2400	32
Rail	200000	0.25	7870	_

The sub-structure characteristics are for a formation level beneath a national heavy haul line with a 26T axle load taken from Transnet's S410 specification.

Table 7.3 Formation layer properties according to Transnet's specification S410 (Transnet Limited S410, 1990)

	LAYER	MATERIAL PROPERTIES										
		SAR INDEX	MINIMUM GRADING MODULUS						PI	MAXIMUM CBR SWELL	MINIMUM COMPACTION % OF MODIFIED AASHTO DENSITY	MINIMUM STRENGTH AFTER COMPACTION CBR
				75	13,2	2,0	0,425	0,075		%		
BALLAST	SSB	<50	2,0	100	60-85	20-50	10-30	5-15	3 - 10	0,5	98	60 (1,5-3Mpa) •
SUB	SB	<80	1,8	100	70-100	20-60	10-40	5-20	3-10	0,5	95	30+ (1,5-3Mpa) •
	A	<110	1,0	-	-	-	-	<40	<12	-	95 100*	20
	B	<155	0,5	-	-	-	-	<70	<17	-	93 98*	10
BULK	EARTHWORKS	-	-	-	-	-	-	-	<25	2	90 95*	5

*These densities apply to non-cohesive soils.

• . Strengths in brackets apply in place of CBR values when sub-ballast is stabilised.

+ Increase to 45 in the absence of layer SSB unless otherwise specified. (Increase not normally required in dry areas).

NOTE: See Appendix A for comparable road materials. The classifications shown may be used by the Contractor at his discretion when preparing preliminary assessments of acceptability of materials for use in the listed layers.

7.2.4 Geosynthetic reinforcement properties:

7.2.4.1 Geosynthetic characteristics:

The existing design guide for a geosynthetically reinforced fill layer is SANS 207 for the South African environment. Chapter 4 concluded that SANS 207 generally over estimates the surface area affected by the presence of the void and did not provide sufficiently accurate results. Due to this, the geosynthetic tensile strength was selected based on available products.

Previous studies performed by Jaros et al. (2009) employed the use of Kaytech's geosynthetic products when reinforcing the Gautrain line against sinkholes. The geosynthetic characteristics are shown in Table 7.4 below:

Table 7.4: Commercially available bi-directional polyester grids

Long term tensile resistance (kN/m)	Ultimate short term tensile resistance Tu (kN/m)	Thickness (mm)	Density (kg/m^3)
26	50	2	150
52	100	2	150
105	200	3	150

Creep and time dependent stresses are used in long term solutions, the geosynthetic solution proposed is a short term means of preventing catastrophic collapse. The long term tensile strength takes creep, environmental conditions and long term damage into account hence Tu will not be factored by safety coefficients. A tensile strength of 100 kN/m was selected for the parametric model, in the further investigation phase other tensile strengths were investigated. Full details of the geosynthetic material properties are contained in Appendix A.

7.2.5 Model limitations:

7.2.5.1 Maximum rail stress:

A maximum rail stress of 120 MPa is allowable on heavy haul lines (see section 7.4.1.1)

7.2.5.2 Maximum ballast bed deformation:

The allowable deformation in ballast beds as per the specifications set out in Section 2.8.1. SANS 207 was as follows:

$$\frac{d_s}{D_s} \leq 0.002$$

A similar ballast bed deformation was employed in the German design guide EBGEO: 2011 for heavy haul lines.

$D_s = D + (2H/\tan\theta_d)$

D = Selected sinkhole diameter, 2m (Sinkhole diameter selected depends on the geological history of the selected site)

H = SSB H + SB H + A H+ B H

= (200 + 200+ 200+200) mm

= 0.8 m

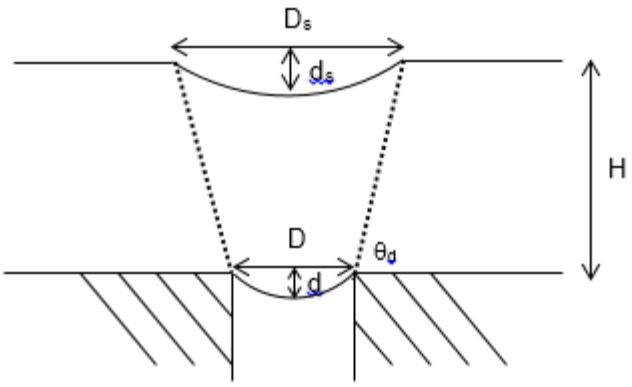

Figure 7.8 Upward propagation of a subgrade void assumed geometry (South African National Standard SANS 207, 2006)

In SANS 207 the angle of draw is equal to the frictional angle of the soil above the geogrid layer, the material above the geogrid layer has varying properties in terms of the frictional angle. From previous investigations performed by de Lange (2016) a value of 60^0 is used. Hence θ_d = $60^{0.}$ The maximum diameter of the settlement trough Ds =

$D_s = D + (2H/\tan\theta_d)$

$= 2 + (2*0.8/\tan(60^0))$

= 2.924 m

$$\frac{d_s}{D_s} = 0.002$$

Hence the maximum ballast bed settlement

$d_s = 2.924*0.002$

= 5.847 mm

7.3 Methodology:

When developing the parametric model, the first step is to construct a suitable geometric representation of the problem. The development of the model geometry included the following elements: Rail, sleeper, ballast, SSB, SB, A, B and BE soil layer. The geometric characteristics of the layer works are set out in Table 7.1.

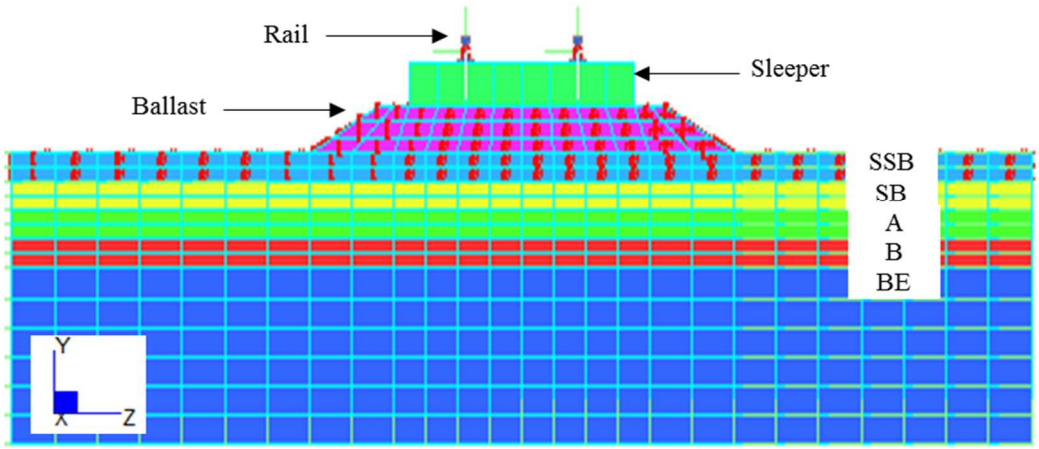

Figure 7.9: Cross section of parametric model in YZ Plane

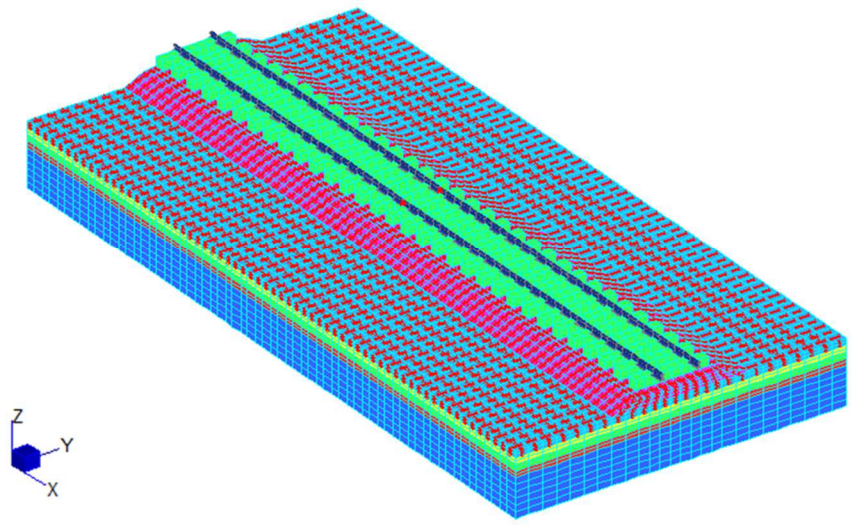

Figure 7.10: Parametric model 3D

Figure 7.9 & Figure 7.10 above show the cross sectional and 3D view of the model geometry used.

7.3.1 Parametric model mesh:

The geometry of the mesh was selected such that the ballast, sleeper and rail were aligned to one another, to ensure compatibility of the mesh. The geometry of the mesh of the various track elements is shown in Figures 7.11 – 7.13 below:

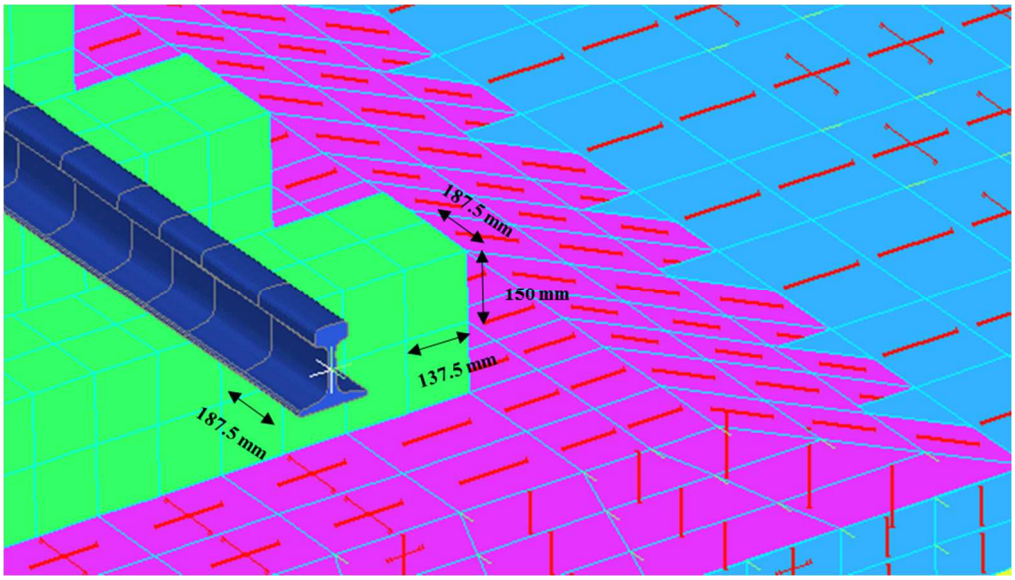

Figure 7.11: Mesh geometry of concrete sleeper in parametric model

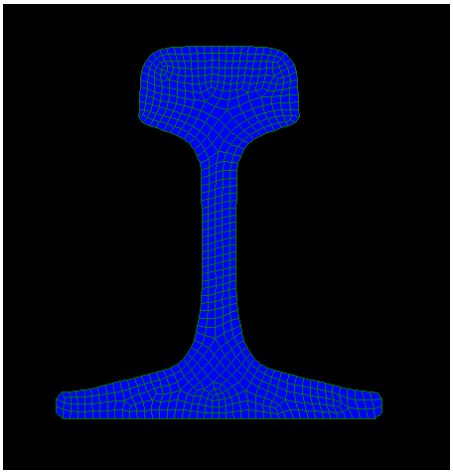

Figure 7.12: Mesh geometry of rail

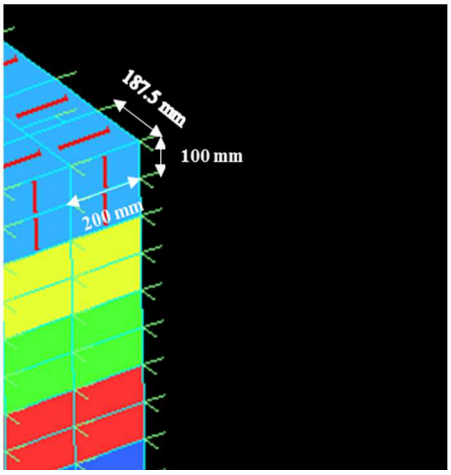

Figure 7.13: Mesh geometry of formation layers

One of the factors that affected the computational time of 3D models was the density of the mesh. Due to the size of the model a smaller mesh greatly increased the running time, resulting in simulations taking several hours. The dimensions shown above are the minimum mesh sizes that give a relatively reasonable 3D model computational time of an hour.

7.3.2 Type of element:

- The soil was modelled using 8-noded brick elements.
- The geogrid is modelled using a 3D membrane element.

In 3D applications where fabric type structures need to be modelled, Strand 7 uses 3D membrane elements. 3D membranes carry in plane stresses alone and have no bending stiffness. The use of membrane elements in modelling geosynthetics was validated in previous studies Potts (2007), Mifsud (2005), Grabe (2003).

7.3.3 Restraint conditions:

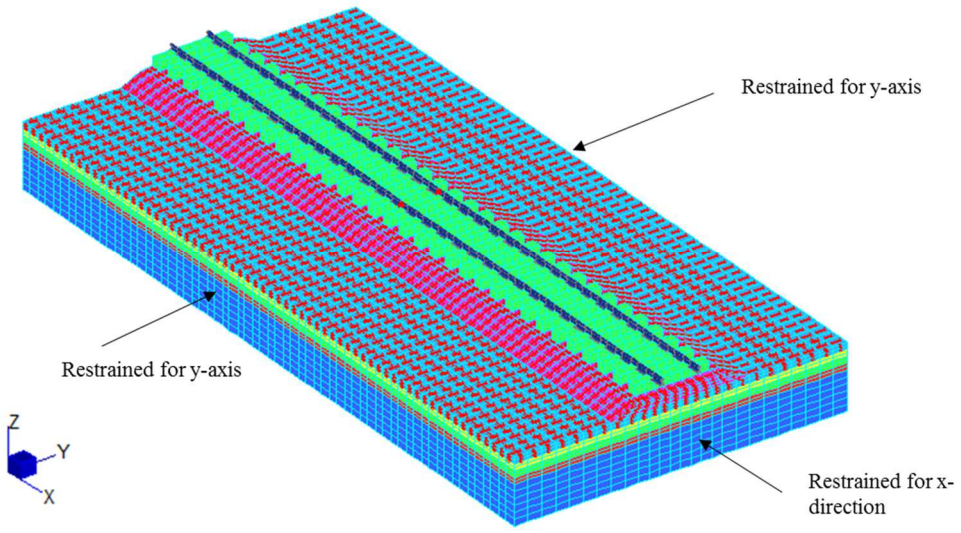

Figure 7.14: Restraint conditions used in the parametric model

The boundary of the model was restrained from horizontal movement but free in the vertical z-direction.

7.3.4 Loading conditions:

The line load was 26T for a 60kg/m heavy haul rail line. A 13T axle load was added to both rail line 1 and line 2. The loading cases were considered as a rolling load present on the sleeper and between the sleepers. There were 60 load cases considered in total (See Appendix B).

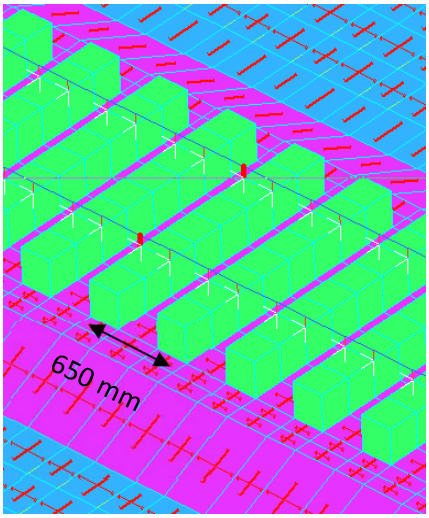

The load applied to the model was a static load applied in "stages". A dynamic load would be more appropriate, however only a static mode was provided in this specific Strand 7 program package. Applying the static load in moving stages however accounted for the movement of the wheel axle load when passing over the rail line. The sleepers in the parametric model are spaced at 650mm at each loading stage in the model, the axle load was applied either onto the sleeper or in the 650mm section between the sleepers.

Figure 7.15: Sleeper spacing used in all parametric models

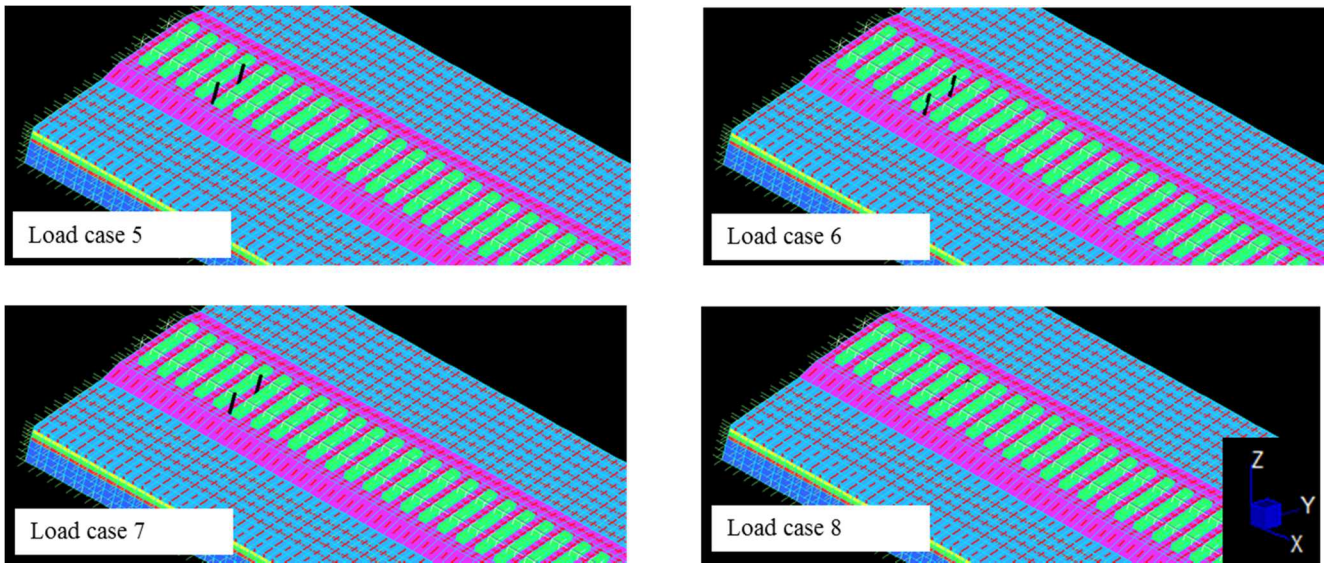

Figure 7.16: Load cases position along rail line

The position along the x-axis and the vertical loading are shown in Appendix B.

7.3.5 Void formation:

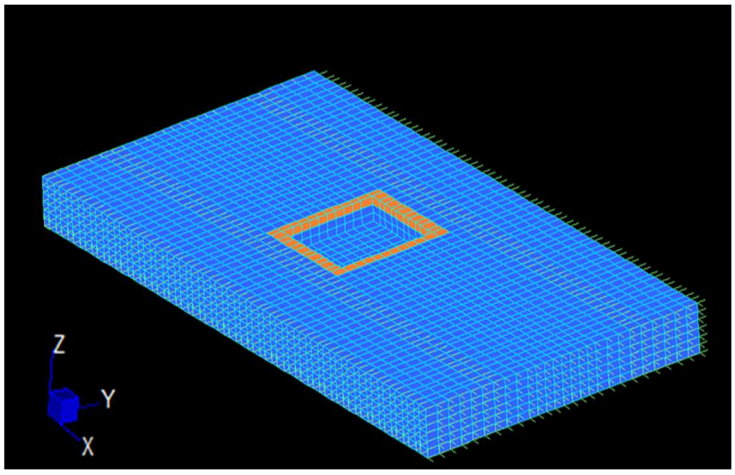

After the model geometry, restraint and loading conditions were developed, the void was formed. A 2 x 2 m void was created in the pre-existing bulk earthworks layer that supports the engineered fill layers above. The void was positioned directly underneath the rail line for maximum effect.

Figure 7.17 Void developed within the bulk earth works layer (natural formation) beneath the engineered formation fill layers of the parametric model

A geogrid layer represented by 3D membrane reinforcement was positioned above the void.

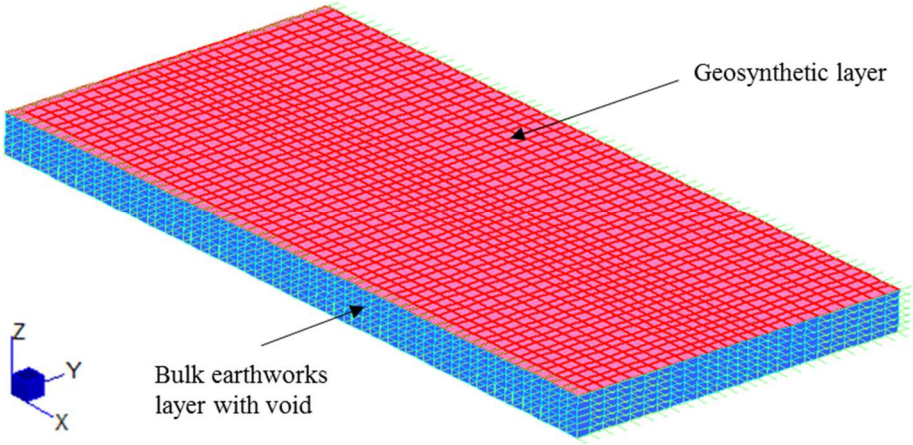

Figure 7.18: Geogrid reinforcement positioning above the void in the parametric model

The reinforcement was unrestrained along the edges such that movement and interlocking was allowed between the soil and the geosynthetic.

7.4 Results parametric study:

7.4.1 Reference model:

The reference model was a formation level, ballast, sleeper and rail model with no void or geogrid reinforcement. The model was developed so that a reference point for rail deflection is observed and the results between a geogrid reinforced formation level and a non-reinforced formation level are compared.

The following results were observed in the reference model:

- Maximum rail deflection
- Maximum rail stress
- Maximum formation level deflection

7.4.1.1 Model limits:

Rails are made of structural steel with a yield strength of 830 MPa. Due to the dynamic loading the line was constantly undergoing, a safety coefficient of 1/3 is multiplied to the steels ultimate tensile strength to prevent rail fatigue. The presence of welds in the rails was also taken into account by multiplying the rail UTS by a value of 0.6. The rail experienced longitudinal stresses due to temperature increase and an additional safety coefficient of 0.75 is used. Hence the serviceability limit on the rail becomes: UTS*0.333*0.6*0.75 = 124.3 MPa, the stress limit in rails was thus taken as 120 MPa.

7.4.1.2 Rail deflection:

The results in terms of rail deflection are shown in Figure 7.19 & Figure 7.20 below. A maximum rail displacement of 2.175 mm was predicted by the FEM model. The rail showed an uplift of 0.1 mm before the maximum rail deflection, this was due to the longitudinal forces in the rail.

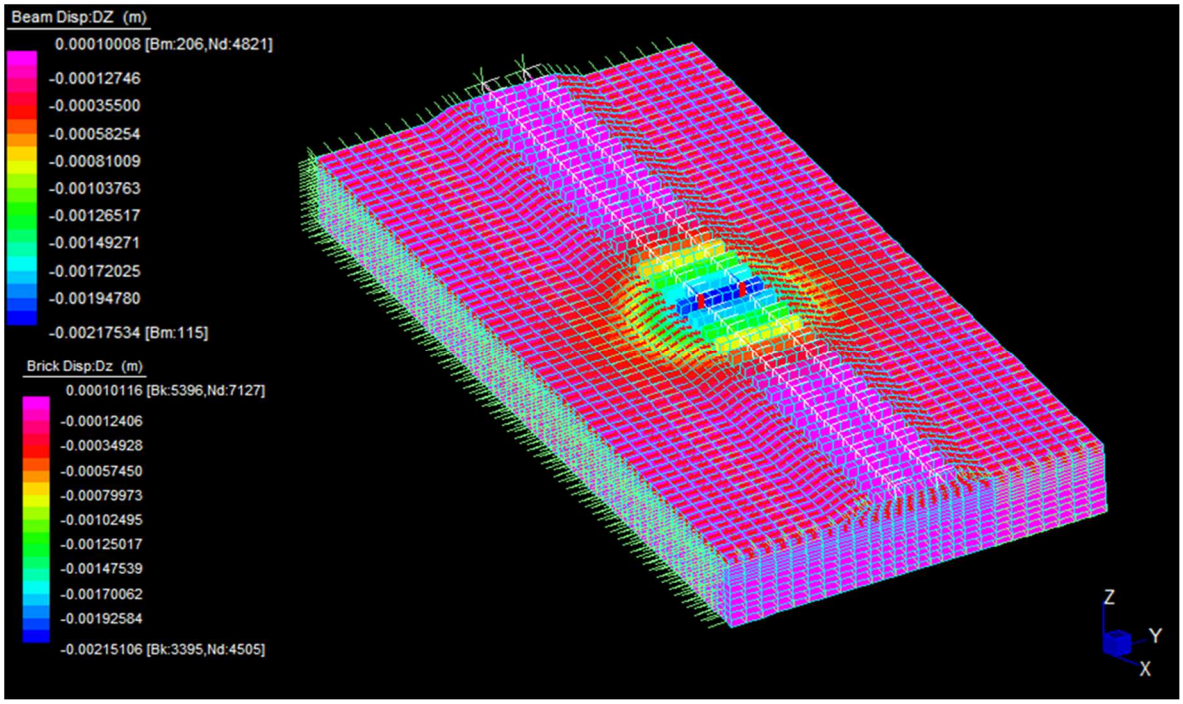

Figure 7.19: Vertical displacement contours for load case 31

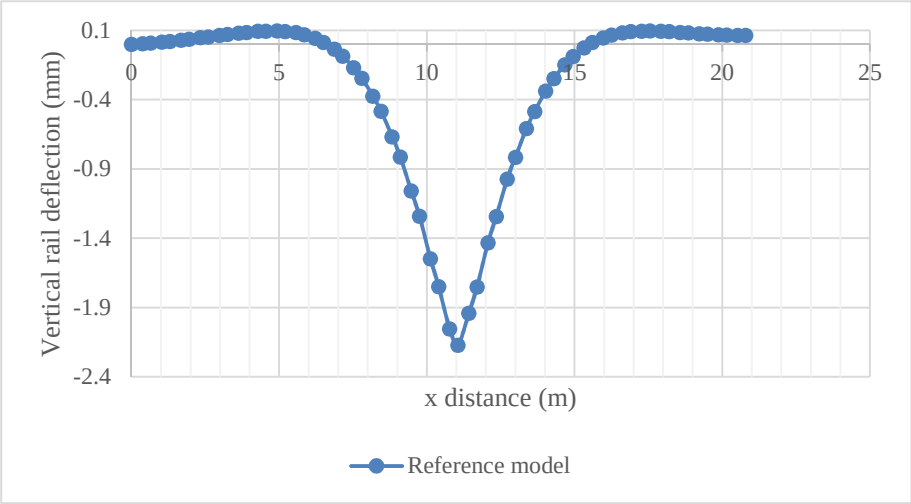

Figure 7.20: Maximum vertical rail deflection in the reference model:

7.4.1.3 Rail stress

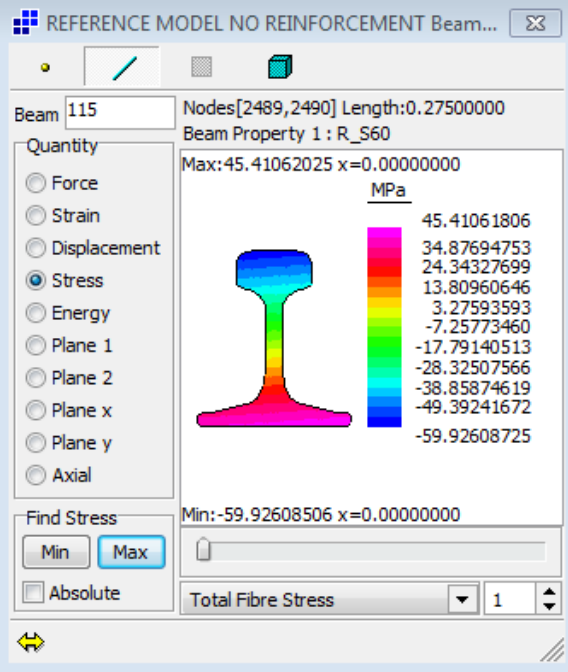

The maximum stress in the rail was a compressive force of 59.93 MPa. In similar loading applications performed in Prokon, the maximum rail stress predicted for a 60kg/m rail with a 26T axle load was ± 60MPa in compression. The FEM program thus predicts a reasonable indication of the rail stress under normal track conditions.

Figure 7.21: Maximum rail stress in the reference model of parametric investigation

7.4.1.4 Summary of results: Reference model:

A summary of the results obtained from the reference parametric model are shown in the table below:

Table 7.5: Summary of results for the reference parametric model

	Value
Maximum rail deflection	2.175 mm
Maximum rail stress	59.926 MPa
Maximum formation level deflection	2.151 mm

The reference model provided a reasonable estimation of the rail stress and was used through the course of the parametric investigation for comparative purposes.

7.4.2 Geosynthetically reinforced parametric model

For the first stage of the investigation, the reference model with the addition of a layer of geogrid reinforcement placed at a depth of 0.2 m was used. (Below the SSB layer). The analysis was performed and the maximum rail stress, deflection, formation level deflection and geogrid deflection were observed. The deformed shape of the 3D membrane representing the geotextile layer is shown in Figure 7.22 below.

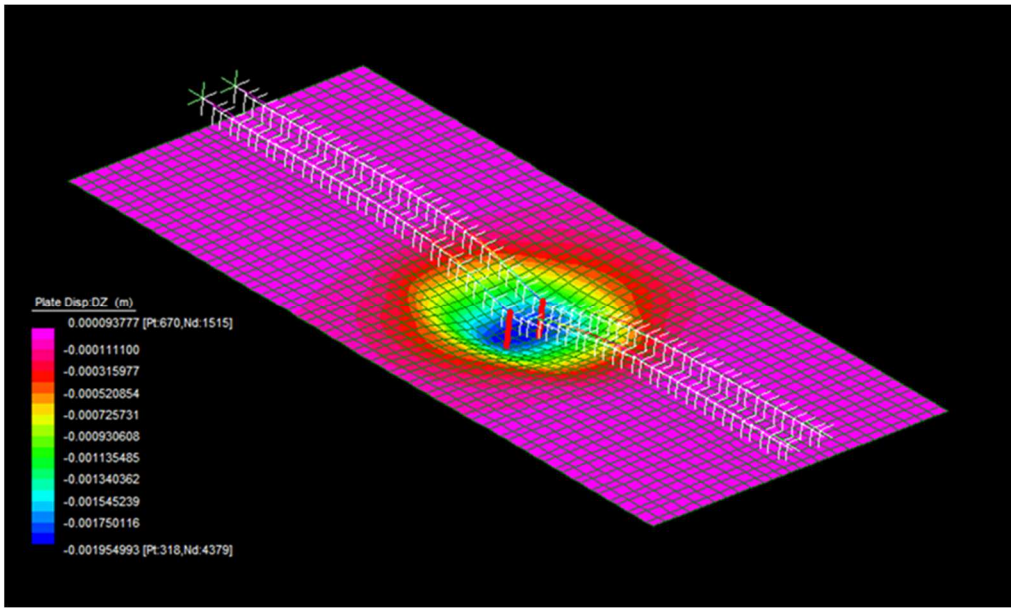

Figure 7.22: Deformed shape of geosynthetic layer

7.4.3 Results: Geosynthetically reinforced parametric mode:

The resulting rail, formation level and geosynthetic deflections are shown in Table 7.6 below

Table 7.6: Results: Geosynthetically reinforced parametric model

	Rail		Maximum formation level deflection (mm)
	Maximum deflection (mm)	Stress (MPa)	
Reference model	2.175	59.926	2.151
Model with geosynthetic reinforcement	2.175	59.923	2.149

The stress in the rail decreased by 0.005%. The formation level shows a 0.09% decrease in deflection when the geogrid layer is included. The decrease in rail stress is negligible with geosynthetic reinforcement present.

7.4.4 Geogrid reinforced parametric model with void

In this stage of the investigation a 2 x 2m void was created in the un-engineered bulk earthworks layer. The vertical sides of the void were restrained in DX and DY, so as to prevent collapse of the material surrounding the void.

7.4.4.1 Geogrid reinforced parametric model with void

The results of the investigation when a void was included are shown in Table 7.7 below:

Table 7.7: Result comparison geogrid reinforced section with void

	Rail		Maximum formation level deflection (mm)	Maximum geogrid deflection (mm)
	Maximum deflection (mm)	Stress (MPa)		
Reference model	2.175	59.926	2.151	-

Model with single layer geogrid	2.175	59.923	2.149	1.950
Model with void and single geogrid layer	4.504	75.30	4.368	4.254

The addition of the void in the model resulted in an increase in rail deflection, stress and settlements as expected. The rail stress when a void has formed was still however below the maximum allowable stress value of 120 MPa. This indicated that the rail did not fail when the void formed beneath it.

Figure 7.23 below showed the increase in rail deflection with the formation of the subgrade void.

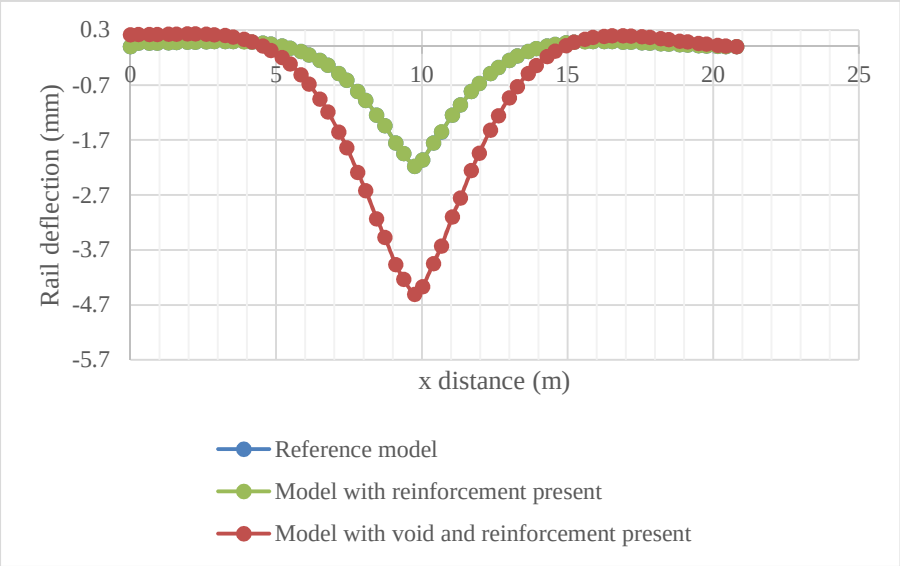

The maximum allowable deflection at ballast level according to the calculations carried out in section 7.2.5.2 was 5. 85 mm.

Figure 7.23: Comparison in vertical rail deflection between the reference models, reinforced model and reinforced model with a void present.

The maximum ballast deflection obtained was 4.368mm, this is lower than the maximum allowable surface settlement. With the reasonable prediction of the rail defections and stresses obtained, an investigation into how different formation layer characteristics/ geometric conditions change the predicted surface settlements and rail stresses was undertaken.

7.5 Soil parameters:

All FEM simulations performed used the Mohr-Coulomb failure criterion to predict the behaviour of the soil. The Mohr-Coulomb failure criterion was used in the FEM program to predict the shear strength in soil at different effective stress values, governed by the failure equation:

$$\tau = c' + \sigma_n \tan(\varphi')$$

The Mohr-Coulomb soil model was elastic-perfectly plastic. The elastic behaviour of soil/ how the soil behaves up to yield was governed by the Young's modulus (E) and Poisson's ratio (μ) values of compressibility. On the onset of plastic behaviour, the soil follows the failure equation stated above and is governed by the angle of internal friction (φ) and the cohesion (c).

The Young's modulus (E), angle of internal friction (φ), earth pressure coefficient (K_0) and cohesion are altered and the effects these parameters had on the deformations/stresses in the geogrid layer were observed.

Table 7.8 below shows the range of values considered in the SSB soil layer during the parametric investigation.

Table 7.8: Soil parameters variations in the SSB layer of the parametric investigation

Parameter	Value
Young's modulus (MPa)	100, 160, 200
Friction angle (Deg)	40, 50
Earth pressure coefficient	0.357, 0.5, 1
Cohesion (kPa)	1
Density (kN/m^3)	19

7.5.1 Young's Modulus (E)

The Young's modulus was an indication of the elasticity of the soil, the E value controlled the compressibility of the material prior to yield. There are multiple formation layers in a track structure, for the sake of simplicity and to limit the number of variables, only the soil properties in the SSB layer were altered. In site conditions when formation rehabilitation occurs, the SSB layer is generally selected for improvement as this is the most cost effective choice and

minimises excavation. A Young's modulus value of 160 MPa was used in the SSB layer for the previous simulations.

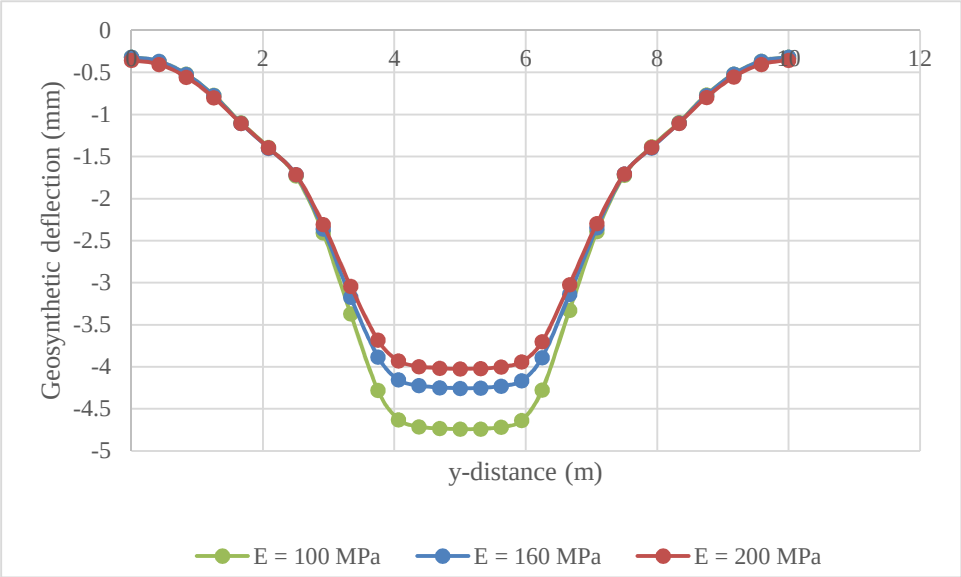

Figure 7.24: Change in geosynthetic deflection in a geotextile present in a geosynthetically reinforced formation level with a subgrade void present when the Young's modulus of the formation level is increased.

Increasing the Young's modulus of the SSB layer from 100 MPa to 200 MPa decreases the compressibility of the material above the void, this would result in a decrease in geotextile deflection as predicted by the FEM model. The rail deflection shows a similar decrease with an increase in the Young's Modulus and was illustrated in Figure 7.25 below. The rail stress decreases from 75.30 MPa when E = 160 MPa to 71.458 MPa when E = 200 MPa.

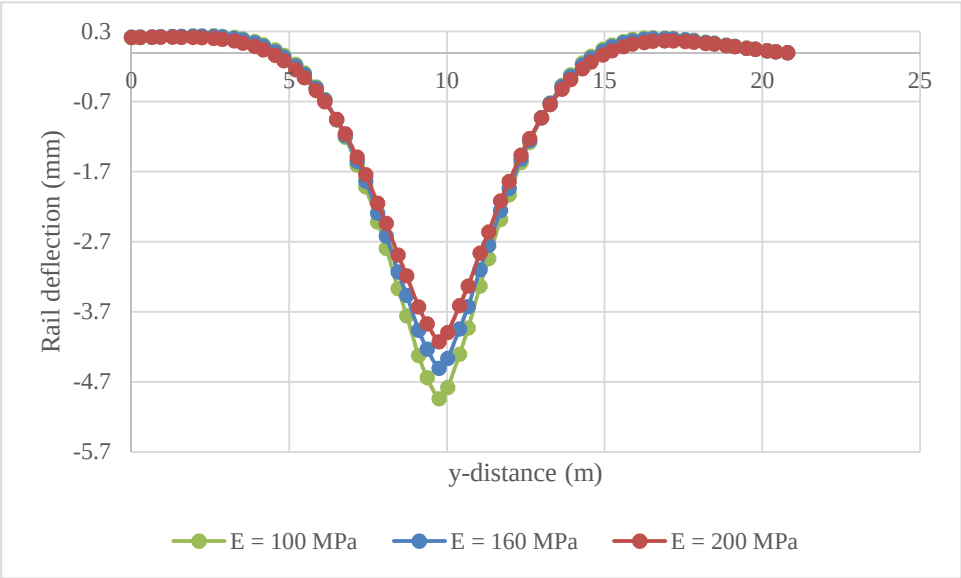

Figure 7.25 Change in deflection of rail line over a geosynthetically reinforced formation level with a subgrade void present when the Young's modulus of the formation level is increased.

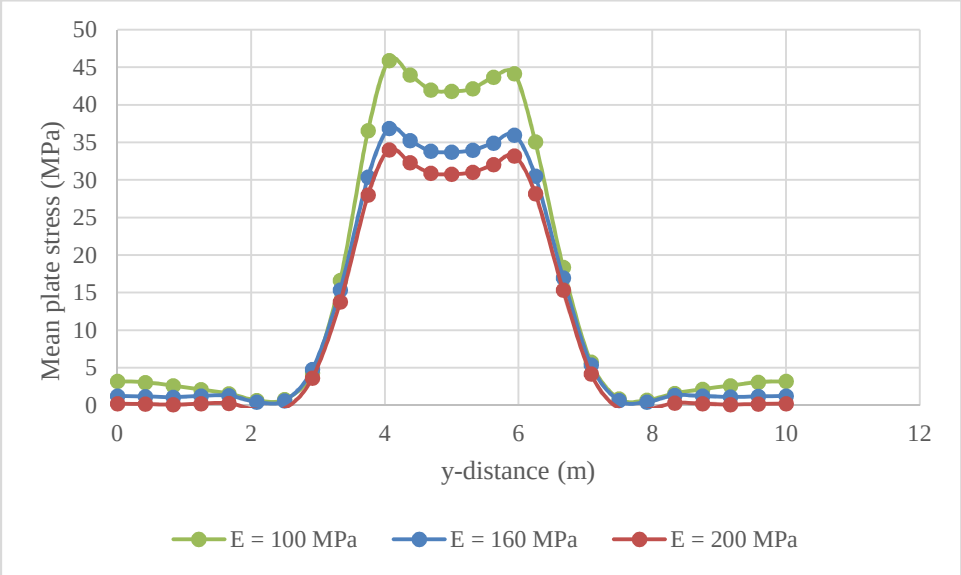

In Figure 7.26 the stress developed in the geosynthetic decreased from 36.003 MPa to 33.207 MPa when the SSB layers Young's modulus was increased.

Figure 7.26: Change in stress at geotextile level present in a geosynthetically reinforced formation level with a subgrade void present when the Young's modulus of the formation level is increased.

In a rail model the E value of the formation layers can be increased by including soil stabilising agents (cementing). However, concrete stabilised subgrades have exhibited problems such as cracking and excessive rail movement in long term Transnet applications. Although stabilisation is still practised in track, it is time consuming when compared to geosynthetic reinforcement and generally more expensive.

7.5.2 Angle of internal friction (φ)

The angle of internal friction provided an indication of a soils/rocks ability to withstand shear force. The angle of shearing resistance in the SSB layer was increased from 40 to 50^0.

A general angle of internal friction of 40^0 was used in the SSB layer as per Transnet's specifications (Transnet Freight Rail S406, 1998). The angle of friction of 50^0 represented an SSB layer with a large amount of ballast stones present, hence a larger angle of internal friction.

With a larger angle of shearing resistance in the layer the geosynthetic deflections should decrease. The maximum rail stress underwent a decrease with an increase in the angle of internal friction.

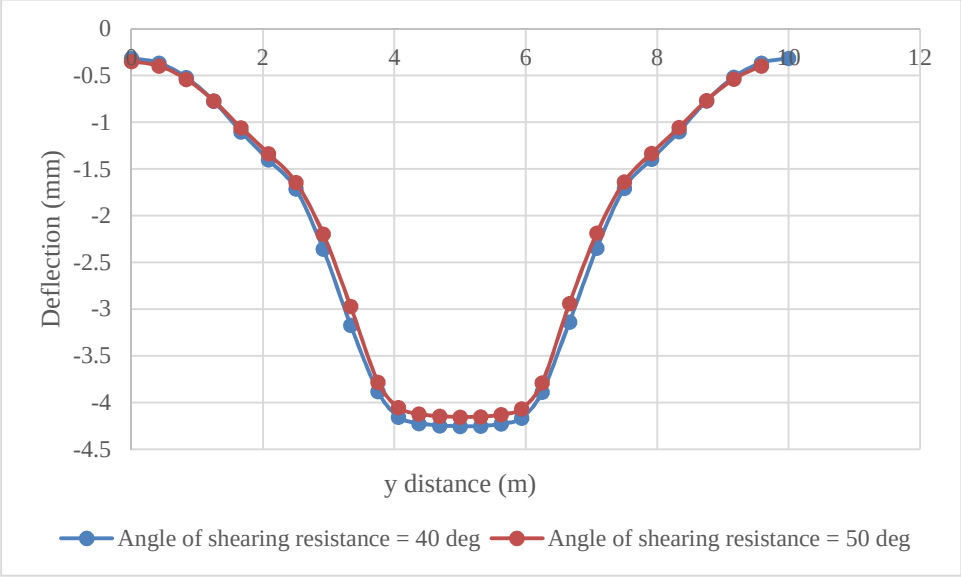

Figure 7.27: Change in geosynthetic deflection in a geotextile present in a geosynthetically reinforced formation level with a subgrade void present when the angle of shearing resistance of the formation level was increased

Table 7.9: Parametric model results with angle of internal friction and Young's Modulus increase

Soil parameters	Maximum geosynthetic stress (MPa)	Maximum rail stress (MPa)
E = 160 MPa, φ =40^0	36.003	75.30
E = 160 MPa, φ =50^0	35.003	74.242
E = 100 MPa, φ =40^0	44.156	81.942
E = 200 MPa, φ =40^0	33.206	71.458

The stress within the geosynthetic fabric itself decreased as the angle of internal resistance increased as shown in Figure 7.28 below.

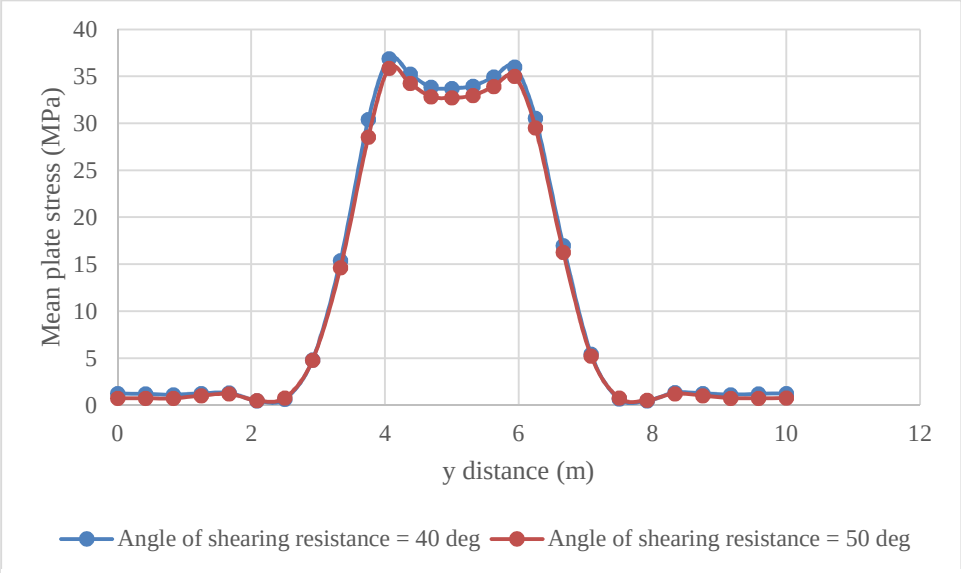

Figure 7.28: Change in stress at geotextile level present in a geosynthetically reinforced formation level with a subgrade void present when the angle of shearing resistance of the formation level was increased

Increasing the angle of shearing resistance decreased the settlement and the geosynthetic stress. In track conditions, the angle of shearing resistance can be increased by increasing the ratio of ballast stones to gravel in the SSB layer.

7.5.3 Earth pressure coefficient:

The coefficient of earth pressure at rest is used in the FEM program in order to accurately predict pre-existing in-situ stress in the soil due to the formation layer height, elevation of the element relative to any fluid (drained conditions are considered in all cases) as well as the material above each element. The equation describing K_0 for normally consolidated soil is taken as:

$K_0 = 1 - \sin(\varphi)$, where φ = Angle of internal friction (Jaky's Formulae)

Jaky's formulae shows the relationship between the angle of internal resistance and the earth pressure coefficient. For all other parametric models a K_0 of 0.357 was used for the SSB layer.

K_0 = 1- sin (40^0) = 0.357 (for the SSB layer)

K_0 was then increased to 0.5 and 1, and the resulting geogrid deflection and rail stress are observed.

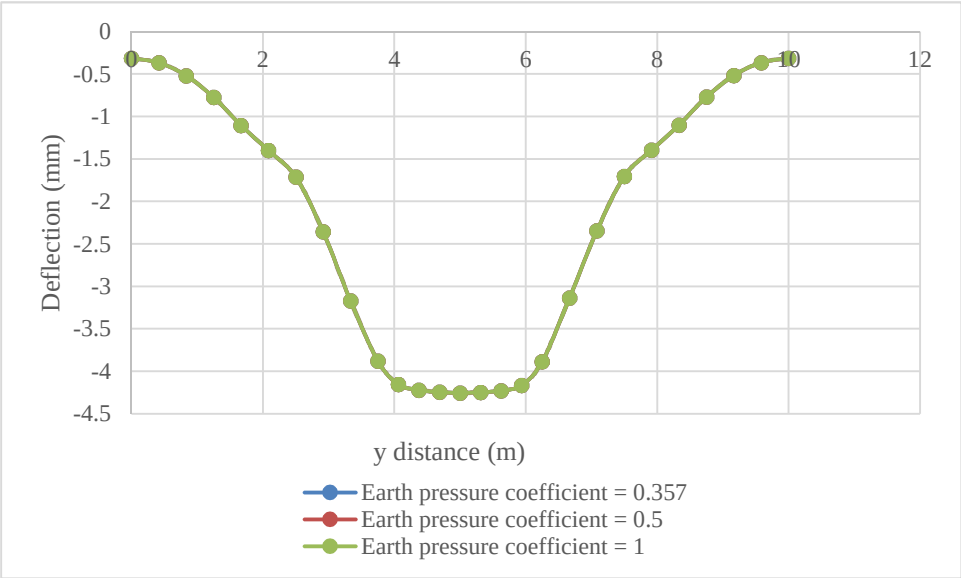

The geogrid deflection does not change with the increase in the earth pressure coefficient.

Theoretically it is expected that the geogrid

Figure 7.29: Change in geosynthetic deflection in a geotextile present in a geosynthetically reinforced formation level with a subgrade void present when the coefficient of earth pressure at rest in the formation level was increased

deflections and subsequent soil surface deflections will decrease with an increase in the soil pressure coefficient, this is however not the case. The maximum rail stress remains at 75.30 MPa throughout.

Similar results were obtained in Potts (2007) and Mifsud (2005) where the increase in K_0 did not result in any change in the geogrid deflection, stress or soil surface settlement. Potts (2007) theorised that according to Tezarghis soil arching equation,

$$\sigma_v = \frac{D(\gamma - 2c/D)}{2K\tan\phi}\left(1 - e^{\frac{-2Kz}{D}\tan\phi}\right) + w_s e^{\frac{-2Kz}{D}\tan\phi}$$

And increase in the coefficient of earth pressure would increase the fills ability to arch. With an increased probability of an arch forming in the soil, it is expected that smaller stresses in the geogrid and a decrease in soil as well as geogrid deflection will take place. The parametric models SSB layer H/D ratio is small (0.2), hence the probability of a soil arch taking place is quite low. The wheels axle point load would also play a role in preventing any possible soil arch formation.

7.5.4 Cohesion:

The cohesion value of soils is the shear strength in the soil when the compressive stresses are equal to zero. A minimal cohesion value of 1 kPa was selected for the SSB Layer, as the FEM solver will not run with a cohesion value of 0 MPa.

7.5.5 Density:

The density of the SSB layer depends mainly on the amount of compaction that the layer has undergone during the construction process as well as the mineral make-up of the soil and how the particles pack together. The SSB layer density as per Transnet's specifications is 19 kN/m^3.

7.6 Loading conditions:

In this phase of the parametric study, the axle loading on the railway line was changed and the effect that this parameter change had on the geosynthetic stress and deflection was observed.

A 26 T axle load was considered in the previous parametric simulations, however the majority of the rail lines in South Africa carry a 20 T axle load.

Certain lines are being upgraded to a 30 T axle load in order to facilitate the transport of larger tonnages and more goods. With the increase in axle load the formation layers are tested to see if they conform to Transnet's standards.

Figure 7.30: Perway network South Africa where the legend represents the tonnages carried as indicated by the colour of the rail line

For research purposes expected axle load was increased in the existing model from 26T to 30T while keeping the formation level parameters the same.

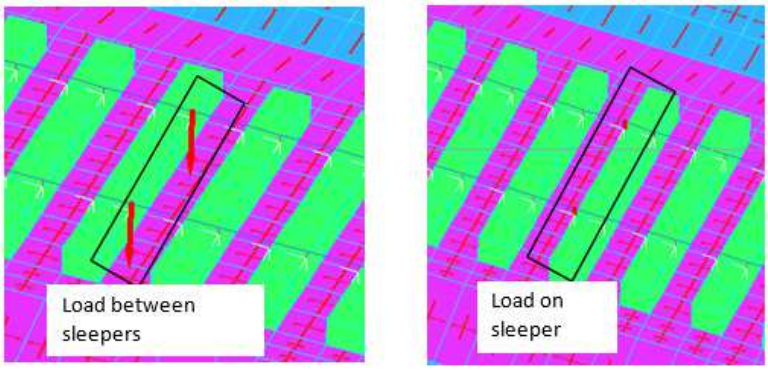

The axle load was applied in 60 stages to simulate the movement of a locomotives wheel over the rail. The axle load in all the load cases was increased to 30T and the results observed (Appendix B).

Figure 7.31: Load position on track moving from on top of the sleeper itself to between the two sleepers

The results of the axle load increase are shown in Table 7.10 below:

Table 7.10: Geosynthetic strain with increase in axle load

Axle load (T)	Maximum rail stress (MPa)	Maximum geosynthetic stress (MPa)	Status
26	75.30	36.003	Acceptable
30	Non convergence		Unacceptable

The ultimate tensile strength of the selected geosynthetic was 100 kN/m, the thickness of the fabric was 2mm hence the stress limit in the reinforcement was 50 MPa. At an axle load of 30 T, the ultimate stress limit in the fabric was exceeded and the model did not converge when the load was directly above the void. Indicating that with an axle load increase the formation needs to be removed and a geogrid layer with increased tensile strength should be installed (or multiple reinforcement layers).

7.7 Geosynthetic reinforcement parameters:

In this phase of the parametric investigation, the geosynthetic reinforcement properties were varied in terms of the strength requirements and the number of geosynthetic layers used.

Table 7.11: Geosynthetic reinforcement parameters: compare to in field geogrids

Parameter	Value range
Tensile modulus (kN/m)	50, 100, 200
Poisson's Ratio	0.2
Density (kg/m^3)	150
Thickness (mm)	2-3
Number of geogrid layers	1 - 4

7.8 Tensile modulus (T):

The tensile modulus values were selected from existing products, the testing details are found in Appendix A. The following geosynthetic tensile resistance values were considered through the course of the parametric investigation:

Table 7.12: Commercially available bi-directional polyester grids

Long term tensile resistance (kN/m)	Ultimate short term tensile resistance T_u (kN/m)	Thickness (mm)	Density (kg/m^3)	Cost (R/m^2)
26	50	2	150	36.55
52	100	2	150	39.82
105	200	3	150	57.55

The long term tensile resistance value was the Tu value multiplied by factors of safety for creep and various environmental factors. For the purpose of the investigation creep and environmental factors are disregarded, hence the Tu value was considered as it is. The results of the analysis are shown in Table 7.13 below:

Table 7.13: Geosynthetic strain with change in geosynthetic tensile modulus

Geosynthetic modulus (kN/m)	Maximum rail stress (MPa)	Maximum geosynthetic stress (MPa)	Status
50	Non convergence		Unacceptable
100	75.30	36.003	Acceptable
200	68.491	59.263	Acceptable

In Table 7.13 as the geosynthetic modulus (T) increases there was a decrease in the surface settlement and the subsequent rail deflections. The maximum stress in the rail also showed a decrease with increased stiffness of the geosynthetic layer. The resulting stress values were acceptable when $T \geq 100$ kN/m.

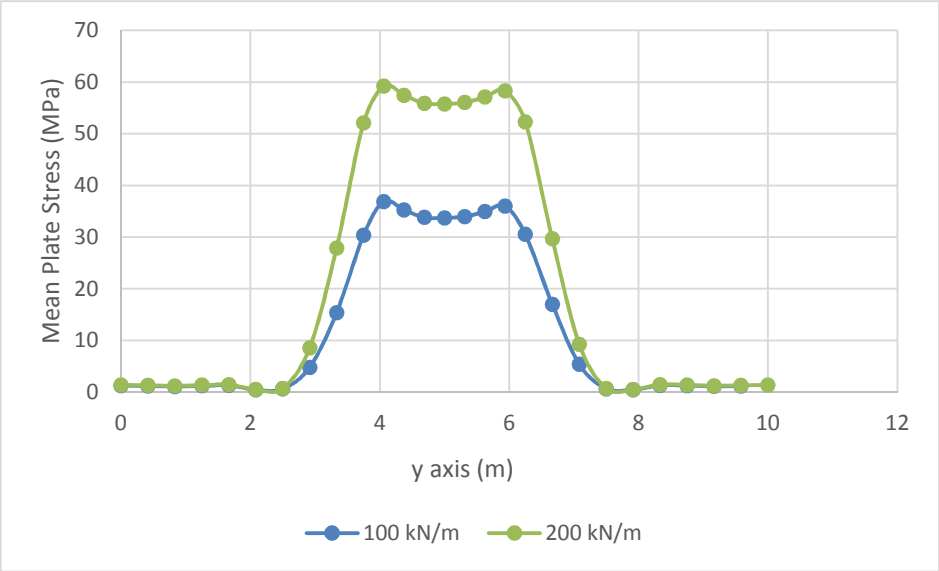

Figure 7.32 Change in stress at geotextile level present in a geosynthetically reinforced formation level with a subgrade void present when different commercially available geosynthetic products were used

Increasing the tensile modulus of the geosynthetic caused an increase in the geosynthetic stress itself. A similar result was obtained in Potts (2007) where increasing the tensile modulus of the geogrid resulted in the geogrid attracting a larger load and ultimately moved the geogrid stress closer to the ultimate tensile strength when the tensile modulus was very high. This lead to the conclusion that a stiffer reinforcement layer attracts more load.

7.9 Number of geosynthetic reinforcement layers:

The use of a geosynthetic layer as basal reinforcement has been covered in SANS 207 and the British Code. The use of multi-layered geosynthetic reinforcement however has not been extensively researched, in this section of the parametric study up to four layers of geosynthetic reinforcement were used.

The void considered remains at 2m. The addition of the reinforcement layers caused the overall formation stiffness to increase, thus minimising the deflection in the model. In the study the use of 1 – 4 reinforcement layers was considered with a geosynthetic modulus of 100 kN/m.

In previous investigations performed by Mifsud (2005) and Potts (2007) it was seen that the soil deformations decreased slightly with the use of multiple geosynthetic layers. The inclusion of a second reinforcement layer did improve results in terms of the geosynthetic stress and

deflection, the addition of a 3rd and 4th layer of reinforcement resulted in no improvement in the results.

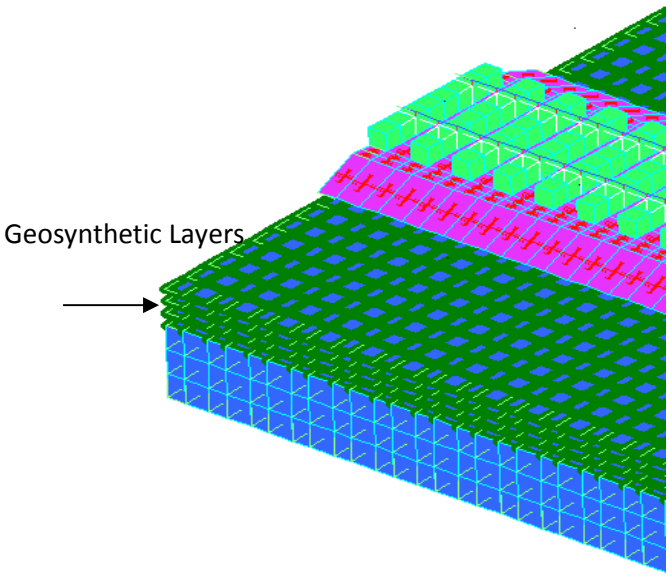

Figure 7.33: Layout of geosynthetic reinforcement in formation at 200mm spacing

The geosynthetic layers were positioned as illustrated in Figure 7.33.

Layer 1: Below SSB Layer

Layer 2: Below SB Layer

Layer 3: Below A Layer

Layer 4: Below B Layer

The model was constructed from the bottom upward, with the bulk earthworks layer developed first, with the subsequent placement of the lowermost reinforcement layer. The B layer of soil was then placed above the system followed by the subsequent reinforcement layer. This continued until 1 – 4 layers of reinforcement were present in the formation. The results of the analysis are shown in Table 7.14 below:

Table 7.14: Geosynthetic stress with increase in number of reinforcement layers.

Number of geosynthetic layers	Maximum rail stress (MPa)	Maximum geosynthetic stress at lowermost layer (MPa)	Status
1	75.30	36.003	Acceptable
2	75.021	34.167	Acceptable
3	74.633	32.527	Acceptable
4	74.170	31.234	Acceptable

When additional geosynthetic layers were included in the parametric model, a decrease in rail stress was observed. The inclusion of the second layer of reinforcement resulted in the most apparent decrease in geosynthetic stress. Further layers resulted in a stress decrease but to a smaller degree as illustrated in Figure 7.34 below.

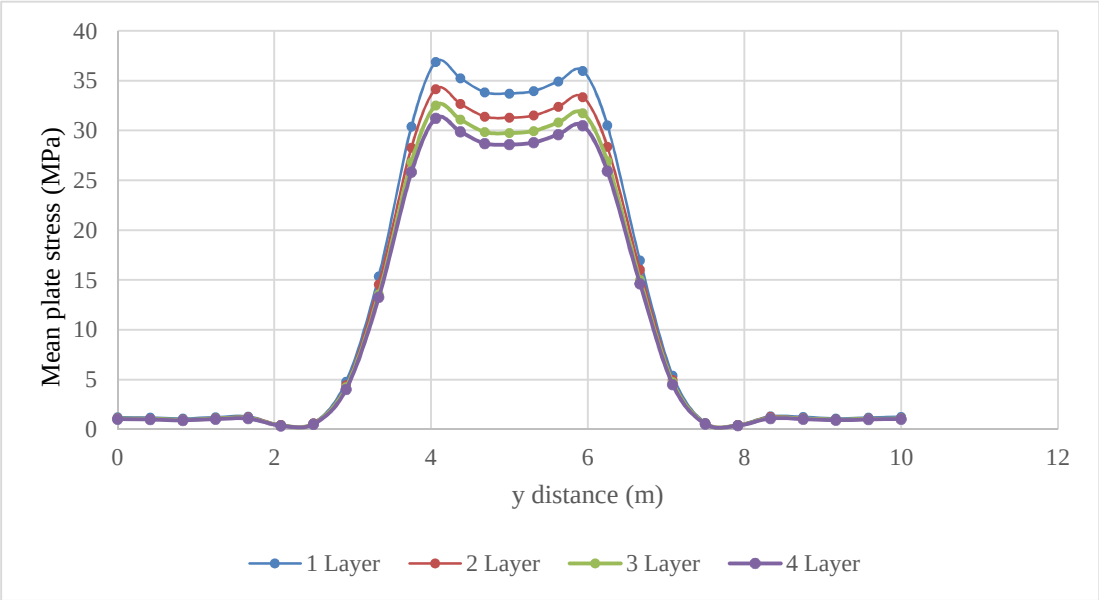

Figure 7.34 Change in stress at geotextile level present in a geosynthetically reinforced formation level with a subgrade void present when the number of reinforcement layers in the formation level were increased

7.9.1 Discussion of results:

Increasing the number of geosynthetic layers decreased the soil deformations. When a second layer was added the stiffening effect was most prominent, more than two layers of reinforcement resulted in a decrease in the soil deformations but to a lesser degree.

The parametric model in general showed an under prediction in the soil deformations due to dilation, the inclusion of multiple geosynthetic layers did result in a change in the deflection values, but to a very small degree. Which was expected due to the models deflections being generally under predicted.

The geosynthetic layers are 200mm apart. In the models considered by Potts (2007) and Mifsud (2005) the spacing between the geosynthetic layers was set at 600mm. No improvement of results was observed in these models beyond the 2nd layer, Potts (2007) attributed this to the distance between the geosynthetic layers and the height of the model. In addition to this Potts

(2007) concluded that the use of geosynthetic reinforcement beneath each formation layer creates a discontinuity in the soil fill and stops soil arching from taking place. Placing the reinforcement 200mm apart as opposed to 600mm creates a larger overall stiffness.

In de Lange (2016) the laboratory model showed a definitive decrease in soil surface deflections with the presence of multiple layers of reinforcement. The reinforcement strength characteristics were not changed with the addition of more layers, i.e. a higher overall stiffness would be expected. In the laboratory FEM model the reinforcement layer strength used was the same with the addition of geosynthetic layers, this higher overall stiffness resulted in a larger decrease in surface deflections with that addition of more geosynthetic layers.

From the results of Chapter 6, it was concluded that using multi-layered geosynthetic reinforcement exhibited improved results when compared to using basal reinforcement alone. The improvement in results however diminished with each additional reinforcement layer, indicating that the number of reinforcement layers, reinforcement strength and the spacing of these layers must be further investigated to develop an optimal model.

8. CHAPTER 8: CONCLUSIONS AND RECOMMENDATIONS

8.1 Introduction

The previous chapters described a study into the deflection behaviour of horizontally reinforced sand spanning over a developing subgrade void. The study comprised a series of FEM simulations of previously reported laboratory experiments (Potts, 2007 and de Lange, 2016) as well as an assessment of methods described in various design guides and methods (SANS 207 and RAFAEL) used to determine the required tensile strength and stiffness of a reinforced fill layer.

The primary aim of the investigation was to develop a finite element model that would be useful in the design of reinforcement for an embankment fill that might experience a loss of support due to subsidence of the underlying ground. The numerical accuracy of the FEM models was within 10% of the experimental model. The overall behaviour of the reinforced fill was predicted by the FEM model in terms of the deflected shape of the geosynthetic and the soil surface deflection shape.

The FEM model that most closely simulated the behaviour of the physical test models was then extended to include the track superstructure and substructure. This composite model was developed to identify the key variables that influence the strength and stiffness of the reinforced fill in order to improve applications of the soil reinforcement technique.

8.2 Experimental models:

The initial aim of this investigation was to examine how finite element analysis could best be applied to provide a useful representation of a reinforced soil mass and how the reinforced soil mass reacted to a loss of subgrade support. In order to prove this, two laboratory modelling scenarios were considered. The first being a case study involving recreating a laboratory model developed at the University of London in Potts (2007) and the second creating an FEM model of a laboratory model developed at the University of Kwa Zulu Natal (de Lange, 2016).

The laboratory model developed by de Lange (2016) considered both a reinforced and unreinforced design. The number of geosynthetic layers as well as the H/D ratio were varied in the laboratory model. The findings of the laboratory experiment are listed below:

8.2.1 Unreinforced model:

- The unreinforced laboratory model developed by de Lange (2016) used a concrete ring filled with loose sand and formed a reference point whereby the effect that geosynthetic reinforcement had on the system could be observed. The presence of the geosynthetic reinforcement reduced the soil surface settlement and gave an indication of the deflection improvement provided by the use of geosynthetics.

8.2.2 Reinforced model:

The reinforced laboratory modelled developed by de Lange (2016) used a concrete ring filled with loose sand and reinforced with layers of mesh. The mesh layers were used to represent the geosynthetic reinforcement. Due to the small scale of the model (fill height was 300 mm) commercially available geosynthetic reinforcement would have been disproportionately stiff in relation to the self-weight of the soil. Lacking the facility (a centrifuge) to increase the load it was necessary to find a substitute fabric. The essential criteria was that the fabric be strong enough to carry the load without tearing and to have linear elasticity, at least at small strains, and to have a tensile modulus low enough to allow sufficient downward movement of the soil to be clearly visible, measurable and of a similar physical scale (several millimetres) as the model itself. A mosquito net mesh was found to reasonably match these criteria and the aperture size of the mesh allowed particle interlock to occur through the mesh while still retaining all but the finest of the constituent particles. The actual loss of fines through the basal reinforcing layer of the trapdoor void was insignificant.

From the reinforced laboratory model the shape of the soil deflection cone was investigated as well as the degree of soil settlement. A summary of the reinforced laboratory experiment findings are listed below:

- Increasing the H/D ratio resulted in a decrease in the soil surface settlement through the majority of the tests.

- The use of multiple layers of reinforcement decreased the expected soil surface settlements when $H/D < 1.5$, suggesting that little or no arching took place over the void.

- When $H/D \geq 1.5$ lower than expected surface deflection was attributed to the occurrence of soil arching within the soil fill layer. A decrease in the vertical spacing between

reinforcing layers appeared to cause a breakdown of the soil arch and hence cause an unexpected increase in vertical deflection.

- The shape of the deflection surface was more parabolic than conical in shape and the maximum vertical displacement was centred above the void. The angle of draw was approximately 60^0, which was larger than the value assumed in the SANS 207 design approach.

In summary the experimental model showed that both the H/D ratio and the vertical spacing between reinforcing layers had an influence on the potential for soil arching over the void. Higher H/D ratios exhibited an increased occurrence of soil arching, while closely spaced reinforcement layers tended to prevent soil arching from taking place. Further investigation into the influence that the spacing of the reinforcement has on the settlements is thus required.

8.3 Finite element analysis:

A series of finite element analysis models were developed to represent the various de Lange (2016) laboratory experiments. A summary of the conclusions obtained from the FEM model are listed below:

- The general behaviour of the laboratory model was that as H/D increased, the vertical centreline settlement decreased. Both the experimental and FEM model exhibit a 50 % decrease in settlements when the H/D ratio is increased from 1 to 1.5. The FEM values predicted were lower but the general trend followed was the same.

- The FEM vertical deflections were on average 10% lower than the physical test data in terms of deflections. As mentioned in the previous chapters the Strand7 program assumes that the angle of shearing resistance is equal to the angle of soil dilation. The angle of dilation cannot be changed independently from the angle of shearing resistance which resulted in a general under-prediction in soil deflection values due to an over prediction of soil dilation. For the purpose of providing reasonable prediction of the behaviour of reinforced fill layer undermined by a void the potential for arching needs to be further investigated.

- In the FEM model using multiple layers of reinforcement resulted in a decrease in the soil surface settlement taking place. The deflection decrease provided diminished with increasing geosynthetic layers. This indicated that multiple reinforcement layers improves the fills overall performance but stops beyond reinforcing at a certain height above the void itself. The general trend discovered was that reinforcing above the mid height of the embankment had a diminished improvement of results. That being said, changing the spacing of the reinforcement layers should optimise the geosynthetics settlement reduction capabilities.

- The shape of the deflection cone generated when multiple layers of reinforcement were present was parabolic throughout the investigation. This was evident in both the experimental model and the design approaches SANS 207 and RAFAEL. The angle of void propagation however was on average 45^0. The actual angle of void propagation was closer to 60^0, indicating that the FEM model predicted a shallower settlement cone affecting a larger area. Some of the factors influencing the angle of void propagation predicted are the angle of shearing resistance of the soil and the soil dilation angle. If these can be changed independently from one another using different FEM software, a more realistic angle of draw can be predicted by the FEM model.

- Plane strain analysis provided a deeper and more concentrated settlement trough when compared to the axisymmetric conditions modelled using FEM. The settlement trough geometry predicted by the plane strain model was a better representation of the experimental results, exhibiting a more accurate angle of draw. The settlements were however over predicted hence improvement to the model is required going forward. In future FEM simulations plane strain analysis should be considered as it provides a deeper more concentrated settlement trough hence mitigation measures for the worst case scenario can be designed for.

- The 3D model was developed to validate the simplification assumptions made in the 2D model. The settlement values predicted between the 2D and 3D model were the same, with the overall under-prediction of deflections. The 3D model confirmed that modelling the geosynthetic fabric as line elements in 2D generated the same results as

the 3D membrane elements. It was thus concluded that the 2D model provides a sufficiently accurate representation of the 3D model and can be used to minimise computational time.

In conclusion FEM provides a means of predicting soil surface and geosynthetic deflections in a geosynthetically reinforced soil mass undermined by a subgrade void. The accuracy of the results can be improved in future with more detailed attention to material properties such as the angle of soil dilation.

8.4 Design approaches:

The aim of the analytical model was to assess the appropriateness of the assumptions made in developing the existing design guides. Calculations based on SANS 207 and RAFAEL design approaches were performed on the de Lange (2016) experimental model. The observations and conclusions derived from the reinforced analytical model calculations are listed below:

- It was evident from the design calculations that both SANS 207 and the RAFAEL method have limitations when estimating the diameter of the surface settlement cone. The diameter is calculated directly from the angle of void propagation. SANS 207 suggests that the angle of draw is equal to the angle of shearing resistance of the soil. This value is too small and results in the void propagating outward to an extent that surpassed the laboratory model boundary. To create a more realistic result the cone diameter from the laboratory model itself was used to calculate a revised angle of draw of approximately 60^0. RAFAEL on the other hand assumes a perpendicular angle of draw, resulting in the settlements being concentrated entirely above the void. Neither method provided an accurate indication of the angle of draw and the subsequent settlement cone diameter.

- Another factor affecting the accuracy of the design calculations is the soil dilation. SANS 207 assumes that no dilation of the soil occurs upon shearing while the soil used in the experimental model showed a propensity towards dilation. With the adjusted angle of draw, the vertical soil surface settlements are overestimated by SANS 207. Given the soils tendency toward dilation, the SANS 207 method does not provide an accurate prediction of the settlement values.

- The RAFAEL design method however takes soil dilation into account. The degree of dilation is dictated by the soils coefficient of expansion. The expansion coefficient was selected from both the German design guide EBGEO: 2011 and Potts (2007) for granular fill layers resulted in an inaccurate prediction of results. The use of Potts (2007) expansion coefficient resulted in upward heave taking place, while the German code value resulted in defections up to 90% larger than the experimental model. Further investigation into the coefficient of expansion is thus required before any meaningful conclusions with regard to RAFAEL's design approach can be made. Calculation of the coefficient of expansion based on RAFAEL's equation of the surface settlement while substituting in de Lange (2016) actual experimental data yielded a lower C_e value. This C_e of 1.0076 was calculated based on a single set of available data so to make more meaningful conclusions with regard to the coefficient of expansion, further investigation in which the volumetric change in the fill layer is monitored is thus required.

The overall conclusion is that when employing existing design techniques, the limitations with regard to the angle of draw and the degree of soil dilation must be taken into account or the design will not be the optimal solution.

8.5 Parametric model:

The aim of the parametric model was to determine which factors have an effect on the behaviour of the geosynthetically reinforced fill layer, and to what extent these factors affect the model results. The load transfer capability of the geosynthetically reinforced fill layer was influenced by the stiffness of both the fill layer and the geosynthetic reinforcement, the number of geosynthetic reinforcement layers used, the shearing resistance of the fill, as well as the loading applied to the rail superstructure. The behaviour of the reinforced fill layer when subjected to void formation is summarised below:

- The soil stiffness was found to have a considerable effect on the soil surface settlement. Previous studies also revealed that using a geosynthetically reinforced fill layer and a stabilised subgrade improves the performance of the subgrade when subjected to void formation. The parametric model in which the upper 200 mm of SSB (below the ballast) was stabilised showed an improvement in terms of the soil surface settlement and the geosynthetic strain. The stiffer SSB layer tends to "attract" more load when subjected

to the overhead train. This results in less load being applied to the geosynthetic reinforcement itself hence smaller strains and deformations. However, concrete stabilisation of the subgrade has found to have certain negative long term effects. Such as subgrade cracking, brittleness when subgrade is over stabilised, and excessive rail movements. When compared to geosynthetic reinforcement, sub grade stabilisation is more time consuming and subsequently costs more. The ease of application of geosynthetic reinforcement indicates that less manpower and equipment is required when compared to cement stabilising the subgrade. Due to this, it will be more feasible to consider using multiple layers of geosynthetic reinforcement instead of stabilising the subgrade.

- An increase in the soils shearing resistance resulted in smaller soil surface deflections and a decrease in geosynthetic strain but to a smaller degree. In the Strand 7 program the angle of shearing resistance is taken as being equal to the angle of soil dilation. It is thus expected that an increase in the angle of shearing resistance to have a considerable effect on decreasing the soil surface settlements as the angle of dilation would subsequently be increasing too but this was not the case. The angle of dilation cannot really be commented on as it cannot be changed independently from the angle of shearing resistance.

- The various geosynthetic products considered were selected based on their previous use in reinforcing void prone topography. The range of tensile strength values considered showed that higher strength reinforcement fared better for the 2 m void diameter selected. Tensile strength of 50 kN/m would fail for the specified void diameter. It was also found that geosynthetic reinforcement with a higher tensile strength tends to attract more load. Increasing the tensile strength of the geosynthetic will decrease the formation settlement but up to a certain degree.

- With regard to the use of multiple layers of reinforcement, adding more than 2 geosynthetic layers decreases the deflections the fill layer further but to a smaller degree with each additional reinforcement layer. When compared to alternate methods such as cement stabilisation however, multiple layers of geosynthetic reinforcement is more

feasible. Further investigation is required into what spacing, strength and frequency of reinforcement layers is required in order to develop an optimised model.

- The loading conditions in the track superstructure also plays an important role. A relatively large axle load of 26 T was used in the parametric model, over recent years many South African heavy haul lines have been upgrading to 30 T axle loads. If the line modelled were to be upgraded i.e. use a 30 T axle load, it was found that the geosynthetic reinforcement would not be able to maintain the increased load when subjected to a subgrade void. Hence when upgrading the tonnages of a line, it should be noted that an upgrade in the tensile resistance of the reinforcement used may be required.

- The use of a continuous strain monitoring system should be considered in identified sinkhole prone areas. Transnet currently employs the use of various monitoring systems in lines that are prone to temperature related disturbances and derailments. The system monitors the strain and settlement of the rail, when the strain is excessive the user is notified and subsequent rehabilitation techniques can be employed. For sinkhole prone areas specifically this will serve as a quick means of identifying whether a void has formed and long term solutions can be provided for the line. The geosynthetic reinforcement will minimise the deflections till full rehabilitation can occur and prevent full collapse but does not serve as a long term solution.

In summary the parametric model helped identify the various factors affecting the soil surface deflection. Increasing the strength and frequency of the reinforcement layers improved the settlements in track. In order to develop an optimal model in terms of number of geosynthetic layers required and their spacing and strength further investigation is required.

8.6 Recommendations for future work:

The laboratory experiments that will be used as a basis for the FEM model should undergo certain improvements during future investigations:

- The simple nature and small scale of de Lange (2016) laboratory model provided a platform to perform a simplified FEM model with a limited number of variables. This also makes it difficult to get a realistic indication of the soil and geosynthetic strains, a

larger model that uses actual geosynthetic fabric and not a scaled down representation of it should be considered. Performing the tests in a centrifuge will provide a more accurate indication of the strains in the soil mass and will remove any scaling problems as a result of the size of the model.

- The multi-layered reinforced laboratory model developed by de Lange (2016) used the same strength of geosynthetic fabric. A laboratory study where one strong basal layer of reinforcement and multiple layers of lower strength reinforcement are used should be performed. This will give a better indication of basal vs multi-layered reinforcement performance, and will help in the development of the most economical design. The spacing of the layers should be changed in future experimental models.

- Further investigation is required to determine an accurate coefficient of expansion and angle of dilation in the soil fill layers used in future testing.

- The strain monitoring system can be improved in the laboratory experiment, soil pressure transducers have been employed at Transnet to observe the pressure at various depths in a fill layer.

- In addition to the warning system, measures should be put in place in the event of the sinkhole forming, such as speed restrictions on the train in the area of void formation and informing all personnel involved.

The FEM model representing the laboratory experiment requires certain modifications to improve the accuracy of the results obtained:

- The under prediction of soil deformations in the FEM model was attributed to the automatic assignment of the angle of soil dilation by the program. Further investigation into modelling the dilation as an independent variable from the angle of shearing resistance is thus required. Currently Strand 7 does not allow this, hence a different FEM program should be used so that the soil deflection is not underestimated.

The analytical calculations covered an investigation into current design methods:

- The analytical calculations indicated that both design methods investigated in SANS 207 and the RAFAEL method showed some inaccuracies in terms of the soil surface deflection predictions. Revision of SANS 207 should take into account the dilative nature of soil. The angle of void propagation currently used in SANS 207 results in an over prediction of the settlement cone diameter and a shallower wider settlement cone. Further investigation into the angle of void propagation is thus required. To improve the RAFAEL design assumptions further testing with regard to the expansion coefficient of the sand must be performed.

The parametric model did exhibit a general under prediction in the soil surface deflections, this is partially attributed to the soil design capabilities in Strand 7 but also because the model needs to be refined further.

- Rail models are complex in that the connection between the concrete sleepers and the ballast stones are not fixed. The sleeper and ballast generally move relative to one another when the train is passing over the rail way line. Going forward a connection should be placed between the sleeper base and the ballast stones such that a gap is allowed between them when loading occurs. This can be done in the form of contact elements that allow movement between the ballast and the sleeper to a specified degree.

- The effect of the rail fastening system must also be taken into account more comprehensively. In the current model the rail is connected to the sleeper such that their meshes are aligned, hence they behave as if they are fixed to one another. This is not actually the case as relative movement between the rail and the sleeper should be allowed so that the rail uplift wave can be more accurately modelled when considering a train load.

- The modelling of the ballast stones also requires refining, generally discrete element analysis methods are considered when modelling particles and interlocking. The ballast layer was modelled as a soil layer but with a higher Young's modulus and an increased void ratio and angle of shearing resistance. Investigation into the accurate modelling of ballast stones is currently being undertaken at Transnet Freight Rail.

- The manner in which the load is applied to the rail must be revised, the current Strand 7 package available allows only static loading conditions, and dynamic loading conditions more representative of the trains axle load are available but were not purchased with this specific Strand 7 package.

- The modelling of soil using Strand 7 has resulted in general underestimation of the soil deformations, this is probably due to overestimation of soil dilation in the program. This can be overcome by regarding the soils angle of dilation separately from the angle of internal friction, Strand 7 is capable of modelling soil but for a more accurate representation of soil conditions, a different software should be considered.

REFERENCES

1. Alexiew, D., Elsing, A. & Ast, W., 2002. *FEM analysis and dimensioning of a sinkhole overbridging system for high speed trains at Groebers in Germany.* Germany, Proceedings of the 7th IGC geosynthetics conference.

2. Atkinson, J. H., 1981. *Foundations and slopes: an introduction to applications of critical state soil mechanics.* 1 ed. Sydney: McGraw-Hill.

3. Augarde, C., Lyamin, A. & Scott, S., 2003. Prediction of undrained sinkhole collapse. *Geotechnical and geoenvironmental engineering,* 129(3), pp. 197-198.

4. Bakhshipour, Z., Huat, B.K., Ibrahim, S., Asadi, A., Kura, N.U., 2013. Application of geophysical techniques for 3D geohazard mapping to delineate cavities and potential sinkholes in the Northern part of Kuala Lumpur, Malaysia. *The scientific world journal,* 2013(Article ID 629476), p. 11.

5. Bartlett, S. F., 2012. *Civil Utah Education.* [Online]
   Available at:
   http://www.civil.utah.edu/~bartlett/CVEEN6920/MohrCoulomb%20Model.pdf
   [Accessed 12 April 2016].

6. Blivet, J. C., Gourc. J.P., Villard. P., Giroud. H., Khay., M., Morbois. A., 2002. *Design method for geosynthetic as reinforcement for embankments subjected to localized subsidence.* Nice, Proceedings of 7th international conference on geosynthetics, pp. 341-344.

7. Bocchi, F., 2014. *Yield surfaces and plastic flow rules in Geomechanics,* United Kingdom: COMSOL.

8. Bohagr, A. A., 2013. *FEM modelling of geosynthetic reinforced pavement subgrades,* Washington state university: Masters of science in civil engineering dissertation .

9. Bolton, M. D., 1986. The strenght and dilatancy of sand. *Geotechnique,* 36(1), pp. 65-78.

10. Brink, A. B. A., 1979. *Engineering Geology of South Africa.* 1 ed. Pretoria: Building Publications.

11. British Code BS 8006, 1995. *Code of procedure for strenghtened/reinforced soils and other fills,* London: British standards institute.

12. Caudron, M., Emeriault, F., Kastner, R. & Al Heib, M., 2006. *Numerical modelling of soil structure interactions during sinkholes,* France,: Institut national de l'environment industriel et des risques.

13. Caudron, M. & Marwan, A. H., 2008. *Collapse of underground cavities and soil structure interactions.* Goa, The 12th international conference of International association for computer methods and advances in geomechanics.

14. Coetzee, C. J., Bassan, A. H. & Vermeer, P. A., 2006. Discrete and continuum modelling of silo discharge. *R & D Journal,* 22(2), pp. 26-38.

15. Craig, R. F., 2004. *Craig soil mechanics.* 7th ed. London: SPON Press.

16. Craig, W. H., 2001. *The seven ages of centrifuge modelling,* Asconia; University of Manchester: Workshop on constitutive and centrifuge modelling.

17. Das, B. M., 2006. *Principles of geotechnical engineering.* 4 ed. Sacramento: Thomson.

18. de Lange, H., 2016. *Physical modelling of the behaviour of a multi-layer reinforced embankment over a developing subgrade void,* Universoty of Kwa Zulu Natal: Msc disseration in draft.

19. El-Emam, M., 2011. *Experimental and numerical study of at rest lateral earth pressure of overconsolidated soil.* [Online] Available at:

http://www.hindawi.com/journals/ace/2011/524568/
[Accessed 10 May 2016].

20. Gallego, E., Rombach, G. A., Neumann, F. & Ayuga, F., 2010. Simulations of granular flow in silos with different finite element programs. *Tranasctions of the ASABE,* 3(53), pp. 819-829.

21. Geotech data information, 2013. *Soil elastic Young's modulus - Geotechdata.info.* [Online]
Available at: http://www.geotechdata.info/parameter/soil-young's-modulus.html
[Accessed 10 May 2016].

22. German design guide EBGEO, 2011. *Recommendations for design and analysis of earth structures using geosynthetic reinforcements,* Munchen: German geotechnical society.

23. Giroud, J. P., Bonaparte, R., Beech, J. F. & Gross, B. A., 1990. Design of soil layer-geosynthetic systems overlying voids. *Geotextiles and geomembranes,* Volume 9, pp. 11-50.

24. Goodings, D. J. & Abdulla, W. A., 2002. Stability charts for predicting sinkholes in weakly cemented sand over karst limestone. *Engineering geology,* Volume 65, pp. 179-184.

25. Grabe, H., 2003. *Thabazimbe formation rehabilitation test sections,* Johannesburg: Transnet freight rail, Internal technical report.

26. Han, J., n.d. *Overview of Geosynthetic Materials, Their Characteristics, Applications, and Design Considerations.* [Online]
Available at: http://www2.ku.edu/~kutc/pdffiles/GeoProperties-Han5-9-12.pdf
[Accessed 15 June 2016].

27. Hutton, D. V., 2004. *Fundementals of finite element analysis.* 0-07-112231-1 ed. New York: Mc Graw-Hill.

28. Jaros, M. B., James, G. M. & Gewanlal, C., 2009. *Multi layer geosynthetic reinforcemed embankment over potential sinkholes for rapid rail link in South Africa.* Cape Town, Proceedings of GIGSA Geo Africa conference.

29. Kae, J., 2003. *The use of geosynthetics as reinforcement in formation layers*, Johannesburg: Transnet Freight Rail, Internal technical report.

30. Lee, Y. J., Kim. D.H., Kim. G.D., Kim. P.U., Lee. S.H., Cho. J.H., Kim. M.N., 2006. FEA of small acoustic filters for the hearing protection device. *World congree on medical physics and biomedical engineering,* 2(14), pp. 827-830.

31. Ling, H. I. & Lui, K., 2003. Finite element studies of asphalt concrete pavement reinforced with geogrid. *Engineering mechanics ASCE,* Volume 129, pp. 801-811.

32. Madabhushi, G., 2011. *Principles of centrifuge modelling*, Proceedings of TNA workshop on centrifuge modelling: University of Cambridge.

33. Messafer, T., 1996. Boundary element analysis of reinforced soil systems using geotextiles. *Engineering analysis with boundary elements,* 17(3), pp. 183-192.

34. Mifsud, A., 2005. *A parametric study on the behaviour of a geosynthetically-reinforced granular fill as voids develop directly below,* London: Masters dissertation Imperial College.

35. Montanelli, F. & Recalcati, P., n.d. *Geogrid reinforced railways embankments: Design concepts and experiemental test results.* [Online]
Available at: http://www.tenax.net/geosynthetics/tech-doc/geogrid-reinforced-railways-embankments.pdf
[Accessed 13 October 2015].

36. Muller, W. W. & Saathoff, F., 2015. Geosynthetics in geoenvironmental engineering. *Science and technology of advanced materials*, 16(3), pp. 1-20.

37. Munian, D., 2010. *Numerical modelling of strains in a sandmass when undermined by a developing subgrade void,* Kwa-Zulu Natal: Bachelor's degree dissertation University of Kwa-Zulu Natal.

38. Oosthuizen, A. C. & Richardson, S., 2011. *Sinkholes and subsidence in South Africa,* Capetown: Council for geoscience Internal technical report.

39. Perkins, S. W., 2001. *Numerical modelling of geosynthetically reinforced flexible pavement,* Montana: Montana department of transportation internal technical report.

40. Pinto, M. I., 2003. Applications of geosynthetics for soil reinforcement. *Ground Improvement,* 7(2), pp. 61-72.

41. Piza, C. G., 2009. *Geosynthetic reinforced fill to bridge voids,* London: Masters degree dissertation Imperial College.

42. Potts, D. & Zdravkovic, L., 1999. *Finite element analysis in geotechnical engineering theory.* 1 ed. London: Thomas Telford.

43. Potts, V., 2007. *Geosynthetically reinforced fill as a load transfer platform to bridge voids,* London: Phd Thesis Imperial college.

44. Rajagopal, K., n.d. *Different types of geosynthetics and their applications,* Chennai: IIT Madras lecture notes.

45. Roylance, D., 2001. *Finite element analysis,* Cambridge: Massachusetts institute of technology Internal course notes.

46. Sanad, A. M., Ooi, J. J., Heist, J. M. & Rotter, J. M., 2001. Computation of granular flows and pressure in a flat bottomed silo. *Journal of engineering mechanics,* 127(10), pp. 1033-1043.

47. Sayas, F.-J., 2008. *A gentle introduction into finite element analysis.* [Online] Available at: http://arturo.imati.cnr.it/~marini/didattica/Metodi-engl/Intro2FEM.pdf [Accessed 7 December 2015].

48. Schofield, A. & Wroth, P., 1986. *Critical state soil mechanics.* Cambridge: University of Cambridge.

49. Sherif, M. A., Fang, Y. S. & Sherif, R. I., 1984. Ka and Ko behind rotating and non-yielding walls. *Journal of geotechnical engineering,* 110(1), pp. 41-56.

50. Smith, M., 2014. Slope stabilization and the arching phenomena. *Civil + Structural engineer,* 1(4), pp. 49-51.

51. South African National Standard SANS 207, 2006. *The design and construction of reinforced soils and fills,* Pretoria: Standards South Africa.

52. Sparks, S., 2012. *A physical study of the angle of dilation of cohesion less soils,* Kwa Zulu Natal: Bachelor's degree dissertation University of Kwa Zulu Natal.

53. Steinman, D. B., 1957. *A practical treatise on suspension bridges.* 2nd edition ed. New York: John Wiley & Sons.

54. Strand 7 verification manual, 2013. *Verification tests for the Strand 7 finite element analysis system,* Sydney: Strand 7 Pty Ltd.

55. Terzagi, K., 1943. *Theoretical soil mechanics.* 1 ed. Michigan: J Wiley & Sons inc.

56. Ting, T. M., 1989. Discrete numerical model for soil mechanics. *Journal of geotechnical engineering,* 115(3), p. 381.

57. Transnet Freight Rail BBB0481, 2012. *Manual for track maintenence,* Johannesburg: Transnet SOC Ltd, Internal technical manual.

58. Transnet Freight Rail S406, 1998. *Specification for the supply of stone contents,* Pretoria: Transnet SOC Ltd, Internal technical document.

59. Transnet Freight Rail S413, 1985. *South African transport services specification for stabilisation,* Johannesburg: Transnet SOC Ltd, Internal technical manuals.

60. Transnet Limited S410, 1990. *Specification for railway earthworks,* Johannesburg: Transnet SOC Ltd, Internal technical manual.

61. University of Colorado, 2012. *University of Colorado education.* [Online]
Available at:
http://www.colorado.edu/engineering/CAS/courses.d/Structures.d/IAST.../IAST.Lect05.pdf
[Accessed 15 June 2016].

62. Van Baars, S., 1995. *Discrete element analysis of granular materials.* 1 ed. England: Delft.

63. Villard, P. & Briancon, L., 2008. Design of geosynthetic reinforcement for platforms subjected to localised sinkholes. *Canadian geotechnical journal,* Volume 45, pp. 196-209.

64. Villard, P., Chevalier, B., Le Hello, B. & Combe, G., 2009. Coupling between finite and discrete element methods for the modelling of earth structures reinforced by geosynthetics. *Computers and geotechnics,* Volume 36, pp. 709-717.

65. Villard, P., Gourc, J. P. & Giraud, H., 2000. A geosynthetic reinforcement solution to prevent the formation of localized sinkholes. *Canadian Geotech Journal,* Volume 37, pp. 987-999.

66. Wang, M. C., Feng, Y. X. & Jao, M., 1996. Stability of geosynthetic-reinforced soil above a cavity. *Geotextiles and geomembranes,* Volume 14, pp. 95-109.

67. Wieckowski, Z., 2003. Modelling of silo discharge and filling problems by the material point method. *Al Politechniki,* 6(4), pp. 701-721.

APPENDIX LIST

Geosynthetic testing results

The results of the geosynthetic testing for both the de Lange (2016) laboratory model and the parametric investigation is described in Appendix A.

Soil testing results

The results of the soil testing is described in Appendix B.

Design Procedures:

The results of the analytical study of the current design methods are attached in the Appendix C.

Potts FEM Case Study:

The results of the Strand 7 FEM analysis describing the Potts case study are attached in the Appendix D.

UKZN Laboratory Tests:

The results of the Strand 7 FEM analysis describing the UKZN laboratory tests are attached in the Appendix E.

Parametric Study:

The position of the loading conditions along the x axis is shown in Appendix B.

The results of the Strand 7 FEM analysis describing the parametric model are attached in the Appendix F.

APPENDIX A:

Laboratory results for geogrid testing:

The geosynthetic reinforcement used in de Lange (2016) was tested at the Geosynthetic Laboratory. The results of the tests are attached below:

Table A1: Results of testing of geosynthetic sample used in de Lange (2016)

GEOSYNTHETIC
LABORATORY

11 Livingstone Road; Pinetown
P.O. Box 116
3600
Tel: 031 717 2360
Fax: 031 702 4477
E-mail: prakash@geolaboratory.com
Webpage: www.geolaboratory.com

SANS 10221-07 : Tensile Test

TEST REPORT

Test Number	: P2010069	Test speed	: 60 mm/min
Customer	: UKZN	Sampled	: Elgie
Manufacturer	: N/A	Tester	: Elgie
Project	: UKZN Dissertation Tensile test Strength	Start	: 2010-12-07
		Finish	: 2010-12-07
Specimen ID	: 250mm X 250mm	Atmosphere	: @ start Temp 23.7°C Humid 54.9% rh @ end Temp 23.0C Humid 53.5% rh
Sample details	: Sample 2 White K - MF Mosquito Net		
Date Recev	: 2010-12-07		
Date Sampled	: 2010-12-07		
Sub-series Identifier	: Diagonal white	Deviation	: None
Condition of test	: Dry	Specimen grips	: 250mm Wide width
Pre-load	: 5 N	Zwick UTM	: Type : 1488 Fmax : 200kN Ser Num : 109494/04 Extenso : Exoptic 001 Ser Num : 811603/05
		Observation	:

Results:

Diagonal white Nr	Max Force N	Tult kN/m	ε Strain @ Fmax. mm	E-Modulus MPa	Gauge Length mm	Date Test
29	257.718	1.03	24.21	8.63	80.00	2010/12/07

Series graphics:

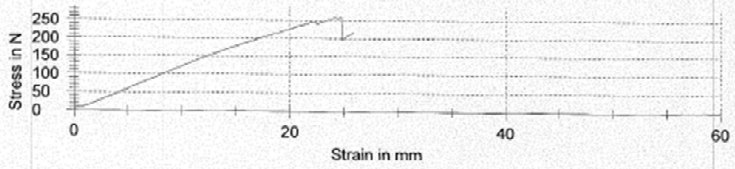

Statistics:

Diagonal white n = 1	Max Force N	Tult kN/m	ε Strain @ Fmax. mm	E-Modulus MPa
x̄	257.718	1.03	24.21	8.63
s	-	-	-	-
v	-	-	-	-

Authorised by: Date:

UKZN Dissertation Tensile P2010069.ZSE

The commercially available geosynthetic properties used in the course of the parametric study are shown in the Table A2 below:

Table A2: Commercially available geosynthetic properties

			50/50	100/100	200/200	
Material		Polyester, staple fibre 150 g/m² needle punched, nonwoven / high strength polyester yarns				
Short Term Tensile Strength (T_u)	Machine	kN/m	50	100	200	ISO 10319
	Across	kN/m	50	100	200	
	Elongation	%	10	10	10	
Long Term Design Strength (LTDS*) 120 Years		kN/m	26	52	105	ISO 10319
Creep Limited Strength 120 Years		kN/m	30	60	120	ISO 13431
Water Flow Rate	Normal to Plane	ℓ/s/m²	150			ISO 11058
	In Plane 20 kPa	ℓ/s/m/hr	20			ISO 12958
Roll Dimensions		m	5 x 100			ISO 12958

$$LTDS = \frac{T_u}{f_c.f_d.f_e.f_m}$$

f_c (creep) = 1.65 (120 years)

f_d (damage) = 1.05 (sand, silt, clay, yarn facing soil)

f_e (environment) = 1.10 (pH 4-9)

f_m (material) = 1.00

APPENDIX B:

Soil testing results:

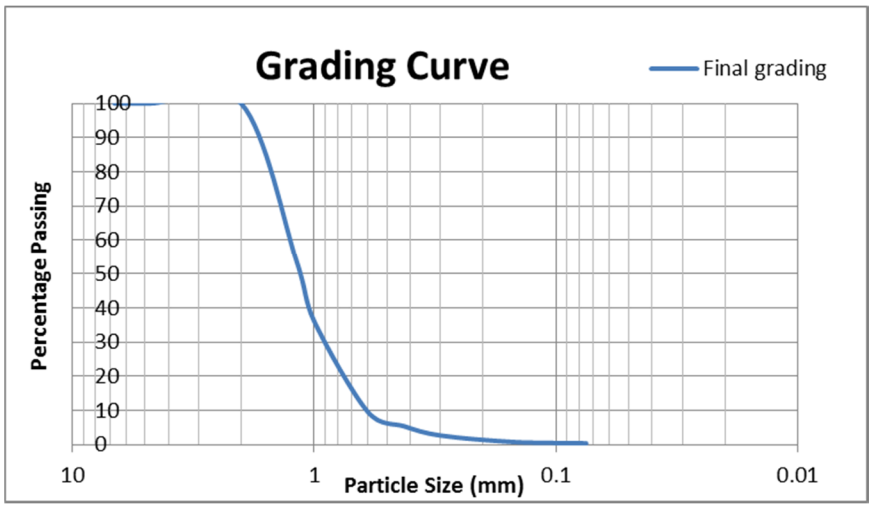

Figure B1: de Lange (2016) results for seive grading analysis

Table B1: Sparks (2011) results for angle of shearing resistance, angle of dilation and dry density of soil samples

	FROM EXPERIMENTAL RESULTS		
Sample	**φ (Deg)**	**ψ (Deg)**	**Dry density (kg/m^3)**
1	43.93	17.61	1439.14
2	41.02	15.57	1698.60
3	42.76	17.94	1680.19
4	45.14	-0.24	1676.10
5	40.36	11.1	1765.63
6	41.33	10.16	1729.28
7	38.54	9.16	1775.09
8	39.62	10.76	1715.89
9	37.91	11.16	1785.52

Table B2: Load cases used in parametric investigation:

Load case	x distance (m)	Sum of loading -z direction (T)
1	-0.275	26
2	0.000	26
3	0.375	26
4	0.650	26
5	1.025	26
6	1.300	26
7	1.675	26
8	1.950	26
9	2.325	26
10	2.600	26
11	2.975	26
12	3.250	26
13	3.625	26
14	3.900	26
15	4.275	26
16	4.550	26
17	4.925	26
18	5.200	26
19	5.575	26
20	5.850	26
21	6.225	26
22	6.500	26
23	6.875	26
24	7.150	26
25	7.525	26
26	7.800	26
27	8.175	26
28	8.450	26
29	8.825	26
30	9.100	26
31	9.475	26
32	9.750	26
33	10.125	26
34	10.400	26
35	10.775	26
36	11.050	26
37	11.425	26
38	11.700	26
39	12.075	26
40	12.350	26

41	12.725	26
42	13.000	26
43	13.375	26
44	13.650	26
45	14.025	26
46	14.300	26
47	14.675	26
48	14.950	26
49	15.325	26
50	15.600	26
51	15.975	26
52	16.250	26
53	16.625	26
54	16.900	26
55	17.275	26
56	17.550	26

APPENDIX C

	D (mm)			
	150	200	300	
Ds (mm)	500.000	500.000	700.000	Geogrid No.
ds (mm)	3.843	9.109	19.594	1
	3.284	7.783	16.741	2
	4.536	10.751	23.126	3
	4.546	10.776	18.551	4
	4.328	10.258	22.065	5
	4.458	10.567	22.729	6

H	300			mm
θ	59.74	63.43	56.3	deg
L geogrid	80			mm

Geogrid No.	Elongation	εmax
1	17.3	0.21625
2	12.63	0.157875
3	24.1	0.30125
4	24.21	0.302625
5	21.94	0.27425
6	23.28	0.291

	D (mm)			
D	150	200	300	Geogrid No.
d	42.71544656	56.95393	85.4308931	1
	36.49753844	48.66338	72.9950769	2
	50.41623622	67.22165	100.832472	3
	50.53116303	67.37488	101.062326	4
	48.10389147	64.13852	96.2077829	5
	49.55110998	66.06815	99.10222	6

SANS207

			D		
			150	200	300
Geogrid No.	Tmax(N)	emax	p (N)	p (N)	p (N)
1	338.295	0.21625	3.389692	2.542269	1.694846
2	232.985	0.157875	2.16664694	1.62498521	1.083323
3	180.943	0.30125	1.93579692	1.45184769	0.967898
4	257.718	0.302625	2.75939879	2.06954909	1.379699
5	241.679	0.27425	2.54139817	1.90604862	1.270699
6	279.558	0.291	2.97223069	2.22917302	1.486115

H			300	mm
Ce			1.03	
H>			1.67 D	

D (mm)		H (mm)	d (mm)	ds (mm)	Ce
150		300	_	2.01	
200		300	7.39	2.81	1.008
300		300	_	6.15	

	D (mm)						
					150	200	300
D	150	200	300	Geogrid No.	1.67D	1.67D	1.67D
d	42.71544656	56.95393	85.4308931	1	71.3348	95.11306	142.6696
	36.49753844	48.66338	72.9950769	2	60.95089	81.26785	121.9018
	50.41623622	67.22165	100.832472	3	84.19511	112.2602	168.3902
	50.53116303	67.37488	101.062326	4	84.38704	112.5161	168.7741
	48.10389147	64.13852	96.2077829	5	80.3335	107.1113	160.667
	49.55110998	66.06815	99.10222	6	82.75035	110.3338	165.5007

	D (mm)			
D	150	200	300	Geogrid No.
ds	24.71544656	38.95393	67.4308931	1
	18.49753844	30.66338	54.9950769	2
	32.41623622	49.22165	82.8324724	3
	32.53116303	49.37488	83.0623261	4
	30.10389147	46.13852	78.2077829	5
	31.55110998	48.06815	81.10222	6

RAFAEL METHOD

		Volume Calculations:		
Void Diameter (mm)	RAFAEL	V (mm^3)	H (mm)	ΔV (%)
	Base	446479.68	50.53	
150 mm	Surface	287436.55	32.53	35.62
	Base	1058322.20	67.37	
200 mm	Surface	775578.87	49.37	26.72
	Base	3571837.44	101.06	
300 mm	Surface	2935664.93	83.06	17.81

		Volume Calculations:		
Void Diameter (mm)	SANS 207	V (mm^3)	H (mm)	ΔV (%)
	Base	446479.68	50.53	
150 mm	Surface	446345.74	4.55	0.03
	Base	1058322.20	67.37	
200 mm	Surface	1057910.94	10.78	0.04
	Base	3571837.44	101.06	
300 mm	Surface	3569538.30	18.55	0.06

Pi	3.141593	
	150	
	200	
	300	
	3.141593	r
	150	250
	200	250
	300	350

V original

Basal												
FEM Model						Lab Model						
Soil surface deflection D=150		Soil surface deflection D=200		Soil surface deflection D=300		Soil surface deflection D=150		Soil surface deflection D=200		Soil surface deflection D=300	
x	y	x	y	x	y	x	y	x	y	x	y
0.00	-1.69	0.00	-2.26	0.00	-5.40	0	-2	0	-2.75	0	-6
10.00	-1.68	10.00	-2.26	10.00	-5.39	50	-1.85	50	-2.5	50	-6
20.00	-1.67	20.00	-2.24	20.00	-5.36	100	-1.68	100	-2.25	100	-5.5
30.00	-1.65	30.00	-2.21	30.00	-5.30	150	-0.9	150	-1.5	150	-3.9
40.00	-1.62	40.00	-2.17	40.00	-5.23	200	-0.5	200	-0.5	200	-2
50.00	-1.58	50.00	-2.12	50.00	-5.14	250	-0.1	250	-0.25	250	-1
60.00	-1.54	60.00	-2.06	60.00	-5.03	300	-0.1	300	-0.2	300	-0.5
70.00	-1.49	70.00	-2.00	70.00	-4.90	350	-0.1	350	-0.2	350	-0.3
80.00	-1.43	80.00	-1.92	80.00	-4.76	400	-0.1	400	-0.2	400	-0.2
90.00	-1.37	90.00	-1.84	90.00	-4.61	450.00	0	450.00	0	450.00	0
100.00	-1.31	100.00	-1.76	100.00	-4.44						
110.00	-1.24	110.00	-1.67	110.00	-4.26						
120.00	-1.18	120.00	-1.58	120.00	-4.08						
130.00	-1.11	130.00	-1.49	130.00	-3.89						
140.00	-1.04	140.00	-1.40	140.00	-3.70						
150.00	-0.97	150.00	-1.31	150.00	-3.51						
160.00	-0.90	160.00	-1.22	160.00	-3.30						
170.00	-0.84	170.00	-1.13	170.00	-3.11						
180.00	-0.77	180.00	-1.04	180.00	-2.92						
190.00	-0.71	190.00	-0.96	190.00	-2.74						
200.00	-0.65	200.00	-0.88	200.00	-2.56						
210.00	-0.60	210.00	-0.81	210.00	-2.38						
220.00	-0.54	220.00	-0.74	220.00	-2.22						
230.00	-0.50	230.00	-0.67	230.00	-2.06						
240.00	-0.45	240.00	-0.61	240.00	-1.89						
250.00	-0.41	250.00	-0.55	250.00	-1.75						
260.00	-0.37	260.00	-0.50	260.00	-1.62						
270.00	-0.33	270.00	-0.45	270.00	-1.49						
280.00	-0.30	280.00	-0.40	280.00	-1.38						
290.00	-0.27	290.00	-0.36	290.00	-1.28						
300.00	-0.24	300.00	-0.32	300.00	-1.18						
310.00	-0.21	310.00	-0.29	310.00	-1.07						
320.00	-0.19	320.00	-0.26	320.00	-0.99						
330.00	-0.17	330.00	-0.23	330.00	-0.92						
340.00	-0.15	340.00	-0.21	340.00	-0.83						
350.00	-0.14	350.00	-0.18	350.00	-0.78						
360.00	-0.12	360.00	-0.17	360.00	-0.70						
370.00	-0.11	370.00	-0.15	370.00	-0.66						
380.00	-0.10	380.00	-0.13	380.00	-0.60						
390.00	-0.09	390.00	-0.12	390.00	-0.57						
400.00	-0.08	400.00	-0.11	400.00	-0.50						
410.00	-0.08	410.00	-0.10	410.00	-0.48						
420.00	-0.07	420.00	-0.10	420.00	-0.42						
430.00	-0.07	430.00	-0.09	430.00	-0.39						
440.00	-0.07	440.00	-0.09	440.00	-0.39						
450.00	-0.07	450.00	-0.09	450.00	-0.38						

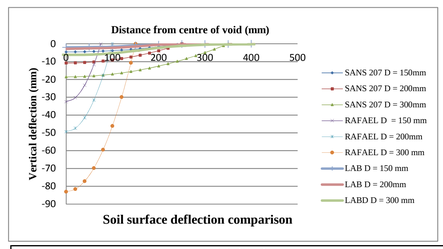

Soil surface deflection comparison

LAB RESULTS					
D = 300mm		D = 200mm		D = 150mm	
x	y	x	y	x	y
0	-6.15	0	-2.81	0	-2.01
50	-6.11	50	-2.51	50	-1.85
100	-5.28	100	-2.25	100	-1.68
150	-3.91	150	-1.51	150	-0.9
200	-2.21	200	-0.52	200	-0.52
250	-1.15	250	-0.25	250	-0.13
300	-0.52	300	-0.24	300	-0.12
350	-0.33	350	-0.23	350	-0.105
400	-0.28	400	-0.23	400	0

RAFAEL: D=150	
x	y
0	-32.5312
20	-30.2178
40	-23.2779
60	-11.7112
75	0

RAFAEL: D=200	
x	y
0	-49.3749
20	-47.3999
40	-41.4749
60	-31.5999
80	-17.775
100	0

RAFAEL: D=200	
x	y
0	-83.0623
20	-81.5857
40	-77.1557
60	-69.7724
80	-59.4357
100	-46.1457
120	-29.9024
140	-10.7058
150	0

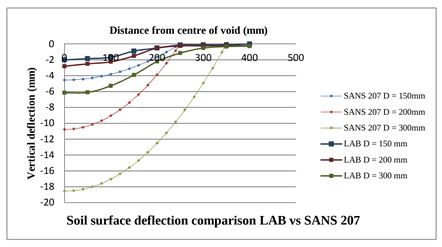

Soil surface deflection comparison LAB vs SANS 207

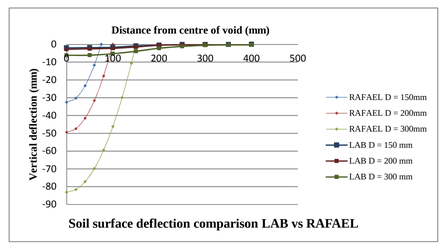

Soil surface deflection comparison LAB vs RAFAEL

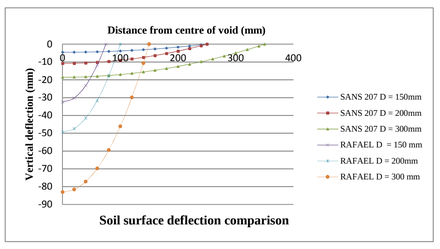

Soil surface deflection comparison

SANS207	D (mm)		
	150	200	300
Ds (mm)	500	500	700
ds (mm)	4.54644	10.77579	18.55052
d(mm)	50.53116	67.37488	101.0623
D (mm)	150	200	300
d/D	0.336874	0.336874	0.336874
r	80.9243	107.8991	161.8486

RAFAEL	D (mm)		
	150	200	300
Ds (mm)	150	200	300
ds (mm)	32.53116	49.37488	83.06233
d(mm)	50.53116	67.37488	101.0623
D (mm)	150	200	300
d/D	0.336874	0.336874	0.336874
r	80.9243	107.8991	161.8486

Soil surface deflection

SANS207: D=150	
x	y
0	-4.54644
20	-4.51734
40	-4.43005
60	-4.28457
80	-4.08088
100	-3.81901
120	-3.49894
140	-3.12068
160	-2.68422
180	-2.18957
200	-1.63672
220	-1.02568
240	-0.35644
250	0

SANS207: D=200	
x	y
0	-10.7758
20	-10.7068
40	-10.4999
60	-10.1551
80	-9.67235
100	-9.05167
120	-8.29305
140	-7.3965
160	-6.36203
180	-5.18962
200	-3.87929
220	-2.43102
240	-0.84482
250	0

SANS207: D=300	
x	y
0	-18.5505
20	-18.4899
40	-18.3082
60	-18.0054
80	-17.5813
100	-17.0362
120	-16.3699
140	-15.5824
160	-14.6738
180	-13.6441
200	-12.4932
220	-11.2212
240	-9.82799
260	-8.31366
280	-6.67819
300	-4.92157
320	-3.0438
340	-1.04489
350	0

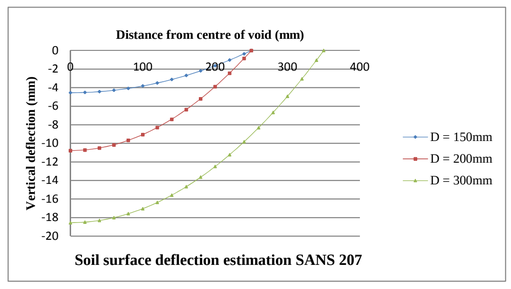

Soil surface deflection estimation SANS 207

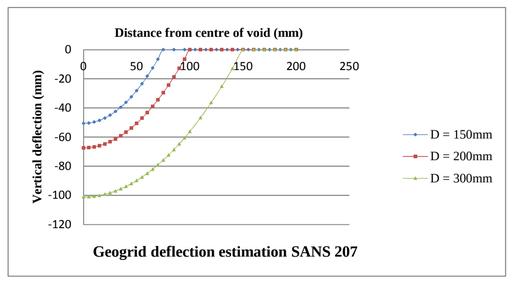

Geogrid deflection estimation SANS 207

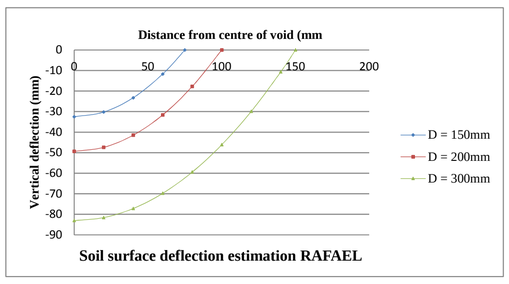

Soil surface deflection estimation RAFAEL

Geogrid deflection: Parabola

SANS207: D=150	
x	y
0	-50.5312
5	-50.3066
10	-49.6328
15	-48.5099
20	-46.9378
25	-44.9166
30	-42.4462
35	-39.5266
40	-36.1579
45	-32.3399
50	-28.0729
55	-23.3566
60	-18.1912
65	-12.5766
70	-6.51291
75	7.11E-15
85	0
95	0
105	0
115	0
125	0
135	0
145	0
155	0
165	0
175	0
185	0
195	0

SANS207: D=200	
x	y
0	-67.3749
5	-67.2064
10	-66.7011
15	-65.8589
20	-64.6799
25	-63.164
30	-61.3111
35	-59.1215
40	-56.5949
45	-53.7315
50	-50.5312
55	-46.994
60	-43.1199
65	-38.909
70	-34.3612
75	-29.4765
80	-24.255
85	-18.6965
90	-12.8012
95	-6.56905
100	0
110	0
120	0
130	0
140	0
150	0
160	0
170	0
180	0
190	0
200	0

SANS207: D=300	
x	y
0	-101.062
5	-100.95
10	-100.613
15	-100.052
20	-99.2657
25	-98.255
30	-97.0198
35	-95.56
40	-93.8757
45	-91.9667
50	-89.8332
55	-87.4751
60	-84.8924
65	-82.0851
70	-79.0532
75	-75.7967
80	-72.3157
85	-68.6101
90	-64.6799
95	-60.5251
100	-56.1457
110	-46.7133
120	-36.3824
130	-25.1533
140	-13.0258
150	1.42E-14
160	0
170	0
180	0
190	0
200	0

RAFAEL: D=150	
x	y
0	-32.5312
20	-30.2178
40	-23.2779
60	-11.7112
75	0

RAFAEL: D=200	
x	y
0	-49.3749
20	-47.3999
40	-41.4749
60	-31.5999
80	-17.775
100	0

RAFAEL: D=300	
x	y
0	-83.0623
20	-81.5857
40	-77.1557
60	-69.7724
80	-59.4357
100	-46.1457
120	-29.9024
140	-10.7058
150	0

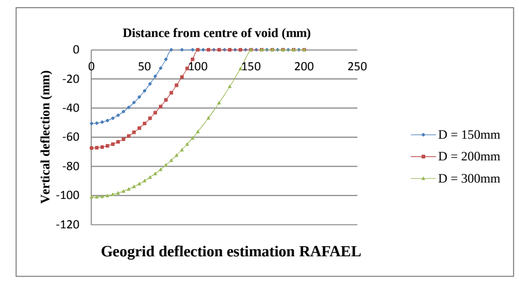

Geogrid deflection estimation RAFAEL

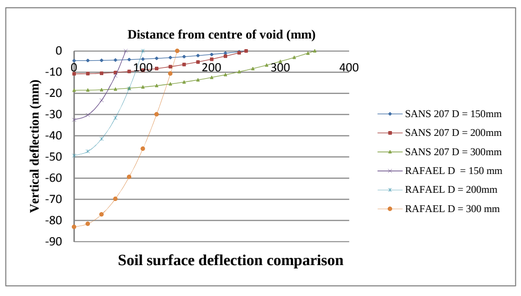

Soil surface deflection comparison

Geogrid deflection: Parabola

RAFAEL: D=150	
x	y
0	-50.5312
5	-50.3066
10	-49.6328
15	-48.5099
20	-46.9378
25	-44.9166
30	-42.4462
35	-39.5266
40	-36.1579
45	-32.3399
50	-28.0729
55	-23.3566
60	-18.1912
65	-12.5766
70	-6.51291
75	7.11E-15
85	0
95	0
105	0
115	0
125	0
135	0
145	0
155	0
165	0
175	0
185	0
195	0

RAFAEL: D=200	
x	y
0	-67.3749
5	-67.2064
10	-66.7011
15	-65.8589
20	-64.6799
25	-63.164
30	-61.3111
35	-59.1215
40	-56.5949
45	-53.7315
50	-50.5312
55	-46.994
60	-43.1199
65	-38.909
70	-34.3612
75	-29.4765
80	-24.255
85	-18.6965
90	-12.8012
95	-6.56905
100	0
110	0
120	0
130	0
140	0
150	0
160	0
170	0
180	0
190	0
200	0

RAFAEL: D=200	
x	y
0	-101.062
5	-100.95
10	-100.613
15	-100.052
20	-99.2657
25	-98.255
30	-97.0198
35	-95.56
40	-93.8757
45	-91.9667
50	-89.8332
55	-87.4751
60	-84.8924
65	-82.0851
70	-79.0532
75	-75.7967
80	-72.3157
85	-68.6101
90	-64.6799
95	-60.5251
100	-56.1457
110	-46.7133
120	-36.3824
130	-25.1533
140	-13.0258
150	1.42E-14
160	0
170	0
180	0
190	0
200	0

APPENDIX D

H = 80 D =160	
H/D = 0.5	
x	y
-400.00	0.01
-390.00	0.01
-380.00	0.01
-370.00	0.01
-360.00	0.01
-350.00	0.01
-340.00	0.01
-330.00	0.01
-320.00	0.01
-310.00	0.01
-300.00	0.01
-290.00	0.01
-280.00	0.01
-270.00	0.01
-260.00	0.01
-250.00	0.01
-240.00	0.02
-230.00	0.02
-220.00	0.03
-210.00	0.03
-200.00	0.03
-190.00	0.03
-180.00	0.02
-170.00	0.00
-160.00	-0.05
-150.00	-0.14
-140.00	-0.28
-130.00	-0.49
-120.00	-0.80
-110.00	-1.25
-100.00	-1.85
-90.00	-2.62
-80.00	-3.52
-75.00	-4.01
-70.00	-4.52
-65.00	-5.04
-60.00	-5.55
-55.00	-6.05
-50	-6.52
-45	-6.97
-40	-7.37
-35	-7.73
-30	-8.05
-25	-8.32
-20	-8.54
-15	-8.71
-10	-8.84
-5	-8.91
0	-8.93814
5	-8.91305
10	-8.83789
15	-8.71301
20	-8.53899
25	-8.31656
30	-8.04666
35	-7.73043
40	-7.36951
45	-6.96636
50	-6.52487
55	-6.05086
60	-5.55229
65	-5.03897
70	-4.52177
75	-4.01168
80	-3.52067
90	-2.61740
100	-1.85368
110	-1.24756
120	-0.80251
130	-0.49122
140	-0.27855
150	-0.13852
160	-0.05231
170	-0.00282
180	0.02262
190	0.03305
200	0.03467
210	0.03157
220	0.02636
230	0.02059
240	0.01514
250	0.01041
260	0.00657
270	0.00359
280	0.00138
290	-0.00019
300	-0.00125
310	-0.00191
320	-0.00230
330	-0.00249
340	-0.00255
350	-0.00254
360	-0.00249
370	-0.00242
380	-0.00237
390	-0.00233
400	-0.00232

H = 80 D =80	
H/D = 1	
x	y
-400.00	-0.00054
-390.00	-0.00057
-380.00	-0.00060
-370.00	-0.00062
-360.00	-0.00063
-350.00	-0.00063
-340.00	-0.00060
-330.00	-0.00051
-320.00	-0.00036
-310.00	-0.00011
-300.00	0.00027
-290.00	0.00081
-280.00	0.00154
-270.00	0.00249
-260.00	0.00365
-250.00	0.00501
-240.00	0.00646
-230.00	0.00781
-220.00	0.00867
-210.00	0.00844
-200.00	0.00615
-190.00	0.00032
-180.00	0.00615
-170.00	0.00032
-160.00	-0.01119
-150.00	-0.01119
-140.00	-0.01119
-130.00	0.00844
-120.00	0.00867
-110.00	-0.11592
-100.00	-0.19230
-90.00	-0.30124
-80.00	-0.45018
-70.00	-0.64439
-60.00	-0.88430
-55.00	-1.01841
-50.00	-1.16080
-45.00	-1.30803
-40	-1.45660
-35	-1.60246
-30	-1.74126
-25	-1.86846
-20	-1.97966
-15	-2.07085
-10	-2.13860
-5	-2.18033
0	-2.19443
5	-2.18033
10	-2.13860
15	-2.07085
20	-1.97966
25	-1.86846
30	-1.74126
35	-1.60246
40	-1.45660
45	-1.30803
50	-1.16080
55	-1.01841
60	-0.88430
70	-0.64439
80	-0.45018
90	-0.30124
100	-0.19230
110	-0.11592
120	-0.06453
130	-0.03142
140	-0.01119
150	0.00032
160	0.00615
170	0.00844
180	0.00867
190	0.00781
200	0.00646
210	0.00501
220	0.00365
230	0.00249
240	0.00154
250	0.00081
260	0.00027
270	-0.00011
280	-0.00036
290	-0.00051
300	-0.00060
310	-0.00063
320	-0.00064
330	-0.00062
340	-0.00060
350	-0.00057
360	-0.00054
370	-0.00052
380	-0.00050
390	-0.00049
400	-0.00049

H = 240 D =80	
H/D = 1	
x	y
-400	-0.00029
-390	-0.00030
-380	-0.00031
-370	-0.00032
-360	-0.00033
-350	-0.00033
-340	-0.00031
-330	-0.00028
-320	-0.00021
-310	-0.00010
-300	0.00007
-290	0.00029
-280	0.00060
-270	0.00099
-260	0.00146
-250	0.00199
-240	0.00254
-230	0.00299
-220	0.00319
-210	0.00287
-200	0.00161
-190	-0.00121
-180	0.00161
-170	-0.00121
-160	-0.00645
-150	-0.01533
-140	-0.02946
-130	-0.02946
-120	-0.02946
-110	-0.05089
-100	-0.08208
-90	-0.12572
-80	-0.18432
-70	-0.25947
-60	-0.35097
-55	-0.40157
-50	-0.45499
-45	-0.50992
-40	-0.56510
-35	-0.61907
-30	-0.67025
-25	-0.71703
-20	-0.75784
-15	-0.79125
-10	-0.81605
-5	-0.83131
0	-0.83646
5	-0.83131
10	-0.81605
15	-0.79125
20	-0.75784
25	-0.71703
30	-0.67025
35	-0.61907
40	-0.56510
45	-0.50992
50	-0.45499
55	-0.40157
60	-0.35097
70	-0.25947
80	-0.18432
90	-0.12572
100	-0.08208
110	-0.05089
120	-0.02946
130	-0.01533
140	-0.00645
150	-0.00121
160	0.00161
170	0.00287
180	0.00319
190	0.00299
200	0.00254
210	0.00199
220	0.00146
230	0.00099
240	0.00060
250	0.00029
260	0.00007
270	-0.00010
280	-0.00021
290	-0.00028
300	-0.00031
310	-0.00033
320	-0.00033
330	-0.00032
340	-0.00031
350	-0.00030
360	-0.00029
370	-0.00027
380	-0.00027
390	-0.00026
400	-0.00026

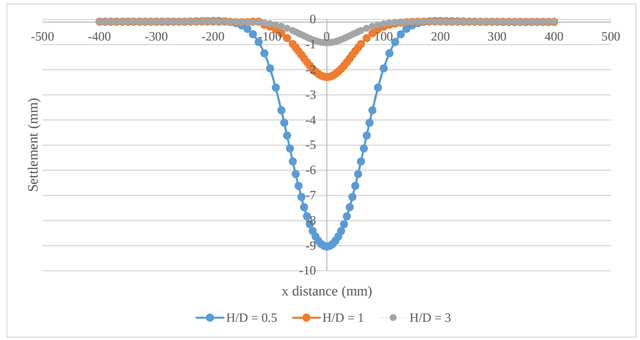

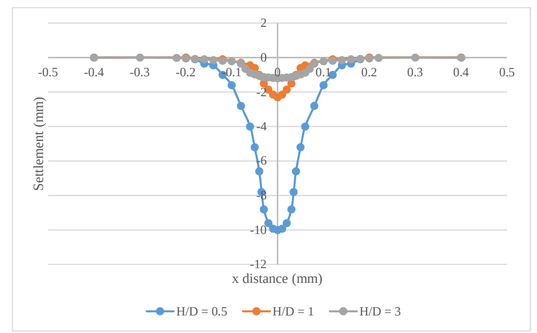

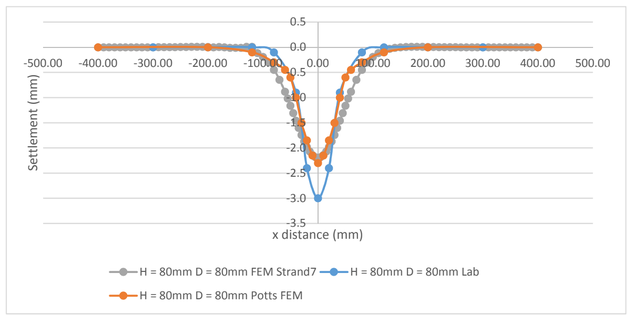

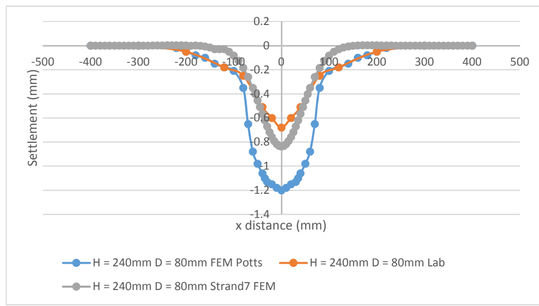

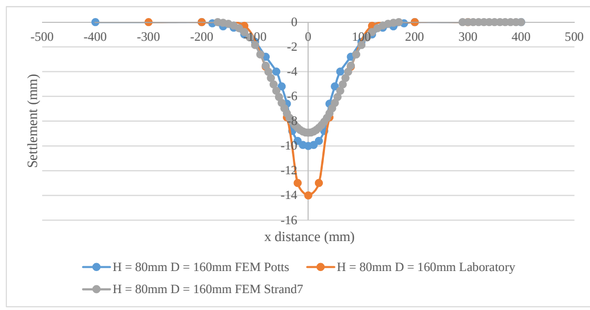

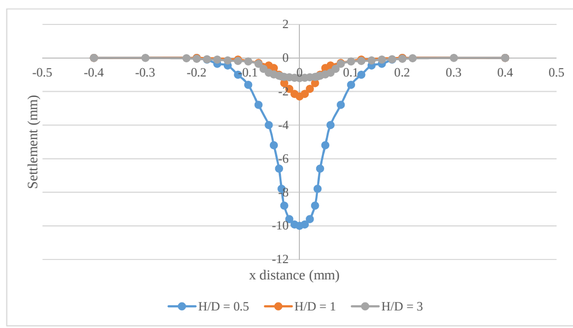

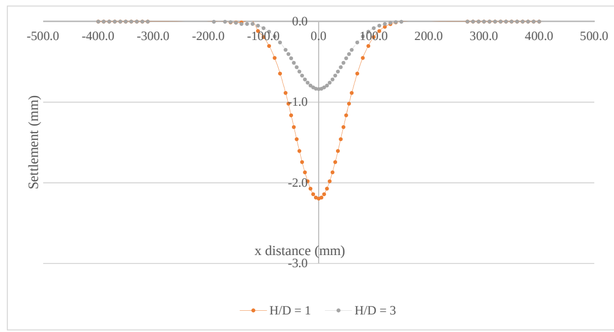

	Maximum Soil Settlement (mm)			
H/D	Lab	FEM	Strand 7	% Difference
0.5	14.014	10.022	8.938	36.220
1	2.981	2.314	2.194	26.386
3	0.651	1.201	0.836	28.488

		Maximum Soil Settlement (mm)		
H / D	Details	Lab	Strand 7	% Difference
0.5	H = 80mm D = 160mm	14.014	8.938	42.786
1	H = 80mm D = 80mm	2.981	2.194	36.667
3	H = 240mm D = 80mm	0.651	0.836	46.154

		Maximum Soil Settlement (mm)		
H / D	Details	Lab	Potts FEM	% Difference
0.5	H = 80mm D = 160mm	14.014	10.022	28.486
1	H = 80mm D = 80mm	2.981	2.314	22.375
3	H = 240mm D = 80mm	0.651	1.201	45.795

POTTS FEM = 80mm, D = 160mm			
	x	y	1000
-0.40	-400.00	0.00	
-0.20	-200.00	0.00	
-0.18	-180.00	-0.10	
-0.16	-160.00	-0.35	
-0.14	-140.00	-0.45	
-0.12	-120.00	-1.00	
-0.10	-100.00	-1.60	
-0.08	-80.00	-2.80	
-0.06	-60.00	-4.00	
-0.05	-50.00	-5.20	
-0.04	-40.00	-6.60	
-0.04	-35.00	-7.80	
-0.03	-30.00	-8.80	
-0.02	-20.00	-9.60	
-0.01	-10.00	-9.93	
0.00	0.00	-10.02	
0.01	10.00	-9.93	
0.02	20.00	-9.60	
0.03	30.00	-8.80	
0.04	35.00	-7.80	
0.04	40.00	-6.60	
0.05	50.00	-5.20	
0.06	60.00	-4.00	
0.08	80.00	-2.80	
0.10	100.00	-1.60	
0.12	120.00	-1.00	
0.14	140.00	-0.45	
0.16	160.00	-0.35	
0.18	180.00	-0.10	
0.20	200.00	0.00	
0.40	400.00	0.00	

POTTS FEM = 80mm, D = 80mm		
	x	y
-0.4	-400	0
-0.2	-200	0
-0.12	-120	-0.1
-0.08	-80	-0.3
-0.06	-60	-0.45
-0.05	-50	-0.6
-0.04	-40	-1
-0.03	-30	-1.5
-0.02	-20	-1.85
-0.01	-10	-2.15
0	0	-2.31
0.01	10	-2.15
0.02	20	-1.85
0.03	30	-1.5
0.04	40	-1
0.05	50	-0.6
0.06	60	-0.45
0.08	80	-0.3
0.12	120	-0.1
0.2	200	0
0.4	400	0

POTTS FEM = 240mm, D = 80mm		
	x	y
-0.4	-400	0
-0.3	-300	0
-0.22	-220	-0.02
-0.2	-200	-0.05
-0.18	-180	-0.08
-0.16	-160	-0.1
-0.14	-140	-0.15
-0.12	-120	-0.2
-0.1	-100	-0.21
-0.08	-80	-0.35
-0.07	-70	-0.65
-0.06	-60	-0.8
-0.05	-50	-0.92
-0.04	-40	-1
-0.035	-35	-1.1
-0.03	-30	-1.13
-0.02	-20	-1.15
-0.01	-10	-1.18
0	0	-1.2
0.01	10	-1.18
0.02	20	-1.15
0.03	30	-1.13
0.035	35	-1.1
0.04	40	-1
0.05	50	-0.92
0.06	60	-0.8
0.07	70	-0.65
0.08	80	-0.35
0.1	100	-0.21
0.12	120	-0.2
0.14	140	-0.15
0.16	160	-0.1
0.18	180	-0.08
0.2	200	-0.05
0.22	220	-0.02
0.3	300	0
0.4	400	0

LAB H = 80mm, D = 160mm			
	x	y	1000
-0.3	-300	0	
-0.2	-200	0	
-0.12	-120	-0.3	
-0.08	-80	-3.6	
-0.04	-40	-7.7	
-0.02	-20	-13	
0	0	-14	
0.02	20	-13	
0.04	40	-7.7	
0.08	80	-3.6	
0.12	120	-0.3	
0.2	200	0	
0.3	300	0	

LAB H = 80mm, D = 80mm		
	x	y
-0.3	-300	-0.3
-0.2	-200	-0.2
-0.12	-120	-0.12
-0.08	-80	-0.08
-0.04	-40	-0.04
-0.02	-20	-0.02
0	0	0
0.02	20	0.02
0.04	40	0.04
0.08	80	0.08
0.12	120	0.12
0.2	200	0.2
0.3	300	0.3

LAB H = 240mm, D = 80mm		
	x	y
-0.3	-300	0
-0.2	-200	-0.05
-0.12	-120	-0.18
-0.08	-80	-0.25
-0.04	-40	-0.51
-0.02	-20	-0.6
0	0	-0.68
0.02	20	-0.6
0.04	40	-0.51
0.08	80	-0.25
0.12	120	-0.18
0.2	200	-0.05
0.3	300	0

APPENDIX E

D = 300mm						
m centre c	Vertical deflection (mm)					
	1 Layer	2 Layers	3 Layers	4 Layers	5 Layers	6 Layers
0	-6.151	-6.133	-3.864	-3.661	-3.642	-3.612
50	-6.112	-6.124	-3.654	-3.452	-3.431	-3.411
100	-5.284	-5.513	-3.125	-2.922	-2.837	-2.811
150	-3.912	-3.922	-2.131	-1.933	-1.823	-1.812
200	-2.213	-2.254	-1.213	-1.011	-0.841	-0.821
250	-1.153	-1.134	-0.512	-0.314	-0.333	-0.322
300	-0.521	-0.514	-0.252	-0.051	-0.052	-0.041
350	-0.331	-0.323	-0.213	-0.011	0	0
400	-0.284	-0.272	-0.181	0.023	0	0
450	0	0	0	0	0	0

D = 200mm						
x (mm)	y (mm)					
	1 Layer	2 Layers	3 Layers	4 Layers	5 Layers	6 Layers
0	-2.8121899	-2.3327109	-1.369624107	-1.7106035	-1.5471264	-0.983334022
50	-2.5134303	-1.7173202	-1.108941844	-1.56020268	-1.31101085	-0.669582253
100	-2.2149765	-0.949825	-0.776553937	-0.83949506	-0.79602829	-0.327720071
150	-1.458805	-0.6249296	-0.526681362	-0.61432726	-0.45448462	-0.159177499
200	-0.5895757	-0.1609753	-0.489021082	-0.5105828	-0.20106507	-0.052337219
250	-0.1367721	-0.2050517	-0.20071726	-0.15451908	-0.07770115	-0.026139777
300	-0.1263319	-0.3796605	-0.260838414	-0.13557087	-0.04128668	-0.0162434
350	-0.1259318	-0.2646981	-0.162968498	-0.06052729	-0.05066068	-0.014457146
400	-0.0589781	0	0	0	0	0
450	0	0	0	0	0	0

D = 150mm						
m centre c	Vertical deflection (mm)					
	1 Layer	2 Layers	3 Layers	4 Layers	5 Layers	6 Layers
0	-2.023	-1.754	-1.205	-1.153	-1.205	-1.103
50	-1.851	-1.652	-1.153	-1.011	-1.153	-1.072
100	-1.68	-1.512	-1.021	-0.753	-0.755	-0.751
150	-0.914	-0.902	-0.654	-0.451	-0.404	-0.405
200	-0.521	-0.431	-0.422	-0.283	-0.272	-0.253
250	-0.133	-0.121	-0.126	-0.112	-0.113	-0.112
300	-0.124	-0.103	-0.091	-0.091	-0.093	-0.081
350	-0.112	-0.091	-0.081	-0.082	-0.064	-0.052
400	0	-0.081	-0.06	-0.05	-0.05	-0.04
450	0	0	0	0	0	0

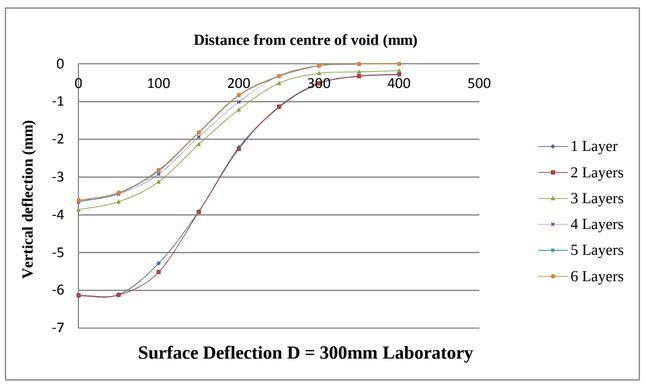

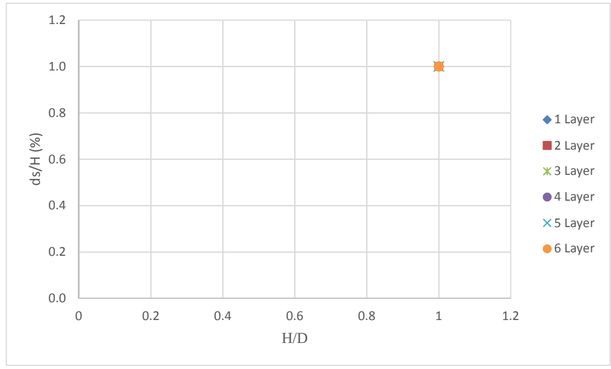

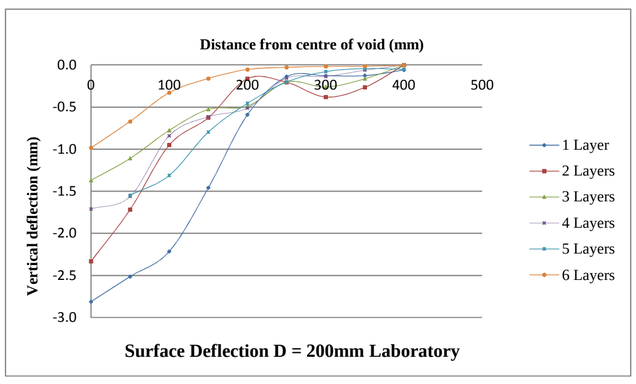

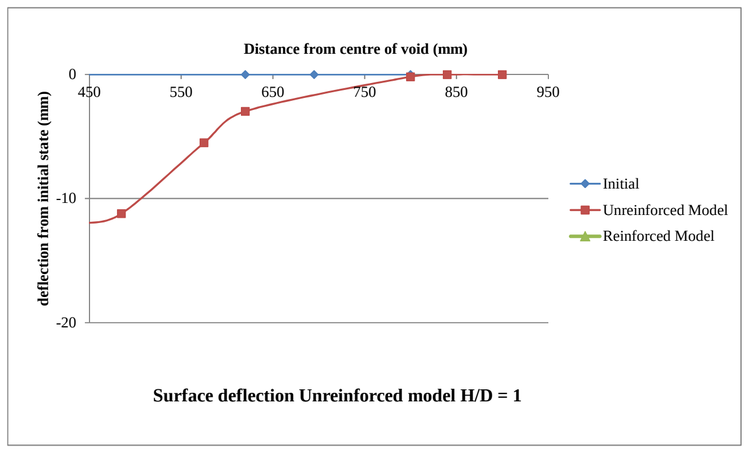

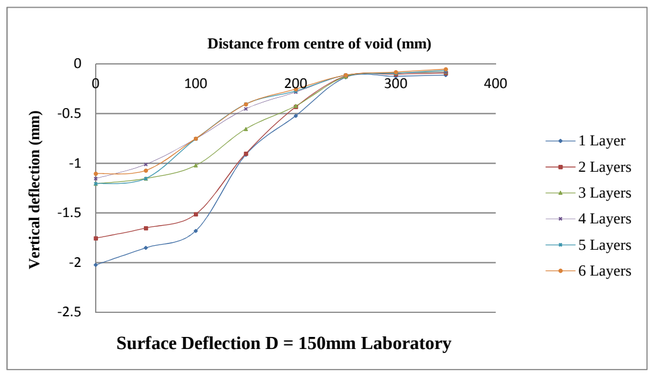

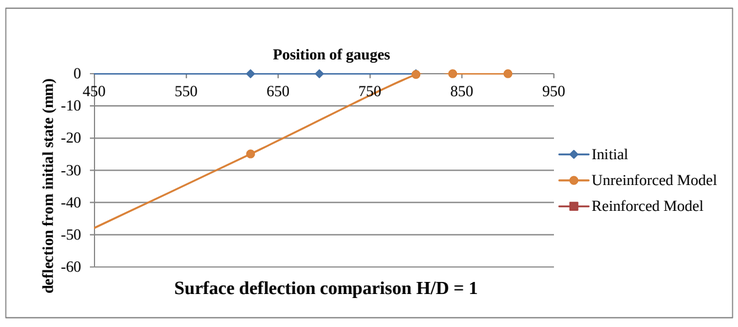

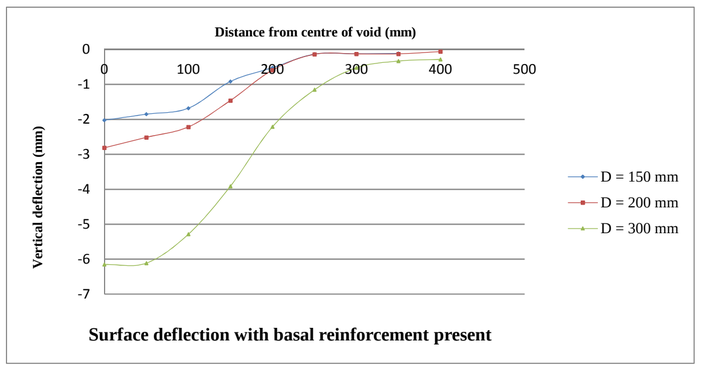

Drop (mm)	ds
10	11.95
20	20.9
30	29.85
40	39.15
50	47.95

3D					
1 Layer		2 Layers		3 Layers	
Geosynthetic deflection (mm)		Geosynthetic deflection (mm)		Geosynthetic deflection (mm)	
x	Deflection	x	Deflection	x	Deflection
0	-6.79636	0	-5.7186	0	-5.2786
4.16667	-6.79132	4.16667	-5.71436	4.16667	-5.27436
8.33333	-6.7776	8.33333	-5.703	8.33333	-5.263
12.5	-6.75616	12.5	-5.68524	12.5	-5.24524
16.6667	-6.72584	16.6667	-5.66016	16.6667	-5.22016
20.8333	-6.68612	20.8333	-5.62728	20.8333	-5.18728
25	-6.6374	25	-5.58696	25	-5.14696
29.1667	-6.5794	29.1667	-5.539	29.1667	-5.099
33.3333	-6.51152	33.3333	-5.48288	33.3333	-5.04288
37.5	-6.39312	37.5	-5.378076	37.5	-4.938076
41.6667	-6.3038	41.6667	-5.304236	41.6667	-4.864236
45.8333	-6.20264	45.8333	-5.220636	45.8333	-4.780636
50	-6.08896	50	-5.126692	50	-4.686692
54.1667	-5.9614	54.1667	-5.021308	54.1667	-4.581308
58.3333	-5.77884	58.3333	-4.863504	58.3333	-4.423504
62.5	-5.618956	62.5	-4.731376	62.5	-4.291376
66.6667	-5.43994	66.6667	-4.583412	66.6667	-4.143412
70.8333	-5.198132	70.8333	-4.37672	70.8333	-3.93672
75	-4.969252	75	-4.187628	75	-3.747628
79.1667	-4.70304	79.1667	-3.967268	79.1667	-3.527268
83.3333	-4.349552	83.3333	-3.667496	83.3333	-3.227496
87.5	-3.981144	87.5	-3.366028	87.5	-2.926028
91.6667	-3.459396	91.6667	-2.89018	91.6667	-2.45018
95.8333	-2.727428	95.8333	-2.283132	95.8333	-1.843132
100	0	100	0	100	0
107.292	0	107.292	0	107.292	0
114.583	0	114.583	0	114.583	0
121.875	0	121.875	0	121.875	0
129.167	0	129.167	0	129.167	0
136.458	0	136.458	0	136.458	0
143.75	0	143.75	0	143.75	0
151.042	0	151.042	0	151.042	0
158.333	0	158.333	0	158.333	0
165.625	0	165.625	0	165.625	0
172.917	0	172.917	0	172.917	0
180.208	0	180.208	0	180.208	0
187.5	0	187.5	0	187.5	0
194.792	0	194.792	0	194.792	0
202.083	0	202.083	0	202.083	0
209.375	0	209.375	0	209.375	0
216.667	0	216.667	0	216.667	0
223.958	0	223.958	0	223.958	0
231.25	0	231.25	0	231.25	0
238.542	0	238.542	0	238.542	0
245.833	0	245.833	0	245.833	0
253.125	0	253.125	0	253.125	0
260.417	0	260.417	0	260.417	0
267.708	0	267.708	0	267.708	0
275	0	275	0	275	0
282.292	0	282.292	0	282.292	0
289.583	0	289.583	0	289.583	0
296.875	0	296.875	0	296.875	0
304.167	0	304.167	0	304.167	0
311.458	0	311.458	0	311.458	0
318.75	0	318.75	0	318.75	0
326.042	0	326.042	0	326.042	0
333.333	0	333.333	0	333.333	0
340.625	0	340.625	0	340.625	0
347.917	0	347.917	0	347.917	0
355.208	0	355.208	0	355.208	0
362.5	0	362.5	0	362.5	0
369.792	0	369.792	0	369.792	0
377.083	0	377.083	0	377.083	0
384.375	0	384.375	0	384.375	0
391.667	0	391.667	0	391.667	0
398.958	0	398.958	0	398.958	0
406.25	0	406.25	0	406.25	0
413.542	0	413.542	0	413.542	0
420.833	0	420.833	0	420.833	0
428.125	0	428.125	0	428.125	0
435.417	0	435.417	0	435.417	0
442.708	0	442.708	0	442.708	0
450	0	450	0	450	0

2D					
1 Layer		2 Layer		3 Layers	
Geosynthetic deflection (mm)		Geosynthetic deflection (mm)		Geosynthetic deflection (mm)	
x	Deflection	x	Deflection	x	Deflection
0	-6.98511	0	-5.8153655	0	-5.116088
12	-6.920205	12	-5.7473465	12	-5.064164
22	-6.816595	22	-5.6385245	22	-4.981276
34	-6.655015	34	-5.469702	34	-4.852012
46	-6.410215	46	-5.216757	46	-4.656172
58	-6.03874	58	-4.840465	58	-4.358992
70	-5.451776	70	-4.2664475	70	-3.8894208
82	-4.476536	78	-3.3561878	78	-3.1092288
92	-2.8653355	86	-1.9275473	86	-1.8202684
95	-1.43266775	92	-0.96377365	92	-0.9101342
100	0	100	0	100	0
110	0	110	0	110	0
120	0	120	0	120	0
130	0	130	0	130	0
140	0	140	0	140	0
150	0	150	0	150	0
160	0	160	0	160	0
170	0	170	0	170	0
180	0	180	0	180	0
190	0	190	0	190	0
200	0	200	0	200	0
210	0	210	0	210	0
220	0	220	0	220	0
230	0	230	0	230	0
240	0	240	0	240	0
250	0	250	0	250	0
260	0	260	0	260	0
270	0	270	0	270	0
280	0	280	0	280	0
290	0	290	0	290	0
300	0	300	0	300	0
310	0	310	0	310	0
320	0	320	0	320	0
330	0	330	0	330	0
340	0	340	0	340	0
350	0	350	0	350	0
360	0	360	0	360	0
370	0	370	0	370	0
380	0	380	0	380	0
390	0	390	0	390	0
400	0	400	0	400	0
410	0	410	0	410	0
420	0	420	0	420	0
430	0	430	0	430	0
440	0	440	0	440	0
450	0	450	0	450	0

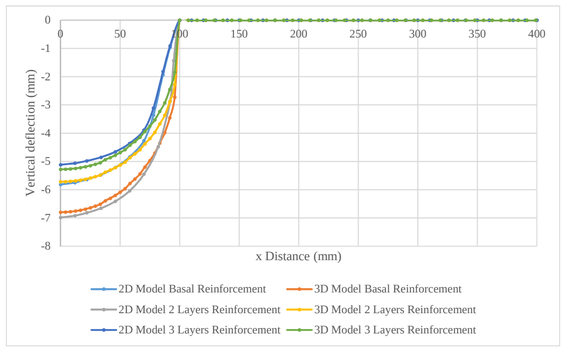

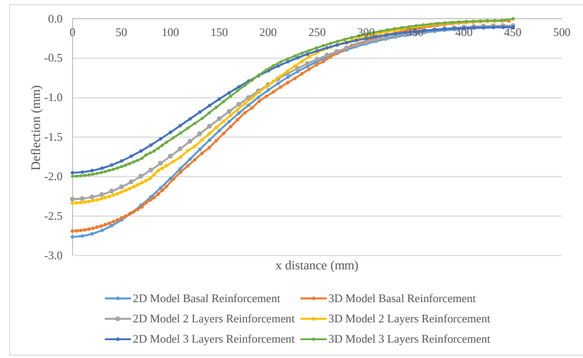

3D					
1 Layer		2 Layers		3 Layers	
Surface deflection (mm)		Surface deflection (mm)		Surface deflection (mm)	
x	Deflection	x	Deflection	x	Deflection
0	-2.69095	0	-2.33589	0	-1.99638
4.16667	-2.68787	4.16667	-2.33329	4.16667	-1.99409
8.33333	-2.68276	8.33333	-2.32896	8.33333	-1.99029
12.5	-2.67562	12.5	-2.32292	12.5	-1.98498
16.6667	-2.66649	16.6667	-2.3152	16.6667	-1.97818
20.8333	-2.65537	20.8333	-2.30579	20.8333	-1.96991
25	-2.64232	25	-2.29476	25	-1.9602
29.1667	-2.62735	29.1667	-2.2821	29.1667	-1.94908
33.3333	-2.61054	33.3333	-2.26789	33.3333	-1.93658
37.5	-2.5919	37.5	-2.25214	37.5	-1.92272
41.6667	-2.57151	41.6667	-2.23491	41.6667	-1.90758
45.8333	-2.54941	45.8333	-2.21624	45.8333	-1.89116
50	-2.52568	50	-2.19621	50	-1.87355
54.1667	-2.50037	54.1667	-2.17485	54.1667	-1.85476
58.3333	-2.47356	58.3333	-2.15223	58.3333	-1.83488
62.5	-2.44532	62.5	-2.12841	62.5	-1.81394
66.6667	-2.41572	66.6667	-2.10347	66.6667	-1.79201
70.8333	-2.38485	70.8333	-2.07746	70.8333	-1.76914
75	-2.33278	75	-2.05045	75	-1.7254
79.1667	-2.29958	79.1667	-2.02252	79.1667	-1.70084
83.3333	-2.26536	83.3333	-1.97373	83.3333	-1.67554
87.5	-2.22018	87.5	-1.92416	87.5	-1.63955
91.6667	-2.17414	91.6667	-1.89388	91.6667	-1.60293
95.8333	-2.12731	95.8333	-1.86296	95.8333	-1.56576
103.125	-2.03125	103.125	-1.80754	103.125	-1.50706
110.417	-1.94349	110.417	-1.75078	110.417	-1.44718
117.708	-1.86447	117.708	-1.67303	117.708	-1.38645
125	-1.78461	125	-1.61466	125	-1.32518
132.292	-1.70431	132.292	-1.536	132.292	-1.26366
139.583	-1.63397	139.583	-1.45739	139.583	-1.19219
146.875	-1.54391	146.875	-1.37911	146.875	-1.121015
154.167	-1.45448	154.167	-1.30144	154.167	-1.050394
161.458	-1.36596	161.458	-1.224619	161.458	-0.980518
168.75	-1.27865	168.75	-1.148887	168.75	-0.91161
176.042	-1.19274	176.042	-1.074407	176.042	-0.84381
183.333	-1.12849	183.333	-1.001383	183.333	-0.777296
190.625	-1.046022	190.625	-0.929921	190.625	-0.712161
197.917	-0.985538	197.917	-0.860177	197.917	-0.648542
205.208	-0.927117	205.208	-0.792209	205.208	-0.596489
212.5	-0.864896	212.5	-0.726126	212.5	-0.546097
219.792	-0.80891	219.792	-0.661949	219.792	-0.507383
227.083	-0.755247	227.083	-0.599744	227.083	-0.470406
234.375	-0.695904	234.375	-0.5395	234.375	-0.435155
241.667	-0.638928	241.667	-0.481249	241.667	-0.401657
248.958	-0.584285	248.958	-0.434957	248.958	-0.369882
256.25	-0.541991	256.25	-0.390629	256.25	-0.339832
263.542	-0.481989	263.542	-0.358211	263.542	-0.311461
270.833	-0.434268	270.833	-0.327688	270.833	-0.284755
278.125	-0.388758	278.125	-0.298996	278.125	-0.259656
285.417	-0.335428	285.417	-0.272105	285.417	-0.236138
292.708	-0.314201	292.708	-0.246945	292.708	-0.214138
300	-0.275031	300	-0.223475	300	-0.193621
307.292	-0.247838	307.292	-0.201624	307.292	-0.174523
314.583	-0.222569	314.583	-0.181344	314.583	-0.156802
321.875	-0.199145	321.875	-0.162567	321.875	-0.140398
329.167	-0.177508	329.167	-0.145243	329.167	-0.125265
336.458	-0.157582	336.458	-0.129307	336.458	-0.111348
343.75	-0.13931	343.75	-0.114708	343.75	-0.0986009
351.042	-0.122622	351.042	-0.101388	351.042	-0.0869722
358.333	-0.10746	358.333	-0.089297	358.333	-0.0764186
365.625	-0.0937629	365.625	-0.0783834	365.625	-0.0668941
372.917	-0.0814768	372.917	-0.0686017	372.917	-0.0583586
380.208	-0.0705471	380.208	-0.0599064	380.208	-0.0507722
387.5	-0.0609255	387.5	-0.0522566	387.5	-0.0440987
394.792	-0.0525655	394.792	-0.0456139	394.792	-0.0383045
402.083	-0.0454247	402.083	-0.0399427	402.083	-0.0333581
409.375	-0.0394638	409.375	-0.0352107	409.375	-0.0292313
416.667	-0.0346475	416.667	-0.0313886	416.667	-0.0258982
423.958	-0.0309464	423.958	-0.0284524	423.958	-0.0233379
431.25	-0.0283308	431.25	-0.0263777	431.25	-0.0215287
438.542	-0.0267651	438.542	-0.0251355	438.542	-0.0204455
445.833	-0.0262515	450	0	450	0
450	0	450	0	450	0

2D					
1 Layer		2 Layer		3 Layers	
Surface deflection (mm)		Surface deflection (mm)		Surface deflection (mm)	
x	Deflection	x	Deflection	x	Deflection
0	-2.7646986	0	-2.28754	0	-1.951741
10	-2.7528896	10	-2.279066	10	-1.943562
20	-2.7255976	20	-2.259457	20	-1.92466
30	-2.6819316	30	-2.228011	30	-1.894418
40	-2.6226386	40	-2.185167	40	-1.853355
50	-2.5489366	50	-2.131671	50	-1.802313
60	-2.4623756	60	-2.068487	60	-1.74236
70	-2.3647396	70	-1.996735	70	-1.674722
80	-2.2579716	80	-1.91765	80	-1.600731
90	-2.1440916	90	-1.832534	90	-1.521769
100	-2.0251266	100	-1.74272	100	-1.439226
110	-1.9030396	110	-1.649527	110	-1.354446
120	-1.7796746	120	-1.554231	120	-1.268699
130	-1.6567066	130	-1.458033	130	-1.183145
140	-1.5356146	140	-1.362037	140	-1.098813
150	-1.4176566	150	-1.267232	150	-1.016589
160	-1.3038666	160	-1.17448	160	-0.937206
170	-1.1950556	170	-1.084512	170	-0.8612484
180	-1.0918266	180	-0.9979286	180	-0.7891557
190	-0.9945911	190	-0.9152008	190	-0.7212343
200	-0.9035944	200	-0.8366815	200	-0.6576713
210	-0.8189367	210	-0.7626133	210	-0.5985496
220	-0.740599	220	-0.6931412	220	-0.543865
230	-0.6684663	230	-0.6283251	230	-0.4935418
240	-0.6023491	240	-0.5681527	240	-0.4474486
250	-0.5420024	250	-0.5125525	250	-0.405412
260	-0.4871421	260	-0.4614053	260	-0.3672292
270	-0.4374592	270	-0.4145557	270	-0.3326786
280	-0.3926312	280	-0.3718214	280	-0.3015284
290	-0.3523316	290	-0.3330021	290	-0.2735442
300	-0.316237	300	-0.2978869	300	-0.2484942
310	-0.2840331	310	-0.2662601	310	-0.2261542
320	-0.2554187	320	-0.2379068	320	-0.2063098
330	-0.2301089	330	-0.2126164	330	-0.1887597
340	-0.2078373	340	-0.1901862	340	-0.1733162
350	-0.1883573	350	-0.1704237	350	-0.1598067
360	-0.17144252	360	-0.1531483	360	-0.1480736
370	-0.15688768	370	-0.1381924	370	-0.1379745
380	-0.1445081	380	-0.1254027	380	-0.1293819
390	-0.13413952	390	-0.11464	390	-0.1221829
400	-0.12563759	400	-0.1057798	400	-0.1162785
410	-0.1188773	410	-0.09871221	410	-0.1115828
420	-0.11375233	420	-0.09334169	420	-0.108023
430	-0.11017519	430	-0.08958769	430	-0.1055388
440	-0.10807431	440	-0.08738184	440	-0.1040806
450	-0.10742692	450	-0.0867036	450	-0.1036339

Axisymmetric					
1 Layer		1 Layer		1 Layer	
Surface deflection 150mm		Surface deflection: 200mm		Surface deflection: 300mm	
x	y	x	y	x	y
0.0000	-2.1484	0.0000	-2.7647	0.0000	-6.1658
10.0000	-2.1393	10.0000	-2.7529	10.0000	-6.1306
20.0000	-2.1184	20.0000	-2.7256	20.0000	-6.0466
30.0000	-2.0848	30.0000	-2.6819	30.0000	-5.9062
40.0000	-2.0392	40.0000	-2.6226	40.0000	-5.7048
50.0000	-1.9824	50.0000	-2.5489	50.0000	-5.4345
60.0000	-1.9157	60.0000	-2.4624	60.0000	-5.1009
70.0000	-1.8401	70.0000	-2.3647	70.0000	-4.7292
80.0000	-1.7574	80.0000	-2.2580	80.0000	-4.3390
90.0000	-1.6688	90.0000	-2.1441	90.0000	-3.9204
100.0000	-1.5761	100.0000	-2.0251	100.0000	-3.5220
110.0000	-1.4805	110.0000	-1.9030	110.0000	-3.1578
120.0000	-1.3836	120.0000	-1.7797	120.0000	-2.8299
130.0000	-1.2866	130.0000	-1.6567	130.0000	-2.5365
140.0000	-1.1907	140.0000	-1.5356	140.0000	-2.2740
150.0000	-1.0970	150.0000	-1.4177	150.0000	-2.0385
160.0000	-1.0061	160.0000	-1.3039	160.0000	-1.8263
170.0000	-0.9188	170.0000	-1.1951	170.0000	-1.6346
180.0000	-0.8357	180.0000	-1.0918	180.0000	-1.4611
190.0000	-0.7571	190.0000	-0.9946	190.0000	-1.3038
200.0000	-0.6833	200.0000	-0.9036	200.0000	-1.1614
210.0000	-0.6143	210.0000	-0.8189	210.0000	-1.0323
220.0000	-0.5503	220.0000	-0.7406	220.0000	-0.9155
230.0000	-0.4912	230.0000	-0.6685	230.0000	-0.8100
240.0000	-0.4368	240.0000	-0.6023	240.0000	-0.7147
250.0000	-0.3870	250.0000	-0.5420	250.0000	-0.6288
260.0000	-0.3416	260.0000	-0.4871	260.0000	-0.5515
270.0000	-0.3004	270.0000	-0.4375	270.0000	-0.4821
280.0000	-0.2632	280.0000	-0.3926	280.0000	-0.4199
290.0000	-0.2296	290.0000	-0.3523	290.0000	-0.3642
300.0000	-0.1995	300.0000	-0.3162	300.0000	-0.3145
310.0000	-0.1726	310.0000	-0.2840	310.0000	-0.2703
320.0000	-0.1486	320.0000	-0.2554	320.0000	-0.2312
330.0000	-0.1274	330.0000	-0.2301	330.0000	-0.1966
340.0000	-0.1087	340.0000	-0.2078	340.0000	-0.1661
350.0000	-0.0923	350.0000	-0.1884	350.0000	-0.1395
360.0000	-0.0781	360.0000	-0.1714	360.0000	-0.1164
370.0000	-0.0658	370.0000	-0.1569	370.0000	-0.0965
380.0000	-0.0553	380.0000	-0.1445	380.0000	-0.0796
390.0000	-0.0466	390.0000	-0.1341	390.0000	-0.0654
400.0000	-0.0394	400.0000	-0.1256	400.0000	-0.0537
410.0000	-0.0337	410.0000	-0.1189	410.0000	-0.0445
420.0000	-0.0294	420.0000	-0.1138	420.0000	-0.0374
430.0000	-0.0263	430.0000	-0.1102	430.0000	-0.0325
440.0000	-0.0246	440.0000	-0.1081	440.0000	-0.0296
450.0000	-0.0240	450.0000	-0.1074	450.0000	-0.0287

Plane strain					
1 Layer		1 Layer		1 Layer	
Surface deflection 150mm		Surface deflection: 200mm		Surface deflection: 300mm	
0.0000	-3.5365	0.0000	-4.1119	0.0000	-8.1890
10.0000	-3.4964	10.0000	-4.0565	10.0000	-8.1437
20.0000	-3.3928	20.0000	-3.9024	20.0000	-7.9710
30.0000	-3.2522	30.0000	-3.6738	30.0000	-7.6499
40.0000	-3.0742	40.0000	-3.3868	40.0000	-7.2274
50.0000	-2.8213	50.0000	-3.0435	50.0000	-6.7032
60.0000	-2.5299	60.0000	-2.6938	60.0000	-6.0887
70.0000	-2.2595	70.0000	-2.3892	70.0000	-5.4135
80.0000	-2.0187	80.0000	-2.1268	80.0000	-4.7091
90.0000	-1.8038	90.0000	-1.8997	90.0000	-4.0108
100.0000	-1.6114	100.0000	-1.7011	100.0000	-3.3197
110.0000	-1.4391	110.0000	-1.5270	110.0000	-2.6487
120.0000	-1.2843	120.0000	-1.3724	120.0000	-2.0597
130.0000	-1.1451	130.0000	-1.2338	130.0000	-1.5778
140.0000	-1.0197	140.0000	-1.1090	140.0000	-1.2205
150.0000	-0.9067	150.0000	-0.9959	150.0000	-0.9728
160.0000	-0.8044	160.0000	-0.8933	160.0000	-0.7916
170.0000	-0.7109	170.0000	-0.7999	170.0000	-0.6509
180.0000	-0.6266	180.0000	-0.7144	180.0000	-0.5333
190.0000	-0.5519	190.0000	-0.6364	190.0000	-0.4443
200.0000	-0.4845	200.0000	-0.5653	200.0000	-0.3768
210.0000	-0.4235	210.0000	-0.5007	210.0000	-0.3233
220.0000	-0.3685	220.0000	-0.4416	220.0000	-0.2793
230.0000	-0.3189	230.0000	-0.3878	230.0000	-0.2424
240.0000	-0.2745	240.0000	-0.3393	240.0000	-0.2107
250.0000	-0.2344	250.0000	-0.2952	250.0000	-0.1829
260.0000	-0.1982	260.0000	-0.2553	260.0000	-0.1583
270.0000	-0.1656	270.0000	-0.2195	270.0000	-0.1364
280.0000	-0.1364	280.0000	-0.1871	280.0000	-0.1170
290.0000	-0.1103	290.0000	-0.1578	290.0000	-0.0996
300.0000	-0.0870	300.0000	-0.1314	300.0000	-0.0842
310.0000	-0.0664	310.0000	-0.1079	310.0000	-0.0706
320.0000	-0.0481	320.0000	-0.0869	320.0000	-0.0586
330.0000	-0.0320	330.0000	-0.0683	330.0000	-0.0481
340.0000	-0.0179	340.0000	-0.0519	340.0000	-0.0390
350.0000	-0.0055	350.0000	-0.0375	350.0000	-0.0311
360.0000	0.0052	360.0000	-0.0250	360.0000	-0.0244
370.0000	0.0144	370.0000	-0.0141	370.0000	-0.0186
380.0000	0.0223	380.0000	-0.0049	380.0000	-0.0137
390.0000	0.0289	390.0000	0.0029	390.0000	-0.0097
400.0000	0.0343	400.0000	0.0094	400.0000	-0.0064
410.0000	0.0386	410.0000	0.0145	410.0000	-0.0037
420.0000	0.0419	420.0000	0.0184	420.0000	-0.0017
430.0000	0.0442	430.0000	0.0212	430.0000	-0.0003
440.0000	0.0456	440.0000	0.0229	440.0000	0.0006
450.0000	0.0461	450.0000	0.0234	450.0000	0.0008

Axisymmetric					
2 Layer		2 Layer		2 Layer	
Surface deflection 150mm		Surface deflection: 200mm		Surface deflection: 300mm	
0.0000	-1.8274	0.0000	-2.2875	0.0000	-5.1354
10.0000	-1.8203	10.0000	-2.2791	10.0000	-5.1099
20.0000	-1.8037	20.0000	-2.2595	20.0000	-5.0498
30.0000	-1.7771	30.0000	-2.2280	30.0000	-4.9516
40.0000	-1.7409	40.0000	-2.1852	40.0000	-4.8097
50.0000	-1.6958	50.0000	-2.1317	50.0000	-4.6267
60.0000	-1.6426	60.0000	-2.0685	60.0000	-4.4082
70.0000	-1.5822	70.0000	-1.9967	70.0000	-4.1424
80.0000	-1.5158	80.0000	-1.9177	80.0000	-3.8464
90.0000	-1.4445	90.0000	-1.8325	90.0000	-3.5402
100.0000	-1.3695	100.0000	-1.7427	100.0000	-3.2373
110.0000	-1.2918	110.0000	-1.6495	110.0000	-2.9469
120.0000	-1.2127	120.0000	-1.5542	120.0000	-2.6741
130.0000	-1.1330	130.0000	-1.4580	130.0000	-2.4211
140.0000	-1.0538	140.0000	-1.3620	140.0000	-2.1882
150.0000	-0.9758	150.0000	-1.2672	150.0000	-1.9744
160.0000	-0.8999	160.0000	-1.1745	160.0000	-1.7783
170.0000	-0.8265	170.0000	-1.0845	170.0000	-1.5987
180.0000	-0.7561	180.0000	-0.9979	180.0000	-1.4343
190.0000	-0.6892	190.0000	-0.9152	190.0000	-1.2839
200.0000	-0.6259	200.0000	-0.8367	200.0000	-1.1467
210.0000	-0.5665	210.0000	-0.7626	210.0000	-1.0217
220.0000	-0.5109	220.0000	-0.6931	220.0000	-0.9079
230.0000	-0.4594	230.0000	-0.6283	230.0000	-0.8047
240.0000	-0.4117	240.0000	-0.5682	240.0000	-0.7111
250.0000	-0.3678	250.0000	-0.5126	250.0000	-0.6265
260.0000	-0.3276	260.0000	-0.4614	260.0000	-0.5502
270.0000	-0.2909	270.0000	-0.4146	270.0000	-0.4816
280.0000	-0.2576	280.0000	-0.3718	280.0000	-0.4199
290.0000	-0.2274	290.0000	-0.3330	290.0000	-0.3647
300.0000	-0.2002	300.0000	-0.2979	300.0000	-0.3154
310.0000	-0.1759	310.0000	-0.2663	310.0000	-0.2715
320.0000	-0.1541	320.0000	-0.2379	320.0000	-0.2325
330.0000	-0.1347	330.0000	-0.2126	330.0000	-0.1981
340.0000	-0.1176	340.0000	-0.1902	340.0000	-0.1678
350.0000	-0.1025	350.0000	-0.1704	350.0000	-0.1413
360.0000	-0.0894	360.0000	-0.1531	360.0000	-0.1183
370.0000	-0.0781	370.0000	-0.1382	370.0000	-0.0984
380.0000	-0.0684	380.0000	-0.1254	380.0000	-0.0816
390.0000	-0.0603	390.0000	-0.1146	390.0000	-0.0674
400.0000	-0.0536	400.0000	-0.1058	400.0000	-0.0558
410.0000	-0.0483	410.0000	-0.0987	410.0000	-0.0466
420.0000	-0.0443	420.0000	-0.0933	420.0000	-0.0396
430.0000	-0.0414	430.0000	-0.0896	430.0000	-0.0347
440.0000	-0.0398	440.0000	-0.0874	440.0000	-0.0318
450.0000	-0.0393	450.0000	-0.0867	450.0000	-0.0309
450.0000	-0.0526				

Plane strain					
2 Layer		2 Layer		2 Layer	
Surface deflection 150mm		Surface deflection: 200mm		Surface deflection: 300mm	
0.0000	-2.2091	0.0000	-2.9036	0.0000	-6.0058
10.0000	-2.1996	10.0000	-2.8949	10.0000	-5.9715
20.0000	-2.1710	20.0000	-2.8693	20.0000	-5.8323
30.0000	-2.1239	30.0000	-2.8270	30.0000	-5.5976
40.0000	-2.0592	40.0000	-2.7690	40.0000	-5.2872
50.0000	-1.9787	50.0000	-2.6964	50.0000	-4.8990
60.0000	-1.8848	60.0000	-2.6105	60.0000	-4.4396
70.0000	-1.7810	70.0000	-2.5130	70.0000	-3.9283
80.0000	-1.6707	80.0000	-2.4055	80.0000	-3.3944
90.0000	-1.5572	90.0000	-2.2901	90.0000	-2.8665
100.0000	-1.4433	100.0000	-2.1687	100.0000	-2.3484
110.0000	-1.3313	110.0000	-2.0431	110.0000	-1.8565
120.0000	-1.2225	120.0000	-1.9152	120.0000	-1.4333
130.0000	-1.1182	130.0000	-1.7868	130.0000	-1.1002
140.0000	-1.0190	140.0000	-1.6593	140.0000	-0.8595
150.0000	-0.9252	150.0000	-1.5340	150.0000	-0.6953
160.0000	-0.8371	160.0000	-1.4122	160.0000	-0.5707
170.0000	-0.7548	170.0000	-1.2947	170.0000	-0.4700
180.0000	-0.6782	180.0000	-1.1821	180.0000	-0.3920
190.0000	-0.6071	190.0000	-1.0752	190.0000	-0.3345
200.0000	-0.5415	200.0000	-0.9741	200.0000	-0.2897
210.0000	-0.4811	210.0000	-0.8791	210.0000	-0.2527
220.0000	-0.4256	220.0000	-0.7904	220.0000	-0.2211
230.0000	-0.3749	230.0000	-0.7078	230.0000	-0.1934
240.0000	-0.3285	240.0000	-0.6314	240.0000	-0.1689
250.0000	-0.2864	250.0000	-0.5609	250.0000	-0.1470
260.0000	-0.2482	260.0000	-0.4962	260.0000	-0.1274
270.0000	-0.2136	270.0000	-0.4370	270.0000	-0.1098
280.0000	-0.1823	280.0000	-0.3831	280.0000	-0.0940
290.0000	-0.1543	290.0000	-0.3341	290.0000	-0.0799
300.0000	-0.1291	300.0000	-0.2898	300.0000	-0.0674
310.0000	-0.1066	310.0000	-0.2499	310.0000	-0.0563
320.0000	-0.0866	320.0000	-0.2141	320.0000	-0.0466
330.0000	-0.0688	330.0000	-0.1822	330.0000	-0.0381
340.0000	-0.0531	340.0000	-0.1538	340.0000	-0.0307
350.0000	-0.0394	350.0000	-0.1287	350.0000	-0.0243
360.0000	-0.0274	360.0000	-0.1068	360.0000	-0.0188
370.0000	-0.0170	370.0000	-0.0877	370.0000	-0.0142
380.0000	-0.0082	380.0000	-0.0713	380.0000	-0.0102
390.0000	-0.0007	390.0000	-0.0574	390.0000	-0.0069
400.0000	0.0054	400.0000	-0.0460	400.0000	-0.0042
410.0000	0.0103	410.0000	-0.0368	410.0000	-0.0020
420.0000	0.0141	420.0000	-0.0297	420.0000	-0.0003
430.0000	0.0168	430.0000	-0.0247	430.0000	0.0008
440.0000	0.0183	440.0000	-0.0217	440.0000	0.0015
450.0000	0.0189	450.0000	-0.0208	450.0000	0.0018

1 Layer	
Surface deflection 150mm	
x	y
0.000	-2.148
10.000	-2.139
20.000	-2.118
30.000	-2.085
40.000	-2.039
50.000	-1.982
60.000	-1.916
70.000	-1.840
80.000	-1.757
90.000	-1.669
100.000	-1.576
110.000	-1.481
120.000	-1.384
130.000	-1.287
140.000	-1.191
150.000	-1.097
160.000	-1.006
170.000	-0.919
180.000	-0.836
190.000	-0.757
200.000	-0.683
210.000	-0.614
220.000	-0.550
230.000	-0.491
240.000	-0.437
250.000	-0.387
260.000	-0.342
270.000	-0.300
280.000	-0.263
290.000	-0.230
300.000	-0.199
310.000	-0.173
320.000	-0.149
330.000	-0.127
340.000	-0.109
350.000	-0.092
360.000	-0.078
370.000	-0.066
380.000	-0.055
390.000	-0.047
400.000	-0.039
410.000	-0.034
420.000	-0.029
430.000	-0.026
440.000	-0.025
450.000	-0.024

1 Layer	
Geogrid deflection 150mm	
x	y

2 Layer	
Surface deflection 150mm	
x	y
0.000	-1.827
10.000	-1.820
20.000	-1.804
30.000	-1.777
40.000	-1.741
50.000	-1.696
60.000	-1.643
70.000	-1.582
80.000	-1.516
90.000	-1.445
100.000	-1.369
110.000	-1.292
120.000	-1.213
130.000	-1.133
140.000	-1.054
150.000	-0.976
160.000	-0.900
170.000	-0.826
180.000	-0.756
190.000	-0.689
200.000	-0.626
210.000	-0.566
220.000	-0.511
230.000	-0.459
240.000	-0.412
250.000	-0.368
260.000	-0.328
270.000	-0.291
280.000	-0.258
290.000	-0.227
300.000	-0.200
310.000	-0.176
320.000	-0.154
330.000	-0.135
340.000	-0.118
350.000	-0.103
360.000	-0.089
370.000	-0.078
380.000	-0.068
390.000	-0.060
400.000	-0.054
410.000	-0.048
420.000	-0.044
430.000	-0.041
440.000	-0.040
450.000	-0.039
450.000	-0.053

1 Layer	
Geogrid deflection 150mm	
x	y

3 Layer	
Surface deflection 150mm	
x	y
0.000	-1.61261
10.000	-1.60619
20.000	-1.59134
30.000	-1.56753
40.000	-1.53513
50.000	-1.49472
60.000	-1.44705
70.000	-1.39301
80.000	-1.33357
90.000	-1.26974
100.000	-1.20256
110.000	-1.13305
120.000	-1.06219
130.000	-0.99091
140.000	-0.92002
150.000	-0.85028
160.000	-0.78232
170.000	-0.71667
180.000	-0.65375
190.000	-0.59389
200.000	-0.53732
210.000	-0.48418
220.000	-0.43455
230.000	-0.38845
240.000	-0.34584
250.000	-0.30662
260.000	-0.2707
270.000	-0.23793
280.000	-0.20815
290.000	-0.1812
300.000	-0.15692
310.000	-0.13513
320.000	-0.11566
330.000	-0.09835
340.000	-0.08304
350.000	-0.06959
360.000	-0.05787
370.000	-0.04774
380.000	-0.0391
390.000	-0.03184
400.000	-0.02587
410.000	-0.02111
420.000	-0.0175
430.000	-0.01497
440.000	-0.01349
450.000	-0.01303
450.000	-0.00263

1 Layer	
Geogrid deflection 150mm	
x	y

4 Layer	
Surface deflection 150mm	
x	y
0.0000	-1.43661
10.0000	-1.43011
20.0000	-1.41508
30.0000	-1.39105
40.0000	-1.35844
50.0000	-1.31795
60.0000	-1.27045
70.0000	-1.21694
80.0000	-1.15851
90.0000	-1.0963
100.0000	-1.03142
110.0000	-0.96496
120.0000	-0.89796
130.0000	-0.83135
140.0000	-0.76594
150.0000	-0.70243
160.0000	-0.6414
170.0000	-0.58329
180.0000	-0.52843
190.0000	-0.47703
200.0000	-0.42921
210.0000	-0.385
220.0000	-0.34437
230.0000	-0.30723
240.0000	-0.27343
250.0000	-0.24282
260.0000	-0.2152
270.0000	-0.19038
280.0000	-0.16816
290.0000	-0.14833
300.0000	-0.13069
310.0000	-0.11506
320.0000	-0.10126
330.0000	-0.08913
340.0000	-0.07852
350.0000	-0.06928
360.0000	-0.0613
370.0000	-0.05446
380.0000	-0.04866
390.0000	-0.04382
400.0000	-0.03986
410.0000	-0.03672
420.0000	-0.03434
430.0000	-0.03269
440.0000	-0.03171
450.0000	-0.03142
450.0000	-0.02263

1 Layer	
Geogrid deflection 150mm	
x	y

5 Layer	
Surface deflection 150mm	
x	y
0.0000	-1.2780
10.0000	-1.2721
20.0000	-1.2583
30.0000	-1.2363
40.0000	-1.2065
50.0000	-1.1696
60.0000	-1.1264
70.0000	-1.0780
80.0000	-1.0252
90.0000	-0.9693
100.0000	-0.9113
110.0000	-0.8521
120.0000	-0.7928
130.0000	-0.7340
140.0000	-0.6767
150.0000	-0.6213
160.0000	-0.5684
170.0000	-0.5183
180.0000	-0.4712
190.0000	-0.4273
200.0000	-0.3867
210.0000	-0.3494
220.0000	-0.3152
230.0000	-0.2841
240.0000	-0.2559
250.0000	-0.2304
260.0000	-0.2075
270.0000	-0.1870
280.0000	-0.1686
290.0000	-0.1523
300.0000	-0.1377
310.0000	-0.1248
320.0000	-0.1135
330.0000	-0.1035
340.0000	-0.0947
350.0000	-0.0871
360.0000	-0.0806
370.0000	-0.0749
380.0000	-0.0701
390.0000	-0.0661
400.0000	-0.0628
410.0000	-0.0602
420.0000	-0.0583
430.0000	-0.0569
440.0000	-0.0561
450.0000	-0.0558
450.0000	-0.0426

1 Layer	
Geogrid deflection 150mm	
x	y

6 Layer	
Surface deflection 150mm	
x	y
0.0000	-1.1323
10.0000	-1.1268
20.0000	-1.1143
30.0000	-1.0944
40.0000	-1.0677
50.0000	-1.0350
60.0000	-0.9971
70.0000	-0.9548
80.0000	-0.9090
90.0000	-0.8607
100.0000	-0.8107
110.0000	-0.7601
120.0000	-0.7095
130.0000	-0.6597
140.0000	-0.6113
150.0000	-0.5648
160.0000	-0.5206
170.0000	-0.4790
180.0000	-0.4402
190.0000	-0.4042
200.0000	-0.3711
210.0000	-0.3408
220.0000	-0.3133
230.0000	-0.2884
240.0000	-0.2660
250.0000	-0.2459
260.0000	-0.2279
270.0000	-0.2119
280.0000	-0.1976
290.0000	-0.1850
300.0000	-0.1739
310.0000	-0.1641
320.0000	-0.1555
330.0000	-0.1480
340.0000	-0.1414
350.0000	-0.1357
360.0000	-0.1308
370.0000	-0.1266
380.0000	-0.1231
390.0000	-0.1201
400.0000	-0.1178
410.0000	-0.1159
420.0000	-0.1145
430.0000	-0.1135
440.0000	-0.1130
450.0000	-0.1128
450.0000	-0.0926

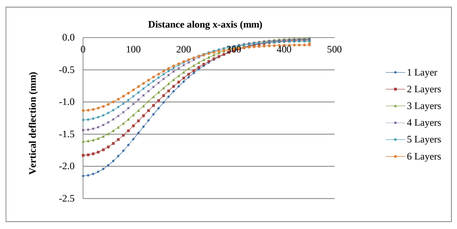

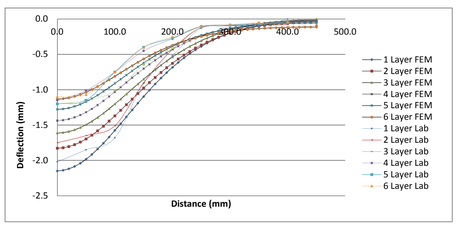

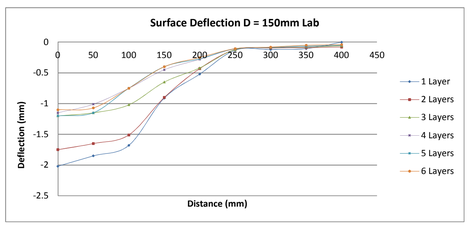

	Maximum surface deflection (mm) H/D = 2					
No. Layers	**1**	**2**	**3**	**4**	**5**	**6**
Laboratory	2.0230	1.7540	1.2050	1.1530	1.2050	1.1030
FEM	2.1484	1.8274	1.6126	1.4366	1.2780	1.1323
% Difference	6.1987	4.1862	25.2762	19.7417	5.7154	2.6558
Average %	**10.629**					
	Maximum surface deflection (mm) H/D = 1.5					
No. Layers	**1**	**2**	**3**	**4**	**5**	**6**
Laboratory	-2.812	-2.333	-1.370	-1.711	-1.547	-0.983
FEM	2.765	2.288	1.952	1.617	1.420	1.236
% Difference	1.612	1.822	29.806	5.760	9.146	20.729
Average %	**11.479**					
	Maximum surface deflection (mm) H/D = 1					
No. Layers	**1**	**2**	**3**	**4**	**5**	**6**
Laboratory	6.1510	6.1330	3.8640	3.6610	3.6420	3.6120
FEM	6.1658	5.1354	4.4196	3.9420	3.4615	3.0817
% Difference	0.2569	16.2246	12.6626	7.1534	5.1562	17.1426
Average %	**9.766**					

10.62

D = 150mm						
x (mm)	y (mm)					
	1	2	3	4	5	6
0	-2.02	-1.75	-1.2	-1.15	-1.2	-1.1
50	-1.85	-1.65	-1.15	-1.01	-1.15	-1.07
100	-1.68	-1.51	-1.02	-0.75	-0.75	-0.75
150	-0.91	-0.90	-0.65	-0.45	-0.40	-0.40
200	-0.52	-0.43	-0.42	-0.28	-0.27	-0.25
250	-0.13	-0.12	-0.12	-0.11	-0.105	-0.105
300	-0.12	-0.095	-0.09	-0.09	-0.086	-0.08
350	-0.105	-0.09	-0.08	-0.075	-0.063	-0.05
400	0	-0.08	-0.06	-0.05	-0.05	-0.04
450	0	0	0	0	0	0

H (opp) 300 mm
Adj 175
57.296

H (opp) 300 mm
Adj 150
57.296

H (opp) 300 mm
Adj 200
57.296

	Experimental model			
H/D	2	1.5	1	Average
D	150	200	300	
Ds	500	500	700	
Angle of draw	59.74	63.44	56.31	59.83
	Numerical model			
H/D	2	1.5	1	Average
D	150	200	300	
Ds	800	800	800	
Angle of draw	42.71	45.00	50.19	45.97

H (opp) 300 mm
Adj 325
57.296

H (opp) 300 mm
Adj 300
57.296

H (opp) 300 mm
Adj 250
57.296

1 Layer	
Surface deflection: 200mm	
x	y
0.0000	-2.7646986
10.0000	-2.7528896
20.0000	-2.7255976
30.0000	-2.6819316
40.0000	-2.6226386
50.0000	-2.5489366
60.0000	-2.4623756
70.0000	-2.3647396
80.0000	-2.2579716
90.0000	-2.1440916
100.0000	-2.0251266
110.0000	-1.9030396
120.0000	-1.7796746
130.0000	-1.6567066
140.0000	-1.5356146
150.0000	-1.4177
160.0000	-1.3038666
170.0000	-1.1950556
180.0000	-1.0918266
190.0000	-0.9945911
200.0000	-0.9035944
210.0000	-0.8189367
220.0000	-0.740599
230.0000	-0.6684663
240.0000	-0.6023491
250.0000	-0.5420024
260.0000	-0.4871421
270.0000	-0.4374592
280.0000	-0.3926312
290.0000	-0.3523316
300.0000	-0.316237
310.0000	-0.2840331
320.0000	-0.2554187
330.0000	-0.2301089
340.0000	-0.2078373
350.0000	-0.1883573
360.0000	-0.17144252
370.0000	-0.15688768
380.0000	-0.1445081
390.0000	-0.13413952
400.0000	-0.12563759
410.0000	-0.1188773
420.0000	-0.11375233
430.0000	-0.11017519
440.0000	-0.10807431
450.0000	-0.10742692

2 Layer	
Surface deflection: 200mm	
x	y
0.0000	-2.2875
10.0000	-2.2791
20.0000	-2.2595
30.0000	-2.2280
40.0000	-2.1852
50.0000	-2.1317
60.0000	-2.0685
70.0000	-1.9967
80.0000	-1.9177
90.0000	-1.8325
100.0000	-1.7427
110.0000	-1.6495
120.0000	-1.5542
130.0000	-1.4580
140.0000	-1.3620
150.0000	-1.2672
160.0000	-1.1745
170.0000	-1.0845
180.0000	-0.9979
190.0000	-0.9152
200.0000	-0.8367
210.0000	-0.7626
220.0000	-0.6931
230.0000	-0.6283
240.0000	-0.5682
250.0000	-0.5126
260.0000	-0.4614
270.0000	-0.4146
280.0000	-0.3718
290.0000	-0.3330
300.0000	-0.2979
310.0000	-0.2663
320.0000	-0.2379
330.0000	-0.2126
340.0000	-0.1902
350.0000	-0.1704
360.0000	-0.1531
370.0000	-0.1382
380.0000	-0.1254
390.0000	-0.1146
400.0000	-0.1058
410.0000	-0.0987
420.0000	-0.0933
430.0000	-0.0896
440.0000	-0.0874
450.0000	-0.0867

3 Layer	
urface deflection: 200mm	
x	y
0.0000	-1.9517
10.0000	-1.9436
20.0000	-1.9247
30.0000	-1.8944
40.0000	-1.8534
50.0000	-1.8023
60.0000	-1.7424
70.0000	-1.6747
80.0000	-1.6007
90.0000	-1.5218
100.0000	-1.4392
110.0000	-1.3544
120.0000	-1.2687
130.0000	-1.1831
140.0000	-1.0988
150.0000	-1.0166
160.0000	-0.9372
170.0000	-0.8612
180.0000	-0.7892
190.0000	-0.7212
200.0000	-0.6577
210.0000	-0.5985
220.0000	-0.5439
230.0000	-0.4935
240.0000	-0.4474
250.0000	-0.4054
260.0000	-0.3672
270.0000	-0.3327
280.0000	-0.3015
290.0000	-0.2735
300.0000	-0.2485
310.0000	-0.2262
320.0000	-0.2063
330.0000	-0.1888
340.0000	-0.1733
350.0000	-0.1598
360.0000	-0.1481
370.0000	-0.1380
380.0000	-0.1294
390.0000	-0.1222
400.0000	-0.1163
410.0000	-0.1116
420.0000	-0.1080
430.0000	-0.1055
440.0000	-0.1041
450.0000	-0.1036

4 Layer	
Surface deflection: 200mm	
x	y
0.0000	-1.6169
10.0000	-1.6101
20.0000	-1.5946
30.0000	-1.5697
40.0000	-1.5358
50.0000	-1.4938
60.0000	-1.4444
70.0000	-1.3887
80.0000	-1.3277
90.0000	-1.2627
100.0000	-1.1946
110.0000	-1.1247
120.0000	-1.0540
130.0000	-0.9834
140.0000	-0.9138
150.0000	-0.8459
160.0000	-0.7803
170.0000	-0.7175
180.0000	-0.6579
190.0000	-0.6017
200.0000	-0.5490
210.0000	-0.5000
220.0000	-0.4546
230.0000	-0.4128
240.0000	-0.3744
250.0000	-0.3394
260.0000	-0.3076
270.0000	-0.2788
280.0000	-0.2528
290.0000	-0.2294
300.0000	-0.2084
310.0000	-0.1897
320.0000	-0.1730
330.0000	-0.1583
340.0000	-0.1453
350.0000	-0.1339
360.0000	-0.1241
370.0000	-0.1156
380.0000	-0.1083
390.0000	-0.1022
400.0000	-0.0972
410.0000	-0.0933
420.0000	-0.0903
430.0000	-0.0882
440.0000	-0.0869
450.0000	-0.0865

5 Layer	
urface deflection: 200mm	
x	y
0.0000	-1.4201
10.0000	-1.4141
20.0000	-1.4001
30.0000	-1.3778
40.0000	-1.3476
50.0000	-1.3101
60.0000	-1.2661
70.0000	-1.2165
80.0000	-1.1625
90.0000	-1.1049
100.0000	-1.0449
110.0000	-0.9835
120.0000	-0.9215
130.0000	-0.8599
140.0000	-0.7993
150.0000	-0.7404
160.0000	-0.6838
170.0000	-0.6297
180.0000	-0.5785
190.0000	-0.5303
200.0000	-0.4854
210.0000	-0.4437
220.0000	-0.4051
230.0000	-0.3697
240.0000	-0.3373
250.0000	-0.3077
260.0000	-0.2809
270.0000	-0.2566
280.0000	-0.2347
290.0000	-0.2150
300.0000	-0.1974
310.0000	-0.1817
320.0000	-0.1677
330.0000	-0.1553
340.0000	-0.1444
350.0000	-0.1348
360.0000	-0.1265
370.0000	-0.1193
380.0000	-0.1132
390.0000	-0.1081
400.0000	-0.1038
410.0000	-0.1005
420.0000	-0.0980
430.0000	-0.0962
440.0000	-0.0951
450.00	-0.0948

6 Layer	
urface deflection: 200mm	
x	y
0.0000	-1.2363
10.0000	-1.2310
20.0000	-1.2189
30.0000	-1.1996
40.0000	-1.1735
50.0000	-1.1411
60.0000	-1.1033
70.0000	-1.0607
80.0000	-1.0143
90.0000	-0.9650
100.0000	-0.9136
110.0000	-0.8611
120.0000	-0.8081
130.0000	-0.7555
140.0000	-0.7039
150.0000	-0.6537
160.0000	-0.6055
170.0000	-0.5595
180.0000	-0.5160
190.0000	-0.4752
200.0000	-0.4371
210.0000	-0.4017
220.0000	-0.3690
230.0000	-0.3390
240.0000	-0.3115
250.0000	-0.2865
260.0000	-0.2638
270.0000	-0.2432
280.0000	-0.2247
290.0000	-0.2080
300.0000	-0.1930
310.0000	-0.1797
320.0000	-0.1678
330.0000	-0.1573
340.0000	-0.1481
350.0000	-0.1400
360.0000	-0.1329
370.0000	-0.1268
380.0000	-0.1216
390.0000	-0.1173
400.0000	-0.1137
410.0000	-0.1109
420.0000	-0.1087
430.0000	-0.1072
440.0000	-0.1063
450.0000	-0.1061

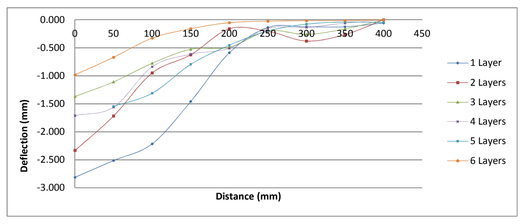

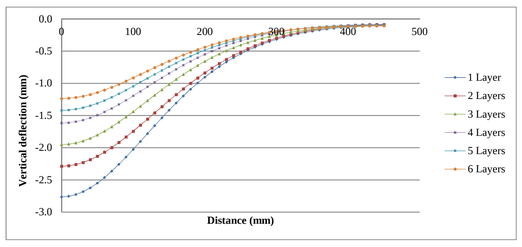

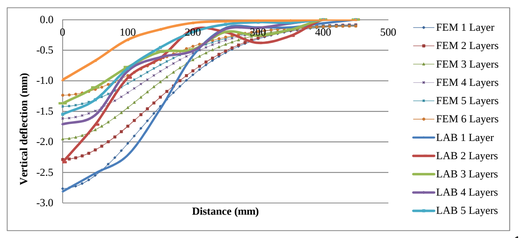

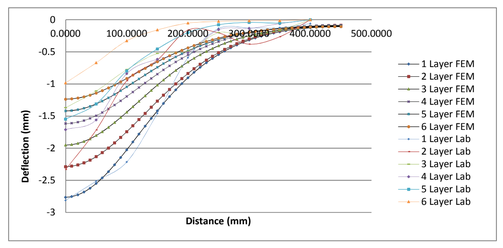

x (mm)	D = 200mm					
	y (mm)					
	1	2	3	4	5	6
0	-2.812	-2.333	-1.370	-1.711	-1.547	-0.983
50	-2.513	-1.717	-1.109	-1.560	-1.311	-0.670
100	-2.215	-0.950	-0.777	-0.839	-0.796	-0.328
150	-1.459	-0.625	-0.527	-0.614	-0.454	-0.159
200	-0.590	-0.161	-0.489	-0.511	-0.201	-0.052
250	-0.137	-0.205	-0.201	-0.155	-0.078	-0.026
300	-0.126	-0.380	-0.261	-0.136	-0.041	-0.016
350	-0.126	-0.265	-0.163	-0.061	-0.051	-0.014
400	-0.059	0.000	0.000	0.000	0.000	0.000
450	0.000	0.000	0.000	0.000	0.000	0.000

-1

	Maximum surface deflection (mm) H/D = 1.5					
No. Layers	**1**	**2**	**3**	**4**	**5**	**6**
Laboratory	2.81219	2.332711	1.37	1.71	1.55	0.98
FEM	2.76	2.29	1.95	1.62	1.42	1.24
% Difference	1.69	1.94	29.83	5.80	8.94	20.46
Average %	**11.44**					

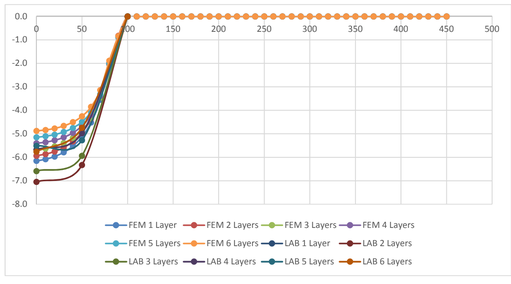

1 Layer	
Geogrid deflection: 200mm	
x	y
0.0000	-6.15382593
10.0000	-6.08184815
20.0000	-5.96669259
30.0000	-5.78804444
40.0000	-5.52037778
50.0000	-5.12218519
60.0000	-4.51475926
70.0000	-3.55152148
80.0000	-2.03973259
90.0000	-0.85185185
100.0000	0.0000
110.0000	0.0000
120.0000	0.0000
130.0000	0.0000
140.0000	0.0000
150.0000	0.0000
160.0000	0.0000
170.0000	0.0000
180.0000	0.0000
190.0000	0.0000
200.0000	0.0000
210.0000	0.0000
220.0000	0.0000
230.0000	0.0000
240.0000	0.0000
250.0000	0.0000
260.0000	0.0000
270.0000	0.0000
280.0000	0.0000
290.0000	0.0000
300.0000	0.0000
310.0000	0.0000
320.0000	0.0000
330.0000	0.0000
340.0000	0.0000
350.0000	0.0000
360.0000	0.0000
370.0000	0.0000
380.0000	0.0000
390.0000	0.0000
400.0000	0.0000
410.0000	0.0000
420.0000	0.0000
430.0000	0.0000
440.0000	0.0000
450.0000	0.0000

1 Layer	
Geogrid deflection: 200mm	
x	y
0.0000	-5.934046
10.0000	-5.864639
20.0000	-5.753596
30.0000	-5.581329
40.0000	-5.323221
50.0000	-4.93925
60.0000	-4.353518
70.0000	-3.424681
80.0000	-1.966885
90.0000	-0.821429
100.0000	0.0000
110.0000	0.0000
120.0000	0.0000
130.0000	0.0000
140.0000	0.0000
150.0000	0.0000
160.0000	0.0000
170.0000	0.0000
180.0000	0.0000
190.0000	0.0000
200.0000	0.0000
210.0000	0.0000
220.0000	0.0000
230.0000	0.0000
240.0000	0.0000
250.0000	0.0000
260.0000	0.0000
270.0000	0.0000
280.0000	0.0000
290.0000	0.0000
300.0000	0.0000
310.0000	0.0000
320.0000	0.0000
330.0000	0.0000
340.0000	0.0000
350.0000	0.0000
360.0000	0.0000
370.0000	0.0000
380.0000	0.0000
390.0000	0.0000
400.0000	0.0000
410.0000	0.0000
420.0000	0.0000
430.0000	0.0000
440.0000	0.0000
450.0000	0.0000

1 Layer	
eogrid deflection: 200mm	
x	y
0	-5.68454
10	-5.62685
20	-5.53475
30	-5.39112
40	-5.17352
50	-4.84332
60	-4.32158
70	-3.4547
80	-2.02252
90	-0.88889
100	0
110	0
120	0
130	0
140	0
150	0
160	0
170	0
180	0
190	0
200	0
210	0
220	0
230	0
240	0
250	0
260	0
270	0
280	0
290	0
300	0
310	0
320	0
330	0
340	0
350	0
360	0
370	0
380	0
390	0
400	0
410	0
420	0
430	0
440	0
450	0

1 Layer	
Geogrid deflection: 200mm	
x	y
0	-5.40323
10	-5.35399
20	-5.27446
30	-5.14922
40	-4.95787
50	-4.66472
60	-4.19374
70	-3.38839
80	-2.00968
90	-0.89552
100	0
110	0
120	0
130	0
140	0
150	0
160	0
170	0
180	0
190	0
200	0
210	0
220	0
230	0
240	0
250	0
260	0
270	0
280	0
290	0
300	0
310	0
320	0
330	0
340	0
350	0
360	0
370	0
380	0
390	0
400	0
410	0
420	0
430	0
440	0
450	0

1 Layer	
Geogrid deflection: 200mm	
x	y
0	-5.14703
10	-5.10414
20	-5.03392
30	-4.92246
40	-4.75131
50	-4.48806
60	-4.06097
70	-3.31365
80	-1.98953
90	-0.88889
100	0
110	0
120	0
130	0
140	0
150	0
160	0
170	0
180	0
190	0
200	0
210	0
220	0
230	0
240	0
250	0
260	0
270	0
280	0
290	0
300	0
310	0
320	0
330	0
340	0
350	0
360	0
370	0
380	0
390	0
400	0
410	0
420	0
430	0
440	0
450	0

1 Layer	
Geogrid deflection: 200mm	
x	y
0	-4.87613
10	-4.8355
20	-4.76897
30	-4.66338
40	-4.50124
50	-4.25185
60	-3.84724
70	-3.13924
80	-1.88481
90	-0.84211
100	0
110	0
120	0
130	0
140	0
150	0
160	0
170	0
180	0
190	0
200	0
210	0
220	0
230	0
240	0
250	0
260	0
270	0
280	0
290	0
300	0
310	0
320	0
330	0
340	0
350	0
360	0
370	0
380	0
390	0
400	0
410	0
420	0
430	0
440	0
450	0

LAB D = 200 mm															
1 Layer	x	2 Layer	x	y	3 Layer	x	y	4 Layer	x	y	5 Layer	x	y	6 Layer	x	y
	0		0	-7.047162		0	-6.58881		0	-5.67508		0	-5.51371		0	-5.75803
	50		50	-6.326663		50	-5.93437		50	-4.97423		50	-5.27465		50	-4.74208
	100		100	0		100	0		100	0		100	0		100	0

1 Layer	
Surface deflection: 300mm	
x	y
0.0000	-6.1658
10.0000	-6.1306
20.0000	-6.0466
30.0000	-5.9062
40.0000	-5.7048
50.0000	-5.4345
60.0000	-5.1009
70.0000	-4.7292
80.0000	-4.3390
90.0000	-3.9204
100.0000	-3.5220
110.0000	-3.1578
120.0000	-2.8299
130.0000	-2.5365
140.0000	-2.2740
150.0000	-2.0385
160.0000	-1.8263
170.0000	-1.6346
180.0000	-1.4611
190.0000	-1.3038
200.0000	-1.1614
210.0000	-1.0323
220.0000	-0.9155
230.0000	-0.8100
240.0000	-0.7147
250.0000	-0.6288
260.0000	-0.5515
270.0000	-0.4821
280.0000	-0.4199
290.0000	-0.3642
300.0000	-0.3145
310.0000	-0.2703
320.0000	-0.2312
330.0000	-0.1966
340.0000	-0.1661
350.0000	-0.1395
360.0000	-0.1164
370.0000	-0.0965
380.0000	-0.0796
390.0000	-0.0654
400.0000	-0.0537
410.0000	-0.0445
420.0000	-0.0374
430.0000	-0.0325
440.0000	-0.0296
450.0000	-0.0287

2 Layer	
Surface deflection: 300mm	
x	y
0.0000	-5.1354
10.0000	-5.1099
20.0000	-5.0498
30.0000	-4.9516
40.0000	-4.8097
50.0000	-4.6267
60.0000	-4.4082
70.0000	-4.1424
80.0000	-3.8464
90.0000	-3.5402
100.0000	-3.2373
110.0000	-2.9469
120.0000	-2.6741
130.0000	-2.4211
140.0000	-2.1882
150.0000	-1.9744
160.0000	-1.7783
170.0000	-1.5987
180.0000	-1.4343
190.0000	-1.2839
200.0000	-1.1467
210.0000	-1.0217
220.0000	-0.9079
230.0000	-0.8047
240.0000	-0.7111
250.0000	-0.6265
260.0000	-0.5502
270.0000	-0.4816
280.0000	-0.4199
290.0000	-0.3647
300.0000	-0.3154
310.0000	-0.2715
320.0000	-0.2325
330.0000	-0.1981
340.0000	-0.1678
350.0000	-0.1413
360.0000	-0.1183
370.0000	-0.0984
380.0000	-0.0816
390.0000	-0.0674
400.0000	-0.0558
410.0000	-0.0466
420.0000	-0.0396
430.0000	-0.0347
440.0000	-0.0318
450.0000	-0.0309

3 Layer	
Surface deflection: 300mm	
x	y
0.0000	-4.4196
10.0000	-4.3978
20.0000	-4.3470
30.0000	-4.2641
40.0000	-4.1480
50.0000	-3.9989
60.0000	-3.8199
70.0000	-3.6158
80.0000	-3.3936
90.0000	-3.1610
100.0000	-2.9256
110.0000	-2.6937
120.0000	-2.4697
130.0000	-2.2562
140.0000	-2.0547
150.0000	-1.8660
160.0000	-1.6901
170.0000	-1.5268
180.0000	-1.3757
190.0000	-1.2363
200.0000	-1.1081
210.0000	-0.9905
220.0000	-0.8830
230.0000	-0.7849
240.0000	-0.6956
250.0000	-0.6147
260.0000	-0.5414
270.0000	-0.4753
280.0000	-0.4158
290.0000	-0.3624
300.0000	-0.3146
310.0000	-0.2720
320.0000	-0.2342
330.0000	-0.2007
340.0000	-0.1712
350.0000	-0.1454
360.0000	-0.1230
370.0000	-0.1036
380.0000	-0.0872
390.0000	-0.0734
400.0000	-0.0621
410.0000	-0.0531
420.0000	-0.0462
430.0000	-0.0414
440.0000	-0.0386
450.0000	-0.0377

4 Layer	
Surface deflection: 300mm	
x	y
0.0000	-3.9420
10.0000	-3.9232
20.0000	-3.8796
30.0000	-3.8089
40.0000	-3.7115
50.0000	-3.5884
60.0000	-3.4417
70.0000	-3.2749
80.0000	-3.0925
90.0000	-2.8999
100.0000	-2.7025
110.0000	-2.5051
120.0000	-2.3113
130.0000	-2.1239
140.0000	-1.9447
150.0000	-1.7746
160.0000	-1.6144
170.0000	-1.4643
180.0000	-1.3243
190.0000	-1.1943
200.0000	-1.0741
210.0000	-0.9633
220.0000	-0.8616
230.0000	-0.7685
240.0000	-0.6835
250.0000	-0.6062
260.0000	-0.5362
270.0000	-0.4728
280.0000	-0.4157
290.0000	-0.3644
300.0000	-0.3184
310.0000	-0.2774
320.0000	-0.2409
330.0000	-0.2085
340.0000	-0.1801
350.0000	-0.1552
360.0000	-0.1335
370.0000	-0.1148
380.0000	-0.0989
390.0000	-0.0856
400.0000	-0.0746
410.0000	-0.0659
420.0000	-0.0593
430.0000	-0.0546
440.0000	-0.0519
450.0000	-0.0511

5 Layer	
Surface deflection: 300mm	
x	y
0.0000	-3.4615
10.0000	-3.4461
20.0000	-3.4104
30.0000	-3.3528
40.0000	-3.2740
50.0000	-3.1751
60.0000	-3.0579
70.0000	-2.9248
80.0000	-2.7788
90.0000	-2.6233
100.0000	-2.4617
110.0000	-2.2974
120.0000	-2.1333
130.0000	-1.9718
140.0000	-1.8148
150.0000	-1.6639
160.0000	-1.5199
170.0000	-1.3835
180.0000	-1.2552
190.0000	-1.1351
200.0000	-1.0233
210.0000	-0.9196
220.0000	-0.8239
230.0000	-0.7359
240.0000	-0.6554
250.0000	-0.5818
260.0000	-0.5149
270.0000	-0.4543
280.0000	-0.3995
290.0000	-0.3502
300.0000	-0.3059
310.0000	-0.2663
320.0000	-0.2311
330.0000	-0.1998
340.0000	-0.1723
350.0000	-0.1481
360.0000	-0.1271
370.0000	-0.1090
380.0000	-0.0936
390.0000	-0.0806
400.0000	-0.0700
410.0000	-0.0615
420.0000	-0.0551
430.0000	-0.0506
440.0000	-0.0479
450.0000	-0.0471

6 Layer	
Surface deflection: 300mm	
x	y
0.0000	-3.0817
10.0000	-3.0689
20.0000	-3.0391
30.0000	-2.9913
40.0000	-2.9260
50.0000	-2.8442
60.0000	-2.7474
70.0000	-2.6375
80.0000	-2.5165
90.0000	-2.3870
100.0000	-2.2515
110.0000	-2.1124
120.0000	-1.9720
130.0000	-1.8323
140.0000	-1.6951
150.0000	-1.5616
160.0000	-1.4331
170.0000	-1.3104
180.0000	-1.1940
190.0000	-1.0843
200.0000	-0.9815
210.0000	-0.8857
220.0000	-0.7969
230.0000	-0.7149
240.0000	-0.6396
250.0000	-0.5706
260.0000	-0.5077
270.0000	-0.4505
280.0000	-0.3987
290.0000	-0.3520
300.0000	-0.3100
310.0000	-0.2725
320.0000	-0.2390
330.0000	-0.2092
340.0000	-0.1830
350.0000	-0.1600
360.0000	-0.1399
370.0000	-0.1226
380.0000	-0.1079
390.0000	-0.0955
400.0000	-0.0854
410.0000	-0.0773
420.0000	-0.0711
430.0000	-0.0668
440.0000	-0.0643
450.0000	-0.0635

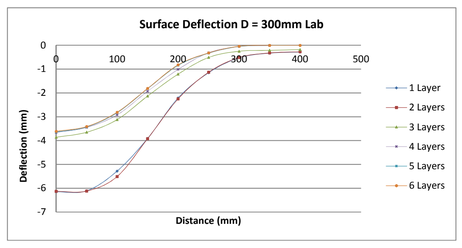

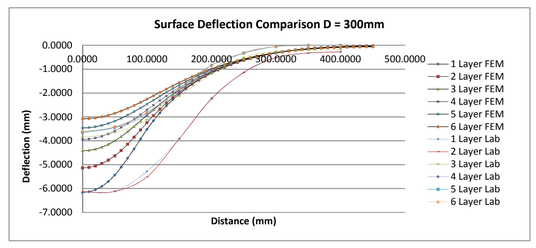

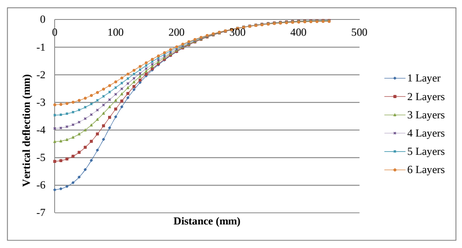

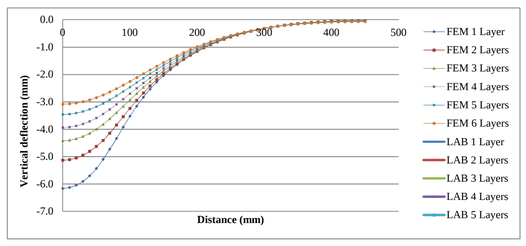

1 Layer	
Geogrid deflection: 300mm	
x	y
0.0000	-13.6588
10.0000	-13.6171
20.0000	-13.5201
30.0000	-13.361
40.0000	-13.137
50.0000	-12.8444
60.0000	-12.4784
70.0000	-12.0325
80.0000	-11.4974
90.0000	-10.8598
100.0000	-10.0998
110.0000	-9.18514
120.0000	-8.06428
130.0000	-6.59869
140.0000	-4.67429
150.0000	0
160.0000	0
170.0000	0
180.0000	0
190.0000	0
200.0000	0
210.0000	0
220.0000	0
230.0000	0
240.0000	0
250.0000	0
260.0000	0
270.0000	0
280.0000	0
290.0000	0
300.0000	0
310.0000	0
320.0000	0
330.0000	0
340.0000	0
350.0000	0
360.0000	0
370.0000	0
380.0000	0
390.0000	0
400.0000	0
410.0000	0
420.0000	0
430.0000	0
440.0000	0
450.0000	0

1 Layer	
Geogrid deflection: 300mm	
x	y
0.0000	-13.1482
10.0000	-13.1081
20.0000	-13.0146
30.0000	-12.8616
40.0000	-12.6459
50.0000	-12.3642
60.0000	-12.0119
70.0000	-11.5827
80.0000	-11.0676
90.0000	-10.4539
100.0000	-9.72224
110.0000	-8.84177
120.0000	-7.76281
130.0000	-6.35201
140.0000	-4.49955
150.0000	0.0000
160.0000	0.0000
170.0000	0.0000
180.0000	0.0000
190.0000	0.0000
200.0000	0.0000
210.0000	0.0000
220.0000	0.0000
230.0000	0.0000
240.0000	0.0000
250.0000	0.0000
260.0000	0.0000
270.0000	0.0000
280.0000	0.0000
290.0000	0.0000
300.0000	0.0000
310.0000	0.0000
320.0000	0.0000
330.0000	0.0000
340.0000	0.0000
350.0000	0.0000
360.0000	0.0000
370.0000	0.0000
380.0000	0.0000
390.0000	0.0000
400.0000	0.0000
410.0000	0.0000
420.0000	0.0000
430.0000	0.0000
440.0000	0.0000
450.0000	0.0000

1 Layer	
Geogrid deflection: 300mm	
x	y
0.0000	-12.6376
10.0000	-12.599
20.0000	-12.5092
30.0000	-12.3621
40.0000	-12.1548
50.0000	-11.8841
60.0000	-11.5455
70.0000	-11.1329
80.0000	-10.6378
90.0000	-10.0479
100.0000	-9.34468
110.0000	-8.4984
120.0000	-7.46134
130.0000	-6.10533
140.0000	-4.32481
150.0000	0.0000
160.0000	0.0000
170.0000	0.0000
180.0000	0.0000
190.0000	0.0000
200.0000	0.0000
210.0000	0.0000
220.0000	0.0000
230.0000	0.0000
240.0000	0.0000
250.0000	0.0000
260.0000	0.0000
270.0000	0.0000
280.0000	0.0000
290.0000	0.0000
300.0000	0.0000
310.0000	0.0000
320.0000	0.0000
330.0000	0.0000
340.0000	0.0000
350.0000	0.0000
360.0000	0.0000
370.0000	0.0000
380.0000	0.0000
390.0000	0.0000
400.0000	0.0000
410.0000	0.0000
420.0000	0.0000
430.0000	0.0000
440.0000	0.0000
450.0000	0.0000

1 Layer	
Geogrid deflection: 300mm	
x	y
0.0000	-12.1574
10.0000	-12.1203
20.0000	-12.0339
30.0000	-11.8923
40.0000	-11.6929
50.0000	-11.4325
60.0000	-11.1067
70.0000	-10.7098
80.0000	-10.2336
90.0000	-9.66607
100.0000	-8.98959
110.0000	-8.17547
120.0000	-7.17782
130.0000	-5.87334
140.0000	-4.16047
150.0000	0.0000
160.0000	0.0000
170.0000	0.0000
180.0000	0.0000
190.0000	0.0000
200.0000	0.0000
210.0000	0.0000
220.0000	0.0000
230.0000	0.0000
240.0000	0.0000
250.0000	0.0000
260.0000	0.0000
270.0000	0.0000
280.0000	0.0000
290.0000	0.0000
300.0000	0.0000
310.0000	0.0000
320.0000	0.0000
330.0000	0.0000
340.0000	0.0000
350.0000	0.0000
360.0000	0.0000
370.0000	0.0000
380.0000	0.0000
390.0000	0.0000
400.0000	0.0000
410.0000	0.0000
420.0000	0.0000
430.0000	0.0000
440.0000	0.0000
450.0000	0.0000

1 Layer	
Geogrid deflection: 300mm	
x	y
0.0000	-11.7113
10.0000	-11.6755
20.0000	-11.5923
30.0000	-11.4559
40.0000	-11.2638
50.0000	-11.013
60.0000	-10.6992
70.0000	-10.3168
80.0000	-9.85801
90.0000	-9.31135
100.0000	-8.6597
110.0000	-7.87545
120.0000	-6.91441
130.0000	-5.6578
140.0000	-4.00779
150.0000	0.0000
160.0000	0.0000
170.0000	0.0000
180.0000	0.0000
190.0000	0.0000
200.0000	0.0000
210.0000	0.0000
220.0000	0.0000
230.0000	0.0000
240.0000	0.0000
250.0000	0.0000
260.0000	0.0000
270.0000	0.0000
280.0000	0.0000
290.0000	0.0000
300.0000	0.0000
310.0000	0.0000
320.0000	0.0000
330.0000	0.0000
340.0000	0.0000
350.0000	0.0000
360.0000	0.0000
370.0000	0.0000
380.0000	0.0000
390.0000	0.0000
400.0000	0.0000
410.0000	0.0000
420.0000	0.0000
430.0000	0.0000
440.0000	0.0000
450.0000	0.0000

1 Layer	
Geogrid deflection: 300mm	
x	y
0.0000	-11.2967
10.0000	-11.2622
20.0000	-11.1819
30.0000	-11.0504
40.0000	-10.8651
50.0000	-10.6231
60.0000	-10.3204
70.0000	-9.95161
80.0000	-9.50905
90.0000	-8.98174
100.0000	-8.35316
110.0000	-7.59668
120.0000	-6.66965
130.0000	-5.45753
140.0000	-3.86592
150.0000	0.0000
160.0000	0.0000
170.0000	0.0000
180.0000	0.0000
190.0000	0.0000
200.0000	0.0000
210.0000	0.0000
220.0000	0.0000
230.0000	0.0000
240.0000	0.0000
250.0000	0.0000
260.0000	0.0000
270.0000	0.0000
280.0000	0.0000
290.0000	0.0000
300.0000	0.0000
310.0000	0.0000
320.0000	0.0000
330.0000	0.0000
340.0000	0.0000
350.0000	0.0000
360.0000	0.0000
370.0000	0.0000
380.0000	0.0000
390.0000	0.0000
400.0000	0.0000
410.0000	0.0000
420.0000	0.0000
430.0000	0.0000
440.0000	0.0000
450.0000	0.0000

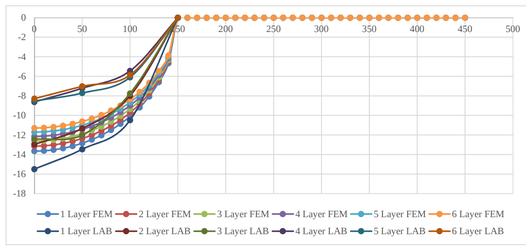

1 Layer	x	y	2 Layer	x	y	3 Layer	x	y	4 Layer	x	y	5 Layer	x	y	6 Layer	x	y
	0	-15.4972		0	-12.9599		0	-12.4382		0	-8.62422		0	-8.52809		0	-8.28672
	50	-13.4655		50	-11.3342		50	-12.019		50	-7.22025		50	-7.71251		50	-7.02618
	100	-10.4878		100	-7.9993		100	-7.74946		100	-5.44454		100	-6.10075		100	-5.86724
	150	0		150	0		150	0		150	0		150	0		150	0

APPENDIX F

Friction angle				Geogrid deflection (mm)		
Geogrid deflection (mm)				Angle = 50		1000
Angle = 40		1000		x	y (m)	y (mm)
x	y (m)	y (mm)		0	-0.0003495	-0.3495
0	-0.00031556	-0.31556		0.4166667	-0.00039741	-0.39741
0.416667	-0.00036651	-0.36651		0.8333333	-0.00054004	-0.54004
0.833333	-0.00052	-0.52		1.25	-0.00076971	-0.76971
1.25	-0.00077379	-0.77379		1.6666667	-0.00105846	-1.05846
1.666667	-0.00110406	-1.10406		2.0833333	-0.00133536	-1.33536
2.083333	-0.00140079	-1.40079		2.5	-0.00164242	-1.64242
2.5	-0.00171289	-1.71289		2.9166667	-0.00219428	-2.19428
2.916667	-0.0023576	-2.3576		3.3333333	-0.00287451	-2.96989
3.333333	-0.00316989	-3.16989		3.75	-0.00346991	-3.78015
3.75	-0.00388015	-3.88015		4.0625	-0.00370015	-4.05347
4.0625	-0.00415347	-4.15347		4.375	-0.00376457	-4.12187
4.375	-0.00422187	-4.22187		4.6875	-0.00378419	-4.14585
4.6875	-0.00424585	-4.24585		5	-0.00379134	-4.15444
5	-0.00425444	-4.25444		5.3125	-0.00378856	-4.15019
5.3125	-0.00425019	-4.25019		5.625	-0.00377086	-4.12823
5.625	-0.00422823	-4.22823		5.9375	-0.00371042	-4.06522
5.9375	-0.00416522	-4.16522		6.25	-0.00349023	-3.78835
6.25	-0.00388835	-3.88835		6.6666667	-0.00286219	-2.937
6.666667	-0.003137	-3.137		7.0833333	-0.00218541	-2.18541
7.083333	-0.00234466	-2.34466		7.5	-0.00163686	-1.63686
7.5	-0.00170547	-1.70547		7.9166667	-0.0013312	-1.3312
7.916667	-0.0013951	-1.3951		8.3333333	-0.00105561	-1.05561
8.333333	-0.00110009	-1.10009		8.75	-0.00076785	-0.76785
8.75	-0.00077121	-0.77121		9.1666667	-0.00053885	-0.53885
9.166667	-0.00051839	-0.51839		9.5833333	-0.00039661	-0.39661
9.583333	-0.00036542	-0.36542		10	-0.00034881	-0.34881
10	-0.00031463	-0.31463				

Rail deflection (mm)			Rail deflection (mm)		
E = 160		1000	50		1000
x	y (m)	y (mm)	x	y (m)	y (mm)
0	0.00021864	0.22099	0	0.0002169	0.2169
0.275	0.0002189	0.22152	0.275	0.00021705	0.21705
0.65	0.00022019	0.22425	0.65	0.00021782	0.21782
0.925	0.00021999	0.22586	0.925	0.00021698	0.21698
1.3	0.0002216	0.23085	1.3	0.00021736	0.21736
1.575	0.00021959	0.23198	1.575	0.00021424	0.21424
1.95	0.00021857	0.236	1.95	0.00021141	0.21141
2.225	0.00021201	0.23358	2.225	0.00020339	0.20339
2.6	0.00020353	0.23125	2.6	0.00019272	0.19272
2.875	0.00018835	0.22063	2.875	0.00017596	0.17596
3.25	0.00016559	0.20425	3.25	0.00015095	0.15095
3.525	0.0001364	0.17919	3.525	0.00012037	0.12037
3.9	0.00009053	0.13863	3.9	0.00007267	0.07267
4.175	0.00004072	0.09129	4.175	0.00002208	0.02208
4.55	-0.00003897	0.01404	4.55	-0.0000584	-0.0584
4.825	-0.00011699	-0.06474	4.825	-0.00013604	-0.13604
5.2	-0.00024264	-0.19317	5.2	-0.00026065	-0.26065
5.475	-0.00035682	-0.31324	5.475	-0.00037267	-0.37267
5.85	-0.00054106	-0.50823	5.85	-0.00055313	-0.55313
6.125	-0.00069869	-0.67898	6.125	-0.00070613	-0.70613
6.5	-0.00095288	-0.95481	6.5	-0.0009529	-0.9529
6.775	-0.00115879	-1.18298	6.775	-0.00115116	-1.15116
7.15	-0.00149001	-1.54909	7.15	-0.00147063	-1.47063
7.425	-0.00174337	-1.83476	7.425	-0.0017131	-1.7131
7.8	-0.00214825	-2.28821	7.8	-0.00210189	-2.10189
8.075	-0.00243669	-2.61754	8.075	-0.00237676	-2.37676
8.45	-0.00288992	-3.1287	8.45	-0.00281101	-2.81101
8.725	-0.00318343	-3.46478	8.725	-0.00309055	-3.09055
9.1	-0.00362633	-3.95992	9.1	-0.00351642	-3.51642
9.375	-0.00386868	-4.22928	9.375	-0.00374994	-3.74994
9.75	-0.0041275	-4.50458	9.75	-0.00400338	-4.40458
10.025	-0.00399422	-4.36292	10.025	-0.00387284	-3.87284
10.4	-0.0036115	-3.94276	10.4	-0.00350236	-3.50236
10.675	-0.00332993	-3.6236	10.675	-0.00323312	-3.23312
11.05	-0.00286279	-3.09769	11.05	-0.00278521	-2.78521
11.325	-0.00256073	-2.75178	11.325	-0.00249762	-2.49762
11.7	-0.00211745	-2.25323	11.7	-0.00207256	-2.07256
11.975	-0.0018385	-1.93651	11.975	-0.00180624	-1.80624
12.35	-0.00146142	-1.51666	12.35	-0.00144348	-1.44348
12.625	-0.00122662	-1.25391	12.625	-0.0012182	-1.2182
13	-0.00092843	-0.92687	13	-0.00092985	-0.92985
13.275	-0.00074368	-0.72403	13.275	-0.00075141	-0.75141
13.65	-0.00052177	-0.48553	13.65	-0.00053526	-0.53526
13.925	-0.0003848	-0.33878	13.925	-0.0004018	-0.4018
14.3	-0.00022973	-0.17663	14.3	-0.00024928	-0.24928
14.575	-0.00013441	-0.07778	14.575	-0.00015532	-0.15532
14.95	-0.00003419	0.02292	14.95	-0.00005534	-0.05534
15.225	0.00002706	0.08349	15.225	0.00000606	0.00606
15.6	0.00008468	0.13753	15.6	0.0000649	0.0649
15.875	0.00011954	0.1692	15.875	0.00010082	0.10082
16.25	0.00014575	0.1898	16.25	0.00012902	0.12902
16.525	0.00016116	0.20087	16.525	0.00014597	0.14597
16.9	0.00016544	0.19895	16.9	0.0001525	0.1525
17.175	0.00016731	0.19626	17.175	0.00015604	0.15604
17.55	0.00015726	0.18038	17.55	0.00014817	0.14817
17.825	0.00015036	0.16929	17.825	0.00014284	0.14284
18.2	0.00013185	0.14587	18.2	0.0001262	0.1262
18.475	0.00011991	0.13045	18.475	0.0001156	0.1156
18.85	0.00009739	0.10418	18.85	0.00009455	0.09455
19.125	0.00008338	0.08755	19.125	0.00008158	0.08158
19.5	0.00006027	0.06196	19.5	0.00005948	0.05948
19.775	0.00004651	0.04658	19.775	0.00004637	0.04637
20.15	0.00002528	0.02446	20.15	0.00002554	0.02554
20.425	0.0000132	0.01226	20.425	0.00001354	0.01354
20.8	0	0	20.8	0	0

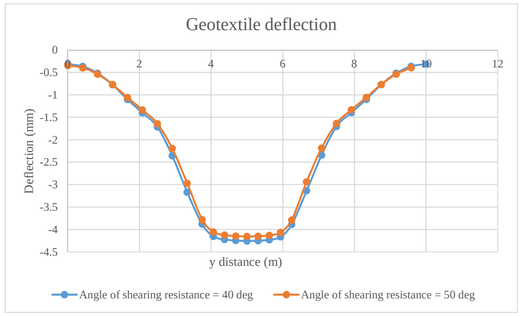

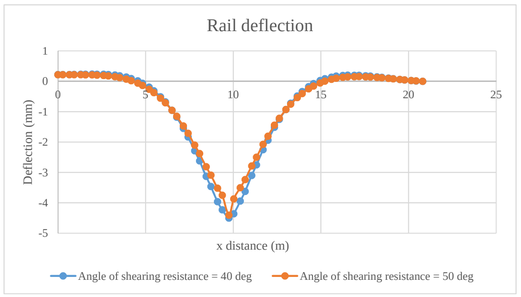

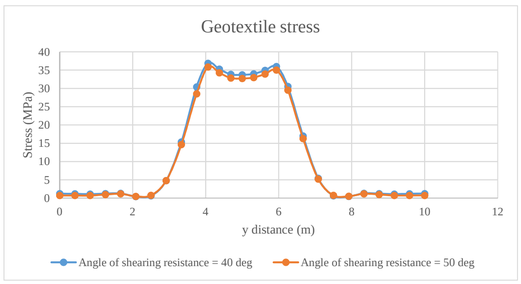

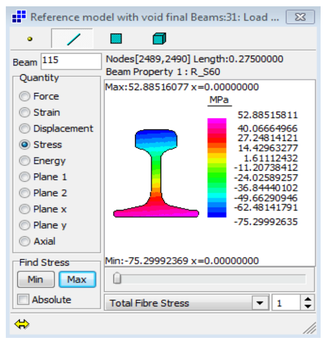

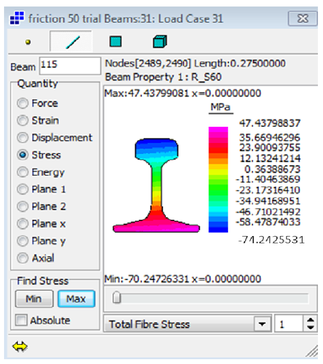

phi	Geo stress	rail stress
40	36	75.3
50	35.003	74.242

Geogrid stress			Geogrid stress		
40		500	50		500
x	y (m)	y (mm)	x	y (m)	y (mm)
0	0.00247816	1.23908	0	0.00148014	0.74007
0.416667	0.00237391	1.186955	0.4166667	0.00143239	0.716195
0.833333	0.00219588	1.09794	0.8333333	0.00144203	0.721015
1.25	0.00247497	1.237485	1.25	0.00197994	0.98997
1.666667	0.00260127	1.300635	1.6666667	0.00237553	1.187765
2.083333	0.00090286	0.45143	2.0833333	0.00098999	0.494995
2.5	0.00127523	0.637615	2.5	0.00152547	0.762735
2.916667	0.00962382	4.81191	2.9166667	0.00957853	4.789265
3.333333	0.03073555	15.36778	3.3333333	0.02928005	14.64003
3.75	0.06080431	30.40216	3.75	0.05708024	28.54012
4.0625	0.07375254	36.87627	4.0625	0.06896669	35.87627
4.375	0.0705067	35.25335	4.375	0.06591866	34.25335
4.6875	0.06767797	33.83899	4.6875	0.06325311	32.83899
5	0.06743875	33.71938	5	0.06302067	32.71938
5.3125	0.06794031	33.97016	5.3125	0.0635189	32.97016
5.625	0.06986895	34.93448	5.625	0.06530852	33.93448
5.9375	0.07200701	36.00351	5.9375	0.06750408	35.00351
6.25	0.06107944	30.53972	6.25	0.05807995	29.53972
6.666667	0.03397248	16.98624	6.6666667	0.03253616	16.26808
7.083333	0.0108239	5.41195	7.0833333	0.01042566	5.21283
7.5	0.0012976	0.6488	7.5	0.00151881	0.759405
7.916667	0.00093123	0.465615	7.9166667	0.00101483	0.507415
8.333333	0.00264656	1.32328	8.3333333	0.00241928	1.20964
8.75	0.00250305	1.251525	8.75	0.00200942	1.00471
9.166667	0.0022224	1.1112	9.1666667	0.00146984	0.73492
9.583333	0.00239647	1.198235	9.5833333	0.0014568	0.7284
10	0.00249965	1.249825	10	0.00150358	0.75179

Tensile modulus = 100 kN/m

Geogrid deflection (mm)		
x	y (m)	1000
0	-0.00031556	-0.31556
0.416667	-0.00036651	-0.36651
0.833333	-0.00052	-0.52
1.25	-0.00077379	-0.77379
1.666667	-0.00110406	-1.10406
2.083333	-0.00140079	-1.40079
2.5	-0.00171289	-1.71289
2.916667	-0.0023576	-2.3576
3.333333	-0.00316989	-3.16989
3.75	-0.00388015	-3.88015
4.0625	-0.00415347	-4.15347
4.375	-0.00422187	-4.22187
4.6875	-0.00424585	-4.24585
5	-0.00425444	-4.25444
5.3125	-0.00425019	-4.25019
5.625	-0.00422823	-4.22823
5.9375	-0.00416522	-4.16522
6.25	-0.00388835	-3.88835
6.666667	-0.003137	-3.137
7.083333	-0.00234466	-2.34466
7.5	-0.00170547	-1.70547
7.916667	-0.0013951	-1.3951
8.333333	-0.00110009	-1.10009
8.75	-0.00077121	-0.77121
9.166667	-0.00051839	-0.51839
9.583333	-0.00036542	-0.36542
10	-0.00031463	-0.31463

Geogrid stress (MPa)	
x	y
0	1.23908
0.416667	1.186955
0.833333	1.09794
1.25	1.237485
1.666667	1.300635
2.083333	0.45143
2.5	0.637615
2.916667	4.81191
3.333333	15.367775
3.75	30.402155
4.0625	36.87627
4.375	35.25335
4.6875	33.838985
5	33.719375
5.3125	33.970155
5.625	34.934475
5.9375	36.003505
6.25	30.53972
6.666667	16.98624
7.083333	5.41195
7.5	0.6488
7.916667	0.465615
8.333333	1.32328
8.75	1.251525
9.166667	1.1112
9.583333	1.198235
10	1.249825

Rail deflection (mm)		
x	y (m)	1000
0	0.00021864	0.22099
0.275	0.0002189	0.22152
0.65	0.00022019	0.22425
0.925	0.00021999	0.22586
1.3	0.0002216	0.23085
1.575	0.00021959	0.23198
1.95	0.00021857	0.236
2.225	0.00021201	0.23358
2.6	0.00020353	0.23125
2.875	0.00018835	0.22063
3.25	0.00016559	0.20425
3.525	0.0001364	0.17919
3.9	0.00009053	0.13863
4.175	0.00004072	0.09129
4.55	-0.00003897	0.01404
4.825	-0.00011699	-0.06474
5.2	-0.00024264	-0.19317
5.475	-0.00035682	-0.31324
5.85	-0.00054106	-0.50823
6.125	-0.00069869	-0.67898
6.5	-0.00095288	-0.95481
6.775	-0.00115879	-1.18298
7.15	-0.00149001	-1.54909
7.425	-0.00174337	-1.83476
7.8	-0.00214825	-2.28821
8.075	-0.00243669	-2.61754
8.45	-0.00288992	-3.1287
8.725	-0.00318343	-3.46478
9.1	-0.00362633	-3.95992
9.375	-0.00386868	-4.22928
9.75	-0.0041275	-4.50458
10.025	-0.00399422	-4.36292
10.4	-0.0036115	-3.94276
10.675	-0.00332993	-3.6236
11.05	-0.00286279	-3.09769
11.325	-0.00256073	-2.75178
11.7	-0.00211745	-2.25323
11.975	-0.0018385	-1.93651
12.35	-0.00146142	-1.51666
12.625	-0.00122662	-1.25391
13	-0.00092843	-0.92687
13.275	-0.00074368	-0.72403
13.65	-0.00052177	-0.48553
13.925	-0.0003848	-0.33878
14.3	-0.00022973	-0.17663
14.575	-0.00013441	-0.07778
14.95	-0.00003419	0.02292
15.225	0.00002706	0.08349
15.6	0.00008468	0.13753
15.875	0.00011954	0.1692
16.25	0.00014575	0.1898
16.525	0.00016116	0.20087
16.9	0.00016544	0.19895
17.175	0.00016731	0.19626
17.55	0.00015726	0.18038
17.825	0.00015036	0.16929
18.2	0.00013185	0.14587
18.475	0.00011991	0.13045
18.85	0.00009739	0.10418
19.125	0.00008338	0.08755
19.5	0.00006027	0.06196
19.775	0.00004651	0.04658
20.15	0.00002528	0.02446
20.425	0.0000132	0.01226
20.8	0	0

Formation deflection (mm)		
x	y (m)	1000
0	0.00014117	0.14117
0.275	0.00014234	0.14234
0.65	0.00014505	0.14505
0.925	0.00014784	0.14784
1.3	0.0001524	0.1524
1.575	0.00015608	0.15608
1.95	0.00016076	0.16076
2.225	0.00016345	0.16345
2.6	0.00016491	0.16491
2.875	0.00016361	0.16361
3.25	0.00015697	0.15697
3.525	0.00014752	0.14752
3.9	0.0001263	0.1263
4.175	0.00010331	0.10331
4.55	0.00005942	0.05942
4.825	0.00001644	0.01644
5.2	-0.00005941	-0.05941
5.475	-0.00012942	-0.12942
5.85	-0.00024675	-0.24675
6.125	-0.0003504	-0.3504
6.5	-0.0005171	-0.5171
6.775	-0.00065892	-0.65892
7.15	-0.00087885	-0.87885
7.425	-0.00105945	-1.05945
7.8	-0.00132844	-1.32844
8.075	-0.00153786	-1.53786
8.45	-0.00182274	-1.82274
8.725	-0.00201523	-2.01523
9.1	-0.00222486	-2.22486
9.375	-0.002323	-2.323
9.75	-0.00236969	-2.36969
10.025	-0.00233927	-2.33927
10.4	-0.00221777	-2.21777
10.675	-0.00206852	-2.06852
11.05	-0.00181152	-1.81152
11.325	-0.00160157	-1.60157
11.7	-0.00131415	-1.31415
11.975	-0.00111348	-1.11348
12.35	-0.00086298	-0.86298
12.625	-0.00069805	-0.69805
13	-0.0005005	-0.5005
13.275	-0.00037532	-0.37532
13.65	-0.00023096	-0.23096
13.925	-0.0001431	-0.1431
14.3	-0.00004602	-0.04602
14.575	0.00001019	0.01019
14.95	0.00006884	0.06884
15.225	0.0001003	0.1003
15.6	0.00012992	0.12992
15.875	0.00014331	0.14331
16.25	0.00015242	0.15242
16.525	0.00015351	0.15351
16.9	0.00014915	0.14915
17.175	0.00014249	0.14249
17.55	0.00013012	0.13012
17.825	0.00011919	0.11919
18.2	0.00010285	0.10285
18.475	0.00009023	0.09023
18.85	0.00007303	0.07303
19.125	0.00006081	0.06081
19.5	0.00004564	0.04564
19.775	0.00003617	0.03617
20.15	0.00002654	0.02654
20.425	0.00002195	0.02195
20.8	0.00001932	0.01932

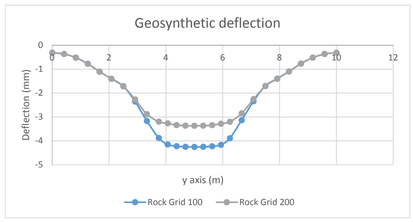

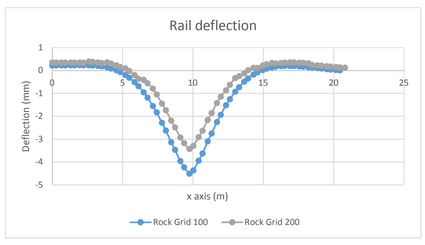

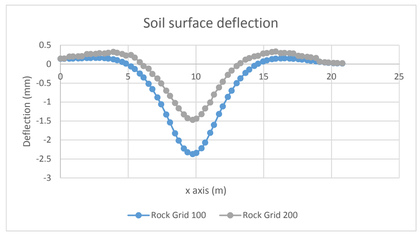

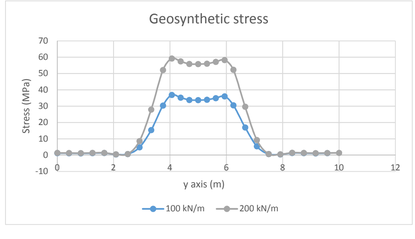

Tensile modulus = 200 kN/m

Geogrid deflection (mm)		
x	y (m)	1000
0	-0.000317138	-0.317138
0.416667	-0.000368343	-0.368343
0.833333	-0.0005226	-0.5226
1.25	-0.0007776 59	-0.777659
1.666667	-0.00110958	-1.10958
2.083333	-0.001407794	-1.407794
2.5	-0.001721454	-1.721454
2.916667	-0.002268888	-2.268888
3.333333	-0.002884239	-2.884239
3.75	-0.003196051	-3.196051
4.0625	-0.003269737	-3.269737
4.375	-0.003338479	-3.338479
4.6875	-0.003362579	-3.362579
5	-0.003371212	-3.371212
5.3125	-0.003366941	-3.366941
5.625	-0.003344871	-3.344871
5.9375	-0.003281546	-3.281546
6.25	-0.003204292	-3.204292
6.666667	-0.002851185	-2.851185
7.083333	-0.002255883	-2.255883
7.5	-0.001713997	-1.713997
7.916667	-0.001402076	-1.402076
8.333333	-0.00110559	-1.10559
8.75	-0.000775066	-0.775066
9.166667	-0.000520982	-0.520982
9.583333	-0.000367247	-0.367247
10	-0.000316203	-0.316203

Geogrid stress (MPa)	
x	y
0	1.362988
0.416667	1.3056505
0.833333	1.207734
1.25	1.1612335
1.666667	1.4306985
2.083333	0.496573
2.5	0.7013765
2.916667	8.593101
3.333333	27.9045525
3.75	52.1423705
4.0625	59.263897
4.375	57.478685
4.6875	55.9228835
5	55.7913125
5.3125	56.0671705
5.625	57.1279225
5.9375	58.3038555
6.25	52.293692
6.666667	29.684864
7.083333	9.253145
7.5	0.71368
7.916667	0.5121765
8.333333	1.455608
8.75	1.3766775
9.166667	1.222232
9.583333	1.3180585
10	1.3748075

Rail deflection (mm)		
x	y (m)	1000
0	0.00034864	0.34864
0.275	0.0003489	0.3489
0.65	0.00035019	0.35019
0.925	0.00034999	0.34999
1.3	0.0003516	0.3516
1.575	0.00034959	0.34959
1.95	0.00034857	0.34857
2.225	0.00034201	0.34201
2.6	0.00039353	0.39353
2.875	0.00037835	0.37835
3.25	0.00035559	0.35559
3.525	0.0003264	0.3264
3.9	0.00036053	0.36053
4.175	0.00031072	0.31072
4.55	0.00023103	0.23103
4.825	0.00015301	0.15301
5.2	0.00009736	0.09736
5.475	-0.00001682	-0.01682
5.85	-0.00020106	-0.20106
6.125	-0.00035869	-0.35869
6.5	-0.00040288	-0.40288
6.775	-0.00055879	-0.55879
7.15	-0.00079001	-0.79001
7.425	-0.00104337	-1.04337
7.8	-0.00144825	-1.44825
8.075	-0.00173669	-1.73669
8.45	-0.00218992	-2.18992
8.725	-0.00248343	-2.48343
9.1	-0.00292633	-2.92633
9.375	-0.00316868	-3.16868
9.75	-0.0034275	-3.4275
10.025	-0.00329422	-3.29422
10.4	-0.0029115	-2.9115
10.675	-0.00262993	-2.62993
11.05	-0.00216279	-2.16279
11.325	-0.00186073	-1.86073
11.7	-0.00141745	-1.41745
11.975	-0.0011385	-1.1385
12.35	-0.00086142	-0.86142
12.625	-0.00062662	-0.62662
13	-0.00032843	-0.32843
13.275	-0.00024368	-0.24368
13.65	-0.00012177	-0.12177
13.925	0.0000152	0.0152
14.3	0.00012027	0.12027
14.575	0.00011559	0.11559
14.95	0.00021581	0.21581
15.225	0.00027706	0.27706
15.6	0.00033468	0.33468
15.875	0.00030954	0.30954
16.25	0.00033575	0.33575
16.525	0.00035116	0.35116
16.9	0.00035544	0.35544
17.175	0.00035731	0.35731
17.55	0.00034726	0.34726
17.825	0.00034036	0.34036
18.2	0.00032185	0.32185
18.475	0.00024991	0.24991
18.85	0.00022739	0.22739
19.125	0.00021338	0.21338
19.5	0.00019027	0.19027
19.775	0.00017651	0.17651
20.15	0.00015528	0.15528
20.425	0.0001432	0.1432
20.8	0.00013	0.13

Formation deflection (mm)		
x	y (m)	1000
0	0.00014617	0.14617
0.275	0.00014734	0.14734
0.65	0.00020005	0.20005
0.925	0.00020284	0.20284
1.3	0.0002074	0.2074
1.575	0.00021108	0.21108
1.95	0.00026576	0.26576
2.225	0.00026845	0.26845
2.6	0.00026991	0.26991
2.875	0.00028761	0.28761
3.25	0.00028097	0.28097
3.525	0.00029952	0.29952
3.9	0.0003213	0.3213
4.175	0.00029731	0.29731
4.55	0.00026842	0.26842
4.825	0.00022624	0.22624
5.2	0.00023959	0.23959
5.475	0.00017058	0.17058
5.85	0.00005325	0.05325
6.125	-0.0000504	-0.0504
6.5	-0.0001171	-0.1171
6.775	-0.00025892	-0.25892
7.15	-0.00037885	-0.37885
7.425	-0.00050945	-0.50945
7.8	-0.00069844	-0.69844
8.075	-0.00083786	-0.83786
8.45	-0.00102274	-1.02274
8.725	-0.00116523	-1.16523
9.1	-0.00132486	-1.32486
9.375	-0.001423	-1.423
9.75	-0.00146969	-1.46969
10.025	-0.00143927	-1.43927
10.4	-0.00131777	-1.31777
10.675	-0.00116852	-1.16852
11.05	-0.00101152	-1.01152
11.325	-0.00080157	-0.80157
11.7	-0.00061415	-0.61415
11.975	-0.00046348	-0.46348
12.35	-0.00028298	-0.28298
12.625	-0.00016805	-0.16805
13	-5.05E-05	-0.0505
13.275	0.00002468	0.02468
13.65	0.00011904	0.11904
13.925	0.0001569	0.1569
14.3	0.00020398	0.20398
14.575	0.00022019	0.22019
14.95	0.00027884	0.27884
15.225	0.0002903	0.2903
15.6	0.00031992	0.31992
15.875	0.00033331	0.33331
16.25	0.00029242	0.29242
16.525	0.00029351	0.29351
16.9	0.00028915	0.28915
17.175	0.00028249	0.28249
17.55	0.00022012	0.22012
17.825	0.00020919	0.20919
18.2	0.00019285	0.19285
18.475	0.00018023	0.18023
18.85	0.00016303	0.16303
19.125	0.00006581	0.06581
19.5	0.00005064	0.05064
19.775	0.00004117	0.04117
20.15	0.00003154	0.03154
20.425	0.00002695	0.02695
20.8	0.00002432	0.02432

Youngs modulus		
Geogrid deflection (mm)		
E = 160 MPa		1000
x	y (m)	y (mm)
0	-0.00031556	-0.31556
0.41666667	-0.00036651	-0.36651
0.83333333	-0.00052	-0.52
1.25	-0.00077379	-0.77379
1.66666667	-0.00110406	-1.10406
2.08333333	-0.00140079	-1.40079
2.5	-0.00171289	-1.71289
2.91666667	-0.0023576	-2.3576
3.33333333	-0.00316989	-3.16989
3.75	-0.00388015	-3.88015
4.0625	-0.00415347	-4.15347
4.375	-0.00422187	-4.22187
4.6875	-0.00424585	-4.24585
5	-0.00425444	-4.25444
5.3125	-0.00425019	-4.25019
5.625	-0.00422823	-4.22823
5.9375	-0.00416522	-4.16522
6.25	-0.00388835	-3.88835
6.66666667	-0.003137	-3.137
7.08333333	-0.00234466	-2.34466
7.5	-0.00170547	-1.70547
7.91666667	-0.0013951	-1.3951
8.33333333	-0.00110009	-1.10009
8.75	-0.00077121	-0.77121
9.16666667	-0.00051839	-0.51839
9.58333333	-0.00036542	-0.36542
10	-0.00031463	-0.31463

Geogrid deflection (mm)		
E = 200 MPa		1000
x	y (m)	y (mm)
0	-0.00035351	-0.3535063
0.41666667	-0.00040382	-0.4038218
0.83333333	-0.00055406	-0.5540576
1.25	-0.00079749	-0.7974878
1.66666667	-0.0011052	-1.1052003
2.08333333	-0.00139441	-1.394414
2.5	-0.00171192	-1.7119218
2.91666667	-0.00230491	-2.3049134
3.33333333	-0.00303896	-3.0389635
3.75	-0.00368108	-3.6810758
4.0625	-0.00392774	-3.9277402
4.375	-0.00399468	-3.9946799
4.6875	-0.00401575	-4.0157537
5	-0.00402351	-4.0235096
5.3125	-0.00402028	-4.0202754
5.625	-0.0040012	-4.0011998
5.9375	-0.00393861	-3.9386067
6.25	-0.00369975	-3.6997497
6.66666667	-0.00302199	-3.0219891
7.08333333	-0.00229475	-2.2947473
7.5	-0.00170576	-1.7057624
7.91666667	-0.00138982	-1.3898202
8.33333333	-0.00110205	-1.1020485
8.75	-0.00079542	-0.7954175
9.16666667	-0.00055275	-0.5527495
9.58333333	-0.00040294	-0.402936
10	-0.00035275	-0.3527544

Geogrid deflection (mm)		
E = 100 MPa		1000
x	y (m)	y (mm)
0	-0.00031674	-0.31674
0.41666667	-0.00036705	-0.36705
0.83333333	-0.00051864	-0.51864
1.25	-0.00076939	-0.76939
1.66666667	-0.00109633	-1.09633
2.08333333	-0.00138973	-1.38973
2.5	-0.0016887	-1.7287
2.91666667	-0.00236675	-2.40675
3.33333333	-0.00332674	-3.36674
3.75	-0.00419959	-4.27959
4.0625	-0.00454654	-4.62654
4.375	-0.00463029	-4.71029
4.6875	-0.00465245	-4.73245
5	-0.0046599	-4.7399
5.3125	-0.00465755	-4.73755
5.625	-0.0046373	-4.7173
5.9375	-0.00455737	-4.63737
6.25	-0.00421424	-4.27424
6.66666667	-0.00328739	-3.32739
7.08333333	-0.00235088	-2.39088
7.5	-0.00167956	-1.71956
7.91666667	-0.00138274	-1.38274
8.33333333	-0.00109146	-1.09146
8.75	-0.0007662	-0.7662
9.16666667	-0.00051664	-0.51664
9.58333333	-0.0003657	-0.3657
10	-0.0003156	-0.3156

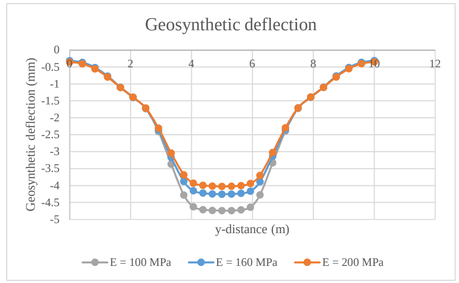

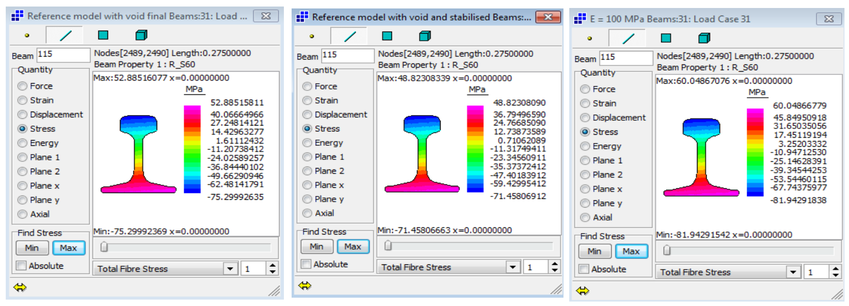

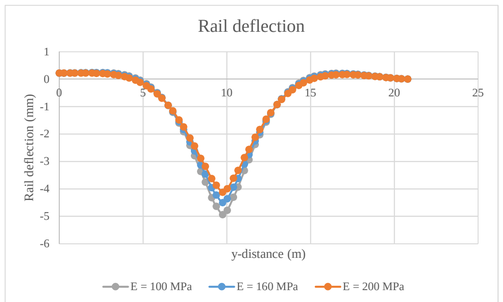

Rail deflection (mm)		
E = 160		1000
x	y (m)	y (mm)
0	0.00021864	0.22099
0.275	0.0002189	0.22152
0.65	0.00022019	0.22425
0.925	0.00021999	0.22586
1.3	0.0002216	0.23085
1.575	0.00021959	0.23198
1.95	0.00021857	0.236
2.225	0.00021201	0.23358
2.6	0.00020353	0.23125
2.875	0.00018835	0.22063
3.25	0.00016559	0.20425
3.525	0.0001364	0.17919
3.9	0.00009053	0.13863
4.175	0.00004072	0.09129
4.55	-0.00003897	0.01404
4.825	-0.00011699	-0.06474
5.2	-0.00024264	-0.19317
5.475	-0.00035682	-0.31324
5.85	-0.00054106	-0.50823
6.125	-0.00069869	-0.67898
6.5	-0.00095288	-0.95481
6.775	-0.00115879	-1.18298
7.15	-0.00149001	-1.54909
7.425	-0.00174337	-1.83476
7.8	-0.00214825	-2.28821
8.075	-0.00243669	-2.61754
8.45	-0.00288992	-3.1287
8.725	-0.00318343	-3.46478
9.1	-0.00362633	-3.95992
9.375	-0.00386868	-4.22928
9.75	-0.0041275	-4.50458
10.025	-0.00399422	-4.36292
10.4	-0.0036115	-3.94276
10.675	-0.00332993	-3.6236
11.05	-0.00286279	-3.09769
11.325	-0.00256073	-2.75178
11.7	-0.00211745	-2.25323
11.975	-0.0018385	-1.93651
12.35	-0.00146142	-1.51666
12.625	-0.00122662	-1.25391
13	-0.00092843	-0.92687
13.275	-0.00074368	-0.72403
13.65	-0.00052177	-0.48553
13.925	-0.0003848	-0.33878
14.3	-0.00022973	-0.17663
14.575	-0.00013441	-0.07778
14.95	-0.00003419	0.02292
15.225	0.00002706	0.08349
15.6	0.00008468	0.13753
15.875	0.00011954	0.1692
16.25	0.00014575	0.1898
16.525	0.00016116	0.20087
16.9	0.00016544	0.19895
17.175	0.00016731	0.19626
17.55	0.00015726	0.18038
17.825	0.00015036	0.16929
18.2	0.00013185	0.14587
18.475	0.00011991	0.13045
18.85	0.00009739	0.10418
19.125	0.00008338	0.08755
19.5	0.00006027	0.06196
19.775	0.00004651	0.04658
20.15	0.00002528	0.02446
20.425	0.0000132	0.01226
20.8	0	0

Rail deflection (mm)		
E = 200		1000
x	y (m)	y (mm)
0	0.00022099	0.21864
0.275	0.00022152	0.2189
0.65	0.00022425	0.22019
0.925	0.00022586	0.21999
1.3	0.00023085	0.2216
1.575	0.00023198	0.21959
1.95	0.000236	0.21857
2.225	0.00023358	0.21201
2.6	0.00023125	0.20353
2.875	0.00022063	0.18835
3.25	0.00020425	0.16559
3.525	0.00017919	0.1364
3.9	0.00013863	0.09053
4.175	0.00009129	0.04072
4.55	0.00001404	-0.03897
4.825	-0.00006474	-0.11699
5.2	-0.00019317	-0.24264
5.475	-0.00031324	-0.35682
5.85	-0.00050823	-0.54106
6.125	-0.00067898	-0.69869
6.5	-0.00095481	-0.95288
6.775	-0.00118298	-1.15879
7.15	-0.00154909	-1.49001
7.425	-0.00183476	-1.74337
7.8	-0.00228821	-2.14825
8.075	-0.00261754	-2.43669
8.45	-0.0031287	-2.88992
8.725	-0.00346478	-3.18343
9.1	-0.00395992	-3.62633
9.375	-0.00422928	-3.86868
9.75	-0.00450458	-4.1275
10.025	-0.00436292	-3.99422
10.4	-0.00394276	-3.6115
10.675	-0.0036236	-3.32993
11.05	-0.00309769	-2.86279
11.325	-0.00275178	-2.56073
11.7	-0.00225323	-2.11745
11.975	-0.00193651	-1.8385
12.35	-0.00151666	-1.46142
12.625	-0.00125391	-1.22662
13	-0.00092687	-0.92843
13.275	-0.00072403	-0.74368
13.65	-0.00048553	-0.52177
13.925	-0.00033878	-0.3848
14.3	-0.00017663	-0.22973
14.575	-0.00007778	-0.13441
14.95	0.00002292	-0.03419
15.225	0.00008349	0.02706
15.6	0.00013753	0.08468
15.875	0.0001692	0.11954
16.25	0.0001898	0.14575
16.525	0.00020087	0.16116
16.9	0.00019895	0.16544
17.175	0.00019626	0.16731
17.55	0.00018038	0.15726
17.825	0.00016929	0.15036
18.2	0.00014587	0.13185
18.475	0.00013045	0.11991
18.85	0.00010418	0.09739
19.125	0.00008755	0.08338
19.5	0.00006196	0.06027
19.775	0.00004658	0.04651
20.15	0.00002446	0.02528
20.425	0.00001226	0.0132
20.8	0	0

Rail deflection (mm)		
E = 100		1000
x	y (m)	y (mm)
0	0.00021468	0.21468
0.275	0.00021529	0.21529
0.65	0.00021867	0.21867
0.925	0.00022116	0.22116
1.3	0.00022778	0.22778
1.575	0.00023054	0.23054
1.95	0.00023715	0.23715
2.225	0.00023704	0.23704
2.6	0.00023815	0.23815
2.875	0.00023038	0.23038
3.25	0.000218	0.218
3.525	0.00019595	0.19595
3.9	0.00015929	0.15929
4.175	0.00011445	0.11445
4.55	0.0000398	0.0398
4.825	-0.00003812	-0.03812
5.2	-0.00016711	-0.16711
5.475	-0.00028968	-0.28968
5.85	-0.00049116	-0.49116
6.125	-0.00067009	-0.67009
6.5	-0.00096203	-0.96203
6.775	-0.00120704	-1.20704
7.15	-0.0016033	-1.6033
7.425	-0.00191757	-1.91757
7.8	-0.00241921	-2.41921
8.075	-0.00279064	-2.79064
8.45	-0.0033681	-3.3681
8.725	-0.00375711	-3.75711
9.1	-0.00432396	-4.32396
9.375	-0.00463851	-4.63851
9.75	-0.00494073	-4.94073
10.025	-0.00478131	-4.78131
10.4	-0.00430449	-4.30449
10.675	-0.00393211	-3.93211
11.05	-0.00333325	-3.33325
11.325	-0.00293805	-2.93805
11.7	-0.0023806	-2.3806
11.975	-0.00202784	-2.02784
12.35	-0.00156842	-1.56842
12.625	-0.00128284	-1.28284
13	-0.00093274	-0.93274
13.275	-0.00071744	-0.71744
13.65	-0.00046779	-0.46779
13.925	-0.00031573	-0.31573
14.3	-0.00015012	-0.15012
14.575	-0.00005038	-0.05038
14.95	0.00004941	0.04941
15.225	0.0001085	0.1085
15.6	0.00015962	0.15962
15.875	0.00018888	0.18888
16.25	0.00020608	0.20608
16.525	0.0002147	0.2147
16.9	0.00020978	0.20978
17.175	0.00020504	0.20504
17.55	0.00018693	0.18693
17.825	0.00017436	0.17436
18.2	0.0001495	0.1495
18.475	0.00013312	0.13312
18.85	0.00010603	0.10603
19.125	0.00008875	0.08875
19.5	0.00006263	0.06263
19.775	0.00004665	0.04665
20.15	0.00002411	0.02411
20.425	0.00001164	0.01164
20.8	0	0

Geogrid stress (MPa)	
E = 160	
x	y (MPa)
0	1.23908
0.41666667	1.186955
0.83333333	1.09794
1.25	1.237485
1.66666667	1.300635
2.08333333	0.45143
2.5	0.637615
2.91666667	4.81191
3.33333333	15.367775
3.75	30.402155
4.0625	36.87627
4.375	35.25335
4.6875	33.838985
5	33.719375
5.3125	33.970155
5.625	34.934475
5.9375	36.003505
6.25	30.53972
6.66666667	16.98624
7.08333333	5.41195
7.5	0.6488
7.91666667	0.465615
8.33333333	1.32328
8.75	1.251525
9.16666667	1.1112
9.58333333	1.198235
10	1.249825

Geogrid stress (MPa)	
E = 200	
x	y (MPa)
0	0.22784
0.41666667	0.17616
0.83333333	0.08764
1.25	0.22453
1.66666667	0.27847
2.08333333	-0.586295
2.5	-0.43193
2.91666667	3.64133
3.33333333	13.766945
3.75	28.006365
4.0625	34.033885
4.375	32.33043
4.6875	30.909095
5	30.7855
5.3125	31.033315
5.625	32.042985
5.9375	33.206715
6.25	28.17811
6.66666667	15.3532
7.08333333	4.19995
7.5	-0.41257
7.91666667	-0.56826
8.33333333	0.30192
8.75	0.23928
9.16666667	0.10146
9.58333333	0.18796
10	0.2391

Geogrid stress (MPa)	
E = 100	
x	y (MPa)
0	3.20363
0.41666667	3.067685
0.83333333	2.628875
1.25	2.12186
1.66666667	1.570935
2.08333333	0.66738
2.5	0.787295
2.91666667	4.338745
3.33333333	16.65188
3.75	36.59748
4.0625	45.91917
4.375	44.013
4.6875	42.00659
5	41.79888
5.3125	42.154575
5.625	43.711815
5.9375	44.156415
6.25	35.082255
6.66666667	18.38298
7.08333333	5.79185
7.5	0.88204
7.91666667	0.691415
8.33333333	1.598315
8.75	2.134745
9.16666667	2.639565
9.58333333	3.074395
10	3.20948

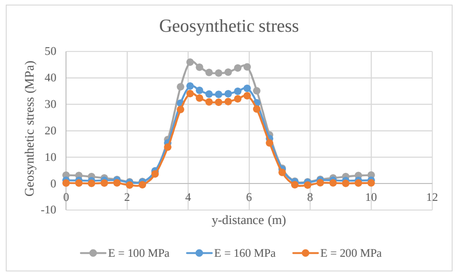

Earth pressure coeficient								
Geogrid deflection (mm)			Geogrid deflection (mm)			Geogrid deflection (mm)		
K = 0.357		1000	K = 0.5		1000	K = 1		1000
x	y (m)	y (mm)	x	y (m)	y (mm)	x	y (m)	y (mm)
0	-0.00031556	-0.31556	0	-0.00031556	-0.31556	0	-0.00031556	-0.31556
0.41666667	-0.00036651	-0.36651	0.41666667	-0.00036651	-0.36651	0.41666667	-0.00036651	-0.36651
0.83333333	-0.00052	-0.52	0.83333333	-0.00052	-0.52	0.83333333	-0.00052	-0.52
1.25	-0.00077379	-0.77379	1.25	-0.00077379	-0.77379	1.25	-0.00077379	-0.77379
1.66666667	-0.00110406	-1.10406	1.66666667	-0.00110406	-1.10406	1.66666667	-0.00110406	-1.10406
2.08333333	-0.00140079	-1.40079	2.08333333	-0.00140079	-1.40079	2.08333333	-0.00140079	-1.40079
2.5	-0.00171289	-1.71289	2.5	-0.00171289	-1.71289	2.5	-0.00171289	-1.71289
2.91666667	-0.0023576	-2.3576	2.91666667	-0.0023576	-2.3576	2.91666667	-0.0023576	-2.3576
3.33333333	-0.00316989	-3.16989	3.33333333	-0.00316989	-3.16989	3.33333333	-0.00316989	-3.16989
3.75	-0.00388015	-3.88015	3.75	-0.00388015	-3.88015	3.75	-0.00388015	-3.88015
4.0625	-0.00415347	-4.15347	4.0625	-0.00415347	-4.15347	4.0625	-0.00415347	-4.15347
4.375	-0.00422187	-4.22187	4.375	-0.00422187	-4.22187	4.375	-0.00422187	-4.22187
4.6875	-0.00424585	-4.24585	4.6875	-0.00424585	-4.24585	4.6875	-0.00424585	-4.24585
5	-0.00425444	-4.25444	5	-0.00425444	-4.25444	5	-0.00425444	-4.25444
5.3125	-0.00425019	-4.25019	5.3125	-0.00425019	-4.25019	5.3125	-0.00425019	-4.25019
5.625	-0.00422823	-4.22823	5.625	-0.00422823	-4.22823	5.625	-0.00422823	-4.22823
5.9375	-0.00416522	-4.16522	5.9375	-0.00416522	-4.16522	5.9375	-0.00416522	-4.16522
6.25	-0.00388835	-3.88835	6.25	-0.00388835	-3.88835	6.25	-0.00388835	-3.88835
6.66666667	-0.003137	-3.137	6.66666667	-0.003137	-3.137	6.66666667	-0.003137	-3.137
7.08333333	-0.00234466	-2.34466	7.08333333	-0.00234466	-2.34466	7.08333333	-0.00234466	-2.34466
7.5	-0.00170547	-1.70547	7.5	-0.00170547	-1.70547	7.5	-0.00170547	-1.70547
7.91666667	-0.0013951	-1.3951	7.91666667	-0.0013951	-1.3951	7.91666667	-0.0013951	-1.3951
8.33333333	-0.00110009	-1.10009	8.33333333	-0.00110009	-1.10009	8.33333333	-0.00110009	-1.10009
8.75	-0.00077121	-0.77121	8.75	-0.00077121	-0.77121	8.75	-0.00077121	-0.77121
9.16666667	-0.00051839	-0.51839	9.16666667	-0.00051839	-0.51839	9.16666667	-0.00051839	-0.51839
9.58333333	-0.00036542	-0.36542	9.58333333	-0.00036542	-0.36542	9.58333333	-0.00036542	-0.36542
10	-0.00031463	-0.31463	10	-0.00031463	-0.31463	10	-0.00031463	-0.31463

Soil surface deflection (mm)			Soil surface deflection (mm)			Soil surface deflection (mm)		
K = 0.357		1000	K = 0.5		1000	K = 1		1000
x	y (m)	y (mm)	x	y (m)	y (mm)	x	y (m)	y (mm)
0	0.00014117	0.14117	0	0.00014117	0.14117	0	0.00014117	0.14117
0.1	0.00013758	0.13758	0.1	0.00013758	0.13758	0.1	0.00013758	0.13758
0.27499682	0.00014273	0.14273	0.27499682	0.00014273	0.14273	0.27499682	0.00014273	0.14273
0.64999249	0.00014553	0.14553	0.64999249	0.00014553	0.14553	0.64999249	0.00014553	0.14553
0.92498931	0.00014809	0.14809	0.92498931	0.00014809	0.14809	0.92498931	0.00014809	0.14809
1.29998498	0.00015265	0.15265	1.29998498	0.00015265	0.15265	1.29998498	0.00015265	0.15265
1.5749818	0.00015611	0.15611	1.5749818	0.00015611	0.15611	1.5749818	0.00015611	0.15611
1.94997746	0.00016072	0.16072	1.94997746	0.00016072	0.16072	1.94997746	0.00016072	0.16072
2.22497429	0.00016308	0.16308	2.22497429	0.00016308	0.16308	2.22497429	0.00016308	0.16308
2.59996995	0.00016456	0.16456	2.59996995	0.00016456	0.16456	2.59996995	0.00016456	0.16456
2.87496677	0.00016263	0.16263	2.87496677	0.00016263	0.16263	2.87496677	0.00016263	0.16263
3.24996244	0.00015632	0.15632	3.24996244	0.00015632	0.15632	3.24996244	0.00015632	0.15632
3.52495926	0.0001457	0.1457	3.52495926	0.0001457	0.1457	3.52495926	0.0001457	0.1457
3.89995493	0.00012538	0.12538	3.89995493	0.00012538	0.12538	3.89995493	0.00012538	0.12538
4.17495175	0.00010042	0.10042	4.17495175	0.00010042	0.10042	4.17495175	0.00010042	0.10042
4.55	0.00005495	0.05495	4.55	0.00005495	0.05495	4.55	0.00005495	0.05495
4.825	0.0000033	0.0033	4.825	0.0000033	0.0033	4.825	0.0000033	0.0033
5.2	-0.00007058	-0.07058	5.2	-0.00007058	-0.07058	5.2	-0.00007058	-0.07058
5.475	-0.00015505	-0.15505	5.475	-0.00015505	-0.15505	5.475	-0.00015505	-0.15505
5.85	-0.00026597	-0.26597	5.85	-0.00026597	-0.26597	5.85	-0.00026597	-0.26597
6.125	-0.00038995	-0.38995	6.125	-0.00038995	-0.38995	6.125	-0.00038995	-0.38995
6.5	-0.000547	-0.547	6.5	-0.000547	-0.547	6.5	-0.000547	-0.547
6.775	-0.00071564	-0.71564	6.775	-0.00071564	-0.71564	6.775	-0.00071564	-0.71564
7.15	-0.00092246	-0.92246	7.15	-0.00092246	-0.92246	7.15	-0.00092246	-0.92246
7.425	-0.0011359	-1.1359	7.425	-0.0011359	-1.1359	7.425	-0.0011359	-1.1359
7.8	-0.00138829	-1.38829	7.8	-0.00138829	-1.38829	7.8	-0.00138829	-1.38829
8.075	-0.00163352	-1.63352	8.075	-0.00163352	-1.63352	8.075	-0.00163352	-1.63352
8.45	-0.00190182	-1.90182	8.45	-0.00190182	-1.90182	8.45	-0.00190182	-1.90182
8.725	-0.00212788	-2.12788	8.725	-0.00212788	-2.12788	8.725	-0.00212788	-2.12788
9.1	-0.002333	-2.333	9.1	-0.002333	-2.333	9.1	-0.002333	-2.333
9.375	-0.00245281	-2.45281	9.375	-0.00245281	-2.45281	9.375	-0.00245281	-2.45281
9.75	-0.00250649	-2.50649	9.75	-0.00250649	-2.50649	9.75	-0.00250649	-2.50649
10.025	-0.00246495	-2.46495	10.025	-0.00246495	-2.46495	10.025	-0.00246495	-2.46495
10.4	-0.0023513	-2.3513	10.4	-0.0023513	-2.3513	10.4	-0.0023513	-2.3513
10.675	-0.00216159	-2.16159	10.675	-0.00216159	-2.16159	10.675	-0.00216159	-2.16159
11.05	-0.00193049	-1.93049	11.05	-0.00193049	-1.93049	11.05	-0.00193049	-1.93049
11.325	-0.00167264	-1.67264	11.325	-0.00167264	-1.67264	11.325	-0.00167264	-1.67264
11.7	-0.0014129	-1.4129	11.7	-0.0014129	-1.4129	11.7	-0.0014129	-1.4129
11.975	-0.00116433	-1.16433	11.975	-0.00116433	-1.16433	11.975	-0.00116433	-1.16433
12.35	-0.00093293	-0.93293	12.35	-0.00093293	-0.93293	12.35	-0.00093293	-0.93293
12.625	-0.00073408	-0.73408	12.625	-0.00073408	-0.73408	12.625	-0.00073408	-0.73408
13	-0.00055091	-0.55091	13	-0.00055091	-0.55091	13	-0.00055091	-0.55091
13.275	-0.00039978	-0.39978	13.275	-0.00039978	-0.39978	13.275	-0.00039978	-0.39978
13.65	-0.00026529	-0.26529	13.65	-0.00026529	-0.26529	13.65	-0.00026529	-0.26529
13.925	-0.00015881	-0.15881	13.925	-0.00015881	-0.15881	13.925	-0.00015881	-0.15881
14.3	-0.0000677	-0.0677	14.3	-0.0000677	-0.0677	14.3	-0.0000677	-0.0677
14.575	0.00000092	0.00092	14.575	0.00000092	0.00092	14.575	0.00000092	0.00092
14.95	0.00005663	0.05663	14.95	0.00005663	0.05663	14.95	0.00005663	0.05663
15.225	0.00009557	0.09557	15.225	0.00009557	0.09557	15.225	0.00009557	0.09557
15.6	0.00012441	0.12441	15.6	0.00012441	0.12441	15.6	0.00012441	0.12441
15.875	0.00014158	0.14158	15.875	0.00014158	0.14158	15.875	0.00014158	0.14158
16.25	0.00015276	0.15276	16.25	0.00015276	0.15276	16.25	0.00015276	0.15276
16.525	0.00015327	0.15327	16.525	0.00015327	0.15327	16.525	0.00015327	0.15327
16.9	0.00014934	0.14934	16.9	0.00014934	0.14934	16.9	0.00014934	0.14934
17.175	0.00014281	0.14281	17.175	0.00014281	0.14281	17.175	0.00014281	0.14281
17.55	0.00013081	0.13081	17.55	0.00013081	0.13081	17.55	0.00013081	0.13081
17.825	0.00011967	0.11967	17.825	0.00011967	0.11967	17.825	0.00011967	0.11967
18.2	0.00010366	0.10366	18.2	0.00010366	0.10366	18.2	0.00010366	0.10366
18.475	0.00009062	0.09062	18.475	0.00009062	0.09062	18.475	0.00009062	0.09062
18.85	0.00007368	0.07368	18.85	0.00007368	0.07368	18.85	0.00007368	0.07368
19.125	0.00006097	0.06097	19.125	0.00006097	0.06097	19.125	0.00006097	0.06097
19.5	0.0000463	0.0463	19.5	0.0000463	0.0463	19.5	0.0000463	0.0463
19.775	0.00003609	0.03609	19.775	0.00003609	0.03609	19.775	0.00003609	0.03609
20.15	0.0000265	0.0265	20.15	0.0000265	0.0265	20.15	0.0000265	0.0265
20.425	0.00002162	0.02162	20.425	0.00002162	0.02162	20.425	0.00002162	0.02162
20.8	0.00001936	0.01936	20.8	0.00001936	0.01936	20.8	0.00001936	0.01936

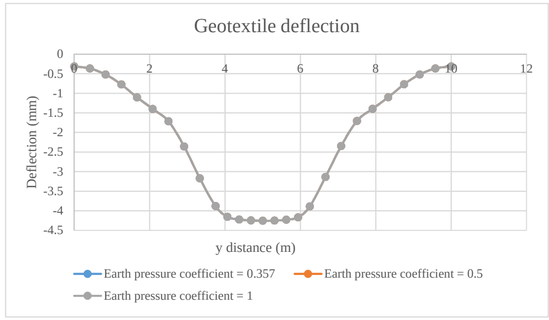

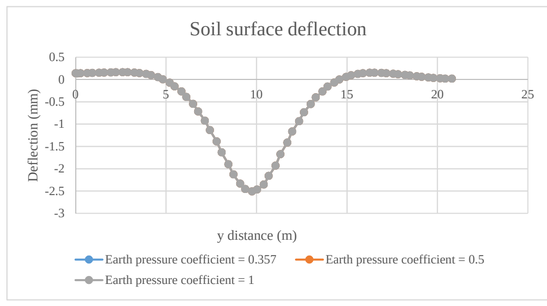

1 Layer

Geogrid deflection (mm)		
x	y (m)	1000
0	-0.00031556	-0.31556
0.41666667	-0.00036651	-0.36651
0.83333333	-0.00052	-0.52
1.25	-0.00077379	-0.77379
1.66666667	-0.00110406	-1.10406
2.08333333	-0.00140079	-1.40079
2.5	-0.00171289	-1.71289
2.91666667	-0.0023576	-2.3576
3.33333333	-0.00316989	-3.16989
3.75	-0.00388015	-3.88015
4.0625	-0.00415347	-4.15347
4.375	-0.00422187	-4.22187
4.6875	-0.00424585	-4.24585
5	-0.00425444	-4.25444
5.3125	-0.00425019	-4.25019
5.625	-0.00422823	-4.22823
5.9375	-0.00416522	-4.16522
6.25	-0.00388835	-3.88835
6.66666667	-0.003137	-3.137
7.08333333	-0.00234466	-2.34466
7.5	-0.00170547	-1.70547
7.91666667	-0.0013951	-1.3951
8.33333333	-0.00110009	-1.10009
8.75	-0.00077121	-0.77121
9.16666667	-0.00051839	-0.51839
9.58333333	-0.00036542	-0.36542
10	-0.00031463	-0.31463

Geogrid stress (MPa)	
x	y
0	1.23908
0.4166667	1.186955
0.8333333	1.09794
1.25	1.237485
1.6666667	1.300635
2.0833333	0.45143
2.5	0.637615
2.9166667	4.81191
3.3333333	15.367775
3.75	30.402155
4.0625	36.87627
4.375	35.25335
4.6875	33.838985
5	33.719375
5.3125	33.970155
5.625	34.934475
5.9375	36.003505
6.25	30.53972
6.6666667	16.98624
7.0833333	5.41195
7.5	0.6488
7.9166667	0.465615
8.3333333	1.32328
8.75	1.251525
9.1666667	1.1112
9.5833333	1.198235
10	1.249825

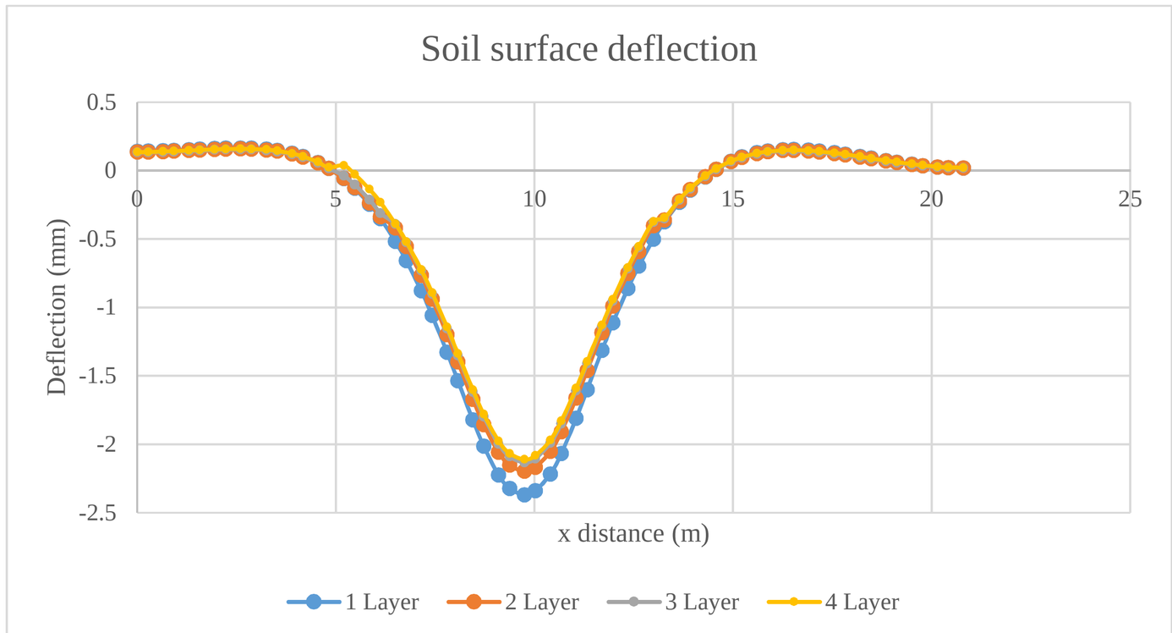

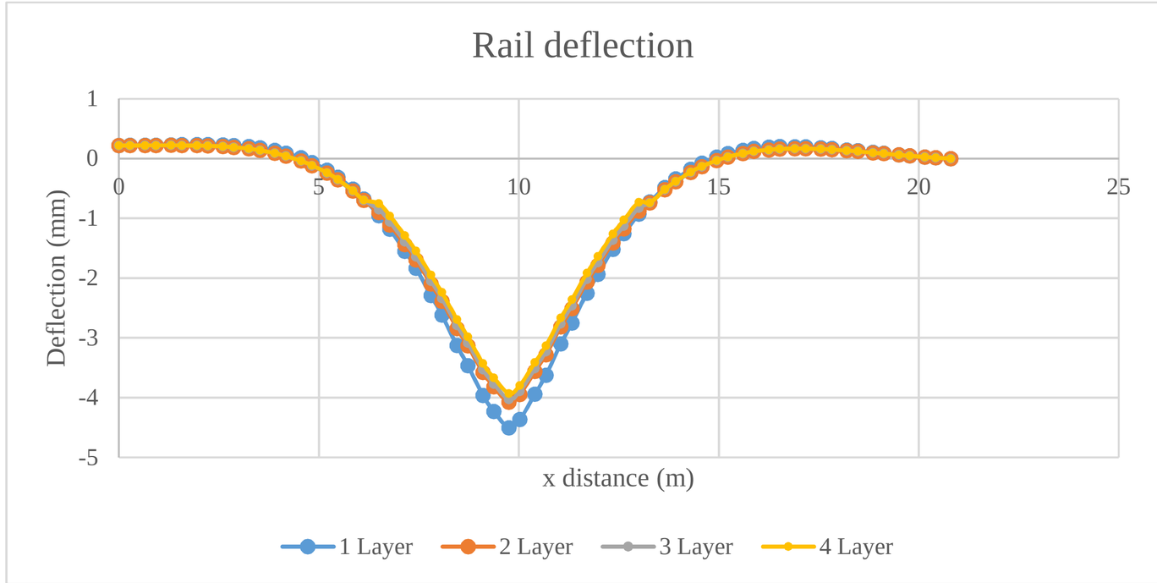

Rail deflection (mm)		
x	y (m)	1000
0	0.00021864	0.22099
0.275	0.0002189	0.22152
0.65	0.00022019	0.22425
0.925	0.00021999	0.22586
1.3	0.0002216	0.23085
1.575	0.00021959	0.23198
1.95	0.00021857	0.236
2.225	0.00021201	0.23358
2.6	0.00020353	0.23125
2.875	0.00018835	0.22063
3.25	0.00016559	0.20425
3.525	0.0001364	0.17919
3.9	0.00009053	0.13863
4.175	0.00004072	0.09129
4.55	-0.00003897	0.01404
4.825	-0.00011699	-0.06474
5.2	-0.00024264	-0.19317
5.475	-0.00035682	-0.31324
5.85	-0.00054106	-0.50823
6.125	-0.00069869	-0.67898
6.5	-0.00095288	-0.95481
6.775	-0.00115879	-1.18298
7.15	-0.00149001	-1.54909
7.425	-0.00174337	-1.83476
7.8	-0.00214825	-2.28821
8.075	-0.00243669	-2.61754
8.45	-0.00288992	-3.1287
8.725	-0.00318343	-3.46478
9.1	-0.00362633	-3.95992
9.375	-0.00386868	-4.22928
9.75	-0.0041275	-4.50458
10.025	-0.00399422	-4.36292
10.4	-0.0036115	-3.94276
10.675	-0.00332993	-3.6236
11.05	-0.00286279	-3.09769
11.325	-0.00256073	-2.75178
11.7	-0.00211745	-2.25323
11.975	-0.0018385	-1.93651
12.35	-0.00146142	-1.51666
12.625	-0.00122662	-1.25391
13	-0.00092843	-0.92687
13.275	-0.00074368	-0.72403
13.65	-0.00052177	-0.48553
13.925	-0.0003848	-0.33878
14.3	-0.00022973	-0.17663
14.575	-0.00013441	-0.07778
14.95	-0.00003419	0.02292
15.225	0.00002706	0.08349
15.6	0.00008468	0.13753
15.875	0.00011954	0.1692
16.25	0.00014575	0.1898
16.525	0.00016116	0.20087
16.9	0.00016544	0.19895
17.175	0.00016731	0.19626
17.55	0.00015726	0.18038
17.825	0.00015036	0.16929
18.2	0.00013185	0.14587
18.475	0.00011991	0.13045
18.85	0.00009739	0.10418
19.125	0.00008338	0.08755
19.5	0.00006027	0.06196
19.775	0.00004651	0.04658
20.15	0.00002528	0.02446
20.425	0.0000132	0.01226
20.8	0	0

Formation deflection (mm)		
x	y (m)	1000
0	0.00014117	0.14117
0.275	0.00014234	0.14234
0.65	0.00014505	0.14505
0.925	0.00014784	0.14784
1.3	0.0001524	0.1524
1.575	0.00015608	0.15608
1.95	0.00016076	0.16076
2.225	0.00016345	0.16345
2.6	0.00016491	0.16491
2.875	0.00016361	0.16361
3.25	0.00015697	0.15697
3.525	0.00014752	0.14752
3.9	0.0001263	0.1263
4.175	0.00010331	0.10331
4.55	0.00005942	0.05942
4.825	0.00001644	0.01644
5.2	-0.00005941	-0.05941
5.475	-0.00012942	-0.12942
5.85	-0.00024675	-0.24675
6.125	-0.0003504	-0.3504
6.5	-0.0005171	-0.5171
6.775	-0.00065892	-0.65892
7.15	-0.00087885	-0.87885
7.425	-0.00105945	-1.05945
7.8	-0.00132844	-1.32844
8.075	-0.00153786	-1.53786
8.45	-0.00182274	-1.82274
8.725	-0.00201523	-2.01523
9.1	-0.00222486	-2.22486
9.375	-0.002323	-2.323
9.75	-0.00236969	-2.36969
10.025	-0.00233927	-2.33927
10.4	-0.00221777	-2.21777
10.675	-0.00206852	-2.06852
11.05	-0.00181152	-1.81152
11.325	-0.00160157	-1.60157
11.7	-0.00131415	-1.31415
11.975	-0.00111348	-1.11348
12.35	-0.00086298	-0.86298
12.625	-0.00069805	-0.69805
13	-0.0005005	-0.5005
13.275	-0.00037532	-0.37532
13.65	-0.00023096	-0.23096
13.925	-0.0001431	-0.1431
14.3	-0.00004602	-0.04602
14.575	0.00001019	0.01019
14.95	0.00006884	0.06884
15.225	0.0001003	0.1003
15.6	0.00012992	0.12992
15.875	0.00014331	0.14331
16.25	0.00015242	0.15242
16.525	0.00015351	0.15351
16.9	0.00014915	0.14915
17.175	0.00014249	0.14249
17.55	0.00013012	0.13012
17.825	0.00011919	0.11919
18.2	0.00010285	0.10285
18.475	0.00009023	0.09023
18.85	0.00007303	0.07303
19.125	0.00006081	0.06081
19.5	0.00004564	0.04564
19.775	0.00003617	0.03617
20.15	0.00002654	0.02654
20.425	0.00002195	0.02195
20.8	0.00001932	0.01932

2 Layer

Geogrid deflection (mm)		
x	y (m)	1000
0	-0.000306093	-0.3061
0.41666667	-0.000355515	-0.3555
0.83333333	-0.0005044	-0.5044
1.25	-0.000750576	-0.7506
1.66666667	-0.001070938	-1.0709
2.08333333	-0.001358766	-1.3588
2.5	-0.001661503	-1.6615
2.91666667	-0.002286872	-2.2869
3.33333333	-0.003026293	-3.0263
3.75	-0.003715246	-3.7152
4.0625	-0.003980366	-3.9804
4.375	-0.004046714	-4.0467
4.6875	-0.004069975	-4.0700
5	-0.004078307	-4.0783068
5.3125	-0.004074184	-4.0742
5.625	-0.004052883	-4.0529
5.9375	-0.003991763	-3.9918
6.25	-0.0037232	-3.7232
6.66666667	-0.00299439	-2.9944
7.08333333	-0.00227432	-2.2743
7.5	-0.001654306	-1.6543
7.91666667	-0.001353247	-1.3532
8.33333333	-0.001067087	-1.0671
8.75	-0.000748074	-0.7481
9.16666667	-0.000502838	-0.5028
9.58333333	-0.000354457	-0.3545
10	-0.000305191	-0.3052

Geogrid stress (MPa)	
x	y
0	1.129297512
0.41666667	1.081790787
0.83333333	1.000662516
1.25	1.127843829
1.66666667	1.231898739
2.08333333	0.457933302
2.5	0.627622311
2.91666667	4.432074774
3.33333333	14.56419014
3.75	28.26652407
4.0625	34.16703248
4.375	32.68790319
4.6875	31.39885093
5	31.28983838
5.3125	31.51839927
5.625	32.39728052
5.9375	33.37159446
6.25	28.39190081
6.66666667	16.03925914
7.08333333	4.97895123
7.5	0.63781632
7.91666667	0.470861511
8.33333333	1.252537392
8.75	1.140639885
9.16666667	1.01274768
9.58333333	1.092071379
10	1.139090505

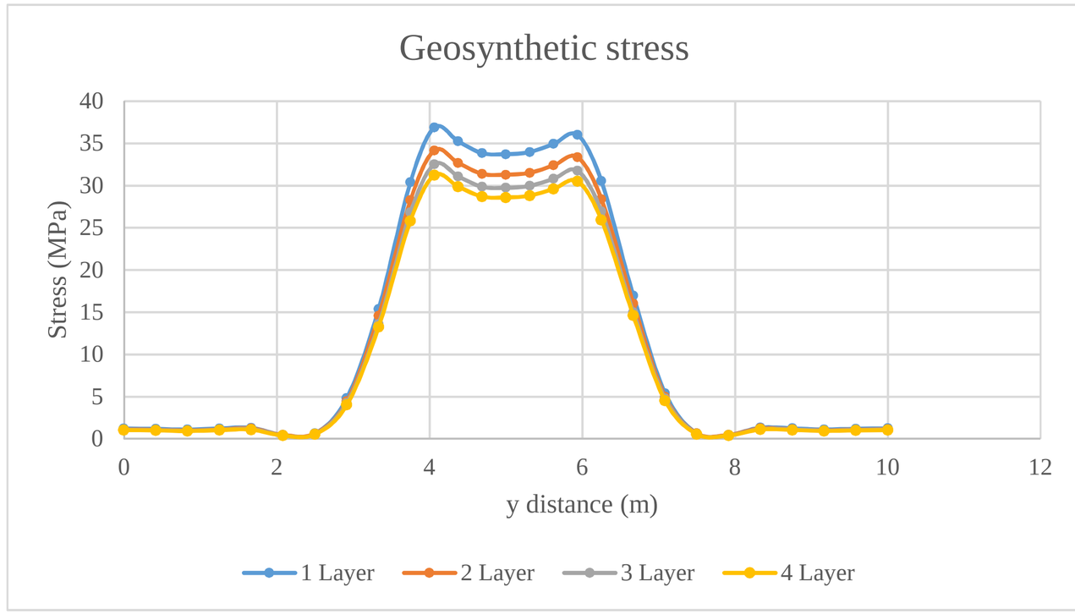

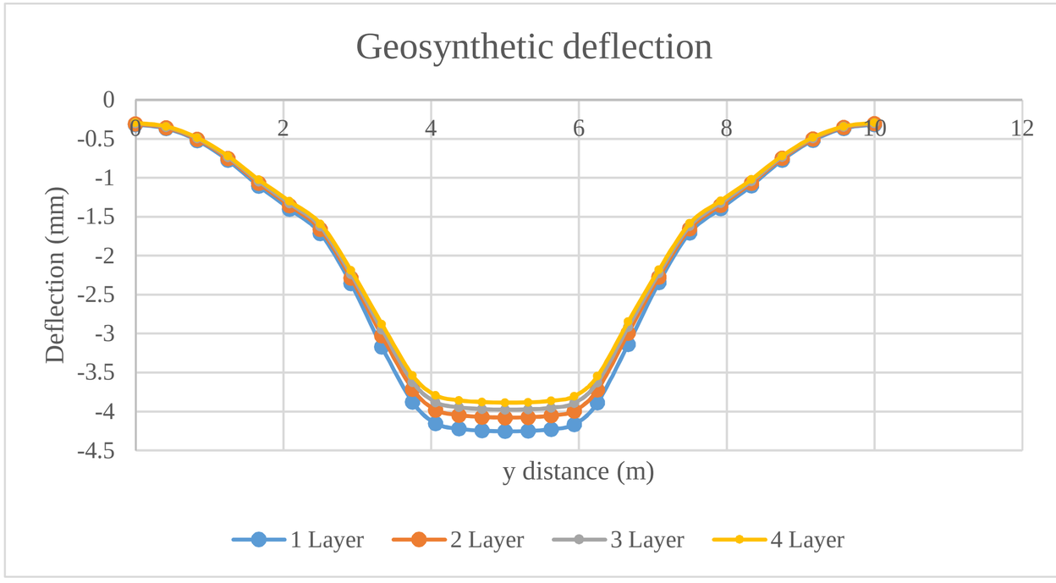

Rail deflection (mm)		
x	y (m)	1000
0	0.00021864	0.21864
0.275	0.0002189	0.2189
0.65	0.00022019	0.22019
0.925	0.00021999	0.21999
1.3	0.0002216	0.2216
1.575	0.00021959	0.21959
1.95	0.00021857	0.21857
2.225	0.00021201	0.21201
2.6	0.00020353	0.20353
2.875	0.00018835	0.18835
3.25	0.00016559	0.16559
3.525	0.0001364	0.1364
3.9	0.00009053	0.09053
4.175	0.00004072	0.04072
4.55	-0.00003897	-0.03897
4.825	-0.00011699	-0.11699
5.2	-0.00024264	-0.24264
5.475	-0.00035682	-0.35682
5.85	-0.00054106	-0.54106
6.125	-0.00069869	-0.69869
6.5	-0.00090288	-0.90288
6.775	-0.00110879	-1.10879
7.15	-0.00144001	-1.44001
7.425	-0.00169337	-1.69337
7.8	-0.00209825	-2.09825
8.075	-0.00238669	-2.38669
8.45	-0.00283992	-2.83992
8.725	-0.00313343	-3.13343
9.1	-0.00357633	-3.57633
9.375	-0.00381868	-3.81868
9.75	-0.0040775	-4.0775
10.025	-0.00394422	-3.94422
10.4	-0.0035615	-3.5615
10.675	-0.00327993	-3.27993
11.05	-0.00281279	-2.81279
11.325	-0.00251073	-2.51073
11.7	-0.00206745	-2.06745
11.975	-0.0017885	-1.7885
12.35	-0.00141142	-1.41142
12.625	-0.00117662	-1.17662
13	-0.00087843	-0.87843
13.275	-0.00074368	-0.74368
13.65	-0.00052177	-0.52177
13.925	-0.0003848	-0.3848
14.3	-0.00022973	-0.22973
14.575	-0.00013441	-0.13441
14.95	-0.00003419	-0.03419
15.225	0.00002706	0.02706
15.6	0.00008468	0.08468
15.875	0.00011954	0.11954
16.25	0.00014575	0.14575
16.525	0.00016116	0.16116
16.9	0.00016544	0.16544
17.175	0.00016731	0.16731
17.55	0.00015726	0.15726
17.825	0.00015036	0.15036
18.2	0.00013185	0.13185
18.475	0.00011991	0.11991
18.85	0.00009739	0.09739
19.125	0.00008338	0.08338
19.5	0.00006027	0.06027
19.775	0.00004651	0.04651
20.15	0.00002528	0.02528
20.425	0.0000132	0.0132
20.8	0	0

Formation deflection (mm)		
x	y (m)	1000
0	0.000135523	0.1355232
0.275	0.000136646	0.1366464
0.65	0.000139248	0.139248
0.925	0.000141926	0.1419264
1.3	0.000146304	0.146304
1.575	0.000149837	0.1498368
1.95	0.00015433	0.1543296
2.225	0.000156912	0.156912
2.6	0.000158314	0.1583136
2.875	0.000157066	0.1570656
3.25	0.000150691	0.1506912
3.525	0.000141619	0.1416192
3.9	0.000121248	0.121248
4.175	9.91776E-05	0.0991776
4.55	5.70432E-05	0.0570432
4.825	1.57824E-05	0.0157824
5.2	-5.70336E-05	-0.0570336
5.475	-0.000124243	-0.1242432
5.85	-0.00023688	-0.23688
6.125	-0.000336384	-0.336384
6.5	-0.000419616	-0.419616
6.775	-0.000555763	-0.5557632
7.15	-0.000766896	-0.766896
7.425	-0.000940272	-0.940272
7.8	-0.001198502	-1.1985024
8.075	-0.001399546	-1.3995456
8.45	-0.00167303	-1.6730304
8.725	-0.001857821	-1.8578208
9.1	-0.002059066	-2.0590656
9.375	-0.00215328	-2.15328
9.75	-0.002198102	-2.1981024
10.025	-0.002168899	-2.1688992
10.4	-0.002052259	-2.0522592
10.675	-0.001908979	-1.9089792
11.05	-0.001662259	-1.6622592
11.325	-0.001460707	-1.4607072
11.7	-0.001184784	-1.184784
11.975	-0.000992141	-0.9921408
12.35	-0.000751661	-0.7516608
12.625	-0.000593328	-0.593328
13	-0.00040368	-0.40368
13.275	-0.000360307	-0.3603072
13.65	-0.000221722	-0.2217216
13.925	-0.000137376	-0.137376
14.3	-4.41792E-05	-0.0441792
14.575	9.7824E-06	0.0097824
14.95	6.60864E-05	0.0660864
15.225	0.000096288	0.096288
15.6	0.000124723	0.1247232
15.875	0.000137578	0.1375776
16.25	0.000146323	0.1463232
16.525	0.00014737	0.1473696
16.9	0.000143184	0.143184
17.175	0.00013679	0.1367904
17.55	0.000124915	0.1249152
17.825	0.000114422	0.1144224
18.2	0.000098736	0.098736
18.475	8.66208E-05	0.0866208
18.85	7.01088E-05	0.0701088
19.125	5.83776E-05	0.0583776
19.5	4.38144E-05	0.0438144
19.775	3.47232E-05	0.0347232
20.15	2.54784E-05	0.0254784
20.425	0.000021072	0.021072
20.8	1.85472E-05	0.0185472

3 Layer

Geogrid deflection (mm)		
x	y (m)	1000
0	-0.000298832	-0.298832
0.41666667	-0.000347235	-0.347235
0.83333333	-0.00049305	-0.49305
1.25	-0.000734151	-0.734151
1.66666667	-0.001047907	-1.047907
2.08333333	-0.001329801	-1.329801
2.5	-0.001626296	-1.626296
2.91666667	-0.00223877	-2.23877
3.33333333	-0.002946796	-2.946796
3.75	-0.003621543	-3.621543
4.0625	-0.003881197	-3.881197
4.375	-0.003946177	-3.946177
4.6875	-0.003968958	-3.968958
5	-0.003977118	-3.977118
5.3125	-0.003973081	-3.973081
5.625	-0.003952219	-3.952219
5.9375	-0.003892359	-3.892359
6.25	-0.003629333	-3.629333
6.66666667	-0.00291555	-2.91555
7.08333333	-0.002226477	-2.226477
7.5	-0.001619247	-1.619247
7.91666667	-0.001324395	-1.324395
8.33333333	-0.001044136	-1.044136
8.75	-0.0007317	-0.7317
9.16666667	-0.000491521	-0.491521
9.58333333	-0.000346199	-0.346199
10	-0.000297949	-0.297949

Geogrid stress (MPa)	
x	y
0	1.092643388
0.4166667	1.046716051
0.8333333	0.968284934
1.25	1.091238034
1.6666667	1.152219499
2.0833333	0.403984973
2.5	0.568032577
2.9166667	4.246003901
3.3333333	13.57614655
3.75	26.82293877
4.0625	32.5272815
4.375	31.09732669
4.6875	29.85112968
5	29.74574131
5.3125	29.96670357
5.625	30.81636592
5.9375	31.75828826
6.25	26.94414729
6.6666667	15.00217606
7.0833333	4.774699145
7.5	0.57788768
7.9166667	0.416483377
8.3333333	1.172172008
8.75	1.103608678
9.1666667	0.97996832
9.5833333	1.056654859
10	1.102110808

Rail deflection (mm)		
x	y (m)	1000
0	0.00021864	0.21864
0.275	0.0002189	0.2189
0.65	0.00022019	0.22019
0.925	0.00021999	0.21999
1.3	0.0002216	0.2216
1.575	0.00021959	0.21959
1.95	0.00021857	0.21857
2.225	0.00021201	0.21201
2.6	0.00020353	0.20353
2.875	0.00018835	0.18835
3.25	0.00016559	0.16559
3.525	0.0001364	0.1364
3.9	0.00009053	0.09053
4.175	0.00004072	0.04072
4.55	-0.00003897	-0.03897
4.825	-0.00011699	-0.11699
5.2	-0.00024264	-0.24264
5.475	-0.00035682	-0.35682
5.85	-0.00054106	-0.54106
6.125	-0.00069869	-0.69869
6.5	-0.00085288	-0.85288
6.775	-0.00105879	-1.05879
7.15	-0.00139001	-1.39001
7.425	-0.00164337	-1.64337
7.8	-0.00204825	-2.04825
8.075	-0.00233669	-2.33669
8.45	-0.00278992	-2.78992
8.725	-0.00308343	-3.08343
9.1	-0.00352633	-3.52633
9.375	-0.00376868	-3.76868
9.75	-0.0040275	-4.0275
10.025	-0.00389422	-3.89422
10.4	-0.0035115	-3.5115
10.675	-0.00322993	-3.22993
11.05	-0.00276279	-2.76279
11.325	-0.00246073	-2.46073
11.7	-0.00201745	-2.01745
11.975	-0.0017385	-1.7385
12.35	-0.00136142	-1.36142
12.625	-0.00112662	-1.12662
13	-0.00082843	-0.82843
13.275	-0.00074368	-0.74368
13.65	-0.00052177	-0.52177
13.925	-0.0003848	-0.3848
14.3	-0.00022973	-0.22973
14.575	-0.00013441	-0.13441
14.95	-0.00003419	-0.03419
15.225	0.00002706	0.02706
15.6	0.00008468	0.08468
15.875	0.00011954	0.11954
16.25	0.00014575	0.14575
16.525	0.00016116	0.16116
16.9	0.00016544	0.16544
17.175	0.00016731	0.16731
17.55	0.00015726	0.15726
17.825	0.00015036	0.15036
18.2	0.00013185	0.13185
18.475	0.00011991	0.11991
18.85	0.00009739	0.09739
19.125	0.00008338	0.08338
19.5	0.00006027	0.06027
19.775	0.00004651	0.04651
20.15	0.00002528	0.02528
20.425	0.0000132	0.0132
20.8	0	0

Formation deflection (mm)		
x	y (m)	1000
0	0.0001327	0.1326998
0.275	0.0001338	0.1337996
0.65	0.000136347	0.136347
0.925	0.00013897	0.1389696
1.3	0.000143256	0.143256
1.575	0.000146715	0.1467152
1.95	0.000151114	0.1511144
2.225	0.000153643	0.153643
2.6	0.000155015	0.1550154
2.875	0.000153793	0.1537934
3.25	0.000147552	0.1475518
3.525	0.000138669	0.1386688
3.9	0.000118722	0.118722
4.175	9.71114E-05	0.0971114
4.55	5.58548E-05	0.0558548
4.825	1.54536E-05	0.0154536
5.2	-3.70454E-05	-0.0370454
5.475	-0.000102855	-0.1028548
5.85	-0.000213145	-0.213145
6.125	-0.000310576	-0.310576
6.5	-0.000392074	-0.392074
6.775	-0.000525385	-0.5253848
7.15	-0.000732119	-0.732119
7.425	-0.000901883	-0.901883
7.8	-0.001154734	-1.1547336
8.075	-0.001351588	-1.3515884
8.45	-0.001619376	-1.6193756
8.725	-0.001800316	-1.8003162
9.1	-0.001997368	-1.9973684
9.375	-0.00208962	-2.08962
9.75	-0.002133509	-2.1335086
10.025	-0.002104914	-2.1049138
10.4	-0.001990704	-1.9907038
10.675	-0.001850409	-1.8504088
11.05	-0.001608829	-1.6088288
11.325	-0.001411476	-1.4114758
11.7	-0.001141301	-1.141301
11.975	-0.000952671	-0.9526712
12.35	-0.000717201	-0.7172012
12.625	-0.000562167	-0.562167
13	-0.00037647	-0.37647
13.275	-0.000350921	-0.3509208
13.65	-0.000215222	-0.2152224
13.925	-0.000132634	-0.132634
14.3	-4.13788E-05	-0.0413788
14.575	9.5786E-06	0.0095786
14.95	6.47096E-05	0.0647096
15.225	0.000094282	0.094282
15.6	0.000122125	0.1221248
15.875	0.000134711	0.1347114
16.25	0.000143275	0.1432748
16.525	0.000144299	0.1442994
16.9	0.000140201	0.140201
17.175	0.000133941	0.1339406
17.55	0.000122313	0.1223128
17.825	0.000112039	0.1120386
18.2	0.000096679	0.096679
18.475	8.48162E-05	0.0848162
18.85	6.86482E-05	0.0686482
19.125	5.71614E-05	0.0571614
19.5	4.29016E-05	0.0429016
19.775	3.39998E-05	0.0339998
20.15	2.49476E-05	0.0249476
20.425	0.000020633	0.020633
20.8	1.81608E-05	0.0181608

4 Layer

Geogrid deflection (mm)		
x	y (m)	1000
0	-0.000293471	-0.2934708
0.416667	-0.000340854	-0.3408543
0.833333	-0.0004836	-0.4836
1.25	-0.000719625	-0.7196247
1.666667	-0.001023986	-1.0239858
2.083333	-0.001299945	-1.2999447
2.5	-0.001590198	-1.5901977
2.916667	-0.002189778	-2.189778
3.333333	-0.002878248	-2.8782477
3.75	-0.00353879	-3.5387895
4.0625	-0.003792977	-3.7929771
4.375	-0.003856589	-3.8565891
4.6875	-0.003878891	-3.8788905
5	-0.003886879	-3.8868792
5.3125	-0.003882927	-3.8829267
5.625	-0.003862504	-3.8625039
5.9375	-0.003803905	-3.8039046
6.25	-0.003546416	-3.5464155
6.666667	-0.00284766	-2.84766
7.083333	-0.002177744	-2.1777438
7.5	-0.001583297	-1.5832971
7.916667	-0.001294653	-1.294653
8.333333	-0.001020294	-1.0202937
8.75	-0.000717225	-0.7172253
9.166667	-0.000482103	-0.4821027
9.583333	-0.000339841	-0.3398406
10	-0.000292606	-0.2926059

Geogrid stress (MPa)	
x	y
0	1.03487962
0.416667	0.99134482
0.833333	0.91699949
1.25	1.03354747
1.666667	1.08890035
2.083333	0.37964434
2.5	0.53514605
2.916667	4.02151723
3.333333	13.2701657
3.75	25.8268799
4.0625	31.2340607
4.375	29.8785979
4.6875	28.6973203
5	28.597422
5.3125	28.8068735
5.625	29.6122735
5.9375	30.5051274
6.25	25.9417741
6.666667	14.6219076
7.083333	4.52267064
7.5	0.54448776
7.916667	0.39149165
8.333333	1.10781346
8.75	1.04527368
9.166667	0.92807424
9.583333	1.00076587
10	1.04385384

Rail deflection (mm)		
x	y (m)	1000
0	0.00021864	0.21864
0.275	0.0002189	0.2189
0.65	0.00022019	0.22019
0.925	0.00021999	0.21999
1.3	0.0002216	0.2216
1.575	0.00021959	0.21959
1.95	0.00021857	0.21857
2.225	0.00021201	0.21201
2.6	0.00020353	0.20353
2.875	0.00018835	0.18835
3.25	0.00016559	0.16559
3.525	0.0001364	0.1364
3.9	0.00009053	0.09053
4.175	0.00004072	0.04072
4.55	-0.00003897	-0.03897
4.825	-0.00011199	-0.11199
5.2	-0.00023764	-0.23764
5.475	-0.00035182	-0.35182
5.85	-0.00053606	-0.53606
6.125	-0.00069369	-0.69369
6.5	-0.00075288	-0.75288
6.775	-0.00095879	-0.95879
7.15	-0.00129001	-1.29001
7.425	-0.00154337	-1.54337
7.8	-0.00194825	-1.94825
8.075	-0.00223669	-2.23669
8.45	-0.00268992	-2.68992
8.725	-0.00298343	-2.98343
9.1	-0.00342633	-3.42633
9.375	-0.00366868	-3.66868
9.75	-0.0039275	-3.9275
10.025	-0.00379422	-3.79422
10.4	-0.0034115	-3.4115
10.675	-0.00312993	-3.12993
11.05	-0.00266279	-2.66279
11.325	-0.00236073	-2.36073
11.7	-0.00191745	-1.91745
11.975	-0.0016385	-1.6385
12.35	-0.00126142	-1.26142
12.625	-0.00102662	-1.02662
13	-0.00072843	-0.72843
13.275	-0.00073868	-0.73868
13.65	-0.00051677	-0.51677
13.925	-0.0003798	-0.3798
14.3	-0.00022473	-0.22473
14.575	-0.00012941	-0.12941
14.95	-0.00003419	-0.03419
15.225	0.00002706	0.02706
15.6	0.00008468	0.08468
15.875	0.00011954	0.11954
16.25	0.00014575	0.14575
16.525	0.00016116	0.16116
16.9	0.00016544	0.16544
17.175	0.00016731	0.16731
17.55	0.00015726	0.15726
17.825	0.00015036	0.15036
18.2	0.00013185	0.13185
18.475	0.00011991	0.11991
18.85	0.00009739	0.09739
19.125	0.00008338	0.08338
19.5	0.00006027	0.06027
19.775	0.00004651	0.04651
20.15	0.00002528	0.02528
20.425	0.0000132	0.0132
20.8	0	0

Formation deflection (mm)		
x	y (m)	1000
0	0.000135008	0.1350081
0.275	0.000136096	0.1360962
0.65	0.000140477	0.1404765
0.925	0.000143071	0.1430712
1.3	0.000147312	0.147312
1.575	0.000150734	0.1507344
1.95	0.000155087	0.1550868
2.225	0.000157589	0.1575885
2.6	0.000158946	0.1589463
2.875	0.000157737	0.1577373
3.25	0.000153422	0.1534221
3.525	0.000144634	0.1446336
3.9	0.000124899	0.124899
4.175	0.000103518	0.1035183
4.55	6.27006E-05	0.0627006
4.825	2.27292E-05	0.0227292
5.2	3.77487E-05	0.0377487
5.475	-2.73606E-05	-0.0273606
5.85	-0.000136478	-0.1364775
6.125	-0.000232872	-0.232872
6.5	-0.000387903	-0.387903
6.775	-0.000519796	-0.5197956
7.15	-0.000724331	-0.7243305
7.425	-0.000892289	-0.8922885
7.8	-0.001142449	-1.1424492
8.075	-0.00133721	-1.3372098
8.45	-0.001602148	-1.6021482
8.725	-0.001781164	-1.7811639
9.1	-0.00197612	-1.9761198
9.375	-0.00206739	-2.06739
9.75	-0.002110812	-2.1108117
10.025	-0.002082521	-2.0825211
10.4	-0.001969526	-1.9695261
10.675	-0.001830724	-1.8307236
11.05	-0.001591714	-1.5917136
11.325	-0.00139646	-1.3964601
11.7	-0.00112916	-1.1291595
11.975	-0.000942536	-0.9425364
12.35	-0.000709571	-0.7095714
12.625	-0.000556187	-0.5561865
13	-0.000372465	-0.372465
13.275	-0.000345328	-0.3453276
13.65	-0.000211073	-0.2110728
13.925	-0.000127503	-0.127503
14.3	-3.72186E-05	-0.0372186
14.575	1.50567E-05	0.0150567
14.95	6.96012E-05	0.0696012
15.225	0.000098859	0.098859
15.6	0.000126406	0.1264056
15.875	0.000138858	0.1388583
16.25	0.000147331	0.1473306
16.525	0.000150204	0.1502043
16.9	0.00014615	0.1461495
17.175	0.000139956	0.1399557
17.55	0.000128452	0.1284516
17.825	0.000118287	0.1182867
18.2	0.000103091	0.1030905
18.475	8.94939E-05	0.0894939
18.85	7.34979E-05	0.0734979
19.125	6.21333E-05	0.0621333
19.5	4.80252E-05	0.0480252
19.775	3.92181E-05	0.0392181
20.15	2.84022E-05	0.0284022
20.425	2.41335E-05	0.0241335
20.8	2.16876E-05	0.0216876

Reference model		
x	Rail deflection (mm)	
0	0.00006433	0
0.275	0.00006478	0.06478
0.65	0.00006699	0.06699
0.925	0.00006892	0.06892
1.3	0.00007375	0.07375
1.575	0.00007673	0.07673
1.95	0.00008326	0.08326
2.225	0.00008631	0.08631
2.6	0.00009284	0.09284
2.875	0.00009435	0.09435
3.25	0.00009819	0.09819
3.525	0.00009582	0.09582
3.9	0.00009304	0.09304
4.175	0.00008353	0.08353
4.55	0.00006867	0.06867
4.825	0.00004773	0.04773
5.2	0.00001364	0.01364
5.475	-0.000024	-0.024
5.85	-0.00008618	-0.08618
6.125	-0.00014655	-0.14655
6.5	-0.00024691	-0.24691
6.775	-0.00033615	-0.33615
7.15	-0.00048501	-0.48501
7.425	-0.00060816	-0.60816
7.8	-0.00081442	-0.81442
8.075	-0.00097382	-0.97382
8.45	-0.00124277	-1.24277
8.725	-0.00143353	-1.43353
9.1	-0.00175227	-1.75227
9.375	-0.00194435	-1.94435
9.75	-0.0021752	-2.1752
10.025	-0.002058	-2.058
10.4	-0.00175226	-1.75226
10.675	-0.00154912	-1.54912
11.05	-0.00124182	-1.24182
11.325	-0.00105932	-1.05932
11.7	-0.00081338	-0.81338
11.975	-0.00066702	-0.66702
12.35	-0.00048363	-0.48363
12.625	-0.00037387	-0.37387
13	-0.0002453	-0.2453
13.275	-0.00016813	-0.16813
13.65	-0.00008444	-0.08444
13.925	-0.00003404	-0.03404
14.3	0.00001529	0.01529
14.575	0.00004516	0.04516
14.95	0.00006982	0.06982
15.225	0.00008492	0.08492
15.6	0.00009301	0.09301
15.875	0.00009815	0.09815
16.25	0.00009596	0.09596
16.525	0.00009489	0.09489
16.9	0.00008699	0.08699
17.175	0.00008243	0.08243
17.55	0.00007193	0.07193
17.825	0.00006575	0.06575
18.2	0.00005464	0.05464
18.475	0.00004806	0.04806
18.85	0.00003753	0.03753
19.125	0.00003132	0.03132
19.5	0.00002202	0.02202
19.775	0.00001665	0.01665
20.15	0.00000888	0.00888
20.425	0.00000455	0.00455
20.8	0	0

1000

Reference model with reinforcement		
x	Rail deflection (mm)	
0	0.000064342	0
0.275	0.000064784	0.064784
0.65	0.000066992	0.066992
0.925	0.000068921	0.068921
1.3	0.000073756	0.073756
1.575	0.000076733	0.076733
1.95	0.000083263	0.083263
2.225	0.000086307	0.086307
2.6	0.000092827	0.092827
2.875	0.000094341	0.094341
3.25	0.00009817	0.09817
3.525	0.000095802	0.095802
3.9	0.000093008	0.093008
4.175	0.000083495	0.083495
4.55	0.000068628	0.068628
4.825	0.000047694	0.047694
5.2	0.000013593	0.013593
5.475	-2.4043E-05	-0.024043
5.85	-8.6222E-05	-0.086222
6.125	-0.00014659	-0.14659
6.5	-0.00024695	-0.246951
6.775	-0.00033618	-0.336175
7.15	-0.00048503	-0.485027
7.425	-0.00060816	-0.608157
7.8	-0.00081439	-0.814391
8.075	-0.00097377	-0.973768
8.45	-0.00124268	-1.242678
8.725	-0.00143341	-1.433409
9.1	-0.00175211	-1.752108
9.375	-0.00194417	-1.944168
9.75	-0.002175	-2.175
10.025	-0.00205781	-2.057808
10.4	-0.00175209	-1.752094
10.675	-0.00154898	-1.548983
11.05	-0.00124173	-1.241732
11.325	-0.00105926	-1.059259
11.7	-0.00081336	-0.813355
11.975	-0.00066701	-0.667014
12.35	-0.00048364	-0.483644
12.625	-0.0003739	-0.373899
13	-0.00024534	-0.245342
13.275	-0.00016817	-0.168171
13.65	-8.4482E-05	-0.084482
13.925	-3.4088E-05	-0.034088
14.3	0.000015246	0.015246
14.575	0.000045114	0.045114
14.95	0.00006978	0.06978
15.225	0.000084883	0.084883
15.6	0.00009298	0.09298
15.875	0.000098129	0.098129
16.25	0.000095945	0.095945
16.525	0.000094876	0.094876
16.9	0.000086981	0.086981
17.175	0.000082418	0.082418
17.55	0.000071928	0.071928
17.825	0.000065744	0.065744
18.2	0.000054643	0.054643
18.475	0.000048059	0.048059
18.85	0.00003753	0.03753
19.125	0.000031319	0.031319
19.5	0.000022026	0.022026
19.775	0.000016652	0.016652
20.15	0.000008883	0.008883
20.425	0.000004555	0.004555
20.8	0	0

1000

Reference model with void and reinforcement		
x	Rail deflection (mm)	
0	0.00022099	0.22099
0.275	0.00022152	0.22152
0.65	0.00022425	0.22425
0.925	0.00022586	0.22586
1.3	0.00023085	0.23085
1.575	0.00023198	0.23198
1.95	0.000236	0.236
2.225	0.00023358	0.23358
2.6	0.00023125	0.23125
2.875	0.00022063	0.22063
3.25	0.00020425	0.20425
3.525	0.00017919	0.17919
3.9	0.00013863	0.13863
4.175	0.00009129	0.09129
4.55	0.00001404	0.01404
4.825	-0.00006474	-0.06474
5.2	-0.00019317	-0.19317
5.475	-0.00031324	-0.31324
5.85	-0.00050823	-0.50823
6.125	-0.00067898	-0.67898
6.5	-0.00095481	-0.95481
6.775	-0.00118298	-1.18298
7.15	-0.00154909	-1.54909
7.425	-0.00183476	-1.83476
7.8	-0.00228821	-2.28821
8.075	-0.00261754	-2.61754
8.45	-0.0031287	-3.1287
8.725	-0.00346478	-3.46478
9.1	-0.00395992	-3.95992
9.375	-0.00422928	-4.22928
9.75	-0.00450458	-4.50458
10.025	-0.00436292	-4.36292
10.4	-0.00394276	-3.94276
10.675	-0.0036236	-3.6236
11.05	-0.00309769	-3.09769
11.325	-0.00275178	-2.75178
11.7	-0.00225323	-2.25323
11.975	-0.00193651	-1.93651
12.35	-0.00151666	-1.51666
12.625	-0.00125391	-1.25391
13	-0.00092687	-0.92687
13.275	-0.00072403	-0.72403
13.65	-0.00048553	-0.48553
13.925	-0.00033878	-0.33878
14.3	-0.00017663	-0.17663
14.575	-0.00007778	-0.07778
14.95	0.00002292	0.02292
15.225	0.00008349	0.08349
15.6	0.00013753	0.13753
15.875	0.0001692	0.1692
16.25	0.0001898	0.1898
16.525	0.00020087	0.20087
16.9	0.00019895	0.19895
17.175	0.00019626	0.19626
17.55	0.00018038	0.18038
17.825	0.00016929	0.16929
18.2	0.00014587	0.14587
18.475	0.00013045	0.13045
18.85	0.00010418	0.10418
19.125	0.00008755	0.08755
19.5	0.00006196	0.06196
19.775	0.00004658	0.04658
20.15	0.00002446	0.02446
20.425	0.00001226	0.01226
20.8	0	0

1000